

**Synthesis of chiral zirconium-based metal-organic
frameworks as solid catalysts in
asymmetric carbon-carbon coupling reactions**

Dissertation

zur Erlangung des akademischen Grades

Doktor rerum naturalium

(Dr. rer. nat.)

vorgelegt

**dem Bereich Mathematik und Naturwissenschaften der
Technischen Universität Dresden**

von

M. Eng. Khoa Dang Nguyen

geboren am 19.01.1989 in Ho Chi Minh city, Vietnam

eingereicht am 20.08.2019

verteidigt am 21.11.2019

Die Dissertation wurde in der Zeit von Januar 2016 bis Dezember 2019 an der
Professur für Anorganische Chemie I angefertigt.

1. Gutachtern

Erstgutachter: Prof. Dr. Stefan Kaskel (Technische Universität Dresden)

Zweitgutachter: Prof. Dr. Christoph Janiak (Heinrich-Heine-Universität Düsseldorf)

2. Rigorosum

Erstprüfer: Prof. Dr. Stefan Kaskel (Technische Universität Dresden)
für Anorganische Materialien

Zweitprüfer: Prof. Dr. Eike Brunner (Technische Universität Dresden)
für Analytische Chemie

3. Promotionskommission

Vorsitzender: Prof. Dr. Andreas Fery (Leibniz Institut für Polymerforschung Dresden e.V.)

Erstprüfer: Prof. Dr. Stefan Kaskel (Technische Universität Dresden)

Zweitprüfer: Prof. Dr. Eike Brunner (Technische Universität Dresden)

Weiteres Mitglied: Prof Dr. Thomas Doert (Technische Universität Dresden)

Acknowledgements

My PhD thesis finally come true. I never imagine that enantioselective synthesis based on chiral metal-organic framework is the title of my research due to my left-right confusion. However, by determining the name of enantiomers during four years, the destiny gives me one great chance to improve myself. Although that is my nightmare at the beginning time of PhD course, beautiful memories with my family, my friends, and my group in Deutschland help me to overcome that difficult period. Therefore, I would like to take this opportunity to show my sincere gratitude and appreciation to them.

First and foremost, I would like to express my sincere gratitude to my supervisor, Prof. Stefan Kaskel, who gives me one chance to arrive to one of the most wonderful cities, Dresden, as well as approach a high level of academic working style. My thesis would not have been finished without his great encouragement and inspiring guidance. I have been learnt very much from his profound knowledge during our course of interactions. Working with him, I have become more and more mature in designing and developing academic projects.

Especial thanks have to be for Dr. Irena Senkowska. Her continuous support and encouragement have always kept me going ahead and made me more self-confidence. She always listens and raises the best solutions for all my troubles in work as well as routine life in “Tête-à-Tête” meetings. I really appreciate her detailed corrections for polishing my drafts using for publications and presentations. I am also grateful to Dr. Volodymyr Bon, who gives me the best guidance how to use crystal visualization software in refining and constructing the structure of MOFs. I really admire the way he “plays” with MOF structures on Materials Studio, he looks like as a true artist.

I express my heartfelt gratitude to Dr. Franziska Drache. Her friendly nature and dedicated introduction have always made me feel at ease with the new laboratory culture as well as experiments in my early days. I also want to thank Dr. Christel Kutzscher, Mr. Sebastian Ehrling, Mrs. Claudia Eßbach, and Mrs. Kerstin Zechel, who are professional in HPLC, SEM, and gas adsorption measurements. My thesis would be impossible to reach this goal without their enthusiastic help. I am especially grateful to Dr. Bikash Garai, Mr. Ubed Sonai Fehrudin Arrozi, and Mr. En Zhang for timely advice, constant support and cooperation.

To all members of Kaskel group, I really appreciate the time we spent together and I am very lucky to work with you, a perfect team. I will miss you so much!

To all my friends, Mrs. Hai Yen, Dr. Hoang Phuoc, Kim Hoang, Hong Nhung, Mai Huong, My An, Kien Pham, Dr. And Phan, Dr. Tien Le, your warmth has pushed me up and kept me smile during my stay here. I will always cherish your friendship.

My special words of thanks should go to thầy Đưa, Prof. Nam Phan, Assoc. Prof. Nhan Le, and all my teachers, who has made it possible for me to reach this goal. I cherish and appreciate their kindness and fruitful knowledge, which have always inspired me.

I gratefully acknowledge the 911 project of Vietnamese Government for providing me financial support. This not only made my PhD come true, but also provided a great opportunity to open my mind and improve myself.

My deepest gratitude, I would like to express Mẹ, chị Tuyền, anh Hà, Quang, and my big family, who never question my decision and always stand strongly behind my back during the tough time of my life. **Thanks you all with love!**

“There can be miracles when you believe” (Stephen Schwartz)

Abbreviation	Description
1D	One-dimensional
2D	Two-dimensional
3D	Three-dimensional
<i>de</i>	Diastereomeric excess
<i>dr</i>	Diastereomeric ratio
<i>ee</i>	Enantiomeric excess
BET	Brauner-Emmett-Teller
BINAP	2,2'-bis(diphenylphosphino)-1,1'-binaphthyl
BINOL	1,1'-bi-2-naphthol
Boc	<i>tert</i> -butyloxycarbonyl
CP	Cross polarization
CPO	Coordination Polymer of Oslo
DFT	Density functional theory
DNP	Dynamic nuclear polarization
DUT	Dresden University of Technology
EA	Elemental analysis
EDX	Energy dispersive X-ray spectroscopy
Equiv.	Equivalent
FID	Flame ionization detector
FT-IR	Fourier-transform infrared spectroscopy
GC	Gas chromatography
HKUST	Hong Kong University of Science and Technology
HPLC	High performance liquid chromatography
ICP	Inductively coupled plasma

Abbreviations

IRMOF	Isoreticular metal-organic framework
MAS	Magic-angle spinning
MIL	Material of Institute Lavoisier
MOF	Metal-organic framework
MS	Mass spectrometry
NLDFT	Non-local density functional theory
NMR	Nuclear magnetic resonance
NU	Northwestern University
PCN	Porous coordination network
PXRD	Powder X-ray diffraction
RT	Room temperature
SBU	Secondary building unit
SEM	Scanning electron microscopy
TGA	Thermogravimetric analysis
UiO	Universitetet i Oslo
wt.%	Weight percent
XRD	X-Ray diffraction

Table of Contents

Acknowledgements	i
Abbreviations	i
Table of Contents	iii
Chapter 1 State of the art	1
1.1 History of metal-organic framework	2
1.2 The art in stable zirconium-based metal-organic frameworks synthesis	8
1.3 Approaching asymmetric catalysis based on Zr-MOFs	12
1.3.1 Enantiopure active sites locating on organic linkers of Zr-MOFs	13
1.3.2 Enantiopure active sites coordinated to inorganic clusters of Zr-MOFs.....	18
1.4 Motivation	20
Chapter 2 Methods of characterization and Experimental section	22
2.1 Methods of characterization	23
2.1.1 Solid-state nuclear magnetic resonance	23
2.1.2 Chiral high-performance liquid chromatography	27
2.2 Equipment and parameter.....	29
2.2.1 Powder X-ray diffraction.....	29
2.2.2 Physisorption measurements	29
2.2.3 Scanning electron microscope and Energy-dispersive X-ray spectroscopy.....	30
2.2.4 Inductively coupled plasma atomic emission spectroscopy.....	30
2.2.5 Thermal gravimetric analysis	30
2.2.6 Fourier-transform infrared.....	30
2.2.7 Nuclear magnetic resonance.....	30
2.2.8 Gas chromatography	32
2.2.9 High-performance liquid chromatography	32
2.3 Used chemicals.....	32
2.4 Materials synthesis	34
2.4.1 Synthesis of DUT-67 and DUT-67-Pro	34
2.4.2 Synthesis of DUT-136 and its derivatives.....	36
2.4.3 Synthesis of DUT-51.....	37
2.4.4 Synthesis of UiO-66	38

Table of contents

2.4.5 Synthesis of UiO-67	38
2.4.6 Synthesis of MOF-808	38
2.5 Catalytic studies	39
2.5.1 Asymmetric Friedel Craft alkylation.....	39
2.5.2 Asymmetric Michael addition reaction	39
2.5.3 Asymmetric Aldol addition reaction	40
2.5.4 Nickel-catalyzed asymmetric Michael addition reaction	41
Chapter 3 Chiral functionalization of a Zr-MOF (DUT-67) as a solid catalyst in asymmetric Michael addition reaction	43
3.1 Introduction	44
3.2 Results and discussion.....	45
3.3 Conclusion.....	57
Chapter 4 Insights into the role of zirconium clusters in proline functionalized Zr-MOF attaining high enantio- and diastereoselectivity in asymmetric Aldol addition reaction	59
4.1 Introduction	60
4.2 Results and discussion.....	61
4.3 Conclusion.....	77
Chapter 5 New 1D chiral Zr-MOFs based on <i>in situ</i> imine linker formation for asymmetric C-C coupling reactions.....	79
5.1 Introduction	80
5.2 Results and discussion.....	81
5.3 Conclusion.....	98
Chapter 6 Conclusions and Outlook.....	100
6.1 Conclusions	101
6.2 Outlook.....	103
Chapter 7 Appendix	105
References	129
Publications and Presentations	a
Curriculum Vitae	c
Erklärung.....	d

Chapter 1

State of the art

1.1 History of metal-organic framework

As one of the most exciting porous solids, metal-organic frameworks (MOFs) have widely contributed to the great development of chemistry, physics, biology as well as material science during the last three decades.¹ These materials are generally constructed from various metal ions or metal ion clusters interlinked by organic linkers in a coordination network (**Figure 1.1**).^{2, 3} It should be noted that the term “MOFs” has also been synonymously used with other names, including porous coordination polymers, and hybrid porous solids.⁴ Although, the idea of this combination originates from the pioneer researches of Tomic, who mentioned the formation of porous coordination polymers built from multi-functionalized organic molecules and inorganic units in 1965, these materials did not attract much attention at that time due to their low stability.⁵

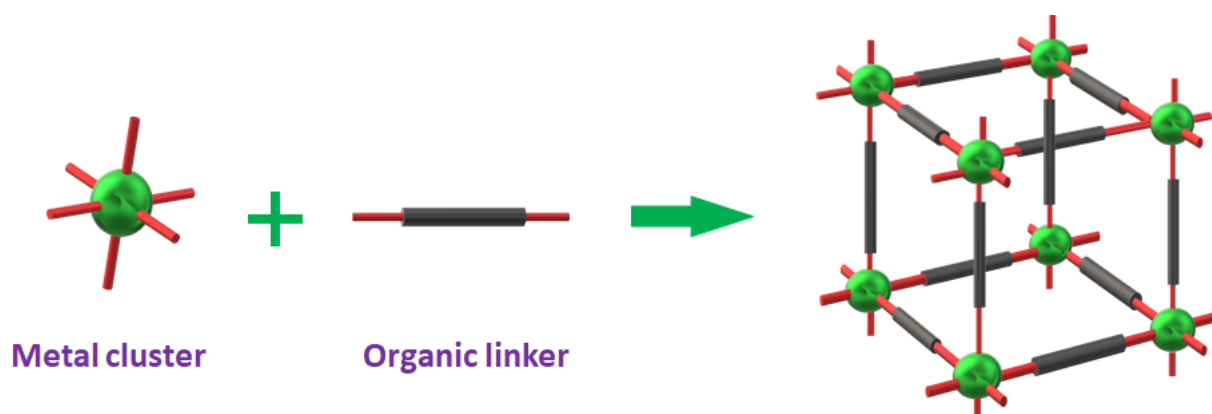


Figure 1.1. Schematic representation of metal-organic framework constructed from metal clusters and organic linkers.

Up to the late 1990s, the appearance of two archetypical MOFs, namely MOF-5 ($\text{Zn}_4\text{O}(\text{BDC})_3$) and HKUST-1 ($\text{Cu}_3(\text{BTC})_2$), led the explosion of studies involving these materials. An enormous number, approximately 70000 metal-organic hybrid solids, is exemplified by reports to date (**Figure 1.2**).⁶⁻⁸ Almost every day, novel MOF structures are being introduced as promising materials towards a wide range of applications, including gas storage and separation, catalysis, biomedical delivery, chemical sensing, etc.⁹ Contributing significantly to this great success of MOFs is the systematic creation of crystalline powders with controlled pore size, shape, and functionality, which could be achieved *via* changing the combinations of organic linkers and metal units.¹⁰ This adjustment has been based on reticular synthesis theory, which had been mentioned by Yaghi and O’Keeffe.¹¹ In reticular chemistry, two components of MOFs, including both organic and inorganic parts, have been considered as secondary building units (SBUs). By

judiciously selecting these building blocks, MOFs can be designed following predetermined topology.¹²

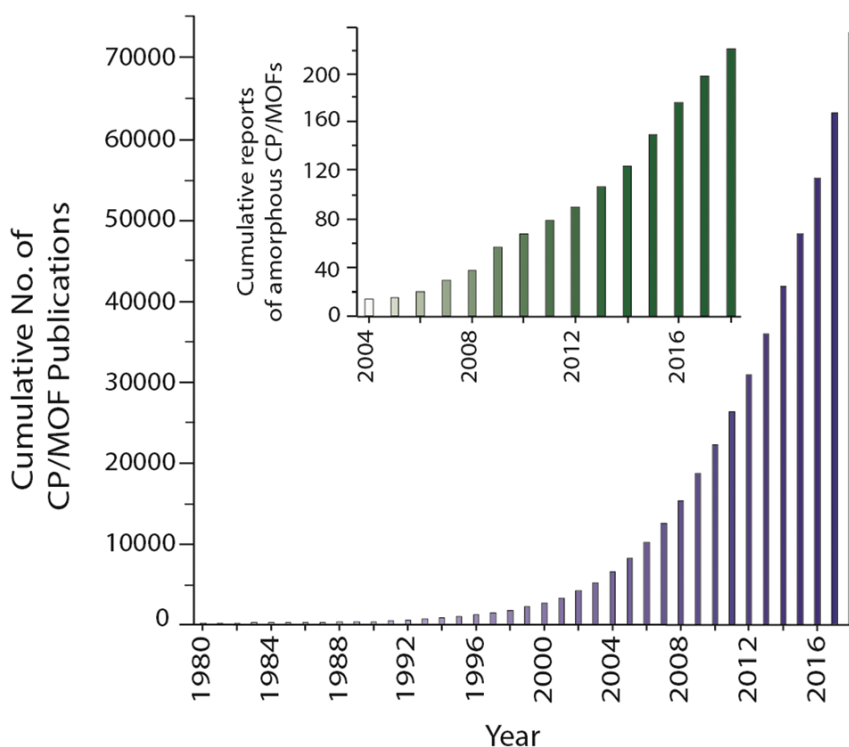


Figure 1.2. The number of crystalline, and non-crystalline MOF structures reported from 1980 to 2018. Reprinted with permission from ref. 6 (Copy right 2019 Royal Society of Chemistry).

The methodology to produce MOF-5 and its derivatives (IRMOF family) have been considered as a benchmark illustration for the feasibility of the reticular synthesis.¹³ The MOF-5, also referred as IRMOF-1, is synthesized from the reaction of $\text{Zn}(\text{NO}_3)_2 \cdot 6\text{H}_2\text{O}$ and terephthalic acid (BDC) in DMF solvent (**Figure 1.3**).^{12, 13} Its structure has primitive cubic (**pcu**) topology, constructed by two building blocks. One is the ditopic linker as “strut”, while the other one is a 6-connected octahedral cluster $\text{Zn}_4\text{O}(\text{CO}_2)_6$ as the “joint”.¹⁴ Considering metal units as metal-oxo-clusters instead of individual atoms opens the possibility to reach orderly predictable 3D structures. There is actually a great number of possible orientations of organic linkers that may coordinate to metal ions, and their geometry can vary during the framework formation.¹⁵ Obviously, the saturated $\text{Zn}_4\text{O}(\text{CO}_2)_6$ SBUs with six bridging carboxylate groups (COO^-), have been used as perfect guidance points with six predetermined directions.¹⁰ Moreover, the metal-oxo clusters have been also found to play a key role in maintaining the porosity of the systems after guest molecule removal, while 3D structures constructed from the isolated metal ions with cyano linkers in early

Robson work tends to collapse due to their fragility.^{10, 16} As a result, the periodic framework of MOF-5 provides approximately 61% empty space of its total volume after the evacuation of solvent molecules.^{3, 17} Unlike any conventional porous material such as zeolites, silicates, or porous carbon, the scaffolding-like nature of MOF-5, meaning the pore without internal walls, provides an ideal space to adsorb gases. Nitrogen gas adsorption measurements at 77 K exhibits a reversible type I isotherm and BET surface area of about 2300 m²/g.³ This value was a significant breakthrough in the gas adsorption field at that time. More importantly, the pore size as well as pore chemistry can also be easily adjusted to meet most of specific application requirement. Toward upgrading the porosity, a new series of porous materials isorecticular to MOF-5 (IRMOF-8 to 10, 12, 14, 16) was developed by replacing BDC with other increasingly complex phenyl-based ditopic carboxylate linkers, including 2,6-naphthalenedicarboxylate, 4,4'-biphenyldicarboxylate, tetrahydropyrene-2,7-dicarboxylate, pyrene-2,7-dicarboxylate, and terphenyl-4,4'-dicarboxylate (TPDC). The pore diameter was gradually increased from 11.2 Å (MOF-5 referred as IRMOF-1) to 19.1 Å (IRMOF-16), and the free volume also reached up to 91.1% in the case of IRMOF-16 with TPDC linker (**Figure 1.3**).^{10, 12} Besides, the moisture stability of material could be improved *via* chemical derivatization of BDC linker.^{18, 19} The highly porous phase of IRMOF-1 collapses into MOF-69c in ambient air, while IRMOF-3, built from 2-amino benzene dicarboxylic acid (**Figure 1.3**), could retain its framework structure in high humidity environment. Furthermore, the moisture stability of IRMOF-3 could be further enhanced by integrating long chain alkyl groups. These hydrophobic molecules could shield the 3D structure when immersed in water.¹⁸ Altogether unprecedented properties relating to gas storage and separation, the functionalization ability of metal-organic frameworks render them as innovative materials. Thus for the first time, the outcome features of new materials could be predicted before starting practical experiments.¹¹

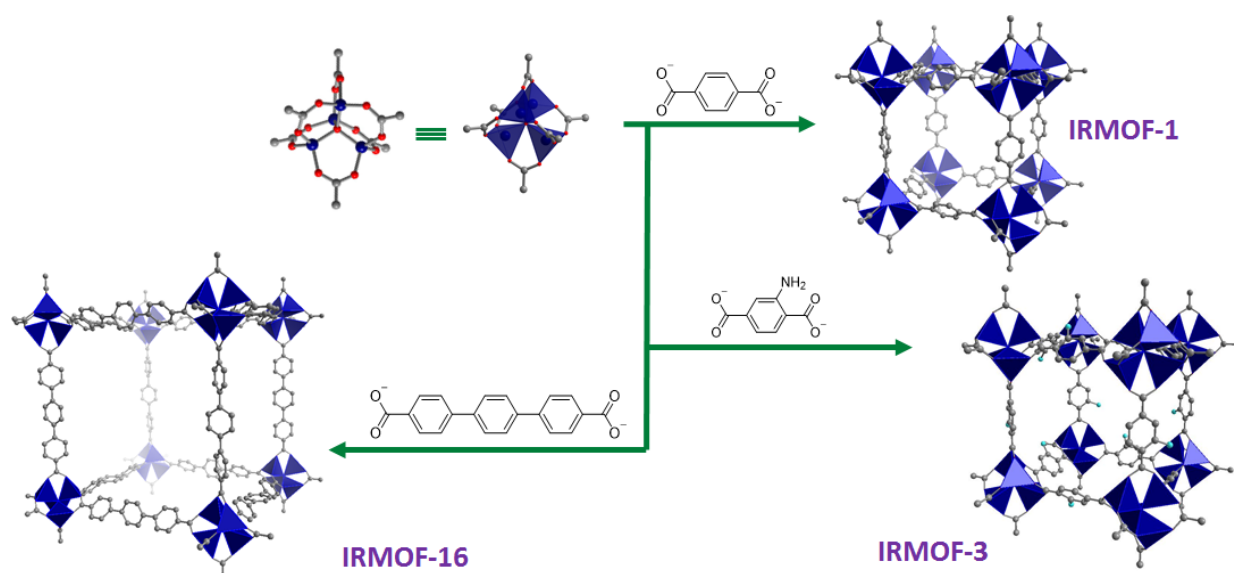


Figure 1.3. Formation of some IRMOF materials and illustration of adjustment pore size as well as pore chemistry by varying the length and functional group on organic building block. Color scheme: Zn (dark blue); O (red); C (grey); N (cyan).

The principle of the reticular chemistry is not only based on 6-connected Zn-clusters and linear dicarboxylic acid linkers, but also expands to various metal clusters and multidentate organic ligands.^{9, 20} The iconic HKUST-1, also called MOF-199 (**Figure 1.4.**), is a typical example. Its octahedral cubic framework with **tpo**-topology is composed of benzene-1,3,5-tricarboxylate (BTC) ligands and dicopper paddle-wheel SBU ($\text{Cu}_2(\text{COO})_4$).^{8, 21} Although, the BET surface area is only about 1600 m^2/g , the existence of open copper sites in the HKUST-1 is a remarkable property, resulting in remarkable advantages in adsorption as well as catalysis.²²⁻²⁴ Several isostructural frameworks have also been developed by using elongated tritopic linkers, such as [4,4',4''-(1,3,5-triazine-2,4,6-triyl)tribenzoate] (TATB – PCN-6'), and 4,4',4''-(4,1,3,5-triyl-tris(benzene-4,1-diyl))tribenzoate (BBC - MOF-399) (**Figure 1.4.**)¹⁰ These materials show a significant increase in cell volume from approximately 18191 \AA^3 for MOF-199 to 101495 \AA^3 for PCN-6' and 318765 \AA^3 for MOF-399.^{25, 26} Noteworthy, MOF-399 also records as one of the lightest metal-organic frameworks as its density is only 0.126 g/cm^3 .¹⁰ Otherwise, the compound isostructural to HKUST-1 ($\text{M}_3(\text{BTC})_2$) could be also designed by replacing metal ions in inorganic paddle-wheel clusters. Indeed, a wide range of structural HKUST-1 analogues could be achieved by solvothermal synthesis with other metal sources, including Zn (II), Mo (II), Cr (II), Ni (II), and Ru (II) instead of copper salts (**Figure 1.4.**)^{3, 27} The ability to diversify metal sites without structure change greatly contributes to the wide range practical application of metal-organic frameworks.

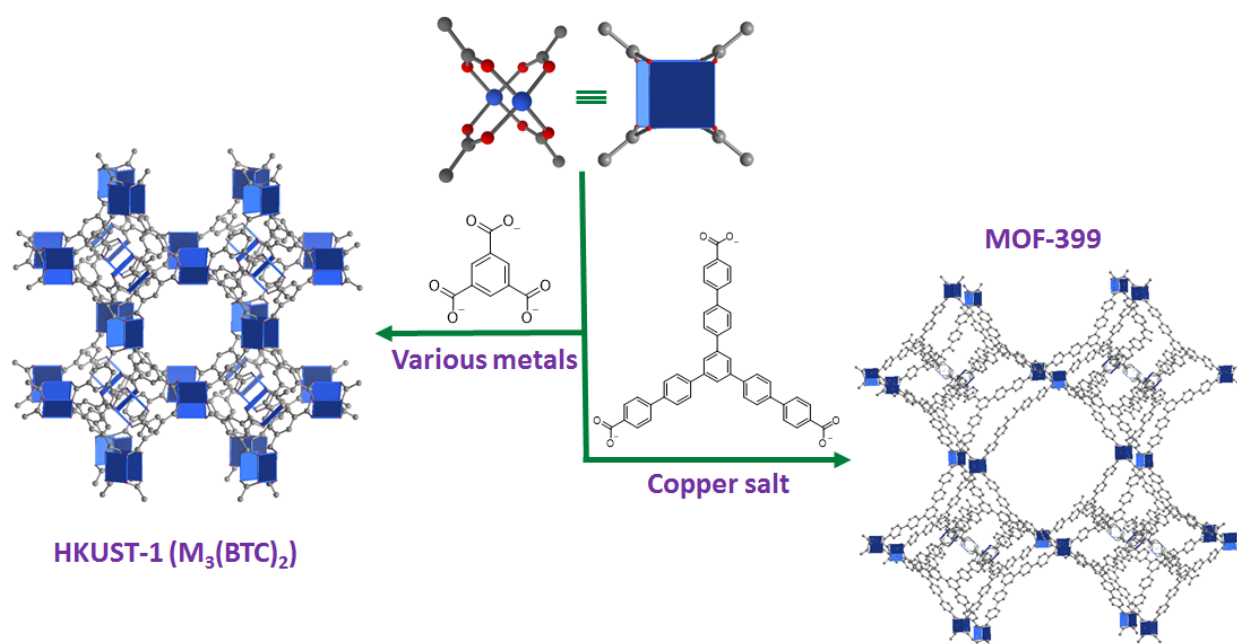


Figure 1.4. Formation of isostructural HKUST-1 materials by changing metal ions or size of tritopic carboxylate linker. Color scheme: metal (blue); O (red); C (grey).

During the next stage of MOFs development, achieving record-breaking values in surface area has always been a special interest of many research groups to determine the limit which the MOFs can reach.²⁸ In a calculation model, the highest surface area of microporous hybrid materials was predicted about 10 577 m²/g as the number of phenyl ring in organic building block reached a maximum level to form poly(*p*-phenylene) frameworks.²⁹ With simple short linkers as BDC, the BET surface area can reach up to 4100 m²/g for MIL-101(Cr₃O(H₂O)₂F(BDC)₃) (**Figure 1.6**),³⁰ while the strategy employing ligand elongation often face to the formation of interpenetrated structures due to high symmetry of MOFs.¹⁰ Only a few of them can be synthesized in the absence of interpenetrated phase and get extremely high BET surface area, such as 5476 m²/g for DUT-49 (Cu₂(BBCDC) – BBCDC = 9,9'-([1,1'-biphenyl]-4,4'-diyl)bis(9H-carbazole-3,6-dicarboxylate) and 7140 m²/g for NU-110 (Cu₃(BHEHPI)- BHEHPI = 5,5',5''- (((benzene-1,3,5-triyltris (benzene-4,1-diyl)) tris(ethyne-2,1-diyl) - tris(benzene-4,1-diyl))tris(ethyne-2,1-diyl)) triisophthalate) (**Figure 1.6**).^{28,29, 31} Therefore, building structures based on the combinations of two linkers to decrease the symmetry of nets has been considered as a suitable approach.²⁸ Actually, a new breakthrough has been recorded at 7839 m²/g (5.02 cm³/g – pore volume) with the discovery of DUT-60 ((Zn₄O(bcpbd))₃(bbc)₄), which was constructed from 1,4-bis-*p*-carboxyphenylbuta-1,3-diene (BCPBD) and 1,3,5-tris (4'-carboxy[1,1'-biphenyl]-4-yl)benzene (BBC) (**Figure 1.6**).³²

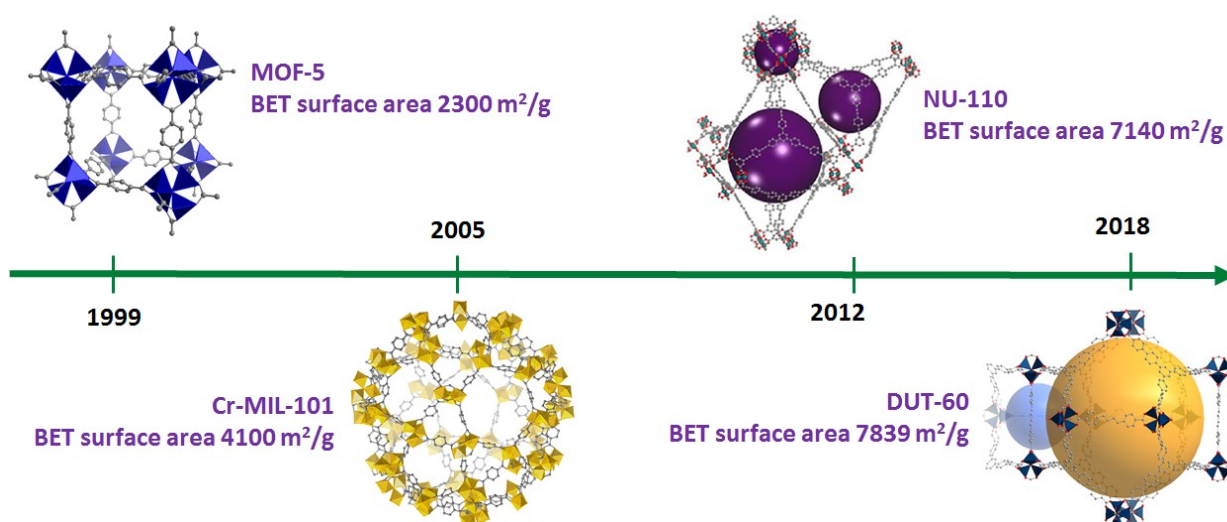


Figure 1.6. Progress in the synthesis of ultrahigh surface area MOFs.

Although the motivation to design metal-organic frameworks derives from the basic requests for storing gaseous fuels (natural gases and hydrogen), the progress in designing highly porous materials expands significantly their application ranges. Based on diversity in combination of building blocks and functionalization ability, MOFs open great opportunities to discover new adsorption behaviours as well as develop *in situ* techniques for characterizing porous materials.³³ Consequently, a tremendous number of reviews related to MOFs and their corresponding applications have been published over 500 papers to date.³⁴ However, MOFs often face to many questions regarding their stability due to the labile nature of coordination bonds. Many of them are in fact characterised by low thermal stability (typically below 350 °C) or instability towards hydrolysis.^{19, 35} Much efforts have been made to synthesize MOFs with enhanced stability, and good results were obtained with the post-synthetic modification (PSM) approach, which was introduced by Cohen and co-workers. PSM permits to incorporate a great number of functionalities into MOF structures but the reduction in surface area and accessible porosity has been frequently observed as a corresponding trade-off.^{36, 37} Therefore, many new methodologies, which include employing azole-based ligands or high valent metal ions (Cr^{3+} , Fe^{3+} , Ti^{4+} , Zr^{4+}), have been devoted to design directly nets with inherent stability.¹⁹ Further along the path of synthesizing stable MOFs, the discovery of UiO-66, constructed from zirconium clusters and the ditopic BDC linkers, has been considered as a remarkable progress. Its structure shows good stability compared with other traditional porous materials. The weight loss of UiO-66 only starts approximately 540 °C via thermogravimetric analysis. Its porous system and crystallinity have been retained in harsh environments.^{35, 38}

1.2 The art in stable zirconium-based metal-organic frameworks synthesis

The robustness and reactivity of MOFs significantly rely on the strength of metal-ligand bonds, which tend to be vulnerable toward increasing temperature or humidity. In some cases, the structure even collapses due to vacuum treatment or exposure to ambient air. For improving the MOFs stability, the general strategy is reinforcing the metal-ligand interactions or increasing the electrostatic interaction between the metal ions and the ligands. This can be easily carried out by using high valence metals with small ionic radius in preparation of metal-organic frameworks.^{2, 19} And, zirconium (IV) ions with high charge density are good candidates. In fact, both of Zr^{4+} and carboxylate ligands are known as hard acid and hard base, respectively. As a result, the combination of these components results in the formation of stable Zr-MOFs, which are tolerant towards water, and even acidic or basic aqueous solutions. In addition, the high abundance, low cost, and low toxicity of zirconium also substantially encourage the development and application of Zr-MOFs.^{35, 39}

The diversity of Zr-MOFs was based on the versatile geometry of Zr-clusters combined with the tunability of multitopic organic building blocks. Although, there is a variety of polyatomic inorganic Zr-containing clusters, the formation of Zr_6O_8 core predominantly appeared in Zr-MOF structures.^{35, 39} In a typical $Zr_6(\mu_3-O)_4(\mu_3-OH)_4$ octahedral cluster, each vertex is a zirconium center with eight-coordination environment. The oxygen atoms form to vertices of a square-antiprismatic coordination geometry. In an ideal case, this $[Zr_6(\mu_3-O)_4(\mu_3-OH)_4]^{12+}$ cluster is fully coordinated by twelve carboxylate groups to form the $Zr_6(\mu_3-O)_4(\mu_3-OH)_4(CO_2)_{12}$ SBU, which is widely found in UiO-family (**fcu** net), such as UiO-66,-67,-68 (**Figure 1.7**).^{35, 40} Aside from 12-connected Zr-clusters, the nets can be also constructed from reduced cluster connectivity, depending on the geometry of linkers. For example, the use of an angular dicarboxylic ligand, such as DTTDC with a bending angle of 148.61° yields 8-coordinated Zr-MOFs, DUT-51 (**reo** topology) (**Figure 1.7**).⁴¹ In its structure, each $[Zr_6(\mu_3-O)_6(\mu_3-OH)_2]^{10+}$ octahedral cluster offers eight of twelve coordination positions to connect 8 carboxylate groups of DTTDC linkers and 4 remaining sites are occupied by DMF and benzoate ligands. The appearance of **reo** structures could be also considered as the absence of one Zr-cluster in the **fcu** structure or as the result of Zr-**fcu**-MOFs with a missing-cluster defect site, which is a unique attribute of using bent ligands. The other types of reduced connectivity Zr-clusters, possessing 4-, 6-, and 10- coordination environment, have been step by step explored to enrich the Zr-MOF chemistry.⁴²⁻⁴⁶

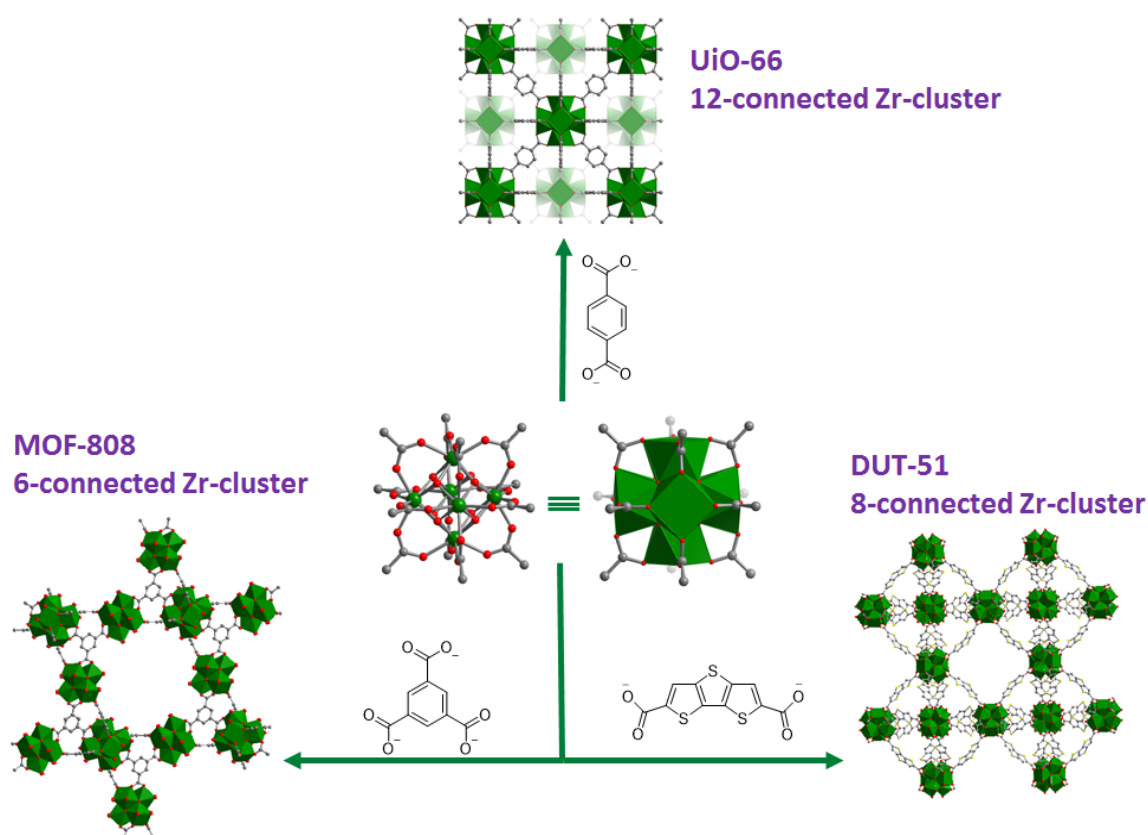


Figure 1.7. Formation of 12-, 8-, and 6-connected Zr-MOFs dependent on configuration of organic building blocks. Color scheme: Zr (green); O (red); C (grey).

However, using high charge density Zr^{4+} ions for stable MOFs synthesis often meets some certain difficulties in obtaining high-quality single crystals for determining their structures.¹⁹ During reaction, the self-repair of network defects, which originates from the lability of the bonds between the metal ions and the carboxylate ligands, plays an essential role in the formation of crystalline materials. In other words, the metal-ligand bonds at metal nodes have been formed with a relative equilibrium, in which any disorder coordination could be replaced by corrected directional bonds.⁴⁷ In the case of high valence metals, these rearrangements slowly occur due to the strong affinity between metal ions and carboxylate ligands. The formation of either microcrystalline powder or amorphous phase has been consequently found as an inevitable result of fast nucleation and precipitation.³⁵

One efficient strategy to regulate the coordination equilibrium is introducing additional chemicals with similar functional groups as organic linkers into the reaction phase. These compounds are also termed modulators, which compete with organic linkers and slow down the reaction rate and nucleation process (**Figure 1.8**).^{35, 46} In addition to this, the modulators have been generally

considered as non-structural moieties, which temporarily bind to metal precursor and be released in an exchange procedure without affecting the nets. Utilization of monocarboxylic acids, such as benzoic acid, acetic acid, formic acid, etc. have been usually preferred in Zr-MOFs synthesis. Together the modulation role in size, shape, and crystallinity of materials, the reproducibility of Zr-MOFs synthesis, affected by purity of organic ligands, metal sources, or solvents, could be further improved in the presence of monocarboxylic molecules as modulators.^{40, 41, 44}

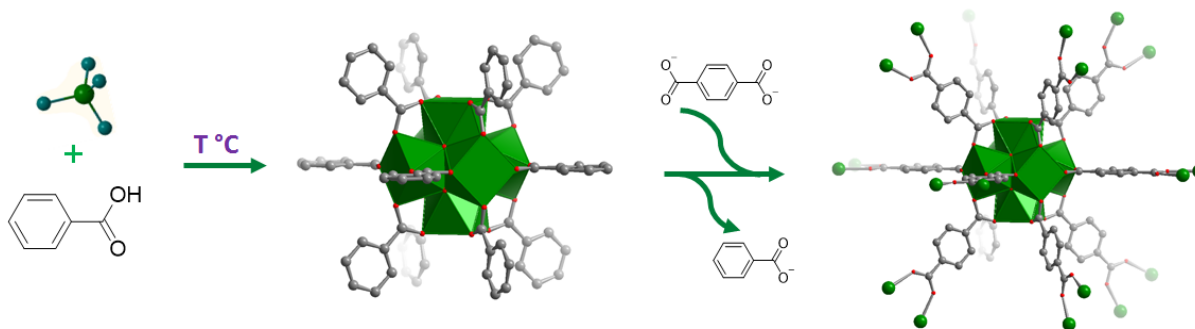


Figure 1.8. Formation of 12-connected Zr-MOF, UiO-66, in the presence of benzoic acid as modulators. Color scheme: Zr (green); O (red); C (grey).

Although, the first Zr-based MOF (UiO-66), constructed from 12-connected Zr-clusters and BDC linkers, was reported in 2008,³⁸ its single-crystal structure determination was only successful after another 3 years.⁴⁰ Behrens and co-workers studied influence of different modulators, including benzoic acid, acetic acid and water, on the formation of UiO-66, Zr-BDC-NH₂ (UiO-66-NH₂), Zr-BPDC (UiO-67), and Zr-TPDC-NH₂ (UiO-68-NH₂). It should be noted that the size and morphology of zirconium-based MOFs can be controlled by varying modulator concentrations. The addition of benzoic acid played a positive role in generating the individual and bigger crystals of UiO-66 and UiO-67, while the water present was essential for the formation of well-ordered structures possessing amino functional groups, such as UiO-66-NH₂, and UiO-68-NH₂. Especially, a mixture of benzoic acid and water as modulators enable enhancing the crystal size of UiO-68-NH₂ adapting single crystal experiment.⁴⁰

Selecting rationally modulators can also lead to the change in coordination geometry of Zr-cluster (**Figure 1.9**). A typical instance was observed in attempts to design isostructural DUT-51 analogues.⁴¹ Using a shortened version of DTTDC as thiophenedicarboxylate linker originally supported the formation of the second isorecticular Zr-**reo**-MOF, DUT-67. However, a variety of topologies based on Zr-TDC system could be also achieved by varying the modulator

concentration. Particularly, DUT-68 in **bon** net was the result of increasing acetic acid content to 183 equiv. instead of 117 equiv. in case of DUT-67 case, while the first 10-connected Zr-MOF (**bct** topology), $Zr_6(\mu_3-O)_4(\mu_3-OH)_4(TDC)_5(OAc)_2$ – DUT-69, was achieved as 50 equiv. of this monocarboxylic acid was applied.⁴⁴ Otherwise, the nature of modulators also maintains a key role in structure formation. This phenomenon was observed in DUT-126 synthesis as acetic acid was replaced by trifluoroacetic acid as modulator. Consequently, an 8,8-connected binodal framework, **hbr** net, was successfully introduced with an improvement in gas accessibility, pore volume of $0.48 \text{ cm}^3/\text{g}$ and BET surface area of $1297 \text{ m}^2/\text{g}$.⁴⁸

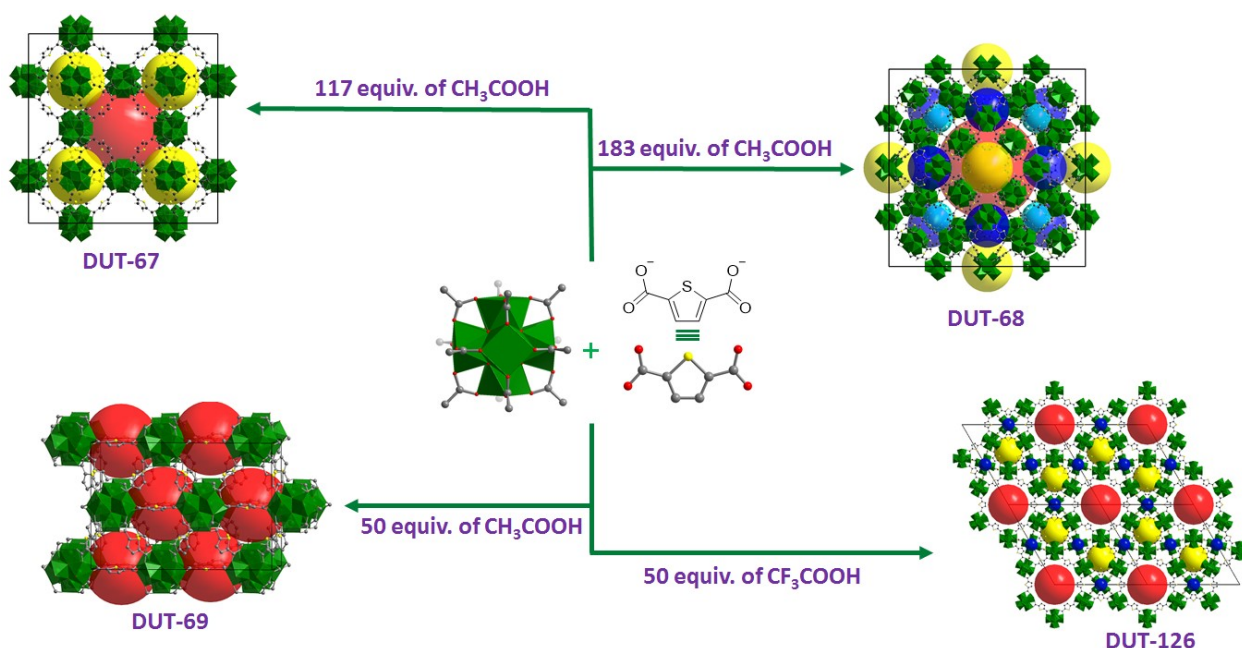


Figure 1.9. Formation of different topologies of Zr-MOF based on various modulators. Color scheme: Zr (green); O (red); C (grey). Adapted with permission from ref.44 (Copy right 2013 American Chemical Society).

Furthermore, the modulators crucially contribute to the formation of defect sites, which greatly determine the nature of pore environment in Zr-MOFs.³⁵ Varying acetic acid concentration systematically results in the presence of missing linker vacancies in UiO-66. A decreasing framework coordination from 12 to 11 would increase the gas accessibility of structure, which showed an enhancement in the pore volume from 0.44 to $1.0 \text{ cm}^3/\text{g}$ and BET surface area from $1000 \text{ m}^2/\text{g}$ to $1600 \text{ m}^2/\text{g}$,⁴⁹ not only affecting the adsorption behaviour, but also the acidic property of Zr-MOFs, origins from ligand defects and open Zr sites, which could be driven by selecting pristine modulators. In particular, the number of defect positions in UiO-66 was mostly improved

by adding trifluoroacetic acid during the synthesis phase. However, to generate open active sites, the releasing of these pristine modulators by post-treatment with HCl, also played a key role in transformation of citronellal. A similar trend was found in case of 8-connected Zr-MOF, DUT-67. By post-treatment with HCl or H₂SO₄, the four coordination sites occupied by DMF and acetate ions was released to form open acid centers, which efficiently catalyze the esterification.⁵⁰

Obviously, the modulated synthesis based on guidance of reticular chemistry offers an efficient approach to design rationally stable MOFs based on zirconium (IV). Despite starting as expansion parts of the UiO-66 discovery, a vast number of Zr-MOF structures with outstanding stabilities has been introduced in recent years.^{35, 46} Their appearance has ushered great possibilities to approach practical applications. In a wide range of MOF applications, asymmetric catalysis is perhaps one of the most fascinating topics to challenge the stability as well as diversity of Zr-MOFs. Although MOF based catalysis have been known as the fastest growing fields, with less than 20 reports in 1997 to over 1100 reports in 2007,³⁴ using MOFs as chiral catalysts is in fact still in its infancy.⁵¹ Only a few reports on chiral MOFs for asymmetric organic transformations have been reported so far due to limitations in stability and remaining chiral environment around active sites under non-ideal reaction conditions.^{51, 52} Therefore, Zr-MOFs with preeminent stability have been recently emerged as promising candidates for designing efficient asymmetric solid catalysts, which not only require appropriate enantiopure active sites, but must also be stable enough towards exposure to reagents, solvents, and high temperature in reactions.⁵³⁻⁵⁶

1.3 Approaching asymmetric catalysis based on Zr-MOFs

Along with inherited basic benefits of a standard MOF supporting efficiently for catalysis, including crystalline nature, high porosity, wide structural and functional variations, chiral environment can be introduced on catalytic sites following various strategies on both organic and inorganic building blocks of Zr-MOFs (**Figure 1.10**).⁵¹

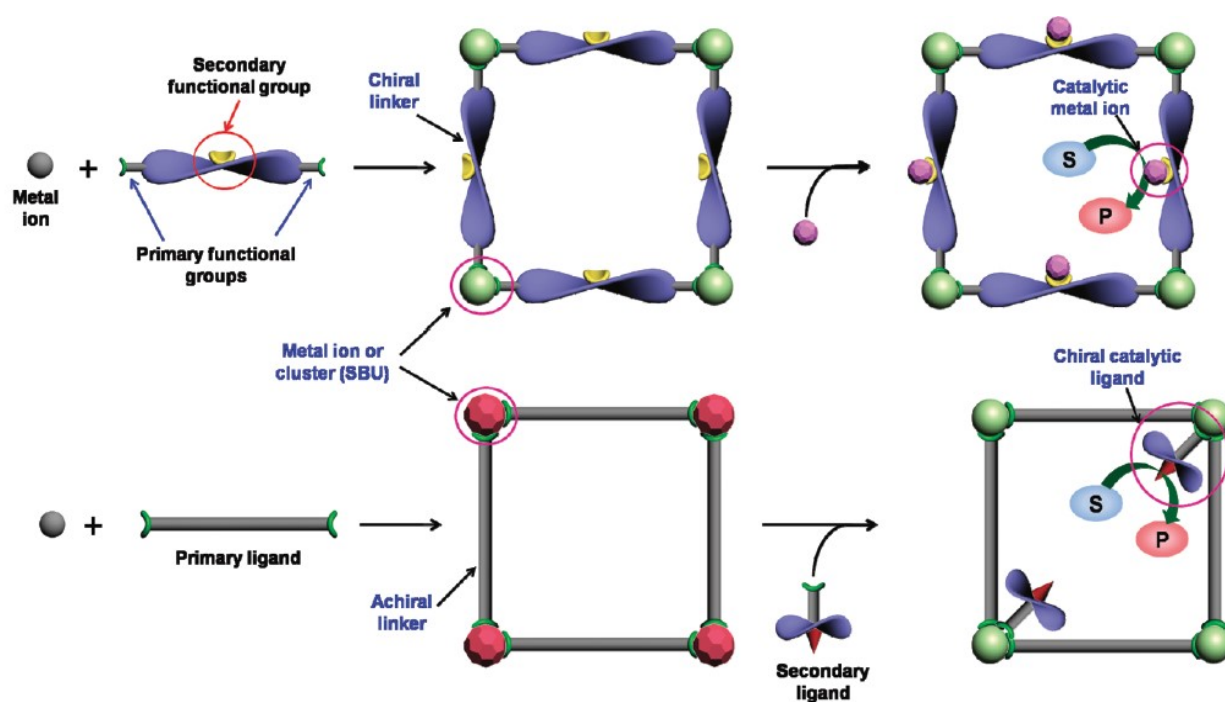


Figure 1.10. Representative strategies to construct MOF-based asymmetric catalysts. Reprinted with permission from ref.51 (Copy right 2011 American Chemical Society).

1.3.1 Enantiopure active sites locating on organic linkers of Zr-MOFs

In order to realize chiral Zr-MOFs, a popular strategy is using readily available chiral ligands as the struts of framework. This method has been inspired by efficiency of chiral auxiliaries, employed as homogeneous asymmetric catalysts. By introducing functional groups to coordinate to zirconium clusters, the homochirality of these precursor linkers can be transferred effectively to resulting solid nets.^{51, 56}

One typical example is utilization of BINOL, and BINAP derivatives to construct zirconium hybrid materials. Lin and co-workers firstly synthesized novel chiral Zr-phosphonated coordination polymers from BINAP structures.⁵¹ Although the zirconium phosphonate compounds are amorphous materials due to non-crystalline nature of coordination polymers, the immobilized Ru active sites in porous system exhibited excellent enantioselectivities for hydrogenation of β -keto esters with above 90% ee for alkyl substitutions and about 80% for aryl derivatives.^{51, 56, 57} Another series of zirconium coordination polymers based on BINOL-derived bisphosphonic linkers was also introduced by Lin and co-workers in 2004. By integrating with $\text{Ti}(\text{OiPr})_4$, these amorphous materials could promote for the transformation of aldehydes to form

chiral secondary alcohols with good conversions and moderate ee values.⁵⁸ Together with the progresses of reticular chemistry and modulated synthesis, truly crystalline Zr-MOF (BINAP-MOF), constructed from 4,4'-bis(4carboxyphenylethynyl) BINAP, in UiO topology was successfully reported on 2015 (**Figure 1.11**).⁵⁵ This material not only possesses a robust framework, but also has been employed to provide chiral environment for coordinated Rh active centers. The resulting catalysts efficiently catalyzed for the asymmetric reductive cyclization and Alder-ene cycloisomerization with excellent performances (about 99% for yields as well as enantioselectivities). However, they were inactive in promoting the asymmetric Pauson–Khand reaction of carbon monoxide and cinnamaldehyde because the steric effect of BINAP structure caused to the insufficient space for bulky reagents.⁵⁵ To increase chemical accessibility of the net, it is essential to replace partly BINAP linkers by other unfunctionalized structs of identical lengths. As a result, another novel Zr-MOF, BINAP-dMOF isorecticular to BINAP-MOF (**Figure 1.11**), was introduced and offered a better reaction space for transformation of cinnamaldehyde. In particular, the activity of Rh-functionalized BINAP-dMOF catalyst was 10 times higher than the homogenous control. These chiral Zr-MOFs could be reused for at least three times without significant loss in yield and enantioselectivity.⁵⁵

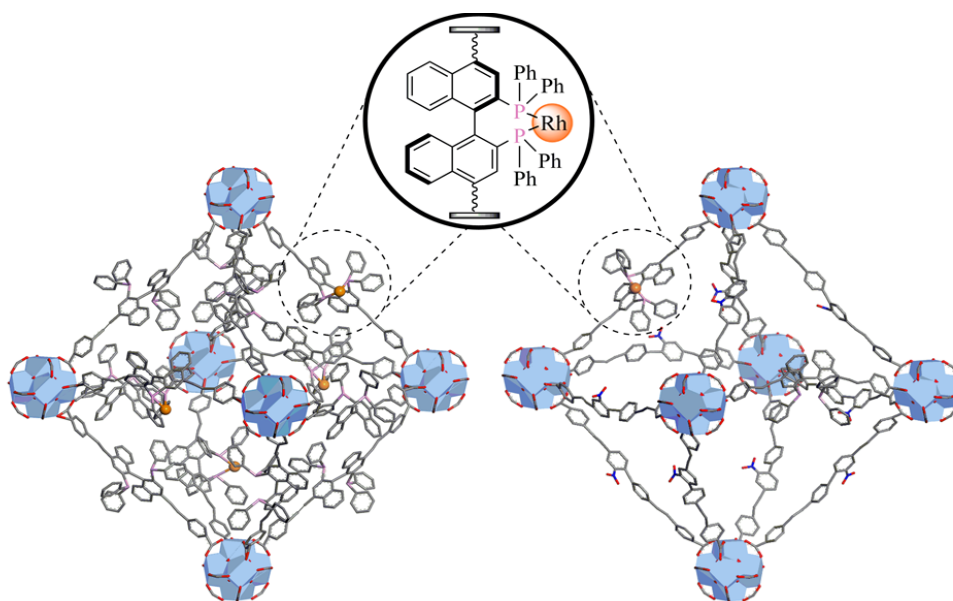


Figure 1.11. Structures of BINAP-MOF·Rh (left) and BINAP-dMOF·Rh (right). Reprinted with permission from ref. 55 (Copy right 2019 American Chemical Society).

Further along the path of designing chiral Zr-MOFs with more open porosity, functionalization of long linear achiral linkers by small chiral molecules has recently emerged as an effective

methodology. In fact, the wealth of chiral compounds, which are accessible from chiral diene derivatives or readily available, inexpensive as amino acids, provides a vast number of possibilities to vary homochiral centers on predetermined Zr-MOFs structures for meeting specific requests in asymmetric organic reactions. Elongated versions of BDC-NH₂ linker are preferably employed as carriers for assembling chiral molecules due to functional ability of amino groups.⁵⁴ In a recent publication of Lin and co-workers in 2015, a derivative of BDC-NH₂, namely 4,4'-((2-amino-[1,1'-biphenyl]-4,4'-diyl) bis(ethyne-2,1-diyl)) dibenzoate linker, was functionalized by chiral diene groups, and this resulting ligand could be then used to synthesize a new chiral Zr-MOF in UiO topology, E₂-MOF (**Figure 1.12**). Its pore accessibility could achieve up to 112 wt.% in uptake of Brilliant Blue R-250. The E₂-MOF after Rh metalation afforded highly efficient solid catalysts for two asymmetric carbon-carbon coupling reactions, including 1,4-additions of arylboronic acids to α , β -unsaturated ketones with a TON of 13 400 (above 90%ee) and 1,2-additions of arylboronic acids to aldimines with almost perfect yield as well as enantioselectivity.⁵⁴

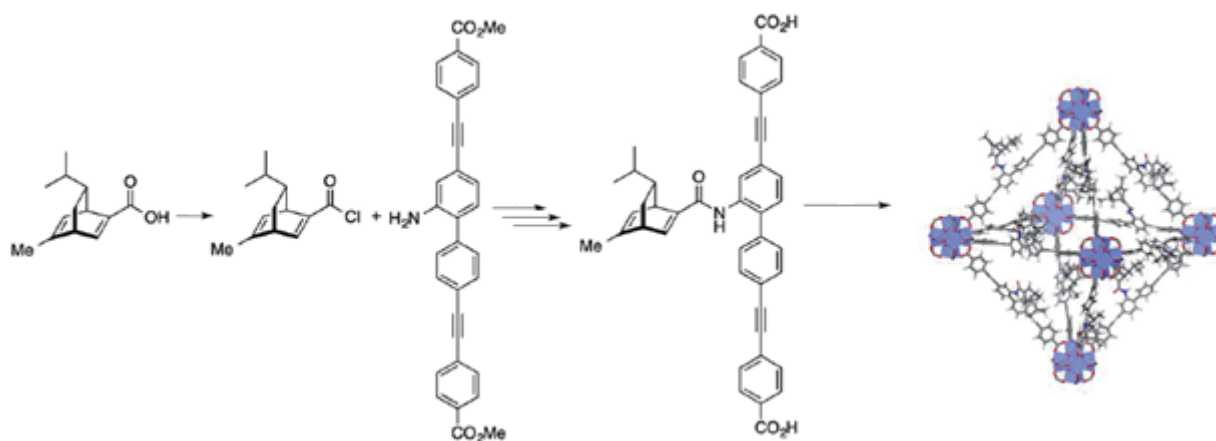


Figure 1.12. Representative scheme of the construction of E₂-MOF. Reprinted with permission from ref.⁵⁴ (Copy right 2015 - Published by The Royal Society of Chemistry).

Otherwise, amino acids are also an important chiral source, which could be applied as efficient organocatalysts in a wide range of enamine-catalyzed reactions. Coupling of well-studied amino acid organocatalysts such as proline enables the generation of enantiopure active sites on achiral linear ligands as BDC-NH₂ derivatives.^{37, 51} However, the protection of catalytic amino groups is essential to prevent coordination to metal ions during the MOFs formation, and the protection groups could be then released to regenerate active centers *via* simple post-synthesis.⁵⁹ Following

this strategy, functionalization of BPDC-NH₂, and TPDC-NH₂ by N-Boc *L*-proline, in which *L*-proline is protected by *tert*-butyloxycarbonyl group, was investigated for synthesis of UiO-67, and UiO-68 analogues, respectively. Interestingly, the *in situ* deprotection of the Boc groups occurred during the Zr-MOFs formation due to the intrinsic acidic nature of Zr⁴⁺ and Zr-clusters. Consequently, two isorecticular chiral Zr-MOFs, UiO-67-NHPro and UiO-68-NHPro, with different window pore size was successfully achieved without involving any post-synthetic procedure (**Figure 1.13**).⁶⁰ Although, no-enantioselectivity was observed as applying these materials as heterogenous catalysts in Aldol addition of 4-nitrobenzaldehyde and cyclohexanone, the predominant formation of *syn*-isomers, which are opposite compared to the reaction catalyzed by homogenous *L*-proline catalyst, gave rise to an interesting phenomenon for future studies relating the role of *L*-proline and zirconium frameworks with the reaction mechanism. The competition of these catalytic activity sites will be deeply investigated in **Chapter 4** to provide a better understanding regarding their effect on reaction pathway.

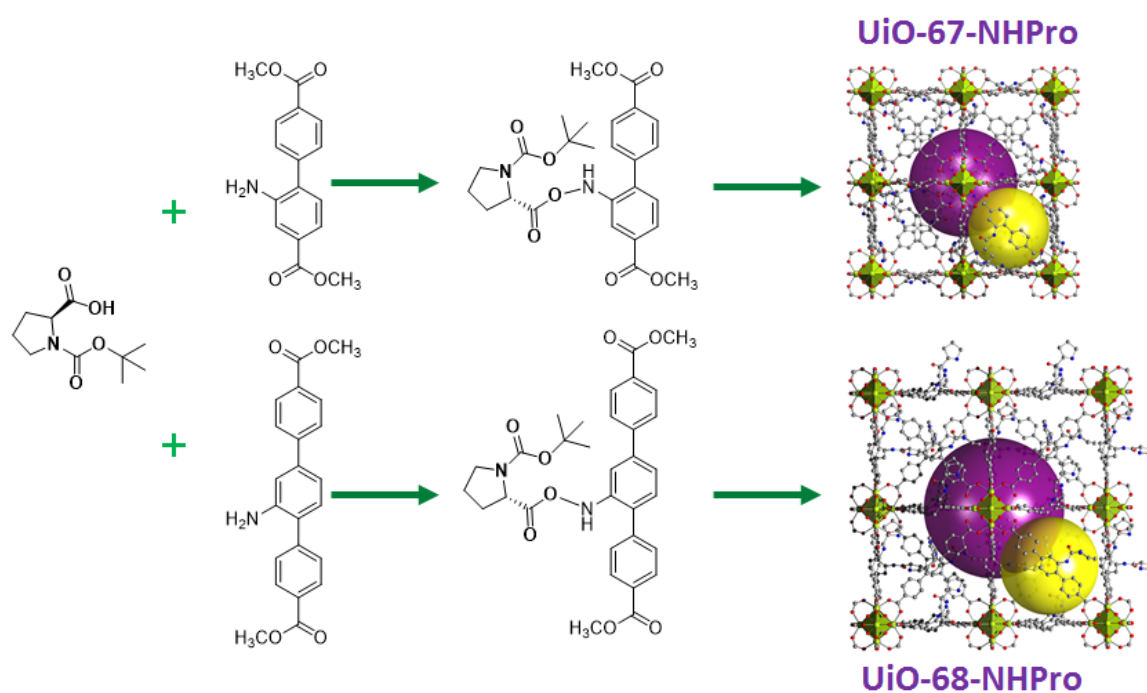


Figure 1.13. Representative strategy to construct two asymmetric Zr-MOFs, UiO-67-NHPro and UiO-68-NHPro. Adapted with permission from ref. 60 (Copy right 2016 American Chemical Society).

Aside from popularity of above described ligand systems, organic linkers based on chiral salen cores, which enable the chelating of various metal ions for challenging asymmetric organic

transformations, are also critically important to build stable chiral Zr-MOFs.^{51,61} In fact, the MOF chemistry based on chiral salen cores was firstly introduced in a report of Hupp and Nguyen et al. in 2006, which mentioned the formation of Zn-MOF containing chiral Mn-salen ligands as struts.^{51,62} This material was then applied as an efficient catalyst for asymmetric epoxidation of olefins with 70% of yield and 82% ee for enantioselectivity.⁶² In the following years, various kinds of chiral metallosalen complexes integrated into organic building blocks was employed to design a great number of MOF structures based on different metal nodes.^{51,63-65} However, assembling the Zr_6 -node and chiral salen ligands not only faces the challenger of rapid nucleation, but also the sensitivity of C-N double bonds in the acidic environment of Zr-synthesis.^{61,66} Therefore, the appearance of chiral zirconium-metallosalen frameworks was only recorded one decade later in 2018 by employing modulated synthesis.

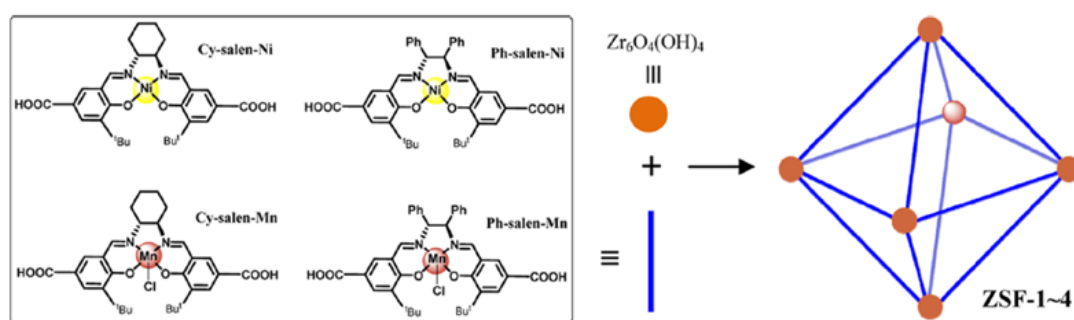


Figure 1.14. Representative synthesis of ZSFs from metallosalen ligands. Reprinted with permission from ref. 66 (Copy right 2018 American Chemical Society).

These novel chiral Zr-MOFs isorecticular to UiO family materials, ZSF-1–4 (**Figure 1.14**), show outstanding chemical stability in aqueous solutions with a wide range of pH. Their high activity was observed in the cycloaddition of CO_2 and epoxides with excellent catalytic efficiency as well as C–H azidation reaction with excellent yield and enantioselectivity.⁶⁶ Moreover, acid labile chiral metallosalen ligands could be introduced into predetermined structures as UiO-68 by a simple ligand exchange procedure (**Figure 1.15**).⁶¹ The chiral UiO-type MOFs contained single- or mixed-metallosalen linkers, afforded high activity in a wide range of asymmetric organic reactions, including cyanosilylation of aldehydes, ring-opening of epoxides, oxidation of secondary alcohols, and aminolysis of stilbene oxide. Importantly, the heterogeneity as well as recyclability of all chiral UiO-68 analogues could be maintained at least for ten cycles without significant loss in activity.⁶¹ These works demonstrate that utilization of chiral metallosalen

linkers is an attractive method to approach stable chiral Zr-MOFs as efficient solid catalysts in asymmetric organic transformations.

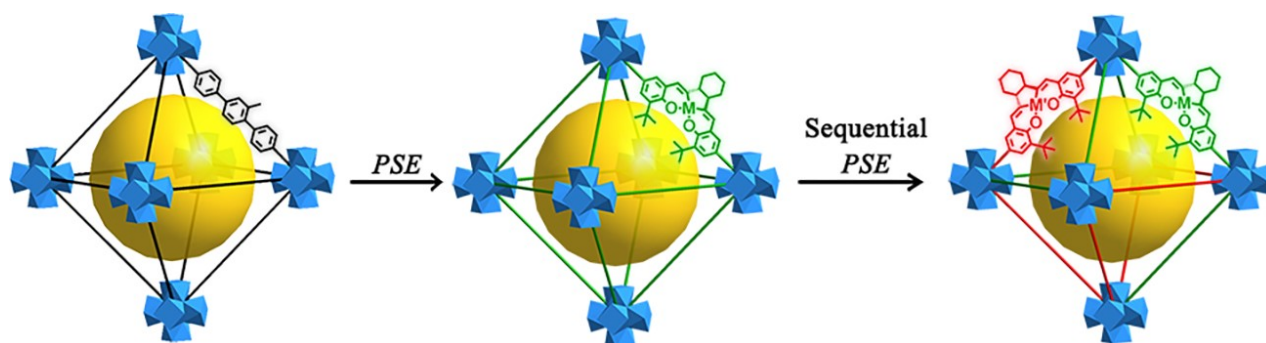


Figure 1.15. Schematic representation of post-synthetic linker exchange method to approach chiral UiO-68. Reprinted with permission from ref. 61 (Copy right 2018 American Chemical Society).

1.3.2 Enantiopure active sites coordinated to inorganic clusters of Zr-MOFs

The enantiopure active sites have been not only located on primary organic linkers, but also introduced on metal nodes. Open metal coordination sites in inorganic clusters can be considered as effective catalytic centers due to their acidic nature.^{51, 67} By providing additional chiral environment, these symmetric metal centers possibly transform into chiral active sites. The chiral environment around open metal nodes could be formed based on chiral auxiliaries of primary organic ligands as neighbouring groups located around the metal cluster. Although, this is an interesting methodology to design chiral catalytic corners in MOF structures, relatively low enantioselectivities were observed in seminal researches of Lin group and Kaskel group.^{68, 69} These results rationalized that the distance and chiral configuration of active metal sites and chiral induction were not compatible to catalyze the asymmetric reaction mentioned in the previous reports. To approach high enantioselectivity, proper chiral environments should be therefore designed to meet specific demands of each transformation, however this is still a huge challenge due to difficulties in chiral linkers synthesis as well as mechanistic insight of the organic reactions.⁵¹

Another alternative method to overcome the problems is utilization of well-studied organocatalysts, originating from nature's "chiral pool", to incorporate to open metal clusters of MOFs. A simple way was introduced by Kim and co-workers in 2009 by introducing chiral active sites on free metal coordination sites in MIL-101, constructed from Cr-clusters and linear BDC linkers.⁶⁷ These open metal sites were formed by removing water molecules, which temporarily

coordinate to chromium trimers. To generate chiral active centers, *L*-proline and its derivatives were after that employed to replace these empty water coordination sites. The resulting materials expectedly showed good performance in asymmetric Aldol reaction with 90% of conversion and good *ee* value of 80%.⁶⁷ Obviously, the introduction of popular privileged organocatalysts into stable achiral MOFs *via* coordinating to their open metal coordination sites is a simple, and effective way to design various catalytically active chiral MOFs.

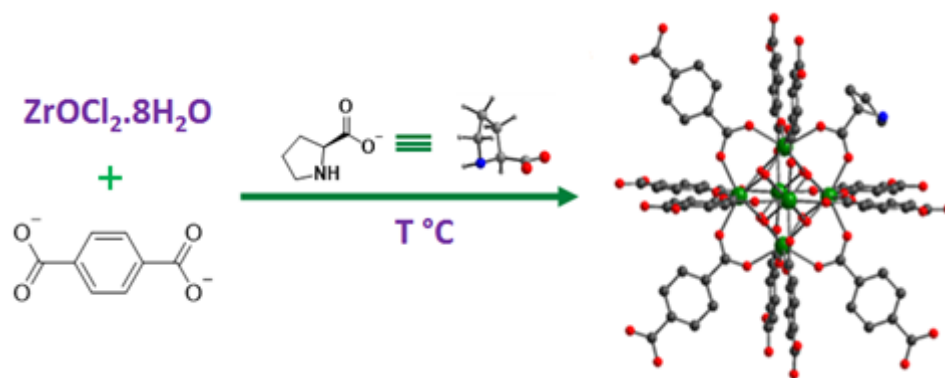


Figure 1.16. Formation of asymmetric UiO-66 in the presence of *L*-proline molecules as modulators. Adapted with permission from ref.66 (Copy right 2018 Elsevier Inc.).

Van Der Voort and co-workers also applied this strategy to synthesize chiral UiO-66 analogues, including UiO-66, DUT-52 and UiO-67 (**Figure 1.16**).⁶⁶ The *L*-proline functionalized modulated Zr-MOFs promoted efficiently the aldol reaction of 4-nitrobenzaldehyde and cyclohexanone with excellent yield and a predominant formation of *syn*-adducts. Once again, the combination of Zr-clusters and *L*-proline sites in catalytic systems resulted in no-enantioselectivity, but shows unexpected diastereoselectivity, which was not observed so far by using homogeneous *L*-proline catalysts.⁶⁶ Apparently, the presence of Zr-clusters affects to the role of proline chirality, which often causes to high enantioselectivity of *anti*-products rather than an inversion in diastereoselectivity. This phenomenon has emerged as an intriguing topic relating effects of Zr-MOFs in asymmetric transformations. It is, however, difficult to control the ratio of Zr-clusters and the presence of *L*-proline due to accidental formation of defect centers in 12-coordinated Zr-MOFs. Thanks to the discovery of Zr-MOF with reduced connectivity, great opportunities could be offered to improve systematically the amount of *L*-proline in Zr-nets for a deep understanding regarding the catalytic role of Zr-clusters and *L*-proline, which will be mentioned in the **Chapter 3** and **Chapter 4**.

1.4 Motivation

Comprehensive understanding of chirality has played a crucial role for ensuring safety and efficacy of drug products. In many cases, two optical configurations of a chiral molecule exhibit substantially different physiological behaviour, and thus the preparation of single enantiomers has become as an essential topic in the pharmaceutical industry.^{51, 52} Enantiomerically pure compounds could generally be achieved by separation from racemic mixtures or direct synthesis of enantiopure molecules. Either way, chiral materials which are employed as stationary phase in chiral columns or chiral catalysis, are a basic condition to decide to enantiomeric excess of resulting mixtures. Despite obtaining high enantiomeric purity, the chiral separation of racemic mixtures is considered as an expensive and inefficient approach due to undesired enantiomers, while asymmetric synthesis, which enables dominant formation of the single enantiomers, is an atom-economical method. However, the development of efficient solid chiral catalysts has been still required further investigations to provide more potential options for asymmetric organic reactions, especially carbon-carbon bond formations, which are key steps in organic synthesis.⁵¹⁻

53

In recent years, metal-organic frameworks have emerged as one of the most intriguing solid porous materials. Together with the highly active catalytic centers, wide structural and functional variations, MOFs have been successfully employed as solid catalysts for a variety of organic transformations.^{70, 71} However, very few achievements relating to MOFs as asymmetric catalysts have been reported to date because of their low thermal and chemical stabilities. Such solid stable frameworks, the Zr-MOFs offers great opportunities for designing novel effective asymmetric catalysts.^{51, 54, 55, 66, 67} This is an interesting, but also challenging topic with many open issues:

- How can we introduce effectively enantiopure active sites into Zr-MOFs?
- Are there any positive or negative impacts of Zr-nets on the performance of chiral catalytic sites?
- If any, is it possible to control these effects during the reaction phase?
- How is the recyclability of these chiral Zr-MOFs?

Finding answers for these questions are the core of this thesis. In **Chapter 3**, a simple method to incorporate a popular chiral organocatalyst, *L*-proline, on Zr-cluster of DUT-67, an 8-connected Zr-MOF will be introduced. A systematic study relating effect of *L*-proline presence into DUT-67 has been also investigated to optimize performance of its catalytic activity in asymmetric

Michael addition reaction. Moreover, the heterogeneity and recyclability of the chiral Zr-MOF are also evaluated to demonstrate its stability.

A further understanding regarding the role of catalytic active sites, including Zr-clusters and *L*-proline, in asymmetric aldol addition of cyclohexanone and 4-nitro-benzaldehyde is investigated in **Chapter 4** to clarify the predominant formation of *syn*-products as well as the absence of enantioselectivity in previous catalytic systems. An approach using benzoic acid as additional modulator to block free acidic active sites in zirconium structure is introduced to drive the reaction to be carried out on enantiopure *L*-proline sites. Moreover, the presence and location of *L*-proline into DUT-67 was confirmed by solid-state MAS and DNP NMR data.

Lastly, *in situ* imine linker formation as an efficient method to synthesize a novel 1D chiral Zr-MOF will be described in **Chapter 5**. The resulting chiral material is characterized by a wide range of physical techniques. Moreover, a variety of C-C bond formation reactions has been employed to evaluate the catalytic activity of new chiral Zr-MOFs.

The research on synthesis of chiral Zr-MOFs and their catalytic behavior in this work are expected to provide a better understanding or at least give to other scientists new ideas for further deeper studies regarding this topic in the future.

Chapter 2

Methods of characterization
and
Experimental section

2.1 Methods of characterization

2.1.1 Solid-state nuclear magnetic resonance

Nuclear magnetic resonance (also referred to as NMR) spectroscopy is one of the preeminent techniques for determination of structures as well as purity of organic compounds for approximately seven decades.^{72, 73} This technique generally bases on the magnetic resonance phenomenon as atomic nuclei of some element isotopes, which have a spinning character, are located into an external magnetic field. Because of their charge, these spinning nuclei produce magnetic field oriented along their rotation axis and could be thus considered as tiny magnets. Not all nuclei behave as though this way, but important isotopes of organic interest, including ^1H , ^{13}C , ^{15}N , ^{19}F , and ^{31}P , fortunately show this behaviour.⁷³ Affected by the local magnetic field (B_0), random distribution of these small magnetic moments could be reorganized to achieve a higher-energy state. This process requests a specific radio frequency wave. When the spinning nuclei return to their base level, the absorbed energy will be released as electromagnetic radiation at the same frequency. This signal depends on both strength of the external magnetic field and the nature of the nuclei and is recorded and analysed in order to yield an NMR spectrum.⁷³

$$\Delta E = \gamma h B_0 / 2\pi$$

where h is Planck's constant ($6.63 \cdot 10^{-34}$ J·s), and γ is constant of the gyromagnetic ratio, characteristic for the nucleus.⁷³

Table 2.1. Properties of Nuclei Most Useful for Biological Studies⁷³

Nucleus	Spin Quantum Number (I)	Natural Abundance (%)	Gyromagnetic Ratio γ ($\text{rad} \cdot \text{T}^{-1} \cdot \text{s}^{-1}$)	Sensitivity (% vs. ^1H)
^1H	$\frac{1}{2}$	99.9844	$267.520 \cdot 10^6$	100
^2H	1	0.0156	$41.067 \cdot 10^6$	0.965
^{13}C	$\frac{1}{2}$	1.108	$67.265 \cdot 10^6$	1.59
^{15}N	$\frac{1}{2}$	0.365	$-27.108 \cdot 10^6$	0.104
^{19}F	$\frac{1}{2}$	100	$251.67 \cdot 10^6$	83.3
^{31}P	$\frac{1}{2}$	100	$108.29 \cdot 10^6$	6.63

Since the NMR spectra enable to access details regarding the electronic structure of small organic molecules and their individual functional groups, it is also a precious tool to determine the composition of MOF crystals, for the characterisation of purity, linker ratios, and efficiency of activation procedure based on leftover solvent content.^{47, 74-76} However, for compounds such as solid porous materials, metal-organic frameworks need to be digested to release the organic components into solution before NMR spectra can be recorded.⁴⁷ This means that information involving host-guest interactions with adsorbed species as well as relative positions of functional groups inside MOF nets could not be obtained when analysing with traditional NMR technique (solution nuclear magnetic resonance). Solid-state NMR spectroscopy has recently emerged as a powerful tool for a deeper understanding about the local chemical environment inside MOFs.^{47, 74-76} However, the signals in solid-state NMR spectra are relatively low in intensity and broad due to strongly line-broadening interactions, including dipole-dipole interactions between nuclei spins, chemical shift anisotropy, electric quadrupole interaction (as $I > 1/2$), and hyperfine interactions with paramagnetic species.⁷⁶ These interactions in mobile fluids could be rapidly averaged by Brownian motion of atomic nuclei and producing high-resolution NMR spectra with a series of very sharp peaks, while they are orientation-dependent in solid-state NMR and yield the low-resolution spectra.^{75, 76} To minimize these anisotropic NMR interactions, one popular line-narrowing technique is employing magic-angle spinning (MAS) method.^{72, 76}

Magic-angle spinning (MAS)

In 1958, E.R. Andrew and I.J. Lowe indicated that the effects of anisotropic dipolar interactions could be reduced by rotating the solid samples around an axis at an appropriate angle β with respect to the applied magnetic field B_0 .^{72, 77, 78} In the best case, these broadening interactions could be nearly removed at $\beta = \arccos((1/3)^{1/2}) = 54.7^\circ$, which is then referred as magic angle. Only one minor problem is the appearance of spinning sidebands (satellite lines) at low spinning rates, but this could be suppressed if the rotors containing the samples could spin at high enough speeds.⁷⁶ Nowadays, the rotating rate of typical MAS units can reach up to 35 kHz (100kHz for maximum rate), which make the spinning sidebands moving out from the center and become weak to achieve high-resolution solid-state NMR spectra.⁷⁶ In some case of nuclear spins with $I > 1/2$, a double spinner, one rotor spinning inside another (double rotation, DOR) or spinning about two axes sequentially (dynamic angle spinning, DAS) could be installed with a second magic angle 30° or 70° to further minimize effect of quadrupolar broadening.^{72, 79}

Moreover, the inherently poor sensitivity also derives from the low equilibrium nuclear spin polarization, which is determined by the Boltzmann equation:

$$\frac{N_{upper}}{N_{lower}} = e^{-\Delta E/kT} = e^{-\gamma h B_0 / 2\pi kT}$$

In the above formula, N_{upper} and N_{lower} are the number of nuclei in upper and lower energy states, respectively for a sample located into the external magnetic field B_0 . k is the Boltzmann constant, and T is the absolute temperature (K).⁷³ Obviously, utilization of higher magnetic fields or lower applied temperatures could lead to increase the population ratio of nuclei on two energy levels, which consequently improve the sensitivity of solid-state NMR technique.^{74, 76} However, these methods are difficult to investigate due to the lack of suitable technology to provide superhigh magnetic fields (max ca. 25 Tesla) or maintain low temperatures for in-vivo spectroscopy.⁷⁴ Therefore, several strategies, which are referred as hyperpolarization experiments, have been developed to affect non-equilibrium nuclear spin polarizations, such as cross polarization (CP) and dynamic nuclear polarization (DNP). By combining MAS and hyperpolarization methods, the high-resolution acquisition of solid-state NMR spectra could be achieved.⁷⁶

Cross polarization (CP)

Cross polarization (CP) is a technique using a double resonance experiment, which allows transferring spin polarization from abundant nuclei with high gyromagnetic ratio γ , such as ^1H , ^{19}F and ^{31}P , to neighbouring nuclei, such as ^{13}C , ^{15}N , ^{29}Si , for improving quality of signals and reducing waiting time between successive scans.⁷⁶ The resulting signals improvement of CP process could be determined by the gyromagnetic ratio of the two coupling nuclei. In fact, cross-polarization under MAS conditions (CP MAS) offers moderate increase in signal-to-noise ratio of solid-state NMR spectra with 4 times ($\epsilon = \gamma^1\text{H}/\gamma^{13}\text{C} \approx 4$) for ^1H to ^{13}C and 10 time ($\epsilon = \gamma^1\text{H}/\gamma^{15}\text{N} \approx 10$) for ^1H to ^{15}N .^{74, 76}

Dynamic nuclear polarization (DNP)

Another strategy to further enhance nuclei population ratio is employing dynamic nuclear polarization method, which enables the spin polarization transfer from unpaired electrons to nuclei *via* microwave irradiation at electron-spin resonance frequency.^{74, 76} The basic idea generally derives from the highly polarized electron spins, which is much higher than that of nuclear spins. The DNP effect was firstly introduced by Overhauser and experimentally demonstrated by

Slichter in the 1950s. Based on this technique, the quality of the solid-state NMR spectra could be significantly enhanced with signal improvements of $\varepsilon = \gamma_{\text{electron}}/\gamma_{\text{H}} \approx 660$ or $\gamma_{\text{electron}}/\gamma_{\text{N}} \approx 6500$.⁷⁴ However, the spin polarization transfer between the electron and the nuclei critically depend on the efficiency of three-spin polarization exchange relating the difference between the coupling strengths of two unpaired electrons. In fact, the bulky nitroxide biradicals (**Figure 2.1.**), such as TAPAPOL, AMUPol, TEKPol or even TEMPO (for water-sensitive samples), have been often employed to provide stable radicals and strong coupling of the electrons in low temperature conditions.^{74, 76}

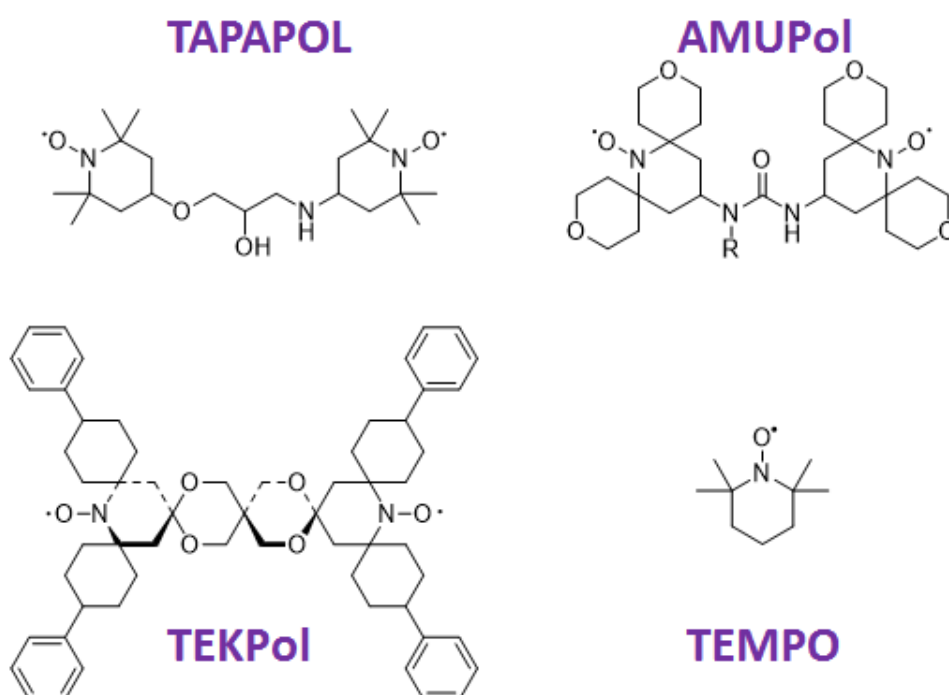


Figure 2.1. Examples of nitroxide radicals used in DNP NMR measurements.

In practice, the transferring process could be carried out following two ways. One is direct DNP, which uses a single polarization step: electron \rightarrow low- γ nucleus. Although a simpler experimental methodology could be offered, especially quadrupolar nuclei, this method often results in lower sensitivity improvements. Another popular strategy is adding one cross polarization transfer as an intermediate step: electron \rightarrow ^1H \rightarrow low- γ nucleus, known as indirect DNP.⁷⁴ This combination provides a good platform to improve significantly the quality of solid-state NMR spectra so that the tiny changes on solid surfaces or into structures could be observed, such as detection of ^{13}C -enriched sucrose or Si active centers adsorbed on low-surface-area by DNP-enhanced $^{13}\text{C}\{^1\text{H}\}$ and $^{29}\text{Si}\{^1\text{H}\}$ CP MAS NMR, respectively.^{74, 80, 81} Besides, this technique has been recently

applied to characterize a number of modified MOFs to clarify the coordination environment of immobilized metal or functional groups. For example, the formation of cis and trans-coordinated Pt complexes into the UiO-66-NH₂ and MOF-253 could be followed by the DNP-enhanced ¹⁹⁵Pt{¹H} BCP NMR spectra or H-bonding interactions of amino acids and frameworks, analysing the distributions of functional groups in MOF nets, was recorded by DNP-enhanced ¹⁵N{¹H} CP MAS NMR.^{82, 83} Obviously, DNP-enhanced CP MAS NMR spectra provide great opportunities to take deeper understandings relating atomic scale characterization, which have not been observed in previous studies. In this context, the relative position of chiral functional groups will be also determined by employing DNP-enhanced CP MAS NMR.

2.1.2 Chiral high-performance liquid chromatography

Inspired from the breakthrough experiment of Pasteur in 1848 regarding the separation of racemic sodium ammonium tartrate, various chiral resolution methods have been so far introduced to obtain high purity of single enantiomers, such as diastereomeric recrystallization, kinetic resolution by chiral reagents or catalysts, and direct chromatographic resolution using chiral stationary phases (CSPs) or chiral mobile phases.⁸⁴ Among these methods, the utilization of CSPs based on high performance liquid chromatography (HPLC) has been considered as a benign and practical way to serve for both quality and quantity purposes. Although the determination of enantiomeric purity (enantiomeric excess) could be investigated by NMR spectroscopy or GC with CSPs, it is simpler and faster as chiral HPLC method to be used.⁸⁴⁻⁸⁶

In general, chiral chromatography is a mass transfer process based on different affinity behaviors of enantiomers on chiral stationary phases, which importantly impact to the efficiency of chiral resolution. All forces, originated from hydrogen bonding, steric effects, inclusion complexation, π - π , dipole-dipole, and ionic interactions, could contribute to resolve racemic mixtures. They also play a decisional role in selection of solvents as mobile phases in HPLC. In fact, there are generally four popular ways to offer an appropriate solvent system,⁸⁷ including:

Table 2.2. Four popular methods used to resolve racemic mixtures.

Method	Dominant interactions	Mobile phase
Normal phase chromatography (NPC)	π - π interaction, hydrogen bonding	Mixture of hydrocarbon solvents (hexane, heptane) and alcoholic solvents (isopropanol, ethanol)
Reversed phase chromatography (RPC)	Inclusion complex, hydrogen bonding	Mixture of organic solvents (Acetonitrile, methanol, THF) and aqueous buffers (triethylamine, NH ₄ OAc)
Polar organic chromatography	Dipole-dipole, hydrogen bonding	Mixture of acetonitrile, methanol, acetic acid, or triethylamine
Polar ionic chromatography	Ionic interaction, hydrogen bonding	Mixture of methanol, acetic acid, and triethylamine

Besides, another key factor of separation based on chiral HPLC is the nature of CSPs. More than one hundred commercial CSPs have been so far designed by immobilizing appropriate chiral molecules on inert carriers as organic polymers or silica gel for resolution of every specific racemic solution.⁸⁴ However, approximately 90% experiments regarding identification of enantiomeric purity has been carried out by polysaccharide-based CSPs. The popularity of these CSPs derives not only from their stability, abundant and non-toxicity, but also resolution ability of a wide range of racemates. Among the polysaccharide-based CSPs, the *tris*-(3,5-dimethylphenylcarbamate) derivative is one of the best chiral recognition. In fact, chiral HPLC columns containing *tris*-(3,5-dimethylphenylcarbamate), which have commercial names as Chiralcel OD, Chiralpak AD, Chiralpak IA, and Amylose-1, enable resolute effectively for a variety of racemic compounds, including aromatic alcohols, amides, pyriproxyfen, amino alcohols, and carboxylic acids.^{84, 85, 87}

The efficiency of CSPs could be evaluated by three parameters, including retention factor (k), separation factor (α) and resolution factor (R_s). These values are determined following below equations:⁸⁴

$$k_1 = (t_1 - t_0) / t_0, k_2 = (t_2 - t_0) / t_0,$$

$$\alpha = (t_2 - t_0) / (t_1 - t_0) = k_2 / k_1$$

$$R_s = 2(t_2 - t_1) / (w_1 + w_2)$$

In these formulas, the retention times of two enantiomers are referred as t_1 and t_2 , respectively. t_0 is the retention time of a non-retained compound, while the peak widths of enantiomers are symbolized by w_1 and w_2 . The k and α value exhibit the interaction degree of enantiomers and the resolution ability of a specific CSP, while resolution factor is affected by both the recognition ability of a CSP and the theoretical plate number of a column. Together nature of CSPs and polarity of mobile phases, external factors, which impact interaction time of enantiomers and CSPs as flow rate and temperature, also obviously contribute to the separation level of enantiomers.⁸⁴ Therefore, a successful chiral resolution based on HPLC method is a result of the right selection, in which the enantiomers are separated by an appropriate mobile solvent on a suitable chiral stationary phase under a specific optimized condition.⁸⁴⁻⁸⁷

2.2 Equipment and parameter

2.2.1 Powder X-ray diffraction

Powder X-ray diffraction (PXRD) patterns were collected using a *STOE STADI P* diffractometer with Cu-K α 1 radiation ($\lambda = 1.5405 \text{ \AA}$) at room temperature in the range of $2\theta = 2\text{--}30^\circ$, step size 0.15° per 90 seconds. For in situ thermo-XRD measurements, the solid samples were prepared in capillaries and analyzed in the range of $2\theta = 2\text{--}45^\circ$ with step size 0.1° per 60 seconds.

2.2.2 Physisorption measurements

Nitrogen physisorption measurements were conducted on a *BELSORP-max* (*MicrotacBEL*, Japan) apparatus at 77 K up to 1 bar using high purity nitrogen gas (99.999 %). CO₂ adsorption isotherms (CO₂ purity: 99.95 %) were performed at 298 K up to 1 bar on *BELSORP-max* device.

2.2.3 Scanning electron microscope and Energy-dispersive X-ray spectroscopy

Scanning electron microscopy (SEM) and Energy-dispersive X-ray spectroscopy (EDX) images were recorded on a *ZEISS DSM-982 Gemini*. The MOF samples were prepared on carbon pellets and then covered by thin gold layers.

2.2.4 Inductively coupled plasma atomic emission spectroscopy

The zirconium content of the solid samples was determined by inductively coupled plasma atomic emission spectroscopy (ICP-OES) using an *Optima 7000 DV* instrument.

2.2.5 Thermal gravimetric analysis

Thermal gravimetric analysis (TGA) and differential thermal analysis measurements were carried out on a STA 409 PC Luxx (Netzsch) thermal device with heating rate 5 K/min in the range of 25 to 1000 °C in air.

2.2.6 Fourier-transform infrared

The Fourier-transform infrared (FT-IR) spectra were obtained on a Vertex 70 instrument, with samples being dispersed on potassium bromide pellets. The measurements were carried out 2 scans with a resolution of 2 cm⁻¹.

2.2.7 Nuclear magnetic resonance

Solution state ¹H and ¹³C-NMR (nuclear magnetic resonance) spectra were recorded on a *Bruker DRX 500 P*. Chemical shifts (ppm) were referenced to tetramethyl silane (0.00 ppm). The samples were digested using a small amount of CsF (ca. 15 mg) with 5 drops of deuterated hydrochloric acid (DCl, 37 %) in deuterated DMSO (1.0 mL) during 6 h.

All room temperature solid-state NMR experiments were carried out on a Bruker AVANCE III HD spectrometer operating at 14 T (¹H frequency of 600.12 MHz), equipped with a Bruker 3.2 mm H/X double resonance probe. ¹³C{¹H} CP MAS NMR spectra were recorded with ¹H excitation pulses of 2.5 μs, a contact time of 2 ms, a repetition delay of 4 s, a MAS spinning rate of 14 kHz and up to 2000 scans. The CP transfer was achieved by fulfilling the Hartmann-Hahn matching condition under MAS, with linearly ramped ¹H amplitude centered at 55 kHz.⁸⁸ Dipolar interactions with protons were decoupled employing SPINAL-64⁸⁹ with an rf field strength of

100 kHz. ^1H MAS NMR spectra were measured using single-pulse excitation, with a 2.5 μs pulse length (90° flip-angle), a MAS spinning rate of 22 kHz, a repetition delay of 4s and up to 32 scans.

All solid-state NMR experiments were carried out at room temperature on a Bruker AVANCE III HD spectrometer operating at 14 T (^1H frequency of 600.12 MHz), equipped with a Bruker 3.2 mm probe. ^{13}C CP MAS NMR spectra were recorded with ^1H excitation pulses of 2.5 μs , a contact time of 2 μs , a repetition delay of 4 s, a MAS spinning rate of 14 kHz and up to 2000 scans. ^1H MAS NMR spectra were measured using single-pulse excitation of 2.5 MHz, a MAS spinning rate of 22 kHz and up to 32 scans.

Samples were prepared for DNP NMR measurements by mixing ca. 10 mg of the sample with ca. 15 μL of the polarizing agent solution, which consisted of a 15 mM solution of TOTAPOL (1-(TEMPO-4-oxy)-3-(TEMPO-4-amino) propan-2-ol)⁵² in $\text{D}_2\text{O}/\text{H}_2\text{O}$ (90:10, v:v). A $\text{D}_2\text{O}/\text{H}_2\text{O}$ (90:10, v:v) solution was used instead of Glycerol- $\text{d}_8/\text{D}_2\text{O}/\text{H}_2\text{O}$ in order to avoid solvent signals in the DNP enhanced ^{13}C CP MAS spectra. This choice of the solvent mixture limits the obtainable signal enhancement since it is not an ideal glass forming matrix.

All solid-state DNP experiments were carried out on a Bruker Avance III 400 MHz NMR spectrometer equipped with an Ascend 400 DNP magnet and a 3.2 mm triple resonance $^1\text{H}/\text{X}/\text{Y}$ low-temperature MAS probe. The microwave (mw) irradiation was provided by a 9.7 T Bruker gyrotron system operating at 263 GHz. The ^1H MAS, $^{13}\text{C}\{^1\text{H}\}$ and $^{15}\text{N}\{^1\text{H}\}$ CP MAS (Cross Polarization Magic Angle Spinning) spectra with and without mw irradiation were acquired with a MAS frequency of 8 kHz. The CP transfer was achieved by fulfilling the Hartmann–Hahn matching condition under MAS, with linearly ramped ^1H amplitude centered at 65 kHz.⁸⁸ The sample temperature was nominally 112 K (without mw) and 124 K (with mw), and was stabilized by a Bruker BioSpin low temperature MAS cooling system. $^{13}\text{C}\{^1\text{H}\}$ and $^{15}\text{N}\{^1\text{H}\}$ CP MAS NMR spectra were recorded with ^1H excitation pulses of 2.5 μs , a contact time of 2 ms, a repetition delay of 4.5 s and 300 to 10000 scans. Dipolar interactions with protons were decoupled employing SPINAL-64 with 100 kHz rf field strength.⁸⁹

DNP enhanced $^{13}\text{C}\{^1\text{H}\}$ and $^{15}\text{N}\{^1\text{H}\}$ heteronuclear correlation (HETCOR) experiments were performed using the pulse sequence proposed by van Rossum et al.,⁹⁰ which employs FSLG (frequency-switched Lee-Goldburg) homonuclear decoupling during the evolution of the chemical shift. A decoupling field of 90 kHz was utilized. Short contact times of 200 μs were used to select the correlations between nearest ^{13}C and ^1H neighbours.

2.2.8 Gas chromatography

Gas chromatography (GC) analyses were performed using a Shimadzu GC 17 A equipped with a flame ionization detector (FID) and a BPX5 column (30 m length, 0.25 mm in inner diameter, and 0.25 mm film thickness). The *n*-hexadecane was used as an internal standard to calculate reaction yields, mass spectra were collected using a Shimadzu GCMS-QP5000 and were compared with database of NIST library.

2.2.9 High-performance liquid chromatography

Enantiomeric excess of various asymmetric carbon-carbon coupling reactions was determined by chiral high-performance liquid chromatography (HPLC), Elite LaChrom System from VWR/HITACHI using a UV L2400 detector and a Lux Amylose-1 chiral column.

2.3 Used chemicals

All reagents and starting materials were purchased from commercial companies and were used as received without any further purification.

Table 2.3. List of solvents.

Chemical	CAS number	Purity	Supplier
1,4-dioxane	123-91-1	99.8%	Sigma-Aldrich
1-methyl-2-pyrrolidinone	872-50-4	99%	Acros Organics
Acetone	67-64-1	99.8%	Sigma-Aldrich
Chloroform-d1	865-49-6	99.8%	Sigma-Aldrich
Dichloromethane	75-09-2	99.8%	Sigma-Aldrich
Dimethylsulfoxide-d6	2206-27-1	99.9%	Sigma-Aldrich
Ethanol	64-17-5	99.8%	VWR
Ethyl acetate	141-78-6	99.8%	Sigma-Aldrich
Isopropanol	67-63-0	99.7%	VWR
Methanol	67-56-1	99.7%	VWR
<i>N,N'</i> -Dimethylformamide	68-12-2	99.8%	Fischer Scientific
<i>n</i> -hexane	110-54-3	99.7%	VWR

Tetrahydrofuran	109-99-9	99%	Th. Geyer
Toluene	108-88-3	99.5%	TH. Geyer

Table 2.4. List of chemicals used for materials synthesis.

Chemical	CAS number	Purity	Supplier
4-bromobenzoic acid	586-76-5	98%	Sigma-Aldrich
4-hydroxybenzoic acid	99-96-7	99%	Sigma-Aldrich
4-mercaptobenzoic acid	1074-36-8	97%	Sigma-Aldrich
4-nitrobenzaldehyde	555-16-8	97%	Sigma-Aldrich
4-tert-butylbenzoic acid	98-73-7	99%	Sigma-Aldrich
Acetic acid	64-19-7	100%	Carl Roth
Benzoic acid	65-85-0	99%	Grüssing
Cyclohexanone	108-94-1	99%	Sigma-Aldrich
Diethylmalonate	105-53-3	99%	Sigma-Aldrich
Formic acid	64-18-6	98%	Carl Roth
Hydrochloric acid	7647-01-0	37%	Honeywell Fluka
<i>n</i> -dodecane	112-40-3	99%	Sigma-Aldrich
<i>n</i> -hexadecane	544-76-3	99%	Sigma-Aldrich
Sodium sulfate	7757-82-6	99%	Sigma-Aldrich
<i>trans</i> - β -nitrostyrene	5153-67-3	99%	Sigma-Aldrich
Trifluoroacetic acid	76-05-1	99%	Alfa Aesar

Table 2.5. List of chemicals used for catalytic study.

Chemical	CAS number	Purity	Supplier
(<i>1R,2R</i>)-1,2-diphenylethylenediamine	35132-20-8	98%	Alfa Aesar
(<i>1S,2S</i>)-1,2-diphenylethylenediamine	29841-69-8	97%	Alfa Aesar
(<i>1R,2R</i>)-1, 2-diaminocyclohexane	20439-47-8	98%	Alfa Aesar
1,3,5- benzenetricarboxylic acid	554-95-0	98%	Alfa Aesar

1,4-Benzenedicarboxylic acid	100-21-0	98%	Sigma-Aldrich
2,5-thiophenedicarboxylic acid	4282-31-9	99%	Sigma-Aldrich
2-methyl-2-butene	513-35-9	95%	Alfa Aesar
4-formyl benzaldehyde	619-66-9	97%	Sigma-Aldrich
4-hydroxybenzoic acid	99-96-7	99%	Sigma-Aldrich
Aqueous sodium chlorite solution (25%)	7758-19-2	p.a.	Sigma-Aldrich
Biphenyl-4,4'-dicarboxylic acid	787-70-2	97%	Sigma-Aldrich
<i>N</i> -(<i>tert</i> -Butoxycarbonyl)- <i>L</i> -proline	115186-37-3	98%	Sigma-Aldrich
<i>L</i> -proline	147-85-3	99%	Sigma-Aldrich
Nickel(II) acetate tetrahydrate	6018-89-9	98%	Sigma-Aldrich
Sodium borohydride	16940-66-2	98%	Sigma-Aldrich
Zirconium(IV) chloride	10026-11-6	99.9%	Sigma-Aldrich
Zirconyl chloride octahydrate	13520-92-8	98%	Sigma-Aldrich

2.4 Materials synthesis

2.4.1 Synthesis of DUT-67 and DUT-67-Pro

The applied DUT-67 and DUT-67-Pro materials in this work are synthesized following two approaches. One is using traditional procedure in the presence of *N,N*-dimethylformamide (DMF) and *N*-methyl-2-pyrrolidone (NMP) as solvents, producing standard **DUT-67-fa (DMF)** and **DUT-67-Pro (DMF)**, which were investigated in Chapter 3. Besides, another greener method, which employed a mixture of ethanol, water and acetic acid as solvents, also allows for a gram-scale synthesis of **DUT-67 (EtOH)** and **DUT-67-Pro (EtOH)** in a high yield. Although these materials are prepared in two different ways, no significant differences in final properties are observed. A detail comparison has been presented in Chapter 4.

DUT-67-fa (DMF): ZrCl₄ (1.38 g, 6.00 mmol) was dissolved in 75.0 mL of DMF/NMP mixture (1:1, v:v) (DMF = *N,N*-dimethylformamide, NMP = *N*-methyl-2-pyrrolidone) in the presence of formic acid (26.8 ml, 120 equiv., 720 mmol). Consequently, a 75 mL solution of DMF and NMP (1:1, v:v) containing 2,5-thiophenedicarboxylic acid (H₂TDC) (0.800 g, 5.71 mmol) was added slowly to the prepared ZrCl₄ solution. The resulting mixture was then sonicated for 5 minutes

before placing it into an oven for 48 h at 120 °C. The solid product was collected, washed three times with DMF and ethanol and was dried under vacuum at 120 °C for 48 h to give activated DUT-67-fa ($\text{Zr}_6\text{O}_6(\text{OH})_2(\text{TDC})_4(\text{HCOO})_2(\text{DMF})(\text{H}_2\text{O})_5$) as a white solid.

Yield: 1.35 g (85% based on zirconium).

$^1\text{H-NMR}$ spectrum after digestion (500 MHz, $\text{DMSO-d}_6/\text{DCI}$): $\delta(\text{ppm})$: 8.10 (s, 1H, formic acid), 7.89 (s, 1H, DMF), 7.66 (s, 2H, TDC), 2.83, 2.66 (s, 6H, DMF)

DUT-67-Pro (DMF): In a representative procedure, DUT-67 (0.15 g) was immersed in 5 mL DMF solution, containing 0.14 g *L*-proline (1.25 mmol, 12 equiv.) and 0.01 mL HCl (1.00 mmol, 1.00 equiv.) at room temperature for 5 days. The white product ($\text{Zr}_6\text{O}_6(\text{TDC})_4(\text{OH})_{4-x}(\text{Pro})_x$) was collected by decantation and washed three times with DMF and ethanol.

Elemental analysis for $\text{Zr}_6\text{O}_6(\text{TDC})_4(\text{OH})_{0.08}(\text{Pro})_{3.92}$: calcd: C 29.5% H 2.22% S 7.23% N 3.11%; found: C 29.4% H 2.05% S 7.09% N 3.01%

$^1\text{H-NMR}$ spectrum after digestion (500 MHz, $\text{DMSO-d}_6/\text{DCI}$): $\delta(\text{ppm})$: 7.67 (s, 2H, TDC), 4.19 (t, 1H, *L*-proline), 3.15 (m, 2H, *L*-proline), 2.22, 1.86 (m, 4H, *L*-proline)

DUT-67 (EtOH): $\text{ZrOCl}_2 \cdot 8\text{H}_2\text{O}$ (1.23 g, 3.82 mmol) was dissolved in 20 mL of water/ CH_3COOH (1:1, v/v). Consequently, a solution of 2,5-thiophenedicarboxylic acid (H_2TDC) (0.800 g, 5.71 mmol) in 20 mL of ethanol was added. The mixture was stirred for 5 minutes, and then was transferred into an oven and heated to 80 °C and annealed for 48h. The resulting powder was filtered, washed three times with ethanol, and dried under vacuum at 120 °C for 24h to get activated DUT-67-EtOH ($\text{Zr}_6\text{O}_6(\text{TDC})_4(\text{CH}_3\text{COO})_4$) as a white solid.

Yield: 79% based on 2,5-thiophenedicarboxylic acid.

Elemental analysis: $\text{Zr}_6\text{O}_6(\text{TDC})_4(\text{CH}_3\text{COO})_4$: calcd.: C 24.1% S 8.06% N 0.00%; found: C 23.6% S 7.74% N 0.00%.

$^1\text{HNMR}$ spectrum after digestion: (500 MHz, $\text{DMSO-d}_6/\text{DCI}$): $\delta(\text{ppm})$: 7.68 (s, 2H, TDC, 1.87 (s, 3H, CH_3COOH).

DUT-67-Pro (EtOH): 0.15 g of activated DUT-67-EtOH was immersed in 5 mL ethanol solution, containing 0.20 g *L*-proline (1.7 mmol) and 0.01 mL HCl (1.0 mmol) at room temperature for 5

days. The resulting product was collected, washed three times with ethanol, and activated under vacuum 120 °C for 24 h.

Elemental analysis: $Zr_6O_6(TDC)_4(Pro)_4 \cdot 5.8EtOH$: calcd: C 32.6% S 6.26% N 2.74%; found: C 30.1% S 6.14% N 2.21%.

1H NMR spectrum after digestion: (500 MHz, DMSO- d_6 /DCI): δ (ppm): 7.65 (s, 2H, TDC), 4.19 (t, 1H, *L*-proline), 3.13 (m, 2H, *L*-proline), 2.19, 1.84 (m, 4H, *L*-proline).

2.4.2 Synthesis of DUT-136 and its derivatives

DUT-136: In a representative procedure, a mixture $ZrCl_4$ (0.92 g, 3.95 mmol) and 4-formylbenzoic acid (0.54 g, 3.60 mmol, 0.91 equiv.) was dissolved in 100 mL of DMF and 15 mL of CH_3COOH (262.5 mmol, 66.5 equiv.). A solution of (1*R*,2*R*)-1,2-diphenylethylenediamine (0.38 g, 1.80 mmol, 0.45 equiv.) in 50 mL of DMF was added dropwise to the $ZrCl_4$ solution. The resulting solution was then sonicated for 10 minutes before distributing into 30 different 10 mL vials. These vials were then heated at 80 °C for 168 hours. The solid product was consequently collected by decanting the mother liquor and washed with DMF (3 × 100 mL). The DMF solvent was exchanged with acetone (5 × 100 mL) at room temperature. The resulting product was then activated at 100 °C for 12 h under vacuum, yielding white solid powders of **DUT-136**.

Yield: 0.91 g (71% based on (1*R*,2*R*)-1,2-Diphenylethylenediamine).

Elemental analysis for $Zr_6O_6(imine-L)_3 \cdot 6(CH_3COO) \cdot 6.8DMF$: calcd: C 50.4% H 4.72% N 6.15%; found: C 49.1% H 4.83% N 6.21%

1H NMR spectrum after digestion: (500 MHz, DMSO- d_6 /DCI): δ (ppm): 10.0 (s, 2H, proton in aldehyde groups of 4-formylbenzoic acid), 7.99 (m, 8H, benzyl groups of 4-formylbenzoic acid), 7.57 (m, 2H, benzyl groups of 1,2-diphenylethylenediamine), 5.21 (s, 2H, CH groups of 1,2-diphenylethylenediamine)

Amine-DUT-136: 0.04 g of DUT-x (0.013 mmol) was slowly stirred into 1.5 mL of methanol for 5 minutes at room temperature before $NaBH_4$ (3 × 0.0025 g, 0.2 mmol, 15.3 equiv.) to be added. After 24 hours, the liquid was removed, while 10 mL of water was used to wash the remaining solid sample. Lastly, the **amine-DUT-136** powder was activated at 100 °C for 12 h under vacuum after washing further with 5 mL of acetone in 5 times.

Elemental analysis for $Zr_6O_6(\text{amine-L})_3(\text{OH})_{5.86} \cdot 0.14(\text{CH}_3\text{COO})$: calcd: C 48.6% H 4.05% N 3.8%; found: C 47.2% H 3.98% N 3.75%

$^1\text{H-NMR}$ spectrum after digestion: (500 MHz, DMSO- d_6 /DCI): δ (ppm): 8.22 (m, 4H, benzyl group of 4-formylbenzoic acid), 7.76 (m, 4H, benzyl groups of 4-formylbenzoic acid), 7.98 (m, 5H, benzyl group of 1,2-diphenylethylenediamine), 7.56 (m, 5H, benzyl groups of 1,2-diphenylethylenediamine), 5.45 (s, 2H, CH groups of 1,2-diphenylethylenediamine)

Amide-DUT-136: 0.04 g of DUT-136 (0.013 mmol) was dispersed into a mixture of 1,4-dioxane (1 mL) and 2-methyl-2-butene (0.62 mL, 5.9 mmol, 450 equiv.). After that, 100 μL of aqueous sodium chlorite solution (3.3 M, 0.33 mmol, 25 equiv) and 35 μL of acetic acid (0.6 mmol, 47 equiv.) were added slowly into the above mixture without stirring. The reaction was carried out in dark for 24h. The resulting powder was then washed with water (2*5 mL) acetone (5*10 mL) before activating at 100 °C for 12 h under vacuum, producing white solid of **amide-DUT-136**.

Elemental analysis for $Zr_6O_6(\text{amide-L})_3(\text{OH})_{5.86} \cdot 0.14(\text{CH}_3\text{COO})$: calcd: C 47.8% H 3.45% N 3.7%; found: C 47.2% H 4.01% N 3.63%

$^1\text{H-NMR}$ spectrum after digestion: (500 MHz, DMSO- d_6 /DCI): δ (ppm): 8.12 (m, 8H, benzyl groups of 4-formylbenzoic acid), 7.95(m, 10H, benzyl groups of 1,2-diphenylethylenediamine), 5.40 (s, 2H, CH groups of 1,2-diphenylethylenediamine)

Ni-DUT-136: 0.05 g of DUT-136 and its derivatives were dispersed into 5 mL of ethanol containing 0.21 g of $\text{Ni}(\text{OAc})_2 \cdot 4\text{H}_2\text{O}$. The immobilized reactions were investigated in 24 hours at room temperature. The resulting solid samples were collected by centrifuging and washing with ethanol (5*10 mL) before activating at 100 °C for 12 h under vacuum. The nickel contents were further confirmed by ICP-OES analysis.

2.4.3 Synthesis of DUT-51

The DUT-51 was prepared according to a procedure reported in the literature.² The mixture of ZrCl_4 (0.22 g, 1.0 mmol) and dithieno[3,2- b;2',3'-d]thiophene-2,6-dicarboxylic acid (H_2dttdc) (0.19 g, 0.67 mmol) was dissolved into 50 mL DMF containing benzoic acid (8g, 65 mmol). The resulting solution was heated in an oven at 120 °C for 3 days. The white powder was collected and washed three times with DMF, HCl and ethanol. After that, the sample was dried under vacuum at 120 °C for 48 h to get activated DUT-51-H.

2.4.4 Synthesis of UiO-66

1,4-Benzenedicarboxylic acid (H₂BDC) (0.27 g, 1.6 mmol) and ZrCl₄ (0.46 g, 2.0 mmol) were added to a mixture of formic acid (9 mL, 225 mmol) and DMF (80 mL). The clear solution was then heated at 80 °C for 48 h. The white powder was collected and washed three times with DMF, HCl and ethanol. After that, the sample was dried in vacuum at 120 °C for 48 h to get activated UiO-66-H.

2.4.5 Synthesis of UiO-67

Synthesis of UiO-67-Form: ZrCl₄ (0.134 g; 0.6 mmol) was dissolved in 15 mL DMF containing HCOOH (2.7 mL, 68 mmol). The resulting solution was then added to the 15 mL DMF solution of biphenyl-4,4'-dicarboxylic acid (0.18 g, 0.7 mmol). The reaction mixture was heated at 80 °C for 3 days. The white product was filtered, washed three times with DMF and ethanol before drying in vacuum at 120 °C for 48 h to get activated UiO-67-form.

Synthesis of UiO-67-H: The as-made UiO-67-form was washed three times with DMF, HCl and ethanol; and was activated in vacuum at 120 °C for 48 h to get activated UiO-67-H.

Synthesis of UiO-67-Benz: A solution of ZrCl₄ (30 mg, 0.13 mmol) and benzoic acid (471 mg, 3.86 mmol, 30 equiv.) in 5 ml DMF (p.a.) was sonicated for 30 min. A suspension formed by addition of biphenyl-4,4'-dicarboxylic acid (31 mg, 0.13 mmol) was thermally treated at 120 °C for 48 hours. The resulting crystalline precipitate was washed with DMF several times. After that the solvent was exchange with acetone. The solid was finally dried in high vacuum and stored under inert gas atmosphere.

2.4.6 Synthesis of MOF-808

In a typical preparation³ a mixture of ZrOCl₂·8H₂O (3.2 g, 3.0 mmol) and 1,3,5-benzenetricarboxylic acid (H₃BTC) was dissolved in a mixture of DMF (150 mL) and formic acid (150 mL). The resulting solution was then heated at 100 °C for 5 days. After that, the product was filtered, washed three times with DMF, HCl and acetone and dried in vacuum at 120 °C for 48 h to get activated MOF-808-H.

2.5 Catalytic studies

2.5.1 Asymmetric Friedel Craft alkylation

In a typical experiment, a mixture of a *trans*- β -nitrostyrene (0.0375 g, 0.25 mmol), indole (0.0585 g, 0.5 mmol) and *n*-hexadecane (0.05 mL) as an internal standard were added into a 10 mL Schlenk tube containing toluene (4 mL) and the pre-determining amount of catalyst. The reaction was performed at 50 °C for 7 days. The conversion was analysed by withdrawing samples from the reaction mixture at different time periods. The organic constituents were then diluted into ethyl acetate (1mL) before dried over anhydrous Na₂SO₄, analyzed by GC and HPLC.

The conversion of reaction was determined by GC with a specific temperature programme. Initially, the samples were heated from 40 to 48 °C with a heating rate of 4 °C/min; then from 48 °C to 100 °C with 15 °C/min and held at 100 °C for 4 mins; after that continuously heated from 100 to 270 °C with 30 °C/min and held at 270 °C for 10 mins. Inlet and detector temperatures were set constant at 270 °C. The *n*-hexadecane was used as an internal standard to calculate reaction conversion. The retention time of the product was recorded at 20.27 min.

Enantiomeric excess of samples was analyzed by HPLC Elite LaChrom System with a UV L2400 detector and a Lux Amylose-1 chiral column. The mobile phase was a mixture of hexane: isopropanol (85:15 v:v) with flow rate of 0.5 mL/min. The product was detected by UV detector operated at $\lambda = 250$ nm. The retention time of two enantiomers was 25.161 and 27.510 min, respectively.

2.5.2 Asymmetric Michael addition reaction

In a standard preparation, *trans*- β -nitrostyrene (0.0375 g, 0.25 mmol), *n*-hexadecane as internal standard (0.05 mL, 0.17 mmol), and catalysts (15 mol%) were placed to a 10-mL Schlenk tube containing 3 mL of a solvent mixture of isopropanol and ethanol (1:1 v:v). And then, 20 equivalents of cyclohexanone (0.50 mL, 5 mmol) were added to the reaction Schlenk tube. The resulting mixture was consequently stirred for 3 minutes before heating up to 50 °C. Reaction progress was monitored by GC as followed: Aliquots (0.20 mL) were withdrawn from the reaction mixture after defined time intervals, diluted with isopropanol (1.00 mL), and dried over Na₂SO₄. The reaction samples were analysed by GC and HPLC.

For the recyclability test, the catalyst was collected by centrifugation, washed intensively with DMF and ethanol to remove any undesired compounds, and activated in vacuum at 120 °C for 24 h, and then reused for a new catalytic run. To ensure the heterogeneity of the catalyst, the MOF catalyst was removed after 72 h of the reaction. The remaining reaction solution was then stirred for further 5 h. Reaction progress, if any, was monitored by GC as previously described.

For determination of reaction yield, the samples were introduced into GC device at 40 °C and heated up to 48 °C in 2 minutes. The temperature was continuously increased to 100 °C with 15 °C/min and maintained at this point for 4 min before elevating up to 270 °C at a rate of 30 °C/min and held at 270 °C for 4 min. The yields were calculated by comparing the area of product peak ($t_{\text{major}} = 16.242$ min and $t_{\text{minor}} = 16.334$ min) with the area of *n*-hexadecane peak ($t = 13.935$ min). The product, 2-(2-nitro-1-phenylethyl) cyclohexanone, was isolated by column chromatography (silica gel, ethyl acetate/hexane = 1:4) as a white solid.

Enantiomeric excesses of 2-(2-nitro-1-phenylethyl)cyclohexanone in product mixtures were determined by HPLC (ELITE LACHROM System from VWR/HITACHI using a UV L2400 detector) using a Lux Amylose I chiral column (0.5 μm, 98/2 (v/v) hexane/isopropanol, 1 mL/min, $\lambda = 225$ nm, retention time $t_{(S)-2((R)-2\text{-nitro-1-phenylethyl})\text{cyclohexan-1-one}} = 48.437$ min (major), $t_{(R)-2((S)-2\text{-nitro-1-phenylethyl})\text{cyclohexan-1-one}} = 31.120$ min, $t_{(S)-2((S)-2\text{-nitro-1-phenylethyl})\text{cyclohexan-1-one}} = 40.887$ min, and $t_{(R)-2((R)-2\text{-nitro-1-phenylethyl})\text{cyclohexan-1-one}} = 33.123$ min.

2.5.3 Asymmetric Aldol addition reaction

In a typical experiment, a mixture of 4-nitrobenzaldehyde (0.0375 g, 0.25 mmol) and *n*-dodecane (0.05 mL, 0.22 mmol) was placed in a 10-mL Schlenk tube containing 1.00 mL of dimethyl sulfoxide (DMSO) and predetermined amount of catalysts. After that, 20 equivalents of cyclohexanone (0.50 mL, 5 mmol) and 0.2 equivalent of benzoic acid as an additive were added. The resulting mixture was magnetically stirred at 25 °C for 7 days. And then, the pure product, 2-(hydroxy(4-nitrophenyl)methyl)cyclohexan-1-one as an orange solid was isolated with 95% isolated yield by column chromatography (silica gel, ethyl acetate/isohexane = 1:3). This product was used as standard compound to record a calibration curve for the determination of GC yield.

For kinetic studies, reaction progress was monitored by GC/MS as followed: Aliquots (0.02 mL) were withdrawn from the reaction mixture at different time, diluted with ethyl acetate (1.00 mL), and dried over Na₂SO₄. The resulting samples were heated from 40 to 48 °C with a heating rate

of 4 °C/min; then from 48 °C to 100 °C with 15 °C/min and held at 100 °C for 4 min; after that continuously heated from 100 to 270 °C with 30 °C/min and held at 270 °C for 5 min. Inlet and detector temperatures were set constant at 270 °C. The yield was identified by comparing the area of product peak ($t = 17.398$ min) with the area of *n*-dodecane peak ($t = 10.555$ min).

In the recycling test, the catalyst was recycled by centrifugation, washed intensively with ethanol to remove any undesired compounds, and activated in vacuum at 120 °C for 24 h, and then reused for a new catalytic run. To ensure the heterogeneity of the catalyst, the DUT-67-Pro was removed after 72 h of the reaction. The remaining reaction solution was then stirred for further 5 h. Reaction progress was monitored by GC as previously described.

Enantiomeric excess of 2-(hydroxy(4-nitrophenyl)methyl)cyclohexan-1-one in product mixture was determined by HPLC (Elite LaChrom System from VWR/HITACHI using a UV L2400 detector) using a Lux Amylose-1 chiral column (0.5 μm , 75/25 (v/v) hexane/isopropanol, 0.5 mL/min, $\lambda = 225$ nm), retention time $t_{((S)-2-((S)-\text{hydroxy}(4\text{-nitrophenyl)methyl})\text{cyclohexan-1-one})} = 19.0432$ min (major), $t_{((R)-2-((R)-\text{hydroxy}(4\text{-nitrophenyl)methyl})\text{cyclohexan-1-one})} = 17.223$ min, $t_{((S)-2-((R)-\text{hydroxy}(4\text{-nitrophenyl)methyl})\text{cyclohexan-1-one})} = 28.113$ min, and $t_{((R)-2-((S)-\text{hydroxy}(4\text{-nitrophenyl)methyl})\text{cyclohexan-1-one})} = 21.103$ min.

2.5.4 Nickel-catalyzed asymmetric Michael addition reaction

In a representative preparation, a mixture of *trans*- β -nitrostyrene (0.0375 g, 0.25 mmol), *n*-hexadecane as internal standard (0.05 mL, 0.17 mmol), and **Ni-DUT-136** (20 mol% based on Ni content) was placed into a 10-mL Schlenk tube containing 3 mL of toluene. The resulting mixture was stirred for 3 minutes before 0.4 mL of diethylmalonate (2.625 mmol, 10.5 equiv.) was added. Reaction progress was monitored by withdrawing aliquots from the reaction mixture at different time intervals, and the organic components were then diluted into ethyl acetate (1 mL), dried over anhydrous Na_2SO_4 , and then analyzed using GC and HPLC.

A GC temperature programming, in which the samples were heated from 40 to 48 °C with a heating rate of 4 °C/min; then from 48 °C to 100 °C with 15 °C/min and held at 100 °C for 4 mins; after that continuously heated from 100 to 270 °C with 30 °C/min and held at 270 °C for 5 mins, was developed to analyze samples. The appearance of product signal was observed at 15.897 min.

For determination of enantiomeric purity, HPLC Elite LaChrom System with a UV L2400 detector and a Lux Amylose-1 chiral column was employed. A mixture of hexane: isopropanol (80:20 v:v) was employed as mobile phase to analyze samples. With a flow rate of 0.5, the retention time of product, which was detected by UV detector operated at $\lambda = 254$ nm, was 23.747 min for R-enantiomer and 67.677 min for S-enantiomer, respectively.

Chapter 3

Chiral functionalization of a Zr-MOF (DUT-67) as a solid catalyst in asymmetric Michael addition reaction

The results in this chapter are reproduced with permission from ref.91. Copyright 2018 American Chemistry Society. (DOI: 10.1021/acs.inorgchem.7b02854)

3.1 Introduction

The asymmetric Michael addition of ketones to nitroalkenes is one of the most effective methods for carbon-carbon bond formation and has been widely applied in natural products and pharmaceutical compounds synthesis.^{92, 93} In recent years, significant improvement in performance has been made using small chiral amines as organocatalysts, typically *L*-proline and its derivatives.⁹⁴⁻⁹⁶ The search for solid catalysts, which enable facile separation of catalyst from liquid-phase products, is always favorable.⁹⁶⁻¹⁰⁰ Therefore, the development of chiral solid catalysts by anchoring chiral molecules onto insoluble supports such as polymers,¹⁰⁰⁻¹⁰² silica materials,^{100, 103} and inorganic nanoparticles¹⁰⁴⁻¹⁰⁶ has recently attracted significant attention.

As mentioned in chapter 1, the Zr-MOFs with reduced cluster connectivity have also emerged as ideal candidates for this strategy. Chiral catalytic sites, such as natural amino acids, can be easily introduced in these solid frameworks *via* solvent assisted linker incorporation (SALI).⁶⁷ Generally, this post-synthetic approach is based on an acid-base reaction between monocarboxylic acids as modulators and free hydroxyl groups on Zr-clusters, which can be generated by HCl pretreatment. For example, in the eight connected $[\text{Zr}_6(\mu_3\text{-OH})_8(\text{OH})_8]^{8+}$ node of NU-1000, containing eight terminal hydroxyl groups in addition to linker molecules, all –OH groups could be substituted by organic molecules containing carboxylic groups.^{107, 108} Thus, fluoroalkanes, dye molecules, and iridium pincer complexes could be incorporated into NU-1000.¹⁰⁹⁻¹¹¹ A similar strategy was applied to modify the hydrophilic/hydrophobic properties of the inner surface of DUT-67.^{44, 112} However, the decoration of Zr-node by chiral molecules for solid asymmetric catalysis remains an unexplored field and offers a great potential because of the simplicity in comparison to the incorporation of chiral linkers. Besides, employing Zr-MOFs with reduced cluster connectivity also results in an important advantage when the presence of enantiopure sites into Zr-MOFs could be systematically controlled. This thing is very difficult for 12-connected Zr-MOFs, such as UiO-66, due to accidental formation of open Zr-nodes.

Such a typical 8-connected Zr-MOF, DUT-67 in this chapter is demonstrated as great platform for the decoration of DUT-67 with *L*-proline and the activity of this new functional material is analyzed in the asymmetric Michael addition involving *trans*- β -nitrostyrene and cyclohexanone.

3.2 Results and discussion

Materials synthesis and characterization

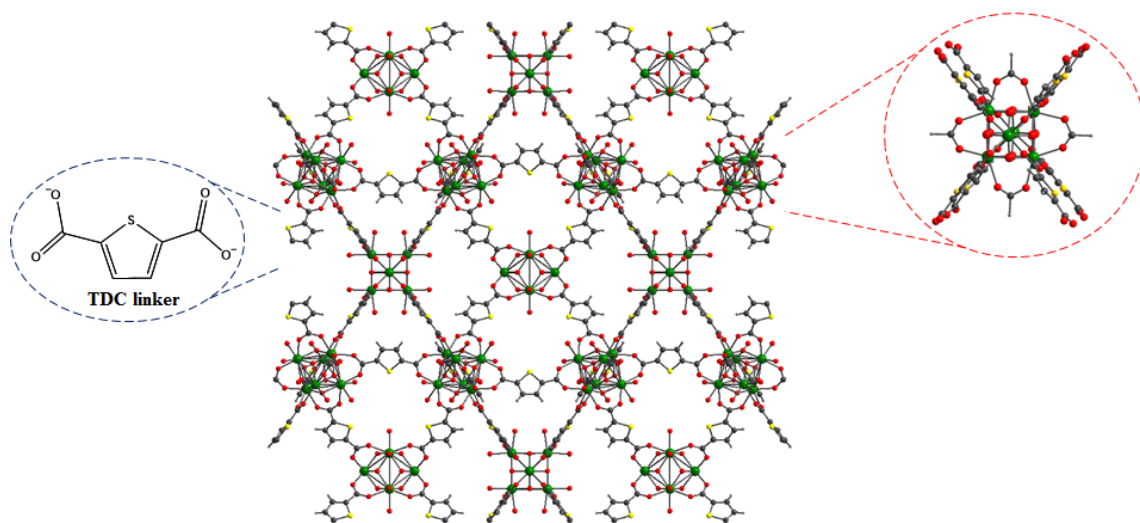


Figure 3.1. Representative structure of DUT-67 constructed from Zr-clusters and thiophene dicarboxylate linkers. Color scheme: Zr (green); O (red); S (yellow); C (grey).

The parent DUT-67-fa synthesized in a mixture of DMF/NMP, containing formate ions as modulators, was synthesized according to a previous report in 85% yield.¹¹² In contrast to UiO-type metal-organic frameworks (12-connected **fcu** net), the octahedral Zr₆-clusters ($[\text{Zr}_6(\mu_3\text{-O})_6(\mu_3\text{-OH})_2]^{10+}$) of DUT-67 crystallizes in **reo** topology (**Figure 3.1**), in which eight of twelve octahedral edges are coordinated to carboxylate linker and the remaining coordination positions are occupied by modulator molecules, formate ions. Usually, these modulators can be easily removed to generate free terminal $\text{-OH}/\text{H}_2\text{O}$ groups through simple acid/base reactions.^{109, 112} This revealed a unique opportunity to functionalize the Zr-clusters when all hydroxyl groups could be substituted by other organic molecules containing carboxylic groups. This approach was applied to improve CO_2 capacity of NU-1000 by decorating the coordinatively unsaturated Zr₆-nodes with perfluoroalkyl carboxylate derivatives.¹⁰⁷

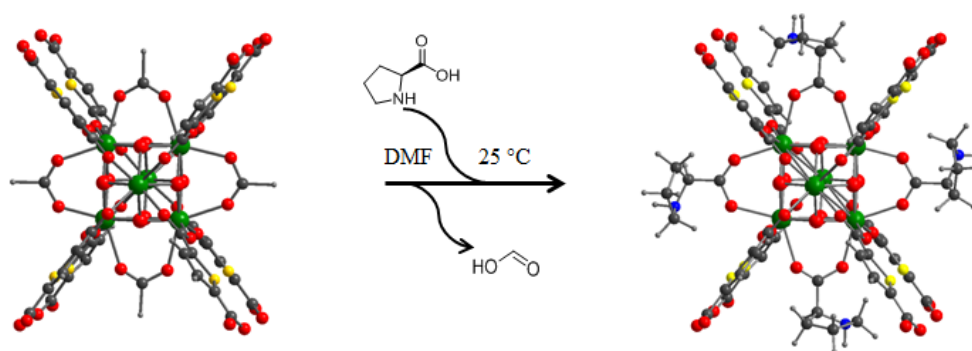


Figure 3.2. Representative scheme of exchange of *L*-proline and formate anions on Zr-cluster. Color scheme: Zr (green); O (red); S (yellow); N (blue); C (grey).

However, the accessibility of Zr-node is also affected by various factors, including solvent polarity, the size of MOF crystals as well as the nature of incoming and outgoing monocarboxylate ligands.^{109, 110, 112} To maximize the efficiency of exchange in most of the reports describing solvent assisted monocarboxylates exchange, the parent Zr-MOFs was usually subjected to a washing step with HCl solution for removing pristine modulators and generating free terminal hydroxyl groups prior to functionalization. It was recently observed that HCl treatment was not actually needed when using fluorinated monocarboxylates, such as trifluoroacetate, or pentafluorobenzoate to replace formate anions as modulators in DUT-67.¹¹²

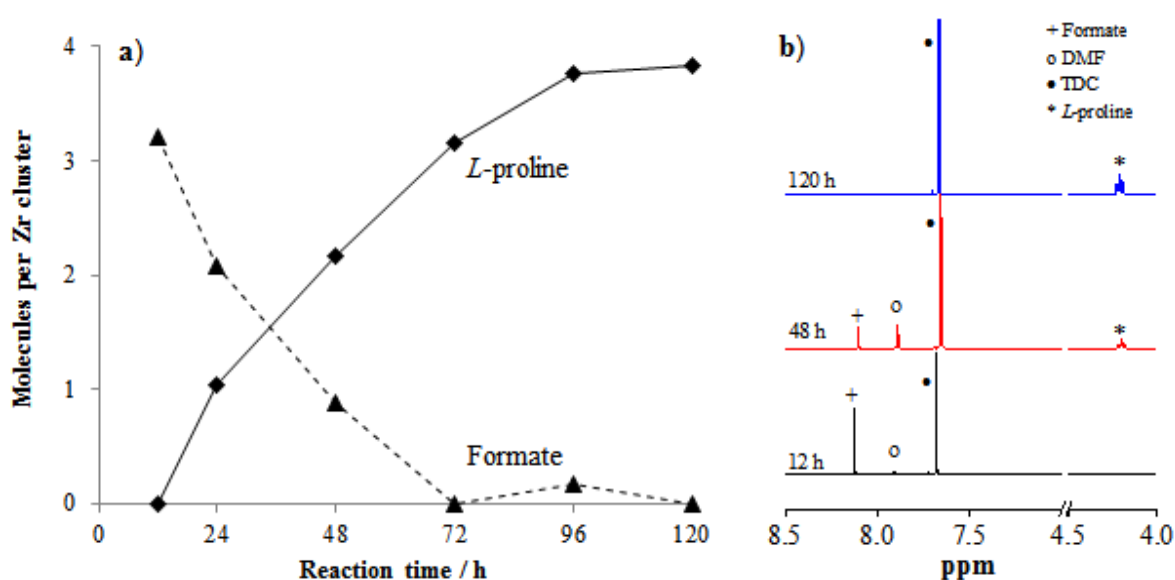


Figure 3.3. a) Exchange rate of formate (triangles) by *L*-proline (diamonds); b) ¹H NMR spectra of digested DUT-67-pro after exposing the samples to *L*-proline solution during different time periods.

Table 3.1. Degree of *L*-proline functionalization.

N	Sample	<i>L</i> -proline		Formate		DMF	
		Molar ratio	Average number of molecules per cluster	Molar ratio	Average number of molecules per cluster	Molar ratio	Average number of molecules per cluster
1	12 h	0	0	0.80	3.20	0.14	0.56
2	24 h	0.26	1.04	0.56	2.24	0.3	1.20
3	48 h	0.54	2.16	0.22	0.88	0.54	2.16
4	72 h	0.78	3.12	0	0	0	0
5	96 h	0.94	3.76	0.06	0.24	0.04	0.16
6	120 h	0.98	3.92	0	0	0	0
7	Used in 2 catalytic cycles	0.98	3.92	0.06	0.24	0.02	0.08
8	HCl treated	0	0	0	0	0	0

The ratios of *L*-proline, formate or DMF to 2,5-thiophene dicarboxylate were determined by $^1\text{H-NMR}$ after digestion of DUT-67 crystals.

In this context, solvent-assisted ligand incorporation method (SALI) was also employed to decorate 8-connected Zr_6 -clusters of DUT-67 with chiral catalytic sites, *L*-proline. This exchange reaction was carried out by suspending DUT-67-fa in *L*-proline solution for up to 5 days giving DUT-67-Pro (**Figure 3.2**). The incoming *L*-proline molecules could also be substituted directly without additional intermediate steps, such as HCl treatment. The functionalization progress was monitored by $^1\text{H-NMR}$ of the digested polycrystalline product (**Figure 3.3b**; **Table 3.1**). The amount of the incorporated *L*-proline per zirconium cluster could be adjusted by controlling the exposure time of DUT-67-fa to *L*-proline solution (**Figure 3.3a**; **Table 3.1**). The exchange rate steadily increased after 12 hours induction period, resulting in an almost complete exchange (4 molecules of *L*-proline per Zr-node) to achieve an idealized 12 connected Zr-cluster (typical, for example, for UiO-66 and UiO-67) after 4 days reaction.

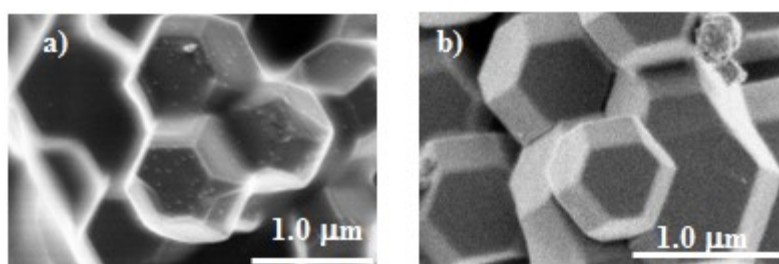


Figure 3.4. SEM images of: a) as made DUT-67-fa synthesized in DMF/NMP; b) as made DUT-67-Pro synthesized in DMF.

The crystallinity of DUT-67 was well maintained during the course of functionalization. No significant differences between X-ray powder diffraction (XRD) patterns of DUT-67-Pro and XRD pattern of parent DUT-67-fa, with only tiny changes in relative intensity of the peaks (**Figure 3.5a**). Besides, according to SEM images (**Figure 3.4**), the morphology as well as crystal size of the new decorated material was preserved well below ca. 550 nm during the exposure course in *L*-proline solution. ICP-OES analysis showed the zirconium content of 3.78 mmol/g and 3.48 mmol/g in DUT-67-fa and DUT-67-Pro, respectively, which is close to the calculated values (3.72 mmol/g for DUT-67-fa and 3.41 mmol/g for DUT-67-Pro (**Table 3.2**).

Table 3.2. Zirconium content in DUT-67 and DUT-67-Pro.

N	Sample	Chemical formula (*)	Zr / wt.% calculated	Zr / wt.% measured
1	As made DUT-67-fa	$Zr_6O_6(TDC)_4(OH)_2(HCOO)_2 \cdot 0.56DMF \cdot 1.2(HCOOH)$	35.43	35.81
2	DUT-67-H	$Zr_6O_6(TDC)_4(OH)_4$	39.28	40.61
3	As made DUT-67-pro	$Zr_6O_6(TDC)_4(OH)_{0.08}(Pro)_{3.92}$	30.84	31.73
4	DUT-67-pro used in two catalytic cycles	$Zr_6O_6(TDC)_4(OH)_{0.08}(Pro)_{3.92}$	30.55	31.15

(*) Based on 1H -NMR spectra.

The nitrogen adsorption experiments at 77 K showed that the porosity of *L*-proline functionalized DUT-67 depends on functionalization degree (**Figure 3.5b**). The specific BET surface area and total pore volume decrease from 1040 m^2/g and 0.44 cm^3/g in the case of parent DUT-67-fa to 730 m^2/g and 0.31 cm^3/g for DUT-67-Pro, possessing approximately 4 *L*-proline molecules on zirconium node. A similar decrease was also observed in case of perfluoroalkane functionalization of DUT-67 and NU-1000.^{107, 112}

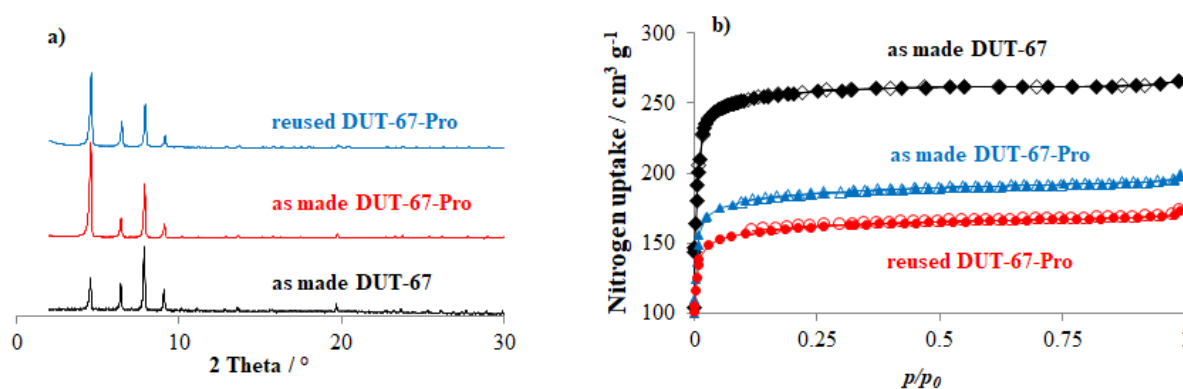


Figure 3.5. (a) XRD patterns and (b) nitrogen physisorption isotherms of as-made DUT-67 synthesized in DMF/NMP, as-made DUT-67-Pro synthesized in DMF, and DUT-67-Pro after two catalytic cycles.

To confirm the existence of the free terminal -OH groups, the original DUT-67-fa was pre-treated by a 2wt% aq. HCl in 4 hours before activating at 120 °C for 24 h to remove completely modulator and solvent molecules coordinated to zirconium clusters because of charge-balancing. This resulting powder could be analyzed by the diffuse reflectance infrared Fourier transform spectroscopy (DRIFTS). The spectrum of parent DUT-67-fa shows a strong absorption at 1595 cm^{-1} (instead of 1670 cm^{-1} as in the spectrum of 2,5-thiophene dicarboxylic acid (H_2TDC)) proving the success of protonation/proving the existence of deprotonated carboxylic groups (**Figure 3.6**). It should be noted that no signal relating to free terminal -OH groups appeared, while the spectrum of activated DUT-67-fa after HCl treatment showed important differences, with two sharp signals at 3670 cm^{-1} and 730 cm^{-1} , which are typically assigned to the free -OH stretching and -OH bending vibrations, respectively (**Figure 3.6**).^{107, 109} It indicates the removal of the modulator molecules as well as DMF molecules to form unsaturated zirconium clusters with free terminal hydroxyl groups. These free hydroxyl groups act as important anchoring points to decorate the Zr-cluster. Disappearance of free -OH signal on the spectrum of the open DUT-67 after soaking into *L*-proline solution 5 days further confirms a successful exchange with formate anions.

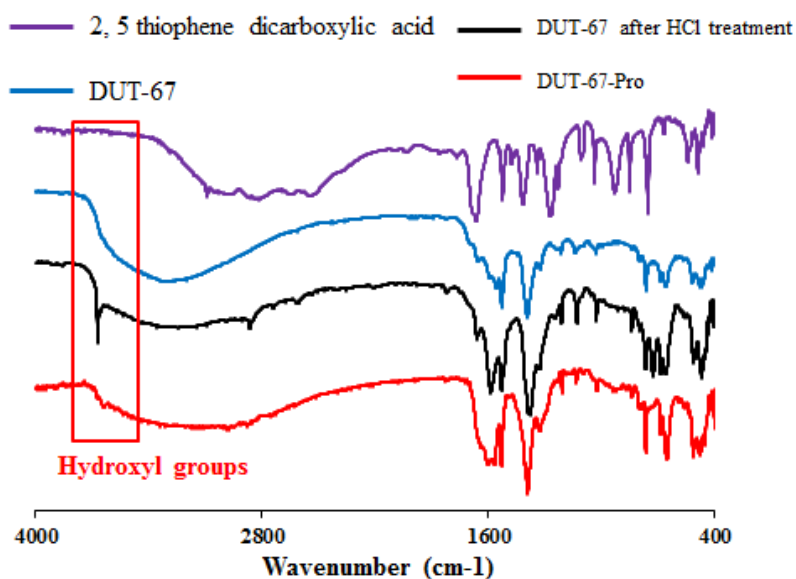


Figure 3.6. IR spectra of DUT-67 after HCl treatment and DUT-67-Pro.

Catalytic study – Asymmetric Michael addition of trans-β-nitrostyrene and cyclohexanone

To evaluate the catalytic activity of the new functionalized chiral DUT-67, the asymmetric Michael addition reaction between *trans*-β-nitrostyrene and cyclohexanone was chosen as model reaction, which yields four stereoisomers of 2-(2-nitro-1-phenylethyl) cyclohexanone as product (**Figure 3.7**), including two pairs of enantiomers originating from *syn*- ($S_{S,R}$ and $S_{R,S}$) and *anti*- addition ($A_{S,S}$ and $A_{R,R}$), respectively (**Figure 7.1**; **Figure 7.2**; **Figure 7.4**).

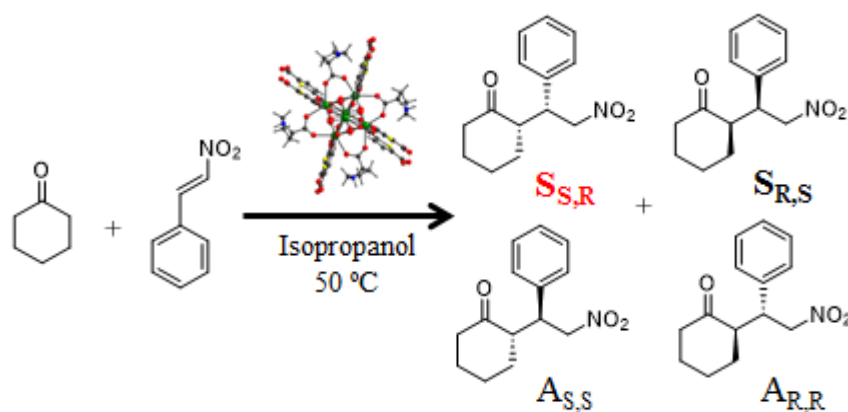


Figure 3.7. Michael addition reaction of *trans*-β-nitrostyrene and cyclohexanone in the presence of DUT-67-Pro catalyst at 50 °C.

As an initial study, a series of experiments was performed to clarify the catalytic role of DUT-67-Pro. The reaction was executed in isopropanol (IPA) as solvent, at 50 °C with a nitrostyrene/cyclohexanone molar ratio of 1:20. In the absence of the catalyst as well as utilizing parent DUT-67 as catalyst (15 mol% catalyst-based on zirconium amount), no adduct was formed after 240 hours of reaction, while a 72% yield was obtained in case of using 15 mol% DUT-67-Pro (based on *L*-proline) after 168 hours, ruling out the catalytic role of the parent MOF and confirming the catalytic activity of DUT-67-Pro to originate from immobilized *L*-proline molecules. It should be noted that the reaction using chiral DUT-67-Pro catalyst leads a comparable enantiomeric excess (*ee*), or even a slightly higher diastereomeric ratio (*dr*) in comparison to the case of employing homogeneous *L*-proline catalyst, 35% to 42% and 95:5 to 90:10 (**Table 3.3**). Obviously, *L*-proline coordinated to the zirconium cluster still retains the enantiopurity, which is not necessarily the case, if proline is incorporated into the framework backbone as a side group of linker molecule.

Table 3.3. Performance of various catalysts in the Michael reaction in isopropanol as solvent.

Entry	Catalyst	Reaction time (h)	Yield (%) [*]	<i>syn:anti</i> ^{**}	<i>ee</i> (%) ^{**}
1	-	240	0	-	-
2	DUT-67-fa	240	0	-	-
3	DUT-67-Pro	168	72	95:5	35
4	<i>L</i> -proline	24	100	93:7	42
5	<i>DL</i> -proline	24	100	90:10	0
6	<i>L</i> -histidine	240	trace	-	-
7	<i>L</i> -tyrosine	240	trace	-	-

* Determined by GC.

** Determined by HPLC.

To improve the catalytic activity of DUT-67-Pro, the effect of different solvents on the rate and selectivity of the reaction was addressed (**Table 3.4**). The series of conventional solvents was employed for the reaction using 20 equivalents of cyclohexanone, in the presence of 15 mol% DUT-67-Pro catalyst at 50 °C. It was observed that the reaction in toluene and chloroform gave only trace amounts of Michael adducts after 240 hours (**Entry 14-16 in table 3.4**). And, the reaction also proceeded with difficulty in polar aprotic solvents, such as THF, 1,4-dioxane, only affording from 5% and 8% yield, respectively (**Entry 11 and 12 in table 3.4**). On the other hand, using alcohol as solvents showed the best performance for this catalyst.^{92, 113} The reaction carried out in ethanol provided 67% yield and 32% *ee*, while isopropanol was found to be more efficient with a 5% increase in both yield and enantioselectivity. Interestingly, these values could be significantly improved to 96% in yield and 94:6 in diastereomeric ratio by using the combination of ethanol and isopropanol (with molar ratio 1:1) as solvent (**Entry 10 in table 3.4**). Indeed, the *L*-proline -catalyzed Michael addition reactions of a non-activated ketone as cyclohexanone to nitro olefins usually show the better performances in the alcoholic solvents than others.^{92, 113} In particular, the modest yields, just below 10%, were reported in the case of using *L*-proline as an organocatalyst in dichloromethane, tetrahydrofuran, while the catalytic activity could be improved greatly in alcoholic solvents.^{92, 113} Steven V. Ley and coworker reported a yield of up to 78% and 47% *ee* when the reaction was carried out in the mixture of ethanol–IPA at room temperature.^{114–116} DMSO was also a good candidate for this reaction, but in most cases the enantioselectivity was low when comparing with using alcohols, 23% in comparison with 47%.^{114, 116} This phenomenon

was also observed in this work, only 36% yield and approximately 25% ee was detected if DMSO was used as solvent. Clearly, solvents can have great impacts on the performance of a heterogeneously catalyzed reaction in different ways, depending on the nature of catalysis.

Table 3.4. Effect of solvents on the performance in the Michael reaction carried out at 50 °C.

Entry	Solvents	Reaction time (h)	Yield (%)*	<i>syn:anti</i> **	<i>ee</i> (%)**
8	isopropanol	168	72	95:5	35
9	ethanol	168	67	92:8	32
10	IPA:EtOH (1:1)	168	96	94:6	38
11	THF	240	5	-	-
12	1,4-dioxane	240	8	-	-
13	DMSO	240	36	91:9	25
14	chloroform	240	trace	-	-
15	toluene	240	trace	-	-
16	cyclohexanone	240	trace	-	-

* Determined by GC.

** Determined by HPLC.

The fact that the formation of the proline enamine intermediates plays a vital role for improving and controlling the stereochemical outcome of the Michael addition reaction, while the protic solvents such as alcoholic systems tends to stabilize the proline enamine intermediates (**Figure 3.8**) formed during catalytic cycle.^{92, 113} Therefore, employing the mixture of ethanol and IPA was essential to reach the best result.

The influence of catalyst amount on the conversion as well as stereochemical outcome of reaction was investigated. It should be noted that no product was detected in the absence of DUT-67-Pro, pointing out the activity of DUT-67-Pro to catalyze for the addition of *trans*- β -nirostyrene. Expectedly, the reaction progress was steadily improved in correlation with increasing amount of catalyst. By using only 5 mol% of catalyst, the reaction could afford 33% yield after 168 hours reaction, while this value was increased up to 96% with 15 mol% DUT-67-Pro applied as catalyst (**Table 3.3 and Figure 3.9**). Utilizing more than 15 mol% catalyst in this study was found to be not efficient as the reaction yield does not change significantly.

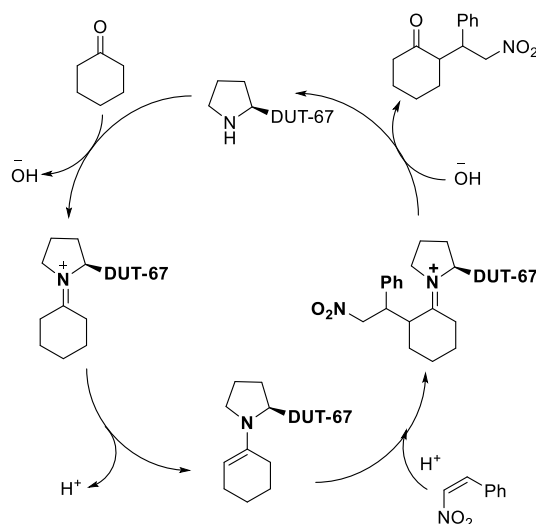


Figure 3.8. Proposed mechanism of Michael reaction using DUT-67-pro as catalyst.

On the other hand, the presence of additives, such as benzoic acid, acetic acid, and formic acid, often leads to significant improvements in the performance of the proline-catalyzed addition reactions, however, adding various amounts of these compound to the reaction system only provided modest progress in conversion of *trans*- β -nitrostyrene to adducts, or even a light drop in enantiomeric excess value (**Entry 21-25 in Table 3.5**).

Table 3.5. The effect of catalyst and additive amounts on the catalytic performance.

Entry	Temp.	Catalyst amount (%)	Additive	Yield*	Syn:anti**	ee (%)**
17	50 °C	5%	-	33	-	-
18	50 °C	10%	-	52	-	-
19	50 °C	20%	-	95	95:5	35
20	RT	15%	-	18	-	-
21	RT	15%	CH ₃ COOH (10%)	66	95:5	31
22	50 °C	15%	-	96	94:6	38
23	50 °C	15%	CH ₃ COOH (10%)	99	91:9	24
24	50 °C	15%	HCOOH (10%)	99	89:11	28
25	50 °C	15%	C ₆ H ₅ COOH (10%)	92	92:8	29

* Determined by GC.

** Determined by HPLC.

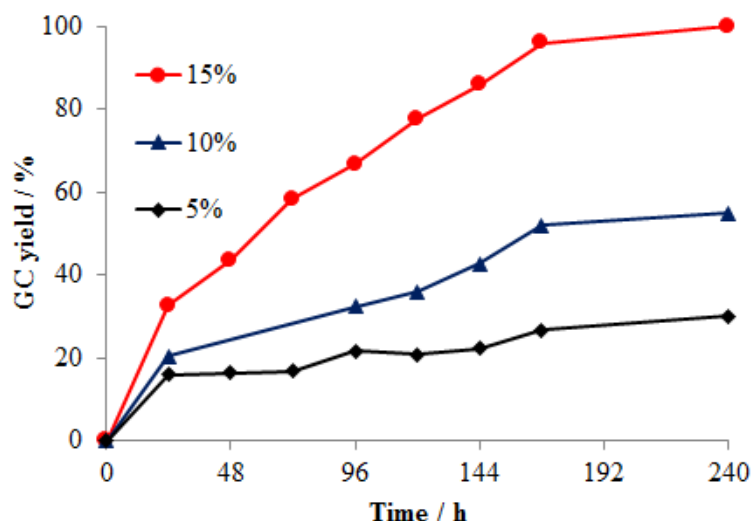


Figure 3.9. Effect of catalyst amount on the rate of the Michael addition reaction.

To investigate the impact of functionalization degree, 4 different samples (containing 1, 2, 3, or 4 *L*-proline molecules per cluster) were prepared and applied as catalysts. The DUT-67-Pro catalyst amounts were adjusted to keep the amount of catalyst at 15 mol% based on *L*-proline unchanged. Interestingly, the formation of product in the asymmetric Michael addition reaction catalyzed by DUT-67-Pro significantly relies on the degree of *L*-proline functionalization. Only 22% yield of 2-(2-nitro-1-phenylethyl) cyclohexanone was obtained after 10 days of reaction with material containing ca. one *L*-proline molecule per cluster, while the reaction could proceed to a yield of 43% with materials containing two *L*-proline molecules per zirconium cluster. A yield as high as 96% was reached in presence of approximately four molecules *L*-proline per zirconium node. This phenomenon could be rationalized since the acidic sites, including the coordinatively unsaturated zirconium as well as hydroxyl groups of DUT-67, were found inactive in this type of reaction as mentioned earlier, but their acidic property could inhibit the active amine sites of connected *L*-proline and hence limit the accessibility of cyclohexanone to the catalytically active center. Consequently, the material DUT-67-Pro with lower *L*-proline loading would tend to be less active in catalyzing Michael addition reaction. In addition, the increasing amount of *L*-proline per cluster does not affect the *ee* value significantly (**Figure 3.10**).

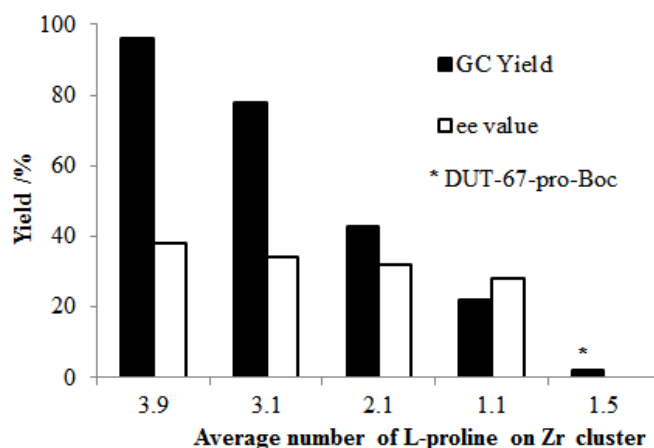


Figure 3.10. The effect of the degree of *L*-proline functionalization.

To gain a deeper understanding of the acidic behaviour of DUT-67-Pro, a control experiment utilizing DUT-67-Pro as heterogeneous catalysis in the Friedel–Crafts alkylation between *trans*- β -nitrostyrene and indole was investigated (**Figure 5.12**). The alkylation reaction was performed at 50 °C in toluene with *trans*- β -nitrostyrene /indole molar ratio of 1:1.5, in the presence of 15 mol% Zr-based catalyst. The pristine DUT-67 exhibited high catalytic activity for the reaction, with a completely conversion after 168 h. In contrast to its high catalytic performance, a steady drop in performance was detected with 80%, 56%, 46%, or even only 18% conversion as DUT-67-Pro with one, two, three, and four molecules of *L*-proline in the structure, respectively (**Figure 3.11**). It can be thus reasoned that the degree of functionalization also affected the acidic activity of DUT-67. Since the new chiral amine sites are generated by coordinating *L*-proline to zirconium cluster, they also act as a blocking moieties and decrease the acidic activity of DUT-67.

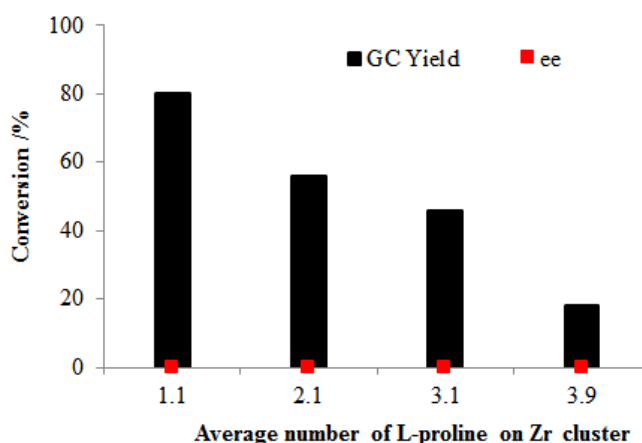


Figure 3.11. The effect of the degree of *L*-proline functionalization.

An additional reaction using DUT-67 with *N*-(*tert*-Butoxycarbonyl)-*L*-proline incorporated (DUT-67-Pro-Boc) as catalyst was carried out to confirm the role of amine groups in the DUT-67-Pro structure as catalytically active sites (**Figure 3.10**). As expected, using the Boc protecting group (*N*-(*tert*-Butoxycarbonyl)) to block amine active sites led to a considerable drop in reaction rate, and only trace amounts of adducts was obtained after 240 h, while a yield of 22% was detected using catalyst possessing the similar *L*-proline functionalization degree (approximately one *L*-proline molecule per zirconium cluster). This result further confirmed that the secondary amine groups of incorporated *L*-proline are the active catalytic sites in Michael addition reaction.

The truly heterogeneous character of the DUT-67-Pro-catalyzed reaction was proven in a leaching test. Hence, the MOF catalyst was separated from reaction mixture by centrifugation after the first 72 hours of reaction (**Figure 3.12a**). It was found that no further product formation takes place in solution, indicating that no availability of homogeneously leached sites and the reaction proceed under real heterogeneous catalysis condition. Moreover, no *L*-proline and no zirconium leaching could be detected according to the analysis of samples after two catalytic cycles (**Table 3.1**; **Figure 7.3c**).

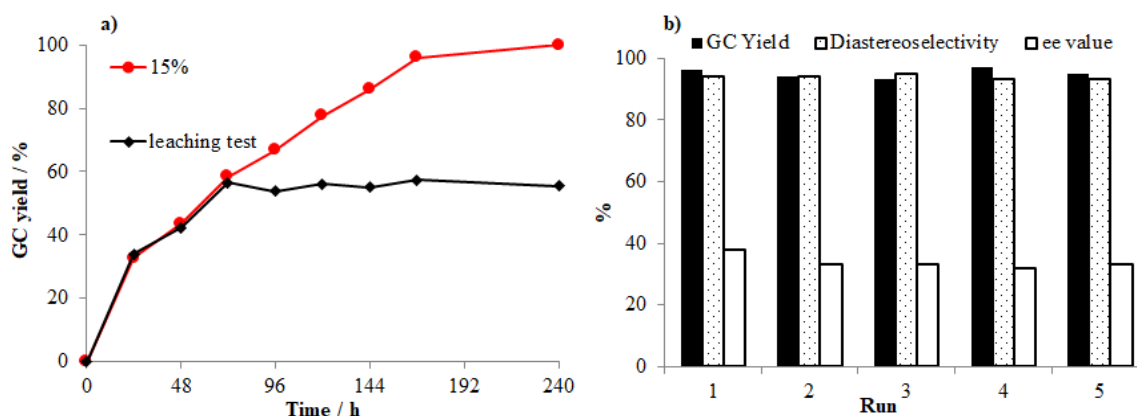


Figure 3.12. a) Leaching test carried out at 50 °C. Kinetics of the reaction with the catalyst (red) and after filtering of the catalyst after 72 h (black). b) Catalyst recycling test.

Highly important for the application of solid catalyst is also the possibility to recover and reuse the catalyst without deactivation. The chiral DUT-67-Pro catalyst was therefore applied in five successive catalytic cycles. For this, the DUT-67-Pro was separated from the reaction mixture after 10 days, washed with DMF and ethanol, dried in vacuum at 120 °C overnight, and reused in the next reaction run. It was found that the DUT-67-Pro could be reused several times without

degradation in catalytic activity. Indeed, similar results in performance were achieved in the 5th run compared with the first run (95% vs 96% for yield and 33% vs. 38% for enantioselectivity) (**Figure 3.12b**).

Moreover, XRD patterns of the reused catalyst revealed that the DUT-67-Pro maintains its crystallinity during the course of the reaction, while the content of zirconium as well as connected *L*-proline also are almost unchanged, confirmed by ¹H-NMR and ICP-OES (**Table 3.1**; **Table 3.2**). The reused catalyst after 2nd run still contains approximately 4 *L*-proline molecules on each zirconium node, and the zirconium loading in MOF is still comparable to fresh catalyst with 3.42 mmol/g and 3.48 mmol/g, respectively (**Table 3.2**). Although, the chiral DUT-67-Pro only showed modest enantioselectivity, the excellent yield as well as diastereoselectivity make it promising for asymmetric Michael addition reaction of unmodified ketones as cyclohexanone to *trans*- β -nitrostyrene.

3.3 Conclusion

The 8-connected Zr-octahedral clusters of DUT-67 were successfully functionalized with chiral catalytic sites (*L*-proline) *via* solvent-assisted ligand incorporation method to obtain a new chiral DUT-67-Pro. Based on ¹H-NMR of the digested functionalized material, it was confirmed that the *L*-proline incorporation degree significantly relied on the exposure time of the parent DUT-67 into in-coming modulator solution. Thereby, a nearly completely exchanged DUT-67-Pro with average of approximately 4 *L*-proline molecules per Zr-node could be achieved after 5 days reaction time.

The resulting chiral DUT-67-Pro was also demonstrated to be a promising solid catalyst for the asymmetric Michael addition of cyclohexanone to *trans*- β -nitrostyrene with excellent yield (up to 96%) and moderate enantioselectivity comparable to that of *L*-proline in homogeneous reaction (*ee* approximately 38%). The solvent was also found to have a marked influence on the performance of DUT-67-Pro. The positive catalytic activity could only be shown in the protic solvent, especially the mixture of ethanol and isopropanol, which could play important role in stabilizing the proline enamine intermediates. In addition, DUT-67-Pro could be separated easily from the products and reused many times without substantial degradation in catalytic activity.

Notably, the acidic nature of DUT-67 catalyst was steadily transformed to become a chiral base catalyst, depending on *L*-proline functionalization degree. Although, these existent acidic sites (including the coordinatively unsaturated zirconium as well as hydroxyl groups of DUT-67) were

found inactive in this type of reaction as mentioned earlier, they could inhibit the active amine sites of connected *L*-proline and hence limit the accessibility of cyclohexanone to the catalytically active center. Consequently, the material DUT-67-Pro with lower *L*-proline amount tends to be less active in catalyzing the Michael addition reaction.

The 8-connected Zr-cluster of DUT-67 is an ideal platform for the incorporation of chiral monocarboxylates into the Zr-nodes by SALI. The great advantage of the proposed approach derived from simplicity of synthetic procedure to achieve an enantiomerically pure MOF by exchanging the monocarboxylic ligand directly by soaking in *L*-proline solution. This facile procedure is also a constructive example, which is utilized to functionalize the majority of 8- or 6- connected Zr-MOFs with carboxylic acids containing specific functional group.

Chapter 4

Insights into the role of zirconium clusters
in proline functionalized Zr-MOF
attaining high enantio- and diastereoselectivity
in asymmetric Aldol addition reaction

The results in this chapter are reproduced with permission from re.117. Copyright 2019 Elsevier Inc. (DOI: 10.1016/j.jcat.2019.07.003)

4.1 Introduction

The asymmetric aldol reaction is one of the most powerful tools for carbon-carbon bond formation,¹¹⁸ particularly with regard to the β -hydroxy ketone and especially β -hydroxy cycloketone products, which are important precursors for bioactive compounds.¹¹⁹ These can be synthesized *via* direct asymmetric aldol reactions of cycloketones with aldehyde derivatives.⁹² Therefore, the search for rational methods integrating chirality efficiently into highly active catalysts has been a challenging goal in organic synthesis and a number of systems have been developed.¹²⁰ Pioneering work describing the application of *L*-proline as an organocatalyst for such reactions was reported approximately 50 years ago (Hajos-Perrish-Eder-Sauer-Wiechert reaction)^{121, 122} and a mechanism involving enamine formation was proposed later.¹²³ Since then, *L*-proline and its derivatives have been widely adopted as catalysts for the asymmetric aldol reaction.¹²⁴⁻¹²⁶ However, the exquisite control of diastereo- and enantioselectivity still remains a challenge, especially in the reaction of unmodified cycloketones and benzaldehyde derivatives. Naturally, formation of *E*-enamines with *L*-proline is thermodynamically favorable and is aided by the steric effect of the cyclohexene ring and substituents of the aldehydes (**Figure 4.12a, 4.12b**).^{127, 128} Hence, formation of *anti*-isomers is usually preferred while the selectivity for *syn*-configuration adducts have been rarely reported for *L*-proline and its derivatives.¹²⁹⁻¹³¹

In recent years, several groups have proposed various strategies to incorporate chiral active sites, especially *L*-proline, into Zr-based MOFs for enantioselective separation, chiral recognition, and asymmetric catalysis.^{51, 132, 133} As mentioned in above literature, a proline-functionalized MOF (UiO-67-NHPro) shows inverse diastereoselectivity (*syn* over *anti*) in the aldol addition reaction of cyclohexanone and 4-nitrobenzaldehyde carried out in ethanol as solvent, but enantioselectivity could not be achieved. Recently, P. Van Der Voort and co-workers reported on the *L*-proline modulated synthesis of UiO-66, UiO-67 and Zr-NDC (DUT-52)⁴² and application of the resulting materials as catalyst in the same aldol reaction.⁶⁶ The preferred *syn* diastereoselectivity was reported (up to 82% in methanol as solvent) also for this system, but also in this case no enantioselectivity was obtained.

The origin for this lack of enantioselectivity in so far reported catalytic systems will be disclosed in the following section. And, DUT-67-Pro will be introduced as an efficient solid catalyst, which catalyzes the asymmetric aldol addition reaction of 4-nitrobenzaldehyde and cyclohexanone toward *syn*-isomers formation with high enantioselectivity.

4.2 Results and discussion

Materials synthesis and characterization

As mentioned in previous reports,^{60, 66} *L*-proline was utilized to introduce chiral active sites into the Zr-based MOF by using functional groups of organic linker (in UiO-67-NHPro) in pre-synthetic modification or modulators in the modulated synthesis of UiO-67 (**Figure 4.1**). Although an unprecedented *syn*-selectivity in the asymmetric aldol addition of 4-nitrobenzaldehyde and cyclohexanone (**Figure 4.7**) was interestingly observed when these proline functionalized Zr-MOFs were applied as solid catalysts, the enantioselectivity was unexpectedly low or absent in comparison to that obtained in the reaction using *L*-proline as homogenous catalyst.⁹² This clearly indicates that the proline chirality, which plays a key role in controlling the configuration of product, was blocked or not sufficient in these Zr-based MOF structure.

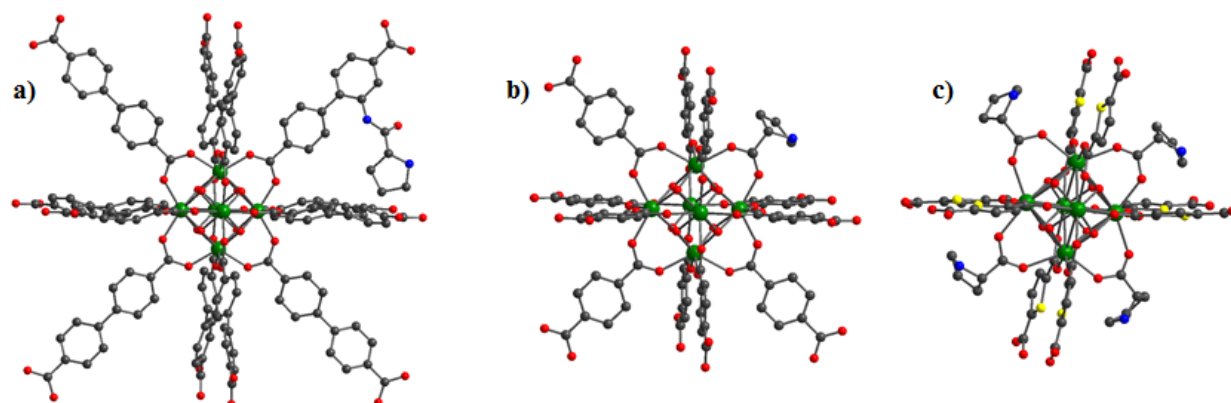


Figure 4.1. a) *L*-proline as functional groups of organic linker (in UiO-67-NHPro) obtained in pre-synthetic modification;³¹ b) *L*-proline as modulator in the modulated synthesis of UiO-66;³³ c) *L*-proline as modulators in the post-synthesis of 8 connected Zr-based MOFs (DUT-67). Color scheme: Zr (green); O (red); N (blue); C (grey); S (yellow).

In contrast to conventional carriers, the Zr-MOFs were usually known as effective catalysts in various acid catalyzed organic transformations.¹³⁴ And, the acidic catalytic activity of Zr-based MOFs originates from the defect positions in framework (uncoordinated Zr-sites, such as Zr^{4+} and hydroxyl groups). They not only catalyze efficiently the direct aldol reaction, but also play a pivotal role in the predominant formation of *syn*-isomers.

To study the effect of the Zr_6 -clusters on the diastereoselectivity, a series of achiral UiO-67 compounds was synthesized in the presence of HCl, formic acid, and benzoic acid as modulators,

(further denoted as UiO-67-H, UiO-67-Form, and UiO-67-Benz, respectively) and employed in heterogeneous catalysis in the aldol reaction between 4-nitrobenzaldehyde and cyclohexanone in our previous work.¹³⁵ Surprisingly, the inverse diastereoselectivity preferring *syn*- over *anti*-adduct was achieved not only for all achiral materials with similar selectivity compared to the chiral modified systems reported earlier, but also for the $Zr_6O_4(OH)_4(OMc)_{12}$ cluster (OMc = methacrylate) applied as homogeneous catalysis.¹³⁶ Clearly, these catalytic sites can react with the carbonyl carbon atom of the cyclohexanone *via* nucleophilic attack to form metal enolates. However, based on steric hindrance between the side groups of these substrates with the Zr-cluster (**Figure 4.2b**), diastereoselectivity is forced into one direction and as consequence *syn*-diastereomer preference. Actually, an exceptional diastereoselectivity of an aza-Diels-Alder [4+2] cycloaddition was observed in a report of Xamena and co-workers using UiO-66 catalyst.¹³⁷ This result was explained by the steric hindrance of bulky substituents within the zirconium cluster, causing the preference to one particular transition state resulting in a high diastereoselectivity of the reaction.¹³⁷ In the case of the previous proline functionalized Zr-MOFs, the aldol transformation could be performed at achiral defect sites, leading to a reversed dr-selectivity and an absence of enantioselectivity.

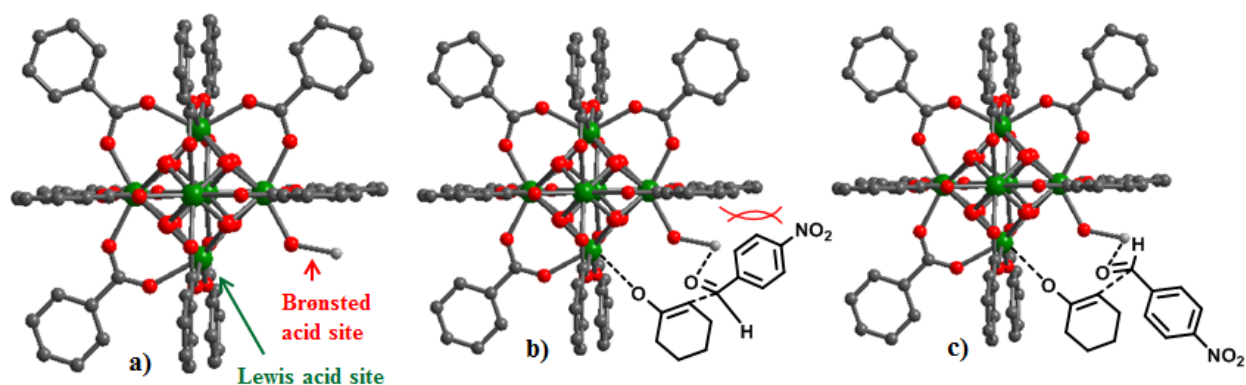


Figure 4.2. a) The defective 12-connected Zr-cluster containing Lewis (Zr^{4+}) and Brønsted acid site (-OH group); b) The proposed pathway for the adduct *anti*-configuration driven by steric effect; c) The proposed pathway for the adduct *syn*-configuration. Color scheme: Zr (green); O (red); C (grey).

To suppress the accessibility and activity of the open metal sites in Zr-MOFs which catalyze the reaction through an achiral pathway without any enantioselectivity, we propose to introduce *L*-proline into frameworks with reduced cluster connectivity (DUT-67-pro) in order to include the modulator as integral part of the framework in the close proximity to the cluster. If *L*-proline would adopt the role of modulator, it may block the Lewis acidic activity of the clusters, as well

as resume the role as enantioselective catalytically active species, maintaining the *syn*-product selectivity arising from the cluster geometry.

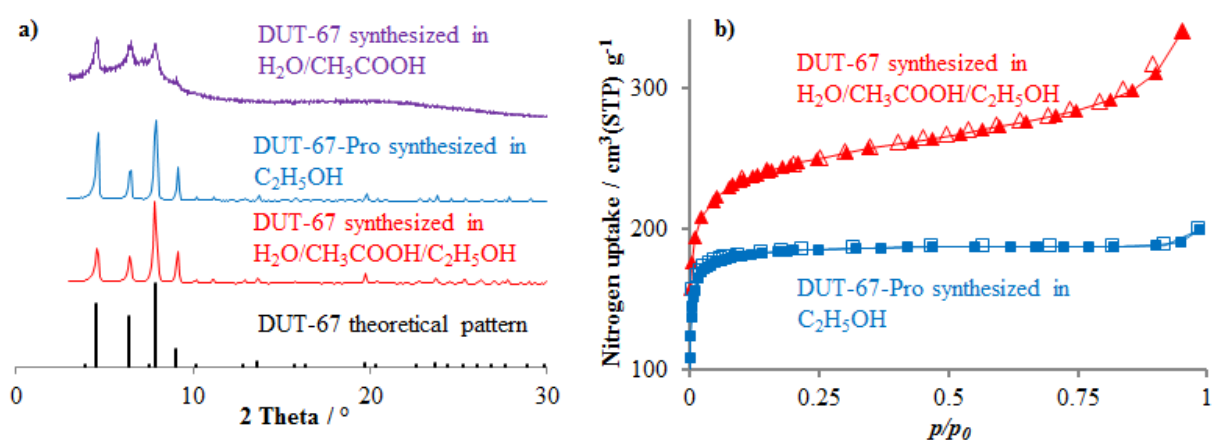


Figure 4.3. (a) XRD patterns and (b) nitrogen physisorption isotherms of DUT-67 synthesized in H₂O/CH₃COOH/C₂H₅OH, DUT-67-Pro synthesized in C₂H₅OH.

In this part, the approach to synthesize DUT-67 differs from the initially reported procedure.^{44, 112} The synthesis reported by Reinsch *et al*,¹³⁸ ZrCl₄ was replaced by ZrOCl₂·8H₂O to enhance the solubility of Zr⁴⁺ in a mixture of water and acetic acid (1:1 v/v), and thus to avoid the use of DMF/DMP. A solution of 2,5-thiophenedicarboxylic acid (TDC) in ethanol was consequently added and the resulting solution was then placed in an oven set at 80 °C for 2 days. Interestingly, this alternative approach also allowed for a gram-scale synthesis of DUT-67 in a high yield (up to 79%). The X-ray diffraction pattern of the resulting powder was in good agreement with previously reported data (**Figure 4.3a**), although slight decreases were observed for the surface area (1093 m²/g vs. 938 m²/g) (**Figure 4.3b**) and crystal size (ca. 750nm vs. 520 nm) (**Figure 4.4**). The crystallinity of DUT-67 phase tends to drastically reduce with increasing water content (**Figure 4.3a**; **Figure 4.4**).

Table 4.1. Zirconium content in DUT-67 synthesized in H₂O/CH₃COOH/C₂H₅OH and DUT-67-Pro prepared in ethanol.

N	Sample	Chemical formula (*)	Zr / wt.% calculated	Zr / wt.% measured
1	DUT-67	$Zr_6O_6(TDC)_4(CH_3COO)_4$	34.4	34.2
2	DUT-67-Pro	$Zr_6O_6(TDC)_4(Pro)_4 \cdot 5.8EtOH$	26.7	26.7
4	DUT-67-Pro used in two catalytic cycles	$Zr_6O_6(TDC)_4(OH)_{0.08}(Pro)_{3.92}$	31.1	30.8

(*) Based on 1H -NMR spectra; TGA; ICP-OES and element analysis.

To introduce the chiral active sites into the zirconium clusters, the activated DUT-67 was then suspended in an ethanol solution containing *L*-proline and HCl at room temperature giving DUT-67-Pro. The presence of *L*-proline in the DUT-67-Pro product was confirmed by 1H NMR (Nuclear Magnetic Resonance) of the digested samples (Fig. S11). A complete exchange of pristine modulator by *L*-proline (4 molecules per cluster) under preservation of crystallinity (**Table 4.1; Figure 7.7 and 7.8**) and an expected decrease in the BET area (from ca. 938 m²/g to ca. 760 m²/g) were observed after 5 days of treatment (**Figure 4.3b**).

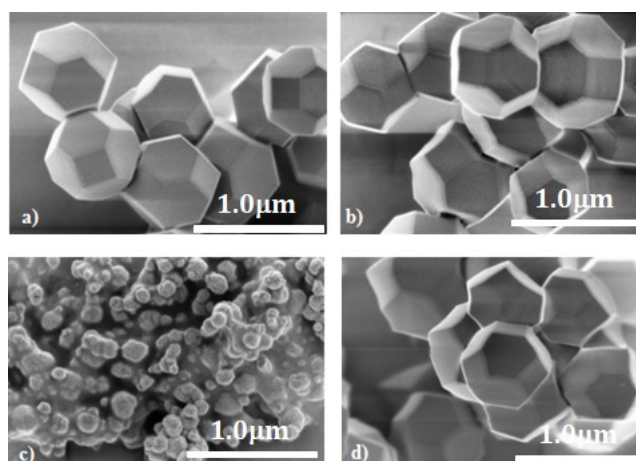


Figure 4.4. SEM images of DUT-67 product, obtained in following synthetic batches: (a) DMF/NMP at 80 °C for 3 days; (b) H₂O/CH₃COOH/ C₂H₅OH at 80 °C for 2 days; (c) H₂O/CH₃COOH at 80 °C for 2 days; (d) DUT-67 exchanged with *L*-proline solution upon 5 days at room temperature.

Since crystallographic techniques could not provide additional insights into location of the *L*-proline molecules in the structure, solid-state NMR techniques were applied to analyze the environment of the *L*-proline in DUT-67-Pro. **Figure 4.5a** shows the solid-state ^{13}C CP MAS (Cross-Polarization Magic Angle Spinning) spectra of the *L*-proline exchanged sample, of the parent DUT-67 material, of neat *L*-proline and of the neat H₂TDC linker. The spectrum of H₂TDC shows three peaks at 168 ppm, 141 ppm and 136 ppm attributed to the carbon atoms 6, 7 and 8 of H₂TDC, respectively (see scheme with signal assignments in **Figure 4.5b**). These three signals are also identified in the ^{13}C CP MAS spectrum of the DUT-67 parent material. Comparison with

the spectrum of H₂TDC shows small chemical shift changes for the lines attributed to carbons 7 and 8, which are most probably related to the conformational changes of the TDC moieties. A split signal is obtained in the carbonyl chemical shift region of the DUT-67 spectrum, with maxima at 172 ppm and 167 ppm. These signals can be attributed to TDC molecules that are coordinated to the Zr metal clusters, giving origin to the MOF structure, as well as to free COOH sites, which are present as defect sites in the MOF structure. Based on the chemical shift information we tentatively attribute the signal at 167 ppm to free COOH sites, while the signal at 172 ppm relates to COO⁻ sites coordinated to the Zr metal cluster. A second strong indication for the coexistence of different TDC sites is the shoulder present in the signal at 135 ppm of carbon 8 in the ¹³C CP MAS spectrum of DUT-67.

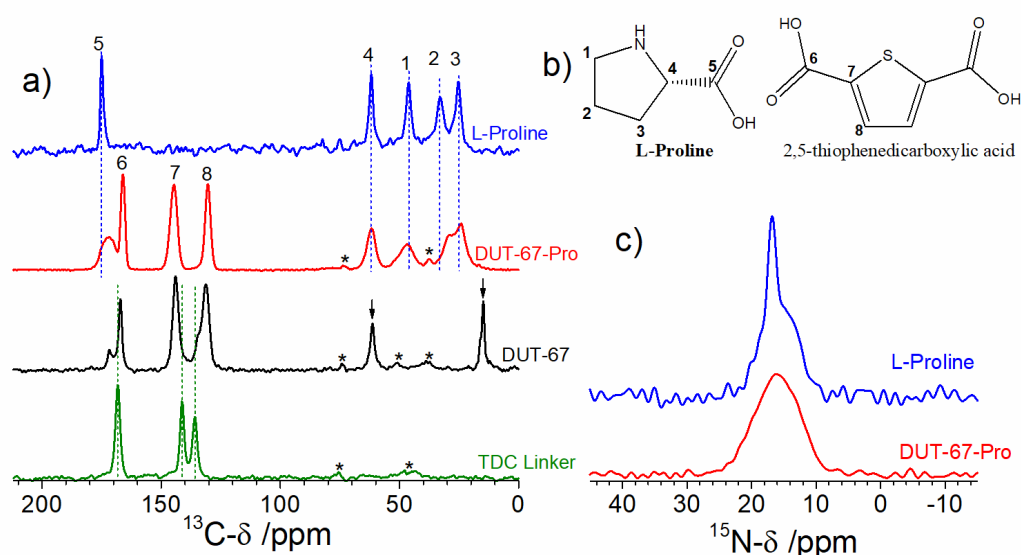


Figure 4.5. a) Conventional solid-state ¹³C{¹H} CP MAS spectra of *L*-proline, TDC, DUT-67 and DUT-67-Pro as well as the assignment of the signals to the carbons in (b). Spectra were recorded at 14 kHz spinning. The peaks indicated by arrows, around 60 ppm and 20 ppm, correspond to reminiscent ethanol in the sample. The spectra were normalized by the maximum intensity. Signals marked with asterisks are spinning sidebands. The total measurement time for the spectra shown in (a) ranged from 8 to 12 h. c) DNP enhanced ¹⁵N{¹H} CP MAS spectra of *L*-proline and DUT-67-Pro. The total measurement times for the spectra in (c) were 1 h for *L*-proline and 2 h for DUT-67-Pro, respectively.

For further structural investigations, we combined solid-state NMR with dynamic nuclear polarization (DNP) to overcome sensitivity limitations of ¹³C and ¹⁵N nuclei.¹³⁹⁻¹⁴¹ Solid-state DNP techniques have been successfully applied in the past for analysis of various MOF systems

and for structure determination of peptide functionalized porous silica materials.^{82, 142-145} Such experiments typically require the impregnation of a sample with a polarization source, which in our case is a matrix containing 1-(TEMPO-4-oxy)-3-(TEMPO-4-amino) propan-2-ol (TOTAPOL) in D₂O/H₂O (90:10, v:v).¹⁴⁶ TOTAPOL was chosen to apply in this series of DNP MAS NMR experiments because of its small size, which allows to access into microporous media with diameter from 5 to 8 Å in Sn-containing zeolites.¹⁴⁷ Thus, this nitroxide biradical could also diffuse well into DUT-67 structure, possessing a larger pore system, including one octahedral cage with diameter approximately 9.1 Å and two cuboctahedral cages with diameter about 14.6 Å and 17.1 Å.^{112, 148} To ensure that the presence of this matrix does not affect the investigated structure, DNP ¹³C{¹H} CP MAS spectra were measured (**Figure 7.15**) and compared with conventional NMR spectra obtained for the dry samples (**Figure 4.5a**). Despite small chemical-shift variations, no considerable changes are observed.

Further insights regarding the assignment of the signals at 167 ppm and 172 ppm is obtained from DNP enhanced ¹³C{¹H} CP MAS experiments with variable contact time, performed for the DUT-67 parent material (**Figure 7.16**). From the analysis of the intensities of these peaks as a function of the CP contact time, two parameters can be extracted, namely: (i) the characteristic time for ¹H → ¹³C polarization transfer T_{HC} , and (ii) the ¹H spin-lattice relaxation time in the rotating frame $T_{1\rho}$. Our analysis (*vide* **Figure 7.16**) yields T_{HC} values of 1.4 ± 0.1 ms and 1.1 ± 0.1 ms and $T_{1\rho}$ of 14 ± 2 ms and 25 ± 1 ms for the lines at 172 ppm and 167 ppm respectively. The shorter T_{HC} value for the signal at around 167 ppm agrees with our attribution of this site to protonated carboxylic groups (COOH) in free TDC sites. On the other hand, somewhat longer T_{HC} values are expected for non-protonated carboxylate groups (COO⁻) belonging to TDC sites coordinated to the Zr₆-clusters.

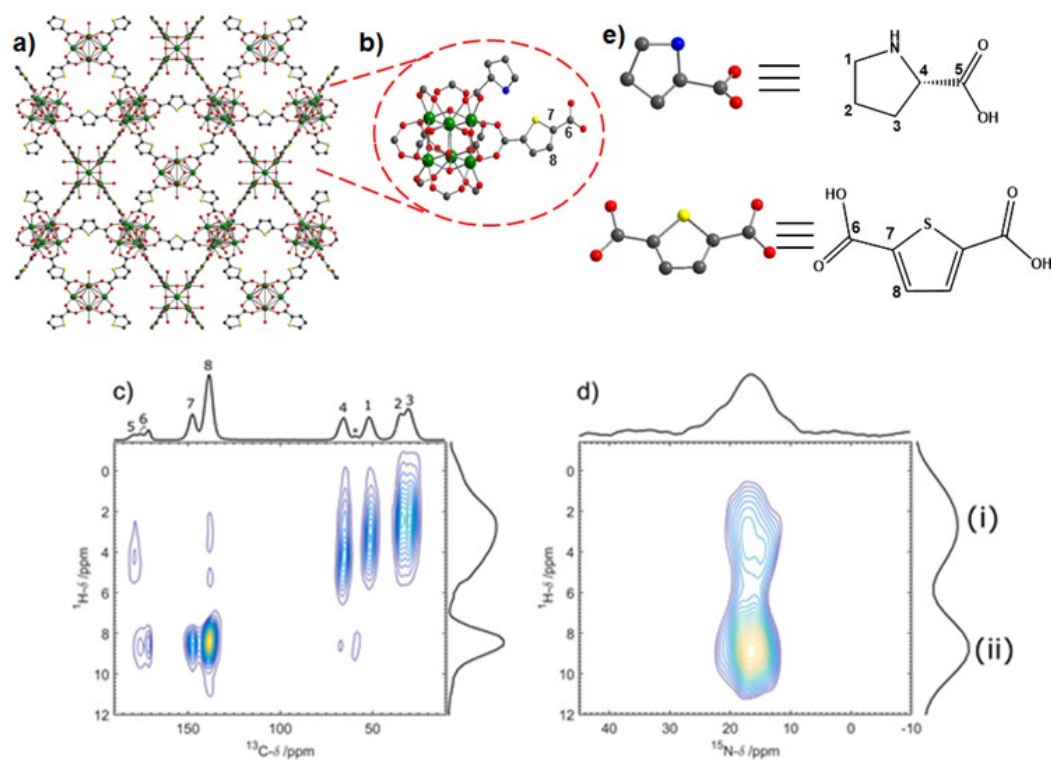


Figure 4.6. a) Structure of the DUT-67 (modulator molecules are omitted); b) Environment of the 8-connected Zr-cluster after exchange of pristine modulator by *L*-proline. c) DNP enhanced $^{13}\text{C}\{^1\text{H}\}$ CP MAS FSLG HETCOR spectrum of DUT-67-Pro. The two signals attributed to C-6 account for the presence of COOH groups in free TDC sites and COO⁻ groups in TDC coordinated to the Zr metal cluster (*vide text*). d) DNP enhanced $^{15}\text{N}\{^1\text{H}\}$ CP MAS FSLG HETCOR spectrum of DUT-67-Pro. (i) *L*-proline protons from carbon atoms labelled as 1 and 4 in Figure 4.5e. (ii) H-N protons from *L*-Proline. Note: The asterisk indicates a spinning sideband. The total measurement times were 4 h for the spectrum in (c) and 20 h for the spectrum in (d), respectively.

Due to the strong signal enhancements in the 1D spectra, it was possible to further study the DUT-67-Pro sample with 2D heteronuclear correlation experiments with homonuclear frequency-switched Lee-Goldburg decoupling (FSLG HETCOR). The improvement of sensitivity provided by the DNP technique is essential to acquire 2D $^{15}\text{N}\{^1\text{H}\}$ CP MAS FSLG HETCOR spectra, which would otherwise take exceedingly long measurement times with standard solid-state NMR. Although, 2D $^1\text{H}/^{13}\text{C}$ HETCOR spectra can in principle be obtained without DNP in a reasonable amount of time, by using modern solid state 2D techniques such as fast MAS and ^1H detection,¹⁴⁹ we have obtained $^{13}\text{C}\{^1\text{H}\}$ CP MAS FSLG HETCOR spectra under DNP conditions to provide a fair comparison of the protons in the coordination environment of both ^{15}N and ^{13}C nuclei. In the $^{13}\text{C}\{^1\text{H}\}$ CP MAS FSLG HETCOR spectrum (**Figure 4.6c**), it is clearly visible that the ^1H signals

between 2 and 4.5 ppm correlate to the carbon signals 1 to 4 of the *L*-proline. A weak ^1H correlation with the carboxylic carbon 5 of the *L*-proline is observed around 4.5 ppm, which occurs due to polarization transfer from the proton bound to the neighbor carbon 4. The ^1H signal at ca. 8.5 ppm correlates to carbon atoms 7 and 8 of TDC and furthermore shows a weak correlation to the carboxylic carbon 6 of TDC. As discussed above, carbon 6 of TDC is represented by two signals corresponding to free COOH sites and COO $^-$ groups coordinated to the Zr metal cluster. Additionally, higher spinning room-temperature ^1H NMR spectra for the whole set of samples (**Figure 7.17**), as well as the low-temperature DNP enhanced ^{13}C CP MAS FSLG HETCOR spectrum for the pure TDC linker are provided as supporting information (**Figure 7.17c**). The ^1H MAS (**Figure 7.17a**) as well as the DNP enhanced $^{13}\text{C}\{^1\text{H}\}$ CP MAS FSLG HETCOR (**Figure 7.17c**) spectrum of TDC exhibits a proton signal around 13 and 14 ppm, clearly attributed to OH protons in carboxylic groups. Such signal is not obtained in the DUT-67-Pro $^{13}\text{C}\{^1\text{H}\}$ CP MAS FSLG HETCOR spectrum (**Figure 4.6c**). In the $^{15}\text{N}\{^1\text{H}\}$ CP MAS FSLG HETCOR spectrum (**Figure 4.6d**) two correlation peaks are observed. The weaker ^1H signal centered around 3.5 ppm corresponds to the protons from carbons 1 and 4 in *L*-proline, while the signal around 8.9 ppm corresponds to the H-N protons in *L*-proline. The $^{15}\text{N}\{^1\text{H}\}$ CP MAS FSLG HETCOR spectrum for DUT-67-Pro is comparable to that obtained for pure *L*-proline in the same experimental conditions (**Figure 7.17b**), confirming that the *L*-proline is possibly coordinated to the Zr-cluster by replacing a terminal modulator group.

Catalytic studies - Asymmetric aldol addition of 4-nitrobenzaldehyde and cyclohexanone

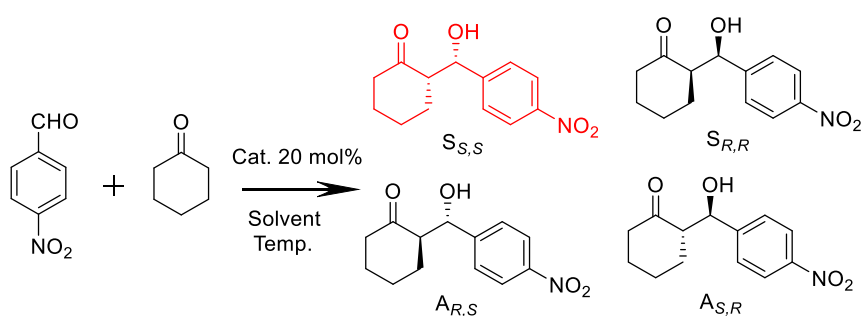


Figure 4.7. Asymmetric aldol reaction of cyclohexanone and 4-nitrobenzaldehyde.

The reaction was conducted at 40 °C, in the presence of 20 mol% catalyst (based on *L*-proline) in various solvents for 168 h to form four products including two *syn*-isomers (S_{S,S} and S_{R,R}) and two *anti*-isomers (A_{S,R} and A_{R,S}) (**Figure 4.7**; **Figure 7.18-7.23**). However, as shown in **Figure 4.8**,

ethanol shows poor compatibility when applying DUT-67-Pro as catalyst. A Lewis acid catalyzed acetalization of 4-nitrobenzaldehyde by ethanol was observed to compete with the desired aldol reaction. Indeed, 84% of 4-nitrobenzaldehyde was converted to 4-nitrobenzaldehyde diethyl acetal instead of the aldol adduct products (**Figure 4.9**).

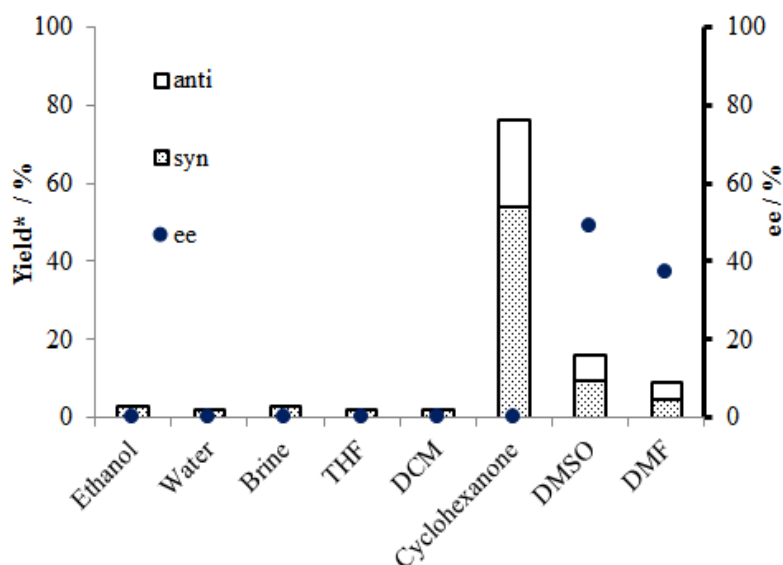


Figure 4.8. The effect of solvent on the catalyst performance in the asymmetric aldol reaction carried out at 40 °C. (*) Isolated yield.

After application of other Zr-based MOFs such as DUT-67, UiO-66, UiO-67, and MOF-808 under same reaction condition the formation of acetal compounds was also observed (**Figure 4.9 and 4.10**), confirming that the Lewis acidic defect sites in Zr-MOFs remain intact even after modification with *L*-proline, and in fact show competing catalytic activity to the *L*-proline units. Consequently, this activity provides a rational explanation for the absence of enantioselectivity of *L*-proline-functionalized Zr-MOFs in the last reports.^{60, 66} In the case of DUT-67-Pro, although a large part of acidic active sites on the Zr-clusters was masked by connected *L*-proline modulators, their activity in alcoholic solvents still maintained strong enough to promote for the formation of 4-nitrobenzaldehyde diethyl acetal instead of the aldol products (**Figure 4.9 and 4.10**). To restrain the acidic activity of Zr-cluster and improve the performance of the *L*-proline active sites, one possibility is using polar aprotic solvents, such as THF, DCM, DMF, or DMSO, in which a slow reaction rate could be offered to increase the interaction opportunity between reagents and *L*-proline active sites.

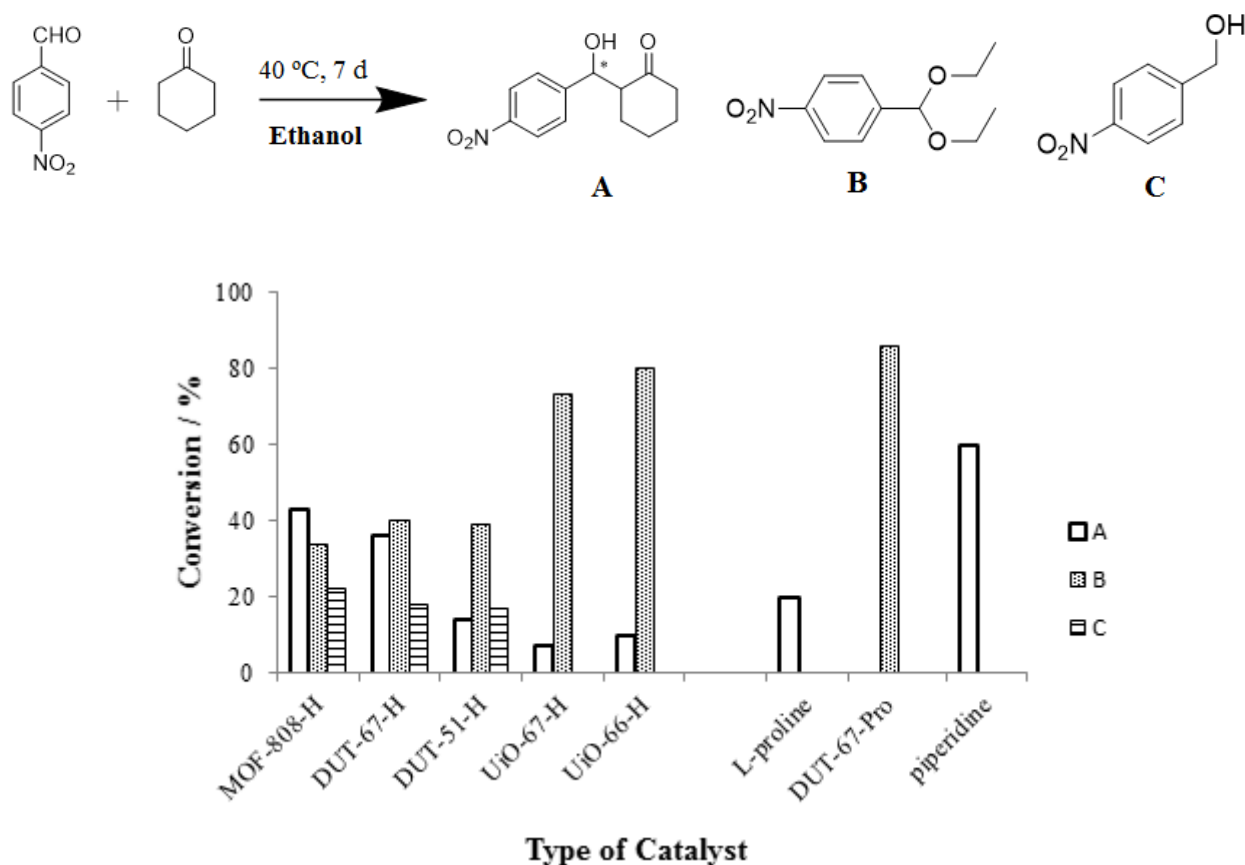


Figure 4.9. Performances of various catalyst in reaction between 4-nitrobenzaldehyde and cyclohexanone in ethanol as solvent.

The literature reports that addition of 1 - 20 mol% water to a homogeneous reaction leads to anti-configuration products with approximately 90% *ee*.^{150, 151} However, in the present study, adding various amounts of water to the DMSO-mediated reaction did not lead to any positive results. No products were found in the reaction mixture containing water even after 7 days. Obviously, water diminishes the reaction performance in contrast to the numerous reports, blocking the open metal sites of the cluster and as consequence changing the acidity of them. Neither dichloromethane nor tetrahydrofuran as solvents resulted in any product formation, not even after 7 days. However, the reaction could proceed slowly in polar aprotic solvent, such as DMF, affording a yield of 9%, and 37% *ee* (**Figure 4.8**). A modest improvement was also recorded when the reaction was investigated in DMSO, producing 16% isolated yield of the product (49% *ee* and 58:42 *dr* (*syn:anti*)). The isolated yield could be significantly improved up to 76% (71:29 *dr* (*syn:anti*)) using cyclohexanone as the solvent, but a racemic product mixture was obtained (**Figure 4.8**). As previously discussed, the catalyst could induce the specific configurations of intermediate states of reaction depending on the nature of solvent.¹⁵² Obviously, in this system, the solvent also plays

a key role in controlling reaction rate as well as stereochemistry of the asymmetric aldol reaction via different impacts on two catalytically active sites (*L*-proline vs. Zr-cluster) in DUT-67-Pro.

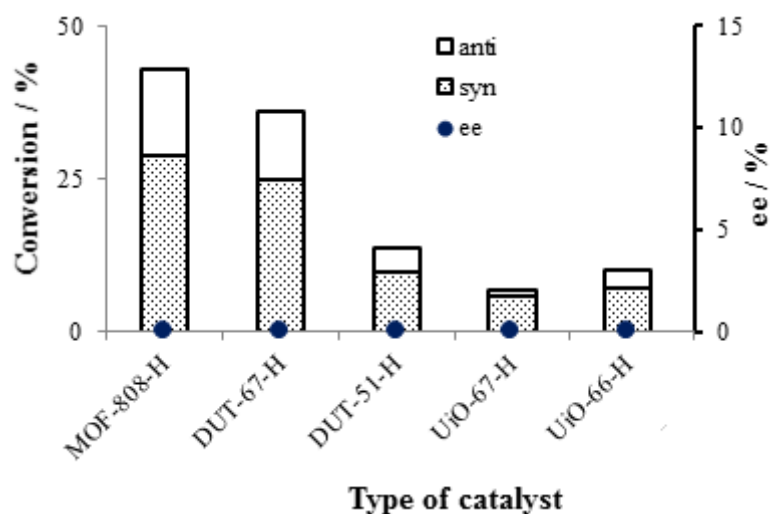


Figure 4.10. Effect of various catalysts on diastereoselectivity in Aldol reaction in ethanol as solvent.

The effect of temperature was also investigated in order to improve the reaction rate and selectivity. Four reactions were carried out in DMSO, using 20 mol% DUT-67-Pro, at various temperatures ranging from 25 °C to 80 °C (**Figure 4.11**). All reactions were terminated after 168h and the reaction progress was monitored by GC. As expected, increasing temperature resulted in a great enhancement in the reaction yield (5%, 86%, and 96% at 25, 60, and 80 °C, respectively, **Figure 4.11**). Although the conversion at 353 K was significantly increased from 8% in the first day to 96% after 7 days of reaction time, the enantioselectivity towards the aldol *syn*-adducts (67:33 dr (*syn:anti*)) was below 19% (**Figure 4.11**). On the other hand, a considerable improvement in enantiomeric excess value to 57% was observed as the reaction was carried out at 298 K. Besides, the ratio of *syn:anti* isomers at this condition was 73:27 (measured after 7 days of reaction time; 5% GC yield) (**Figure 4.11**). This enantioselectivity is comparable to that of the homogeneous *L*-proline catalyst reference, at higher isolated yield (60%) and ca. 54% ee (45:55 *syn:anti*) after 72 h. The preference for anti-product formation for the homogeneous case is known to result from *L*-proline mediated organocatalysis.

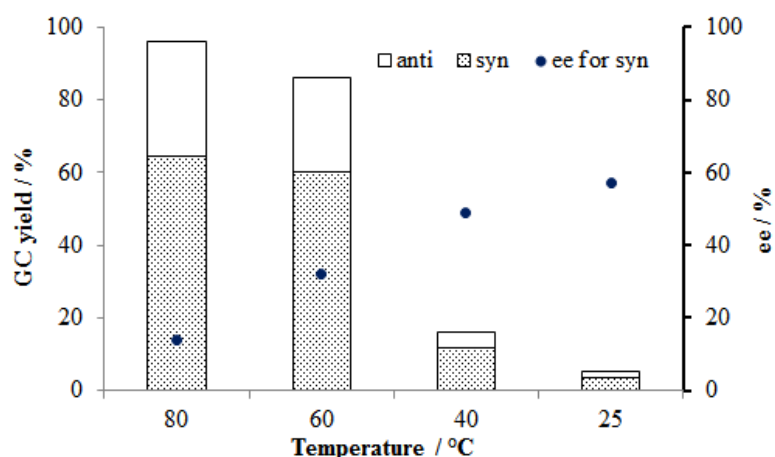


Figure 4.11. The effect of the temperature on the DUT-67-pro catalyst performance in asymmetric aldol reaction carried out in DMSO as solvent. Yield was determined by GC.

The efficiency of proline-based catalysts originates from the formation of reactive enamines and the steric effect between phenyl groups of benzaldehydes and the cyclohexene rings predominately drives intermediates to form anti-adducts. However, a hypothesis was proposed that it is possible to improve the *syn*-selective reaction by using bulky anion groups, which would push the substituted phenyl ring of aldehydes to the opposite side. A plausible explanation for the *syn*-selectivity of DUT-67-pro may be found in the Zr-cluster and the resulting steric hindrance to force the phenyl group in the *syn*-position as indicated in **Figure 4.12c**.

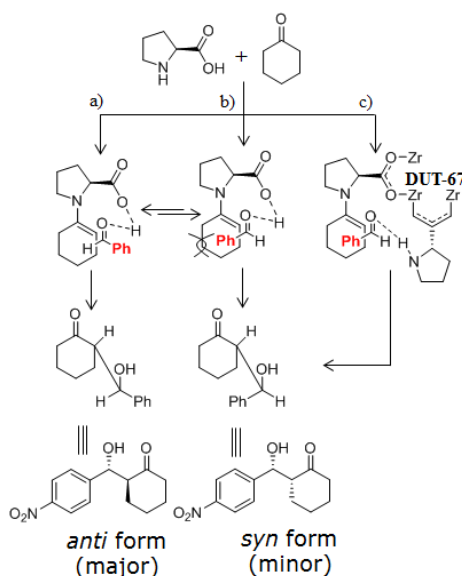


Figure 4.12. The possibilities of enamine intermediate state formation in the presence of *L*-proline (a and b); and DUT-67-Pro (c).

Experimental and theoretical works demonstrate the enantioselectivity-defining step to be highly affected by the presence of additives, such as water, Lewis and Brønsted acids. To study the influence of acids, as compounds competing in coordination with modulator molecules, we investigated a variety of organic acids as well as HCl as additives in the catalyzed reaction. Interestingly, stronger acids such as CH₃COOH, HCOOH, CF₃COOH, and HCl invert the diastereoselectivity to favor the *anti*-product (**Figure 4.13**) with increasing acidity of the additives (**Table 4.2**). In order to clarify the effect of these acidic additives, a control experiment was performed by adding only the acid (0.2 equiv.) but without any DUT-67-Pro catalyst. In this case only traces of product were detected after 7 days of reaction (except for HCl) (**Table 4.2**). This observation rules out the reaction to be catalyzed by 0.2 equiv. of organic acidic additives alone. The observed *anti*-selectivity in the presence of acidic additives thus may be rationalized assuming stronger acidic additives to substitute the *L*-proline moieties at the Zr-cluster, and consequently leading to a leaching of *L*-proline into the homogeneous reaction medium. The high level of similarity especially for diastereoselectivity data compared with those from reactions catalyzed by homogeneous *L*-proline strengthens this assumption. In fact, the ¹H NMR spectra of the MOF catalyst digested after one reaction cycle using strong acid additives show a decreasing *L*-proline content (**Figure 7.9-7.14**). While the *L*-proline content after reaction using MOF catalyst without additives remained unchanged (ca. 4 molecules per Zr-node), this value drops to 1.8, 1.2, 0.64 and 0.16 for CH₃COOH, HCOOH, HCl, and CF₃COOH, respectively.

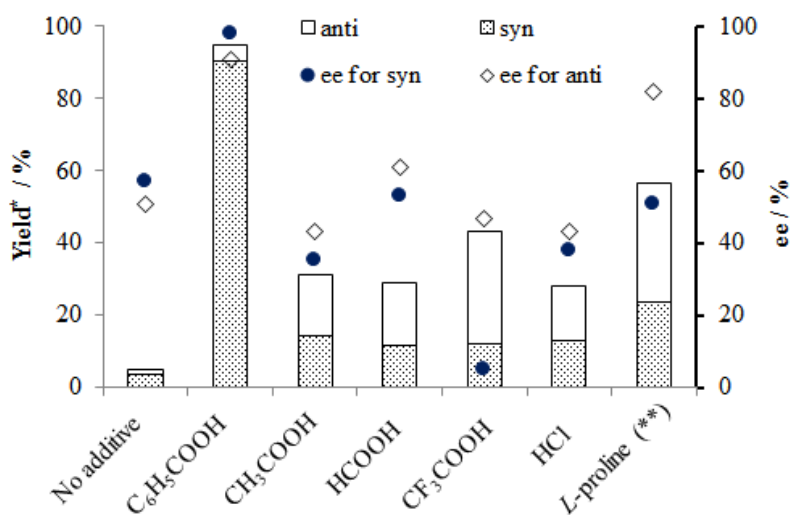


Figure 4.13. The effect of the additives on the performance in the asymmetric aldol reaction carried out in DMSO at 298 K. (*) Isolated yield. (**) The reaction was catalyzed by *L*-proline in the presence of benzoic acid (20 mol%) at 25 °C in 2 days.

The highest conversion and selectivity (namely, 95% in isolated yield, 95:5 for syn:anti and 96% in ee) was obtained with the use of 20 mol% of benzoic acid as additive (**Figure 4.13 and Table 4.2**). In this case no leaching of the *L*-proline into the solution was detected. The amount of *L*-proline in the DUT-67-Pro catalyst remained unchanged, as well as the leaching test confirms the heterogeneity of the catalytic process. A heterogeneity test was carried out for these optimized conditions and monitored by GC (**Figure 4.16a**). After 72 h the catalyst was removed by centrifugation. As expected for a truly heterogeneous reaction, after solid catalyst removal, the aldol reaction essentially stops confirming the purely heterogeneous character of the catalyst.

Table 4.2. The effect of additives on aldol reaction in the presence of DUT-67-Pro catalyst.

N	Additives	pKa ¹⁵³⁻¹⁵⁵	Yield (%)	dr (syn:anti)	ee value (%) (for syn)	ee value (%) (for anti)	<i>L</i> -proline contain**
1	C ₆ H ₅ COOH	4.2 (11.1 in DMSO)	95	95:5	96	3	3.94
2	CH ₃ COOH	4.76 (12.3 in DMSO)	31	46:54	35	43	1.8
3	HCOOH	3.77	19	40:60	53	61	1.2
4	CF ₃ COOH	-0.25	33	28:72	5	47	0.16
5	HCl	-8.0 (1.8 in DMSO)	18	47:53	38	43	0.64
6	4-mercapto-C ₆ H ₄ COOH	4.8	99	83:17	51	41	3.94
7	4-hydroxy-C ₆ H ₄ COOH	4.6	81	68:32	83	33	3.92
8	4-tertbutyl-C ₆ H ₄ COOH	4.4	76	67:33	74	34	3.94
9	4-bromo-C ₆ H ₄ COOH	4.0	56	96:4	62	44	3.90
10*	C ₆ H ₅ COOH	4.2 (11.1 in DMSO)	Trace	-	-	-	
11*	CH ₃ COOH	4.76 (12.3 in DMSO)	Trace	-	-	-	
12*	HCOOH	3.77	Trace	-	-	-	
13*	HCl	-8.0 (1.8 in DMSO)	16%	-	-	-	

*The reaction was carried out in the absence of DUT-67-Pro.

** *L*-proline contain of DUT-67-Pro after using as catalyst was identified by NMR spectra.

The optimized balance between linker, *L*-proline and additive creates a highly efficient catalytic system. The benzoic acid blocks the open metal Lewis-acidic sites and consequently suppresses the catalytic activity of the metal cluster, which would otherwise cause a loss of enantioselectivity.

However, the benzoic acid does not substitute *L*-proline coordinated to the cluster, which would cause leaching and favor the *anti*-isomers formation (Figure 4.13).

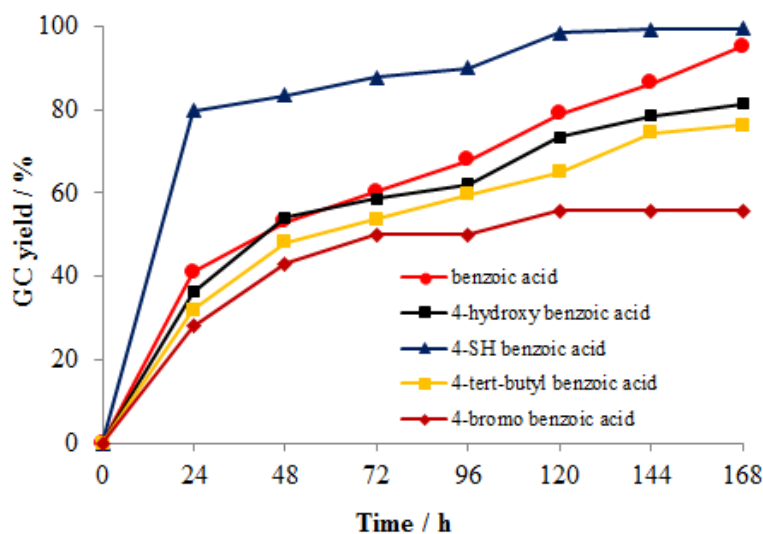


Figure 4.14. The effect of benzoic derivatives on aldol reaction in the presence of DUT-67-Pro catalyst.

To emphasize the role of DUT-67-Pro catalyst, an additional experiment, in which the reaction was catalyzed by both DUT-67 and *L*-proline as separated parts in the use of 20 mol% benzoic acid, was investigated. Expectedly, a substantial drop in diastereoselectivity was recorded, with just 57:43 for *dr* value, while the yield of reaction was 87% (after for 7-day reaction time) and the enantioselectivity was found to be 67% *ee* for *syn*-products (47% *ee* value for *anti*-isomers). Clearly, the combination of DUT-67 inducing *syn*-selectivity and *L*-proline promoting *anti*-*S,R*-enantiomer formation could result in a unique property: preference for *syn*-*S,S*-enantiomer in *syn*-selective aldol addition in the presence of benzoic acid as an additive. Furthermore, the use of various benzoic acid derivatives including 4-bromobenzoic acid (pKa = 4.0), 4-tert-butylbenzoic acid (pKa = 4.4), 4-hydroxy benzoic acid (pKa = 4.6), and 4-mercaptobenzoic acid (pKa = 4.8) as additives was further investigated to clarify the kinetic data of the DUT-67-pro catalyzed aldol reaction (Figure 4.14 and Table 4.2). It should be noticed that the acidic property of additive causes the change in enamine formation and orientation of substrate. Generally, the stereoselectivity as well as yield of reaction is expected to be decreased if the strong acids are applied. The reaction could proceed to 55% yield and 62% *ee* value in the case of 4-bromo benzoic acid, while it produced about 76% yield with 4-tert-butyl benzoic acid. Although a slight increase in reaction rate was recorded in the presence of 4-mercapto benzoic acid, the enantioselectivity

still remained 51% *ee* (Table 4.2). The utilization of aromatic acids clearly leads the better performances than other proton acids.

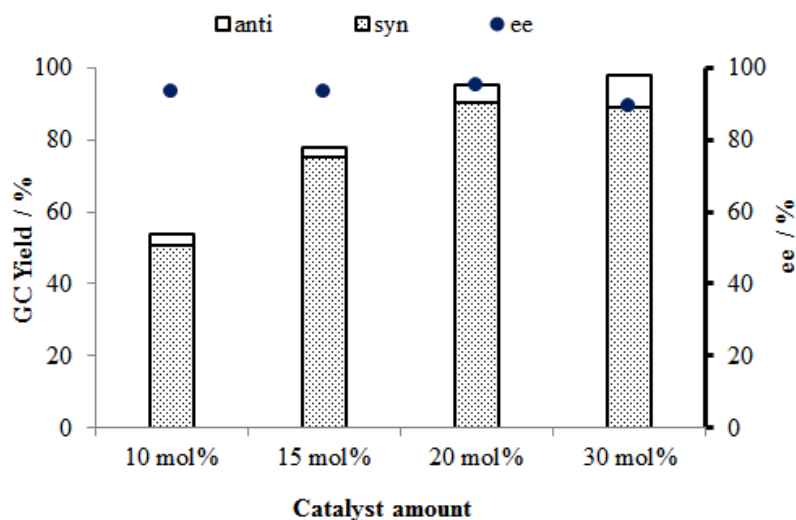


Figure 4.15. The effect of the catalyst amount on the performance in the asymmetric aldol reaction carried out in DMSO at 25 °C.

The influence of catalyst amount was investigated by screening from 0 mol% to 30 mol% DUT-67-Pro. The reaction was carried out in DMSO solvent at 25 °C for 168 hours with the presence of 0.2 equivalents of benzoic acid as additive. As expected, decreasing the mass of catalyst resulted in a significant drop in the reaction conversion (53% for 10 mol% and 78% for 15 mol% DUT-67-Pro), though the enantiomeric excess for *syn*-isomers could still afford to 93% (96:4 *syn:anti*) for both cases. However, it is not essential to employ more than 20 mol% DUT-67-Pro as a slight decrease in stereoselectivity (89% *ee* and 91:9 for *syn:anti*) was observed when 30 mol% catalyst was applied (Figure 4.15). It should be noted that the aldolisation could not be carried out in the absence of DUT-67-Pro.

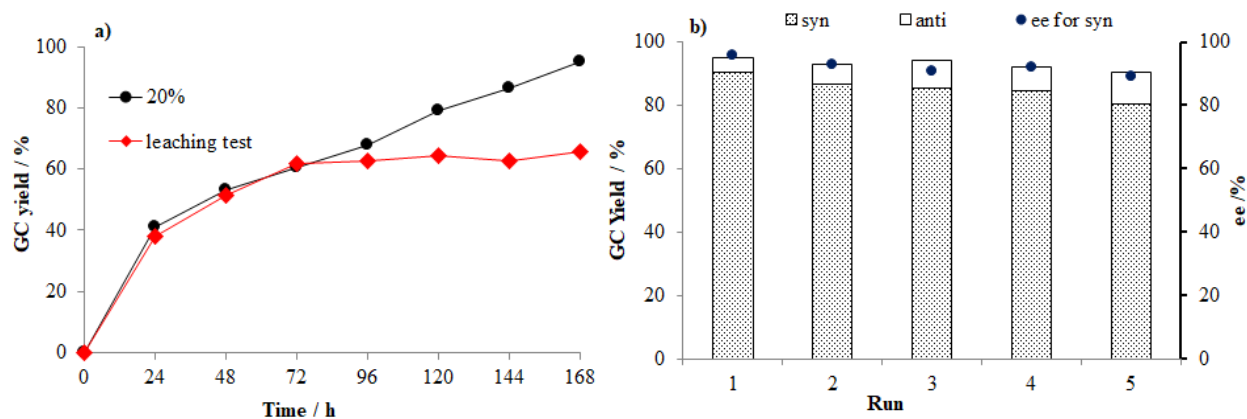


Figure 4.16. a) The leaching test carried out at room temperature. Kinetic progress of the reaction with catalyst (in black cycles) and after filtration of catalyst after 72 h (in red squares). b) Catalyst recycling test. Yield was determined by GC.

An obvious advantage of heterogeneous catalysis is facile and efficient catalyst recycling. The DUT-67-Pro can be reused 5 times with negligible drop in yields and stereoselectivity (only 5% in GC yield and *ee* value after five cycles, **Figure 4.16b**). After a simple recycling procedure (as described in the experimental section), the crystallinity of DUT-67-Pro was well preserved even though the nitrogen adsorption capacity was reduced by approximately 18% to 625 m²/g. The *L*-proline content still remains at ca. 4 molecules per Zr₆-node (**Figure 7.10**). These results show that the DUT-67-Pro catalyst is highly stable under reaction conditions.

4.3 Conclusion

Activity of Zr₆-clusters was found to be origin of high diastereoselectivity in asymmetric aldol addition reactions, predominantly favoring the *syn*-diastereoisomer formation for the addition of cyclohexanone to 4-nitrobenzaldehyde. The catalytic activity and selectivity of Zr₆-clusters, no matter if they are used as homogeneous molecular catalysts or embedded in a solid framework structure, originates from the Lewis acidity of open metal sites and a steric situation with restricted accessibility dictating the preferable *syn*-diastereoselectivity.

In contrast to *L*-proline, a prominent enantioselective catalyst for aldol reactions favoring the *anti*-diastereoisomer formation, *L*-proline functionalized Zr₆-clusters integrated in an 8-connected zirconium-based MOF (DUT-67-Pro) show a high level of diastereoselectivity for preferred *syn*-adduct formation (95 %) combined with excellent enantioselectivity (*ee* = 96 %). The DUT-67 mediated reversed diastereoselectivity combined with high enantioselectivity is a valuable

complement to established organocatalytic catalysts. The crystalline catalyst DUT-67-Pro is easily obtained in a solvothermal reaction in high yields using environmentally benign solvents and subsequent solvent assisted *L*-proline exchange. Solid-state MAS and DNP NMR data of the catalyst localize *L*-proline in close spatial proximity to the TDC linkers in agreement with the expected coordination to the Zr cluster.

Blockage of the Lewis-acidic Zr-sites by adding benzoic acid in the reaction medium is a crucial technique to achieve a high enantioselectivity and cycling stability in this system. Stronger acid additives, in contrast, lead to a loss of selectivity (diastereo- and enantioselectivity) and significant leaching of *L*-proline into the solution as confirmed by NMR analyses.

Cycling and heterogeneity tests render DUT-67-Pro as a highly stable catalyst suitable to heterogeneously catalyze aldol reactions with remarkable enantioselectivity and diastereoselectivity.

Chapter 5

New 1D chiral Zr-MOFs
based on *in situ* imine linker formation
for asymmetric C-C coupling reactions

5.1 Introduction

Schiff-base chemistry has emerged as a simple and useful tool in designing various types of porous solid materials, including metal-organic frameworks (MOFs),¹⁵⁶⁻¹⁵⁹ covalent organic frameworks (COFs),¹⁶⁰⁻¹⁶² and porous organic polymers (POPs).^{163, 164} These imine-based nets generally exhibit high stabilities in most organic solvents, while their nitrogen atoms possibly coordinate to various transition metal ions, offering ideal platforms for catalytic applications.^{51, 165} In fact, metal complexes, based on dynamic imine chemistry, could be employed as effective catalysts for different organic reactions. More importantly, the Schiff-base reactions also are an efficient and environmentally benign approach to generate homochirality.⁵¹ Numerous works recently dedicated to preparation of chiral porous materials based on formations of chiral imine.^{63, 166-168} These materials have not only applied as effective catalysts for asymmetric base-catalyzed reactions, but also offer vast possibilities in post-synthesis *via* chemical conversion of imine groups and metalation.^{64, 169, 170} However, their stabilities are still intrinsic drawbacks to apply in practical applications. Therefore, comprising chiral imine ligands into Zr-based frameworks obviously is an interesting way to prepare crystalline porous materials, possessing high activities as well as outstanding stable structures.^{51, 56}

Attempts for assembling the Zr₆-node and chiral imine ligands into a solid framework structure face two major challenges: (i) The formation of amorphous phases due to rapid nucleation and precipitation, and (ii) The decomposition of imine groups in the acidic environment of Zr-MOFs synthesis. This issue was first mentioned by Zhou and co-workers. Using a mixture of linkers, including (4-[(E)-(4-carboxybenzylidene)amino]benzoic acid) (CBAB) and azobenzene (4,4'-stilbenedicarboxylic acid) (AZDC) forming only a pure phase of Zr-AZDC, PCN-160, in which there was no the presence of CBAB linkers present.¹⁵⁷ This result could be rationalized assuming that the imine bonds in CBAB linkers were broken up during Zr-MOF synthesis, which require either a high temperature (120 °C) or an excess amount of acid modulators.¹⁵⁷ A similar phenomenon was reported by Jiang and Cui on 2018.^{61, 66} Particularly, chiral Zr-MOFs based on salen ligands, in **fcu**-topology, such as UiO-68, could only be obtained through a precious modulated process, while the introduction of these chiral salen linkers into UiO-68 structure could be easily carried out by one- or two-step ligand exchange.⁶¹ In addition, the solubility of chiral diimine linkers also is a certain obstacle to introduce them into Zr-MOF nets.¹⁷¹ However, these disadvantages could be overcome by employing one-pot synthesis, in which either formation of Zr-clusters or imine organic linkers will occur at the same time, limiting the acidic effects of zirconium ion, monocarboxylic acid as

modulators and low solubility of organic linkers. Actually, a series of Ti-MOFs based on imine linkages was successfully synthesized via *in situ* generation of titanium clusters and imine ligands.^{156, 158}

In this chapter, synthesis of a new chiral Zr-MOF, DUT-136, *via in situ* formation of Zr-clusters and chiral imine-organic building blocks is described, and its catalytic activity is evaluated by a wide range of asymmetric C-C coupling reactions.

5.2 Results and discussion

Material synthesis and characterization

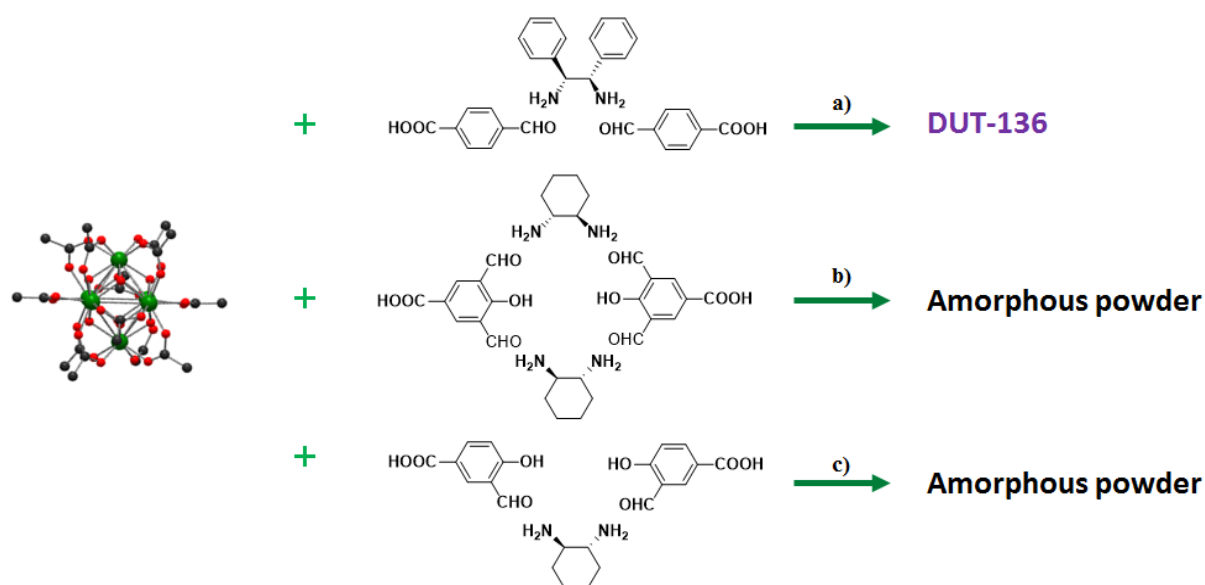


Figure 5.1. Combination of Zr-clusters and some chiral linkers to achieve chiral Zr-MOFs. Color scheme: Zr (green); O (red); C (black).

In our initial work, a systematic study to achieve chiral imine Zr-MOF, assembled from (*R,R*)-1,2-diaminocyclohexane and 3-formyl-4-hydroxybenzoic acid/3, 5-diformyl-4-hydroxybenzoic acid, was carried out. Unfortunately, all efforts following this approach resulted in unknown amorphous phases (**Figure 5.1b and 5.1c**), as indicated by PXRD, while the MOF crystals in **fcu** topology could be successfully reached *via* modulation method as the other derivatives of 3-formyl-4-hydroxybenzoic acid with the *tert*-butyl groups at meta position were employed.⁶⁶ The hydrophobic and bulky groups clearly played an important role in protecting the imine groups from acidic reagents, such as Zr^{4+} , HCl, and modulators in Zr-MOFs synthesis process. Similarly, the diimine ligand built from 4-formylbenzoic acid and (*R,R*)-1, 2-diphenylethylenediamine, in

which the phenyl groups were employed as imine protectors, provided an efficient way to achieve chiral Zr-MOF *via* one-pot synthesis method (**Figure 5.1a**).

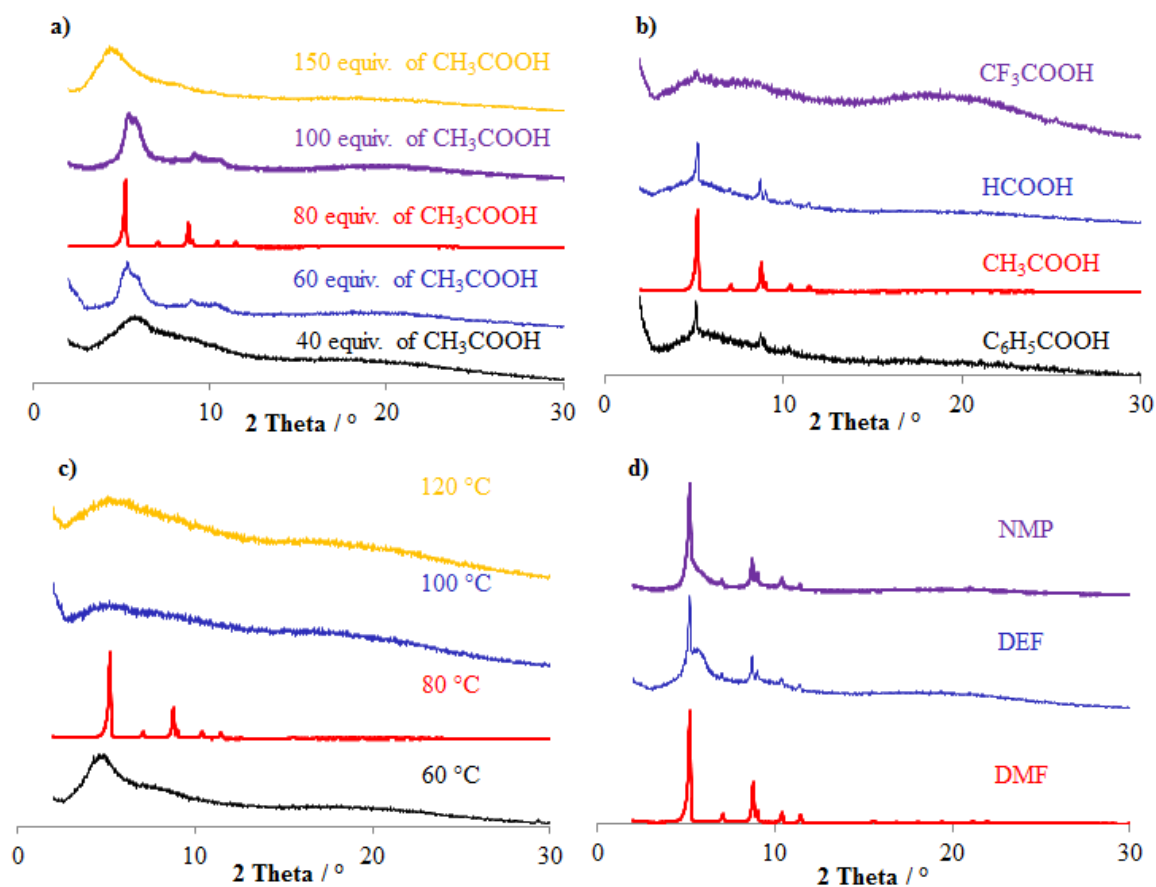


Figure 5.2. Effect of modulator concentration (a); kinds of modulator (b); temperature (c) and solvent (d) on the DUT-136 formation.

As mentioned in the previous reports, the monocarboxylic acids as modulators significantly affect the formation of Zr-MOFs. They not only promote the formation of high quality Zr-MOFs crystals, but also compete with organic building linkers to generate the reduced Zr-cluster connectivity. Hence, a series of various modulators in different concentrations was therefore investigated to obtain the desired products. The reaction was carried out in DMF as solvent at 80 °C in the presence of CH₃COOH as an initial modulator at concentrations from 0 to 150 equivalents to ZrCl₄. However, any attempt with less than 40 equiv. of CH₃COOH only produced amorphous powders, while phases with highest crystallinity were observed with 80 equiv. of CH₃COOH. It was also not reasonable for employing more than 100 equiv. of modulator as no better result was recorded (**Figure 5.2a**).

Besides, the crystallinity was found to be affected by the nature of modulators such as benzoic acid, acetic acid, formic acid, and trifluoroacetic acid. Only poorly crystalline phases were particularly detected in the cases of benzoic acid, and formic acid, while the crystallization was not observed in the presence of CF_3COOH (**Figure 5.2b**). Although, the monocarboxylic acids play a key role in improving the crystallinity of Zr-MOFs, an excess amount of acids could promote the hydrolysis of imine linkers. This explains the formation of the poorly crystallized products in the case of using either a strong acid such as CF_3COOH or a high concentration of modulators. In addition, the fragility of such imine bonds in the acidic environment has also been a major reason for forming non-crystalline powders when diimine linkers are applied directly in zirconium framework assembly. Therefore, the utilisation of one-pot reaction of three components, including 1, 2-diphenylethylenediamine, 4-formylbenzoic acid, and zirconium chloride (**Figure 5.1**) has been found to be an advantageous approach to avoid these inherent drawbacks in the self-assembly synthesis of chiral Zr-MOF based diimine linkers.

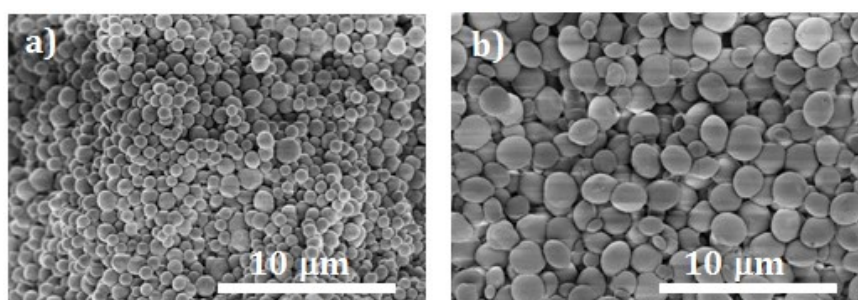


Figure 5.3. SEM images of RR-configuration DUT-136 (a) and SS-configuration DUT-136 (b).

Although, the resulting material was formed as highly crystalline phase, the regular spherical particles with approximately 500 nm observed in the corresponding SEM images (**Figure 5.3**) were inappropriate to be applied to single crystal X-ray diffraction. Consequently, an attempt to improve the quality of crystallites by varying temperature as well as solvent was undertaken in the presence of 80 equiv. of CH_3COOH with stoichiometric ratio of ZrCl_4 :4-formylbenzoic acid:1,2-diphenylethylenediamine being 2:2:1. However, these conditions also lead to poorly crystalline phases. In particular, amorphous powders with a broadened reflection profile were found if conducting the reaction at 60°C in DMF, while further increasing of temperature up to 100°C or 120°C produced only suspended particles with no reflection detected in XRD pattern (**Figure 5.2c**). Besides, the change of solvent to DEF or NMP also resulted in a minor drop in crystallinity (**Figure 5.2d**).

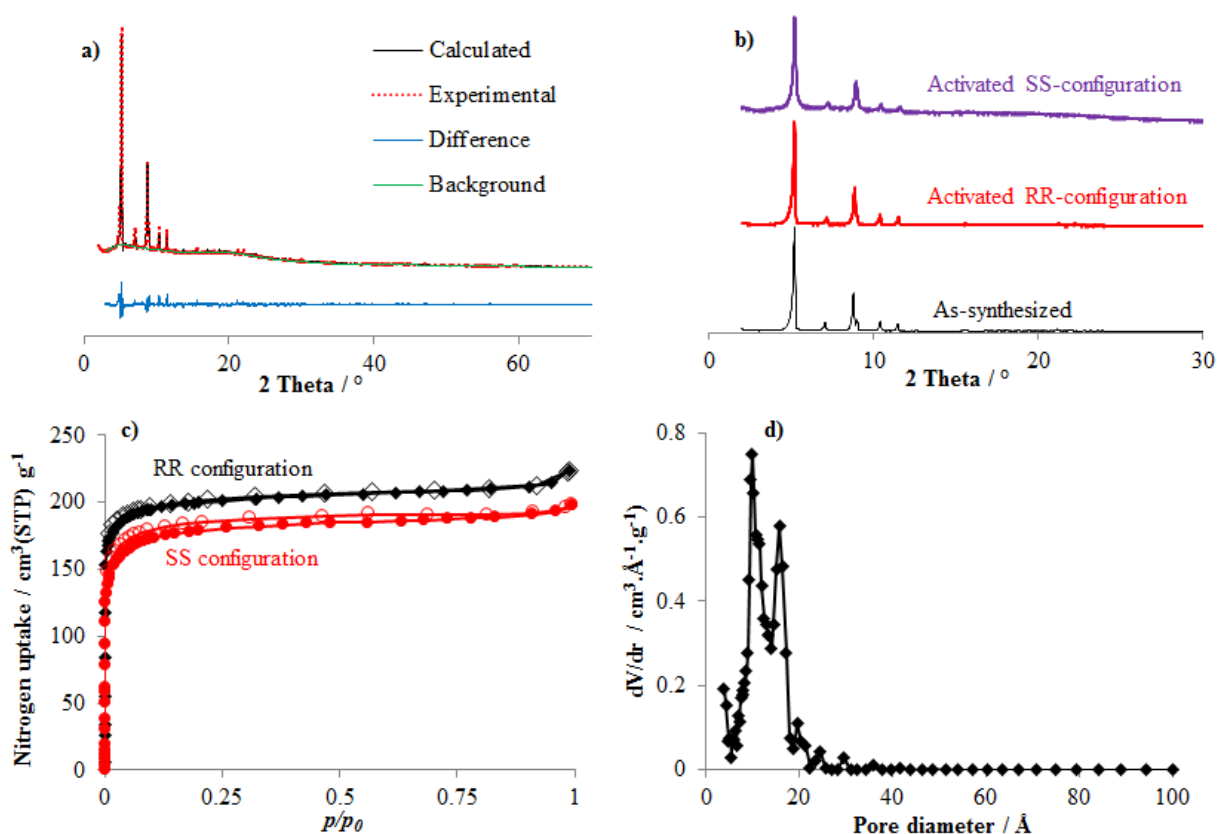


Figure 5.4. a) Rietveld refinement plot of DUT-136; b) PXRD patterns of as-synthesized and activated DUT-136; c) Nitrogen physisorption isotherms of DUT-136 at 77 K; d) Pore size distribution for RR-configuration DUT-136.

Due to the microcrystalline nature of the resulting product, its structure was determined from PXRD data (2θ range of $2\text{--}70^\circ$). Indexing was performed using X-Cell program, which is implemented in Material Studio 5.0 program. The unit cell parameters and PXRD Profile were refined using Pawley fit option of the Reflex module. Since the ligand contains two chiral centers, P3 was chosen a space group. Thompson-Cox-Hastings profile function and Berar-Baldinozzi asymmetry function was used for refinement of profile function and peaks asymmetry. The structure was modelled by using visualization module of material studio. In each unit cell, one Zr_6O_8 cluster was placed and combined with organic linkers. The molar composition of building blocks was based on chemical formula of material, derived from elemental analysis, TG and NMR data. Obtained crystal structure was then optimized using Universal Force Field. This resulting structure was applied as an initial model for the Rietveld analysis. The low data to parameter ratio prompted us to employ the Rietveld refinement with energy option with the energy contribution of 1%. In order to further improve the data to parameter ratio, rigid body option was applied,

resulting in 18 motion groups with 94 degrees of freedom. The main experimental results of the structure refinement are given in the **Table 7.1** and the Rietveld refinement plot is shown in **Figure 5.4a**.

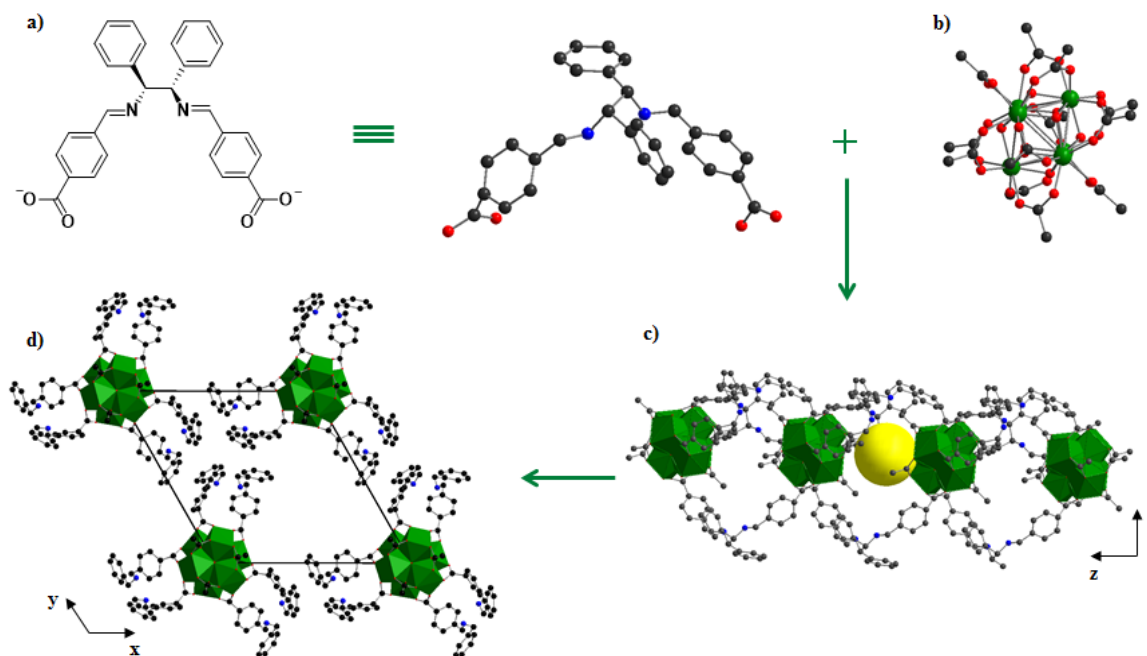


Figure 5.5. Representative schematic of DUT-136 construction: a) organic building block constructed from 4-formylbenzoic acid and (*R,R*)-1, 2-diphenylethylenediamine; b) zirconium cluster; c) connection of Zr-clusters and organic linkers with pore location (yellow sphere); d) unit cell packing diagram of DUT-136. Color scheme: Zr (green); O (red); C (black); N (blue).

In this structure, the interconnection of the well-known hexanuclear cluster $Zr_6O_4(OH)_4$ and diimine building blocks resulted in a 6-connected one-dimensional framework. In other words, each inorganic SBU was connected to six diimine linkers, and each of these linkers was coordinated to two Zr-clusters (**Figure 5.5**). For the charge balance, six molecules of acetate anions were additionally connected at the remaining coordination sites of the Zr-node. Besides, the internal pore of structure with diameters of about 10 Å was determined by zirconium cluster at vertices and the diimine ligand as the edge of cage.

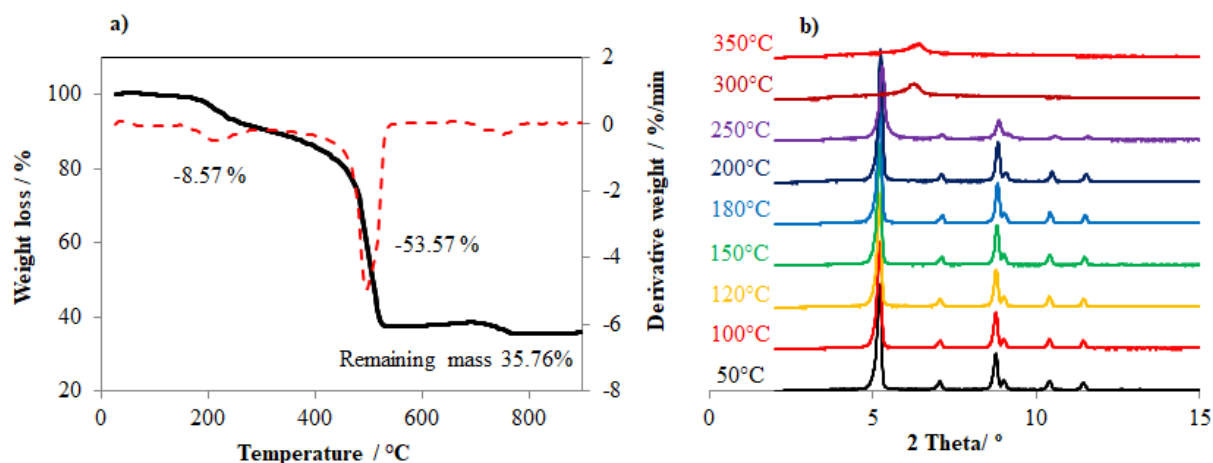


Figure 5.6. a) TGA curve of DUT-136; b) PXRD pattern of DUT-136 dependent on temperature.

The porosity of crystalline material was confirmed by nitrogen adsorption at 77K. After a washing step with acetone and thermal activation at 100°C for 8 hours, the specific BET surface area and total pore volume was recorded as 795 m²/g and 0.35 cm³/g, respectively, in the case of *R,R*-configuration of linker (**Figure 5.4c**). The pore size distribution is based on the none-local density functional theory (NLDFT) for cylindrical pore geometry, shown in **figure 5.4d**. The average pore size was estimated ca. 12 Å, which is close to the pore diameter (10Å) of the cage in the modelled structure. A similar isotherm was also observed for a material containing *S,S*-configuration linkers, which showed 730 m²/g and 0.32 cm³/g for specific BET surface area and total pore volume, respectively.

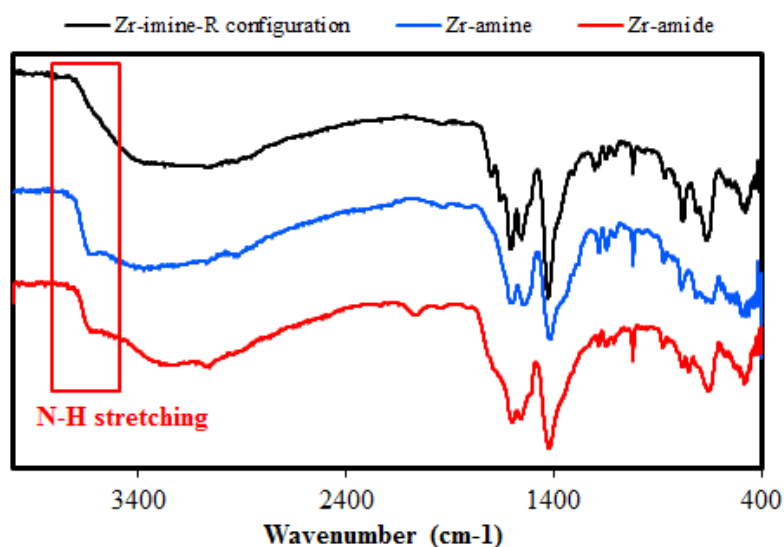


Figure 5.7. DFTIR spectra of imine-DUT-136 and its derivatives.

Furthermore, the thermal stability of the material was investigated by using thermogravimetric analysis and *in situ* thermo-XRD measurement. **Figure 5.6a** contains information about the decomposition of the crystalline product in air following two steps. The first weight loss of 8.57% at 200°C corresponds to the presence of residual DMF solvent and acetate anions as modulators. The next decrease of 53.57% corresponds to the decomposition of the organic building blocks and was observed at 490°C. This oxidation reaction leads to zirconium oxide (ZrO_2) as the final product and its content was recorded as approximately 35.76%, which matches well with zirconium content (27.34%) found by ICP-OES measurement. Together with NMR results of digested samples, a proportion of building blocks was determined in a chemical formula, $\text{Zr}_6\text{O}_6(\text{L})_{2.45}(\text{OH})_2 \cdot (\text{CH}_3\text{COO})_{2.1} \cdot 2.3\text{DMF}$ (L - 4,4'-(((1,2-diphenylethane-1,2-diyl)bis(azaneylylidene))bis(methaneylylidene))- dibenzoic acid). This calculated formula matched well with the composition of refined structure, $\text{Zr}_6\text{O}_6(\text{L})_3(\text{OH})_2 \cdot 6(\text{CH}_3\text{COO})_6$. Otherwise, the variable-temperature powder XRD has been used to ascertain whether the crystallinity of the bulk material is maintained at increasing temperature. The PXRD patterns remained virtually the same up to 250 °C, after that the appearance of amorphous phase was observed following by the decomposition of organic linker starting from 300 °C (**Figure 5.6b**).

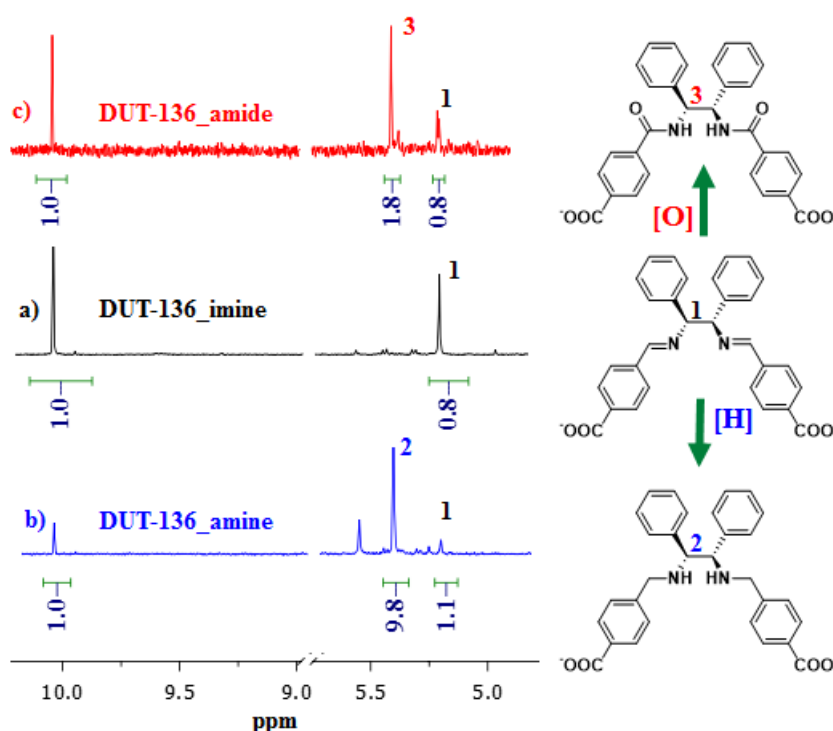


Figure 5.8. $^1\text{H-NMR}$ spectra of digested imine DUT-136 (a), digested amine-DUT-136 (b), digested and amide-DUT-136 (c).

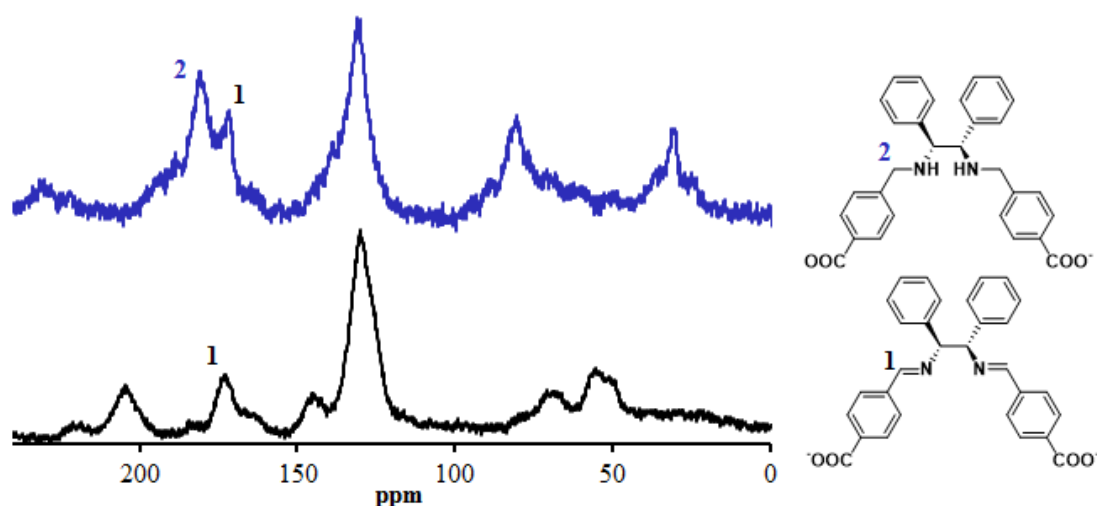


Figure 5.9. Solid state ^{13}C -NMR spectra of imine-DUT-136 (a) and amine-DUT-136 (b).

Utilization of the diimine linkers as organic struts in DUT-136 also offers various possibilities in functionalization *via* chemical conversion of its imine groups. Actually, the amidation and amination of linker in DUT-136 could be carried out under mild conditions. In particular, efforts to generate amine-linker containing structure was achieved up to approximately 92% conversion at room temperature (**Figure 5.8**). The reaction was performed with the presence of sodium borohydride as a reducing reagent in methanol as solvent at room temperature. The success of the reduction was observed by Fourier transform infrared (FT-IR) spectroscopy. The spectrum of reduced material exhibited a broad signal at 3640 cm^{-1} , which was typically assigned to the free N-H stretching (**Figure 5.7**). It indicated that in the structure there are $-\text{NH}$ groups originating from the reduction of imine linker by NaBH_4 . This progression was quantified by NMR spectra of digested samples (**Figure 5.8 and 7.30**). In the spectrum of reduced material, a new signal, attributed to proton at position 2 (**Figure 5.8**), appeared at 5.4 ppm instead of 5.2 ppm characteristic for the parent DUT-136 spectrum (**Figure 5.8**). By comparing the area of these proton peaks, the conversion of the material from imine to amine was calculated to be up to 92%. In addition, the transformation of $-\text{C}=\text{N}$ to $-\text{C}-\text{NH}$ groups was also recorded in solid state ^{13}C -NMR. A new peak, belonging to amine carbon, was observed at 190 ppm along with the signal of imine carbon at 175 ppm, indicating the formation of amine linkages (**Figure 5.9**).

Similarly, the amidation was monitored by FT-IR and NMR techniques. The oxidation reaction was executed by using sodium chlorite as oxidizing reagent in dioxane as solvent. The free N-H

stretching at 3654 cm^{-1} was also observed in the FT-IR spectrum of oxidized material (**Figure 5.7**), however, only 70% conversion of imine linkers, based on the NMR spectrum of functionalized material, was just achieved after 24-hours reaction time (**Figure 5.8 and 7.31**).

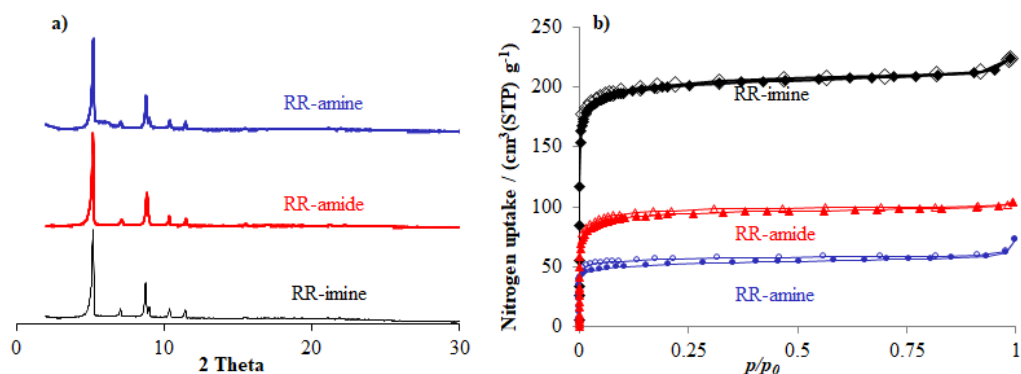


Figure 5.10. PXRD patterns (a) and nitrogen physisorption isotherms at 77 K (b) of imine-DUT-136 (black), amine-DUT-136 (blue) and amide-DUT-136 (red).

The crystallinity of amide- as well as amine-linked framework was confirmed by PXRD measurements (**Figure 5.10a**). The series of sharp peaks in the resulting diffraction patterns was found and matched well with that in the parent DUT-136 pattern. It reveals that no substantial structural rearrangement of the material occurs during the course of chemical transformation. Although, the stability as well as the shape of crystals were still maintained, the nitrogen adsorption capacity at 77 K of oxidized and reduced materials was significantly decreased from $795\text{ m}^2/\text{g}$ to $364\text{ m}^2/\text{g}$ ($0.16\text{ cm}^3/\text{g}$) and $198\text{ m}^2/\text{g}$ ($0.11\text{ cm}^3/\text{g}$), respectively (**Figure 5.10b**). Besides, a similar drop was also found as these materials were tested for CO_2 adsorption capacity at 25°C . A moderate CO_2 uptake of $20.4\text{ cm}^3/\text{g}$ at 1 bar was found in the case of the imine DUT-136, while this value decreased to 10.6 and $6.5\text{ cm}^3/\text{g}$ for the reduced and oxidized material, respectively (**Figure 5.11**).

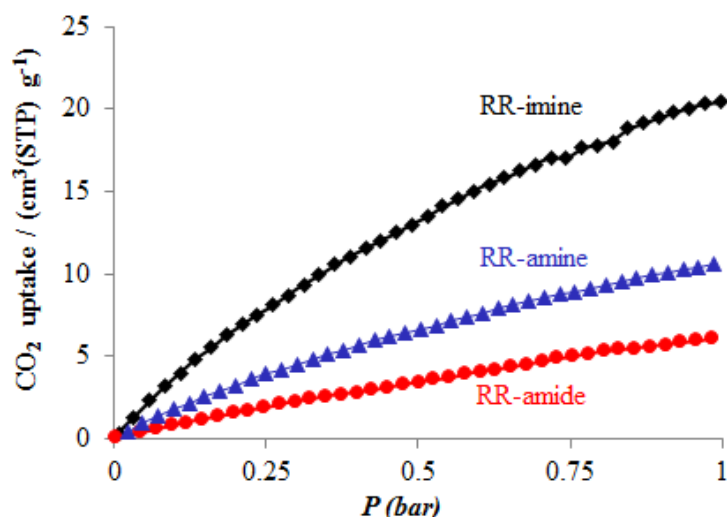


Figure 5.11. CO₂ physisorption isotherms of imine-DUT-136 (black), amine-DUT-136 (blue), and amide-DUT-136 (red).

Catalytic study

To further emphasize the catalytic activity of DUT-136, a wide range of organic transformations, including acid-base and transition metal catalyzed C-C coupling reactions were investigated. As the first model reaction, the Friedel–Crafts alkylation between *trans*- β -nitrostyrene and indole (**Figure 5.12**) was employed to assess the acidic activity of DUT-136. The effect of DUT-136 amount on reaction performance was studied in toluene with *trans*- β -nitrostyrene/indole molar ratio of 1:1.5 at 50 °C (**Figure 5.12**).

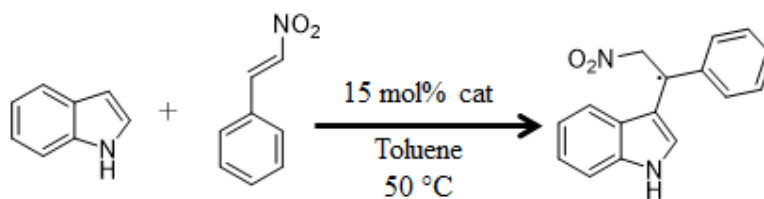


Figure 5.12. Asymmetric Friedel–Crafts alkylation between *trans*- β -nitrostyrene and indole.

A good progress in the reaction conversion was recorded as the catalyst concentration was increased from 5 mol% to 15 mol% (based on Zr content). Particularly, the alkylation of indole was recorded at 33%, and 65% in the presence of 5 mol%, and 10 mol% of DUT-136 catalyst, respectively, while this value in the reaction using 15 mol% of catalyst increases to 88% after 3 days (**Table 5.1**). Clearly, DUT-136 with 6- connected Zr-clusters offers a better way to alkylate

indole than DUT-67, which required 7 days to achieve a similar conversion (90% in yield). However, no enantioselectivity at all was found. This further confirmed that although DUT-136 is built from chiral diimine linkers, the acidic Zr-clusters are non-chiral active sites and the chiral structure has no effect on enantioselectivity of alkylation reaction between *trans*- β -nitrostyrene with indole.

Table 5.1. Performance of various catalysts in the Friedel–Crafts alkylation.

Entry	Catalyst ^a	Reaction time (h)	Gc Yield (%) ^b	<i>ee</i> value ^c
1	DUT-67	168	90	0
2	DUT-67-Pro	168	18	0
3	R-imine-DUT-136	72	88	0
4	R-amine-DUT-136	72	81	0
5	R-amide-DUT-136	72	85	0

^aReaction parameters: 50 °C, 20% mol catalyst based on zirconium content, 1.0 mmol *trans*- β -nitrostyrene, 1.5 mmol indole, 4 mL toluene; ^b Determined by GC; ^c *ee* value was determined by HPLC.

In an effort to demonstrate the function of enantiopure sites in DUT-136, its basic activity based on diimine linkers was investigated *via* an acid-base catalyzed aldol addition of cyclohexanone and 4-nitrobenzaldehyde with the presence of benzoic acid as additive. As expected, a modest enantioselectivity of 5% *ee* for *syn*-isomers (77:23 *dr* (*syn:anti*)) was observed in the reaction carried out in DMSO at 25°C with 20 mol% catalyst (based on diimine linkers) in 7 days (**Entry 4 - Table 5.2**). Although there was a gradual rise in aldolisation yield from 32% to 43% by increasing catalyst amount from 5 mol% to 20 mol%, respectively, to use up to 30 mol% DUT-136 was found to be unnecessary as the reaction performance was not further improved. However, the application of the post-synthetically modified DUT-136 provided a minor enhancement in stereoselectivity. Specifically, the reaction catalyzed by 20 mol% of oxidized material, amide DUT-136, as catalyst could reach up to 48% yield and 7% *ee* for *syn*-isomers (**Entry 6 - Table 5.2**), while this enantiomeric excess in the case of reduced DUT-136, amination form, was 9% (*syn*-isomers) with 55% yield and 77:23 *dr* (*syn:anti*) (**Entry 5 - Table 5.2 and Figure 7.34**).

Table 5.2. Performance of various catalysts in the aldol reaction.

Entry	Catalyst ^a	Cat amount (%)	Gc Yield (%) ^b	dr (<i>syn:anti</i>) ^c	<i>ee</i> for <i>syn</i>
1	R-imine-DUT-136	5	32	-	0
2	R-imine-DUT-136	10	37	-	0
3	R-imine-DUT-136	15	41	-	0
4	R-imine-DUT-136	20	43	73:23	5
5	R-amine-DUT-136	20	55	77:23	9
6	R-amide-DUT-136	20	48	78:22	7

^aReaction parameters: 25 °C, 0.05 mmol benzoic acid, 0.25 mmol 4-nitrobenzaldehyde, 4 mmol cyclohexanone, 1 mL DMSO, reaction time 168h; ^b Determined by GC; ^c *ee* value was determined by HPLC.

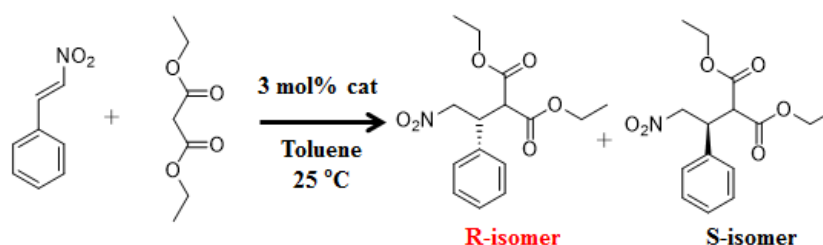
In addition, a similar behaviour was also observed as chiral DUT-136 and its derivatives were used as catalysts in a typical base catalyzed Michael addition of *trans*- β -nitrostyrene and cyclohexanone. Initially, the reaction involving chiral imine DUT-136 catalysts at 50°C in the mixture of isopropanol: methanol proceeded slowly to only 12% yield and 5% *ee* for *syn*-isomers after 7 days reaction time, but a minor progress was detected to 17% yield and 17% *ee* in the presence of trifluoroacetic acid (TFA) as additive (**Entry 3 - Table 5.3**). This recorded value could be even better if the modified DUT-136 materials were used to catalyze the Michael reaction. A yield of 27% with 23% *ee* value was achieved with the chiral amide material, while this value could be improved to 28% yield and a moderate enantioselectivity of 31% *ee* in the case of amine-linked structure (**Entry 7-8 - Table 5.3 and Figure 7.35**). As mentioned in previous part, although the acidic defect sites on Zr-cluster showed inactivity in the Michael reaction, their existence could cause negative effects on performance of the nitrogen-containing functional groups. Hence, the introduction of acid additives not only enhances the formation rate of enamine intermediates, but also improves the ability of DUT-136 and its derivatives in catalyzing the Michael addition of *trans*- β -nitrostyrene and cyclohexanone. Otherwise, by the chemical transformation to amide- as well as amine containing framework, the basicity of DUT-136 material was enhanced. And, this improvement clearly showed better results in enamine-catalyzed reactions.

Table 5.3. Performance of various catalysts in the Michael reaction.

Entry	Catalyst ^a	Cat amount (%)	Additives	Gc Yield (%) ^b	<i>dr</i> (<i>syn:anti</i>) ^c	<i>ee</i> for <i>syn</i> -isomers ^c
1	R-imine-DUT-136	5	TFA	0	-	-
2	R-imine-DUT-136	10	TFA	0	-	-
3	R-imine-DUT-136	20	TFA	17	92:8	17
4	R-imine-DUT-136	20	HCCOH	10	-	-
5	R-imine-DUT-136	20	CH ₃ COOH	11	-	-
6	R-imine-DUT-136	20	C ₆ H ₅ COOH	8	-	-
7	R-amine-DUT-136	20	TFA	28	85:15	31
8	R-amide-DUT-136	20	TFA	27	86:14	23

^aReaction parameters: 50 °C, 0.05 mmol additives, 0.25 mmol *trans*- β -nitrostyrene, 5 mmol cyclohexanone, 4 mL isopropanol:methanol (1:1 v:v); ^b Determined by GC; ^c *ee* value was determined by HPLC.

On the other hand, the diimine linked-frameworks also offer many possibilities for post-synthetic metalation to afford organometallic catalysts. In this context, the DUT-136 and its derivatives were also utilized as solid supports to immobilize nickel (II) catalytic sites to catalyse a cross C-C coupling reaction of *trans*- β -nitrostyrene and diethyl malonate (**Figure 5.13; Figure 7.32-7.33**).

**Figure 5.13.** Asymmetric Ni-catalyzed Michael reaction of *trans*- β -nitrostyrene and diethyl malonate.

Particularly, post-synthetic Ni-metalation of these MOFs materials was performed by immersing it in methanol solution of 1.5 equivalents of Ni(OAc)₂ at 25°C. The resulting materials were then washed several times with methanol to remove unreacted chemicals before activation under vacuum at 100°C in 24h. The presence of modified metal sites was confirmed by ICP-OES, indicating that the immobilization of Ni(II) significantly relied on the nitrogen-containing functional groups in DUT-136. The highest Ni content was found in the amide DUT-136 material with 2.1 wt%, while these results in the case of imine- and amine-linked framework were 1.4 wt%

and 1.7 wt%, respectively. Besides, the PXRD measurement was employed to verify the crystallinity of all resulting samples, which showed no significant change in structure after post synthetic modifications (**Figure 5.14**).

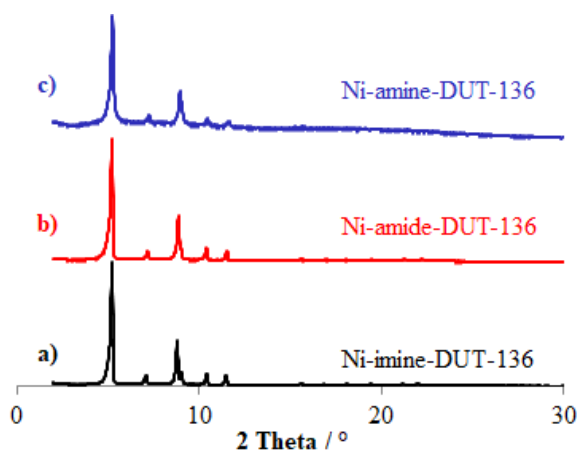


Figure 5.14. PXRD patterns of Ni-imine-DUT-136 (a), Ni-amide-DUT-136 (b), Ni-amine-DUT-136 (c).

To evaluate the catalytic activity, the metallated materials were utilized as solid catalysts in asymmetric cross C-C coupling reaction of *trans*- β -nitrostyrene and diethyl malonate. The reaction was typically carried out in toluene as solvent in the presence of 3 mol% catalyst (based on Ni) at 25°C. It should be noted that no traces of product were detected after 240 hours if the original materials as well as homogeneous Ni(OAc)₂ salt catalysts were utilized, while a yield of 36% could be obtained if Ni(II)-imine DUT-136 was used (**Entry 6 - Table 5.4**). Otherwise, the Ni-catalyzed Michael addition could significantly improve to 63%, and 67% yield as Ni-amide-, and Ni-amine-containing frameworks were applied (**Entry 7 and 8 - Table 5.4**). Moreover, a gradual increase in enantioselectivity toward formation of *R*-configuration isomer was observed. This value improved from 6% *ee* in reactions catalyzed by Ni-imine materials to 16%, and 12% *ee* in reactions catalyzed by Ni-amide-, and Ni-amine-DUT-136, respectively.

Table 5.4. Performance of various catalysts in the Ni-catalyzed Michael reaction.

Entry	Catalyst ^a	Reaction time (h)	Gc Yield (%) ^b	ee value ^c
1	-	240	0	0
2	Ni(OAc) ₂	240	0	0
3	R-amine core + Ni(OAc) ₂	72	100	-34 (S-isomer)
4	S-amine core + Ni(OAc) ₂	72	100	26 (R-isomer)
5	R-imine-DUT-136	240	0	0
6	Ni(II)-R-imine-DUT-136	240	36	6
7	Ni(II)-R-amine-DUT-136	240	67	12
8	Ni(II)-R-amide-DUT-136	240	63	16
9	Ni(II)-S-amide-DUT-136	240	61	18

^aReaction parameters: 25 °C, 3 mol% catalyst based Ni content, 0.25 mmol trans- β -nitrostyrene, 2.5 mmol diethyl malonate, 3 mL toluene; ^b Determined by GC; ^c ee value was determined by HPLC.

More importantly, the utilization of Ni-amide-DUT-136 not only provides a moderate enantioselectivity, but also causes a reversal in enantioselectivity in comparison with the reaction catalyzed by respective homogeneous Ni-complex. In the presence of an organometallic catalyst, obtained from (*R,R*) - 1, 2-diphenylethylenediamine and Ni(OAc)₂, the reaction could proceed to a complete conversion with 34% ee for S-enantiomer, while the ee value toward generating *R*-product was observed to be 26% with the Ni-complex derived from (*S,S*)-diamine core (**Entry 3-4 - Table 5.4 and Figure 7.36-7.37**). Obviously, although Ni-amine-DUT-136 was synthesized from (*R,R*) - 1, 2-diphenylethylenediamine precursor, it promotes the preferable formation of S-enantiomer. To confirm this observation, an additional reaction using Ni-(*S,S*)-amide-DUT-136 as catalyst was investigated under optimized conditions. As expected, the opposite enantioselectivity was also observed with 18% ee for R-isomer (**Entry 9 - Table 5.4**).

Table 5.5. Performance of Ni(II)-R-amide-DUT-136 catalysts in various solvents.

Entry	Catalyst ^a	Solvent	Reaction time (h)	Gc Yield (%) ^b	ee value ^c
10	Ni(II)-R-amide-DUT-136	Toluene	240	63	18
11	Ni(II)-R-amide-DUT-136	THF	240	48	6
12	Ni(II)-R-amide-DUT-136	Dioxane	240	59	8
13	Ni(II)-R-amide-DUT-136	Methanol	240	100	4
14	Ni(II)-R-amide-DUT-136	Ethanol	240	100	5
15	Ni(II)-R-amide-DUT-136	Toluene/Ethanol(1%)	240	100	16
16	Ni(II)-R-amide-DUT-136	Toluene/Ethanol(5%)	240	65	18
17	Ni(II)-R-amide-DUT-136	Toluene/Ethanol(10%)	240	83	19
18	Ni(II)-R-amide-DUT-136	Toluene/Ethanol(15%)	240	98	22
19	Ni(II)-R-amide-DUT-136	Toluene/Ethanol(20%)	240	100	6

^aReaction parameters: 25 °C, 3 mol% catalyst based Ni content, 0.25 mmol *trans*- β -nitrostyrene, 2.5 mmol diethyl malonate, 3 mL toluene; ^b Determined by GC; ^c ee value was determined by HPLC.

Since toluene was inappropriate to achieve better results due to the poor dispersion of chiral DUT-136, the influence of various solvents was investigated to enhance further the performance. It was found that the product formation significantly relies on polarity of reaction solution. In particular, the conversion of *trans*- β -nitrostyrene slowly proceeds in polar aprotic solvents, such as THF, 1,4-dioxane, only affording 48% and 59% yield with modest *ee* values of 6% and 8%, respectively. A perfect conversion was observed when methanol or ethanol was applied as solvent (**Entry 11-14 - Table 5.5**). Although the reaction yield could be significantly improved in polar protic solvents, unexpected low enantioselectivity (*ee* values just remained below 5%) was detected by HPLC. By adjusting the content of ethanol in reaction phase, the polarity could be systematically changed to offer a suitable medium for catalysis. In fact, the yield of reaction could not only gradually increase from 65% to 98% as the ethanol content was changed from 1% to 15%, but also *ee* value could be improved to 22% (**Entry 18 - Table 5.5 and Figure 7.38**). However, further increasing of ethanol content leads to a sharp decrease in enantioselectivity, though the conversion of reaction still reaches an excellent value.

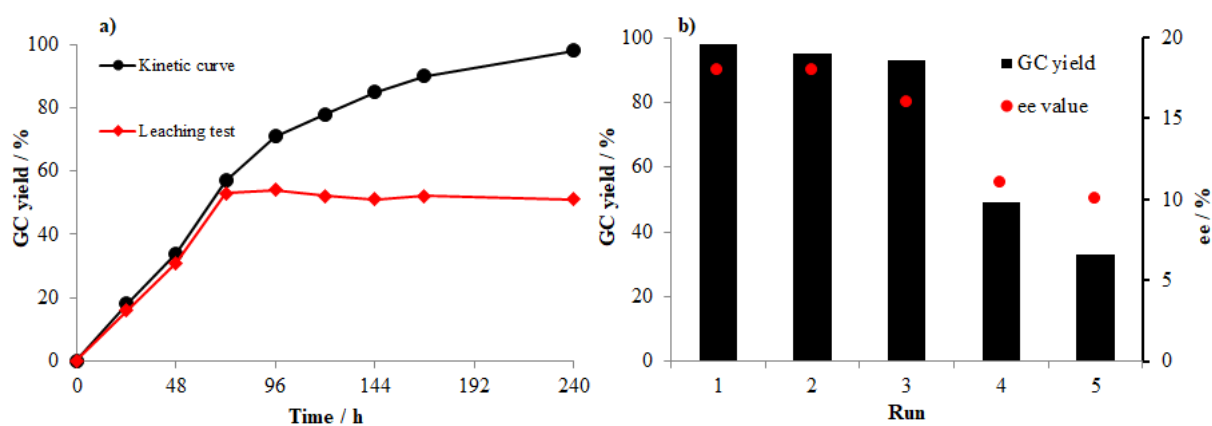


Figure 5.15. a) The leaching test carried out at room temperature. Kinetic progress of the reaction with catalyst (black cycles) and after filtration of catalyst after 72 h (red diamond). b) Catalyst recycling test.

Using the metallated materials as solid catalysts usually results in transfer of metal active sites into the liquid. In this context, the leaching test were performed. Particularly, the reaction was carried out under optimized conditions. The reaction progress was monitored by GC, and the Ni-imine-DUT-136 catalyst was removed by simple centrifugation after the first 72h of reaction time. A similarity in reaction rates was observed, with approximately 42% yield detected after 72h, but no further conversion of main product was found after the solid catalyst was removed (**Figure 5.15a**).

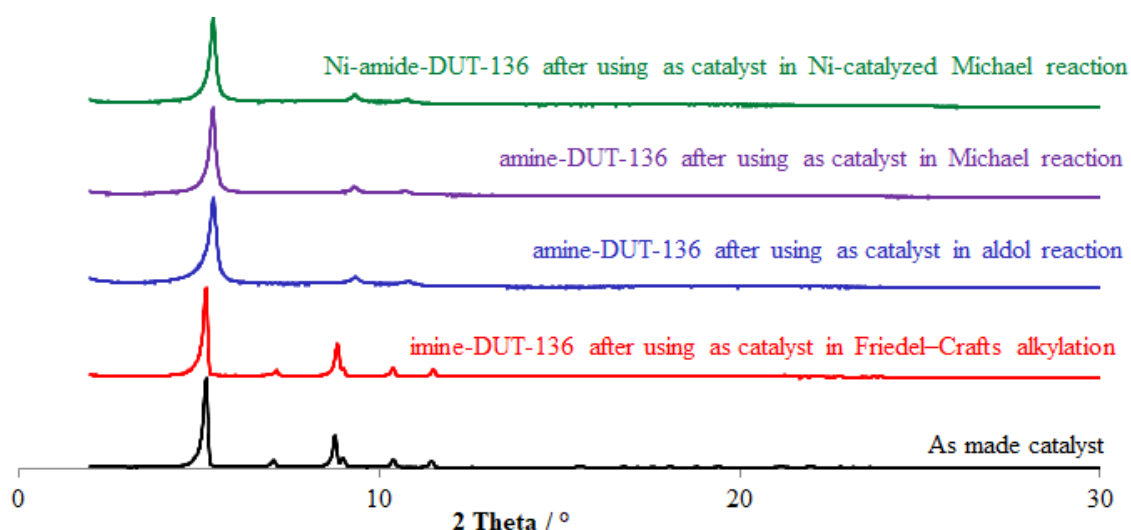


Figure 5.16. PXRD profiles of reused DUT-136 and its derivatives.

Because of the inactivity of nickel salt in presented reaction, ICP-OES measurements were then employed to determine the nickel content in DUT-136, which still maintained at 2.1wt%. This

showed a high stability as well as activity of Ni-amide-DUT-136 after 72h reaction time. To further highlight the advantage of DUT-136 catalyst system, the catalyst recycling experiment was conducted by repeatedly separating the catalyst from reaction phase after every 240h, washing, and activating at 100°C for 8 hours and then reusing it. Expectedly, the reaction performance remains at 62% yield with 18% *ee* for R-isomer after three cycles (**Figure 5.15b**). However, a sudden drop was observed in the 4th run as the reaction only produced 49% yield, while this value has decreased to 33% with 10% *ee* in the next cycle (**Figure 5.15b**). The nickel loading of catalyst dropped to about 1.6 wt%, detected by ICP-OES method, although its high crystallinity remained (**Figure 5.16 and Figure 7.28b**). This shows that the stability as well as activity of Ni-amide-DUT-136 is maintained under these conditions only for three cycles.

5.3 Conclusion

A new chiral metal-organic framework, DUT-136, was synthesized following the one-pot reaction of ZrCl₄, 4-formylbenzoic acid, and (*R,R*)-1, 2-diphenylethylenediamine as an enantiopure core in the presence of CH₃COOH as modulator. Although, the quality of crystalline material was inappropriate for single crystal X-ray analysis, its structure was solved and refined from the experimental PXRD data. In the structure, each hexanuclear Zr-cluster, Zr₆O₄(OH)₄ is coordinated by six diimine linkers, combined from 4-formylbenzoic acids, and 1, 2-diphenylethylenediamine, in one-dimensional chain. Its crystallinity is maintained up to 250 °C, and the BET surface area is at 795 m²/g.

To emphasize the advantages of DUT-136, two chemical approaches to convert it to amide-, and amine-containing frameworks from corresponding chiral imine MOFs were introduced. The oxidized and reduced materials were respectively obtained *via* the amidation and amination under mild conditions, which allowed preserving the original structure. These modified materials also yield better results in asymmetric based-catalyzing reactions. Actually, a moderate performance providing up to 55% yield with 9% *ee* for *syn*-isomers in aldol reaction and 28% yield with 31% *ee* in Michael addition were observed in the presence of the *RR*-amine-DUT-136 as catalyst. However, no enantioselectivity was found for these chiral materials, used in a typical acid-catalyzed reaction, such as the Friedel Craft alkylation. This indicates that although the chiral DUT-136 and its derivatives are built from the chiral struts, the chiral environment maintained no effect on enantioselectivity if the reaction proceeds at the acidic defect sites on Zr-clusters. In

other words, the enantiopure active sites are only located at the nitrogen-containing functional groups, and only provided a moderate enantioselectivity for enamine-catalyzed reactions.

The chiral DUT-136 and its derivatives were employed as effective carriers for immobilizing Ni(II) active sites through a simple post-synthetic metalation. Especially, the Ni-containing chiral amide-DUT-136 materials were highly active in asymmetric carbon-carbon cross coupling reactions of *trans*- β -nitrostyrene and diethyl malonate, affording perfect conversions, while their chiral environment resulted in modest enantiomeric excess values. However, astonishing inversion of enantioselectivities as compared to the reactions catalyzed by the corresponding homogenous Ni-complex catalysts was observed. The materials could be easily reused at least three times without any significant degradation in catalytic activity.

Chapter 6

Conclusions and Outlook

6.1 Conclusions

Because of high hydrolytic stability, the chiral Zr-MOFs are efficient solid catalysts in fine chemical syntheses. In this context, two benign approaches were introduced to produce two potential asymmetric zirconium MOF catalysts:

- (i) One material is obtained in the post-synthetic modification of 8-connected Zr-clusters of a well-known Zr-MOF, DUT-67 with chiral active sites, *L*-proline.
- (ii) Another originates from a one-pot reaction of $ZrCl_4$, 4-formylbenzoic acid and (*R,R*)-1, 2-diphenylethylenediamine as an enantiopure core.

The reduced Zr-cluster connectivity opens up many opportunities to diversify the stable zirconium MOFs. Through solvent-assisted ligand incorporation method, the *L*-proline molecules were successfully coordinated to 8-coordinated Zr-octahedral clusters of DUT-67. This exchange approach could be easily applied to DUT-67, possessing CH_3COOH or $HCOOH$ as original modulators. According to 1H -NMR of the digested modified material, the degree of *L*-proline incorporation substantially depends on the exposure time of the parent DUT-67 to incoming modulator solution. Besides, the location of *L*-proline modulators around Zr-clusters was indirectly confirmed through a close spatial proximity between these chiral compounds and thiophene linkers, observed in solid-state MAS and DNP NMR spectra.

The catalytic activity of DUT-67-Pro was deeply investigated in various asymmetric acid-base catalyzed reactions. The results indicate that the enantiopure sites are connected *L*-proline moieties, while the acidic property of DUT-67, originating from defect sites, has a negative effect on the performance of asymmetric nitrogen-functional groups. This influence was observed as DUT-67-Pro was applied as a solid catalyst in a typical asymmetric Michael addition of *trans*- β -nitrostyrene and cyclohexanone. Following the evolution of the *L*-proline functionalization degree, the reaction performance was significantly improved to 98% yield combined with a moderate enantioselectivity (38% *ee*), which was comparable with that of *L*-proline homogeneous catalyst. The activity of the catalyst also remained at least in 5 recycling cycles.

Moreover, the defect sites of DUT-67-Pro are responsible for the absence of enantioselectivity in aldol addition of 4-nitrobenzaldehyde and cyclohexanone. A potential reason is that the reaction occurs at acidic centers instead of enantiopure *L*-proline sites. However, the Zr-cluster leads to an

interesting inversion in diastereoselectivity. To simultaneously maintain the steric effect of Zr-clusters and enantioselectivity of *L*-proline sites, a strategy using additional modulators as acid blockers was thus employed in reaction phase. Expectedly, the DUT-67 with integrated *L*-proline showed a high level of diastereoselectivity for preferred formation of *syn*-configuration products (95 %) with excellent enantioselectivity (*ee* = 96 %) in the presence of benzoic acid as additive. And, the DUT-67-Pro showed a high stability in recycling test.

In the next effort, the one-pot strategy was applied to produce a novel pair of chiral Zr-MOFs. DUT-136 was obtained from ZrCl₄, 4-formylbenzoic acid, and (*R,R*)-1, 2-diphenylethylenediamine. The 6-connected Zr-clusters in its structure were linked by diimine ligands, formed directly during the synthesis process. Inspired from the facile transformations of the C=N double bond to amide as well as amine groups, two chemical reactions, including oxidation and reduction, were employed to generate the chiral amide- and amine-linked frameworks, respectively. These modified materials were then used as carriers, which could easily coordinate Ni(II) ions *via* a simple post-synthetic metalation.

Despite the presence of chirality on the organic building blocks, a near achiral environment still maintained around the acidic Zr-clusters of DUT-136 and its derivatives, resulting in no enantioselectivity for a typical acid-catalyzed reaction as Friedel Craft alkylation of *trans*- β -nitrostyrene and indole. In the case of enamine-catalyzed reactions proceeding at nitrogen-containing functional groups, including Michael addition of *trans*- β -nitrostyrene and cyclohexanone or aldol reaction of 4-nitro-benzaldehyde and cyclohexanone, moderate enantiomeric excess values could be observed. Besides, this chiral environment around immobilized Ni(II) active centers affords good performance in asymmetric carbon-carbon coupling reactions of *trans*- β -nitrostyrene and diethyl malonate. It should be noted that these catalytic systems also provided an inversion of enantioselectivity as compared to the homogeneous catalyst.

The presented results in this work provides a better understanding regarding synthesis, characterization as well as catalytic behavior of chiral zirconium-based metal-organic frameworks. The Zr-clusters as acidic centers negatively compete in the performance with integrated enantiopure basic active sites. Therefore, it is necessary to choose a proper strategy to use or limit the acidic effect of Zr-clusters for achieving a high stereoselectivity. The Zr-clusters in some asymmetric organic reactions could also act as steric hindrance groups, affording an

inversion in diastereoselectivity or enantioselectivity in comparison with homogeneous catalysts. This, together with high thermal and chemical stability, make chiral Zr-MOFs more interesting for designing new asymmetric catalysis systems.

6.2 Outlook

To further emphasize the role of Zr-clusters in stereoselectivity reversal, a systematic study regarding the size of reagents, such as *trans*- β -nitrostyrene, 4-nitrobenzaldehyde, and cyclohexanone should be intensively investigated. By using other derivatives of these chemicals, the interaction between Zr-clusters and different bulky substituents can be studied and provide a comprehensive understanding about the steric effects of Zr-clusters in asymmetric organic transformations. Computational tools should be also applied to confirm the reaction mechanism pathways in the presence of chiral Zr-MOFs and give predictions when and why Zr-clusters will afford an inversion of enantioselectivity or diastereoselectivity in asymmetric synthesis.

Moreover, the pore accessibility of chiral Zr-MOF is an important factor impacting their catalytic activity. A sufficient reaction space in chiral Zr-MOFs is necessary to accommodate reagents as well as intermediate compounds and release desired products during the reaction phase. In the case of DUT-136 and its derivatives, the steric hindrance of phenyl groups on organic building blocks as well as the small pore size (approximately 10Å) could be a rational reason for their poor enantioselectivity. In the next attempt, strategies using a mixture of chiral and achiral linkers of the same length or prolonging chiral organic linkers could be used to design chiral Zr-MOFs with high accessible reaction spaces.

An efficient method to approach chiral Zr-MOFs with bigger pore sizes is *in situ* imine bond generation, in which the formation of chiral imine linkers as well as Zr-clusters can take place simultaneously. By this approach, length of chiral imine building blocks can be simply adjusted without any trouble regarding poor linker solubility or linker preparation. In addition, the acidic property of zirconium ions has no effect on imine functional groups due to blockage by modulating molecules. Therefore, this strategy needs to be further investigated to diversify organic building blocks.

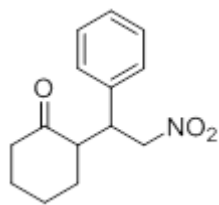
There is remarkable progress in design and application of chiral Zr-MOF in the last decade, however, this field is still in an early phase. A vast number of challenges as well as opportunities remains and need to be solved, for example:

- i) How to improve crystallinity of chiral Zr-MOFs;
- ii) How Zr-clusters affect on the enantiomer formations;
- iii) How to approach a suitable chiral environment in a Zr-based framework for a specific asymmetric organic reaction.

With undeniable advantage regarding high stability, chiral Zr-MOFs will be efficient solid asymmetric catalysts, which could be applied in large-scale asymmetric synthesis of important optically pure organic compounds.

Chapter 7

Appendix



2-(2-Nitro-1-phenylethyl)cyclohexan-1-one: $^1\text{H-NMR}$ (300 MHz, CDCl_3) δ : 7.28 - 7.07(m, 5H), 4.85 (dd, 1H), 4.56(dd, 1H), 3.70(dt, 1H), 2.65-2.62 (m, 1H), 2.38 - 2.35 (m, 2H), 2.00 - 1.99 (m, 1H), 1.65 - 1.45 (m, 4H), 1.18 - 1.14 (m, 1H). $^{13}\text{C-NMR}$ (100 MHz, CDCl_3) δ : 211.91, 137.73, 128.83, 128.25, 127.65, 77.21, 52.52, 43.92, 42.31, 33.19, 28.50, 25.02. MS ($\text{M} + \text{H}^+$) 248.12

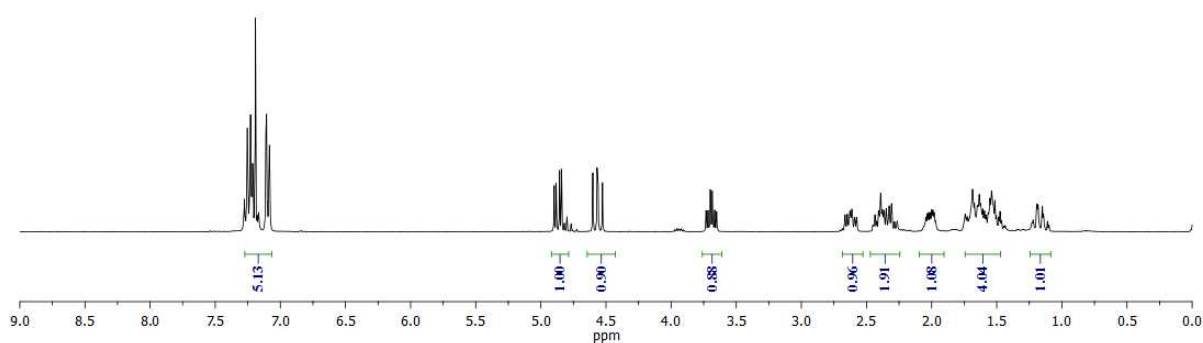


Figure 7.1. $^1\text{H-NMR}$ spectrum of 2-(2-nitro-1-phenylethyl)cyclohexan-1-one.

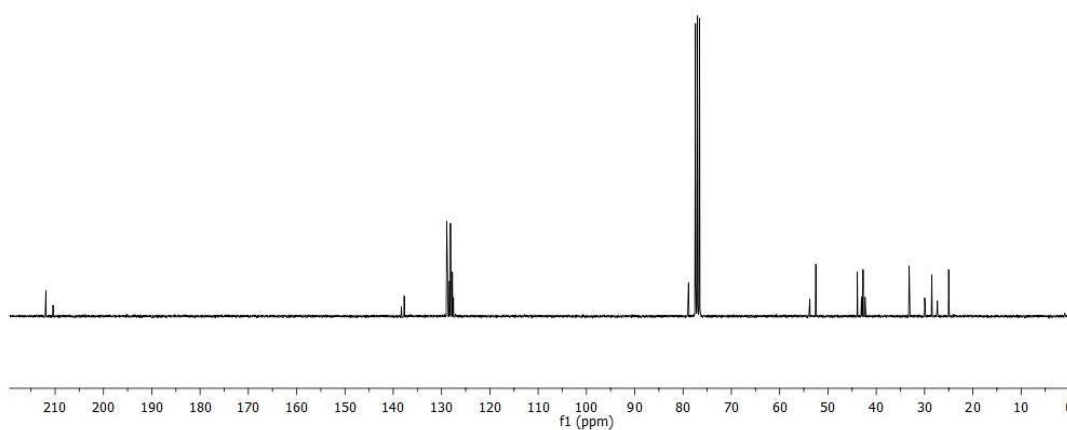


Figure 7.2. $^{13}\text{C-NMR}$ spectrum of 2-(2-nitro-1-phenylethyl)cyclohexan-1-one.

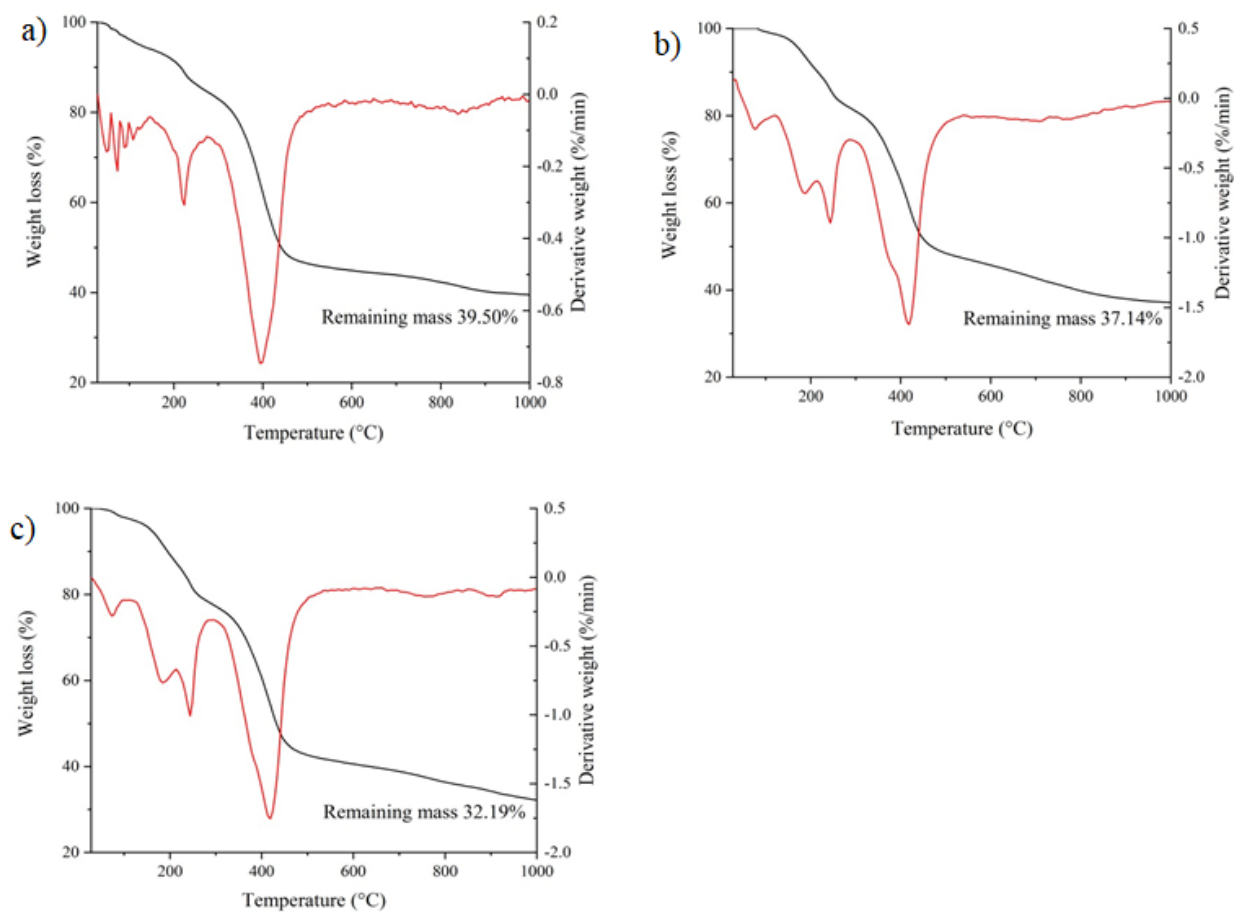


Figure 7.3. (a) TGA curve of DUT-67 synthesized in DMF/NMP, (b) TGA curve of DUT-67-Pro synthesized in DMF, (c) TGA curve of reused DUT-67-Pro.

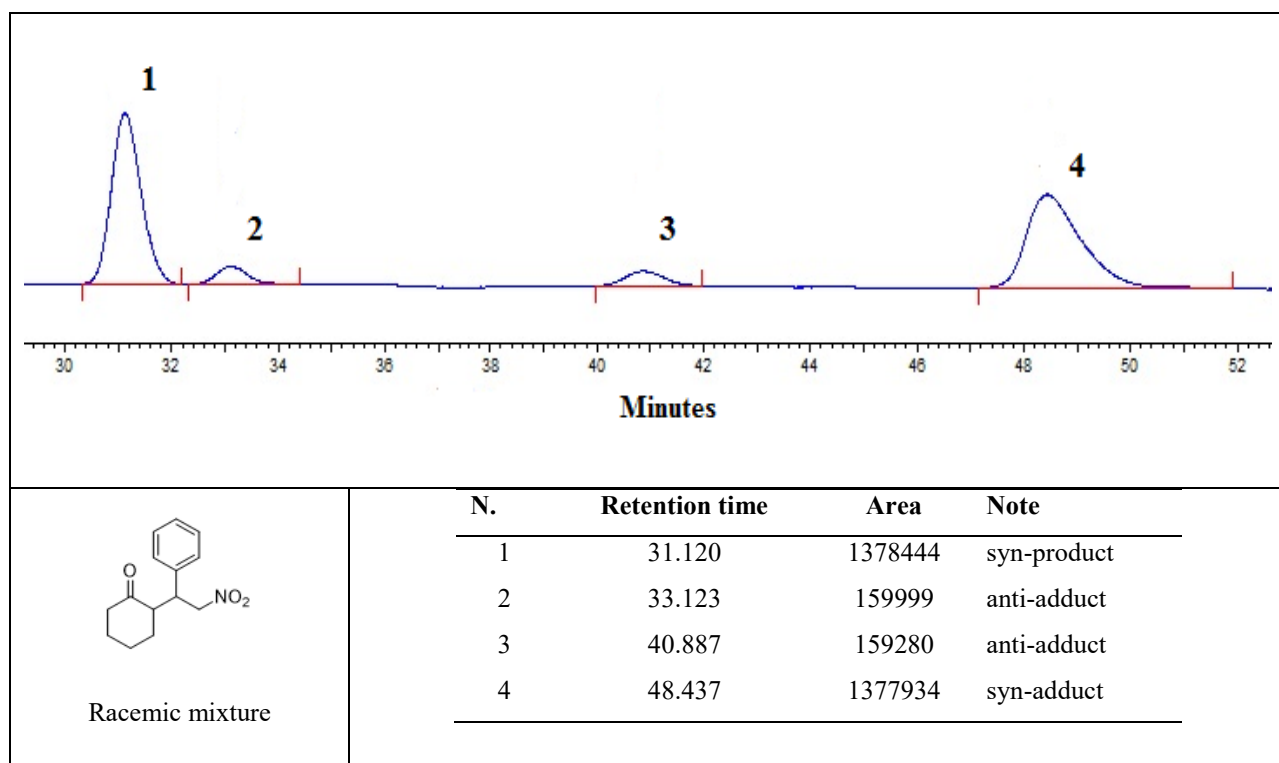


Figure 7.4. HPLC spectrum of the 2-(2-nitro-1-phenylethyl)cyclohexan-1-one enantiomers produced in the presence of *DL*-proline as catalyst.

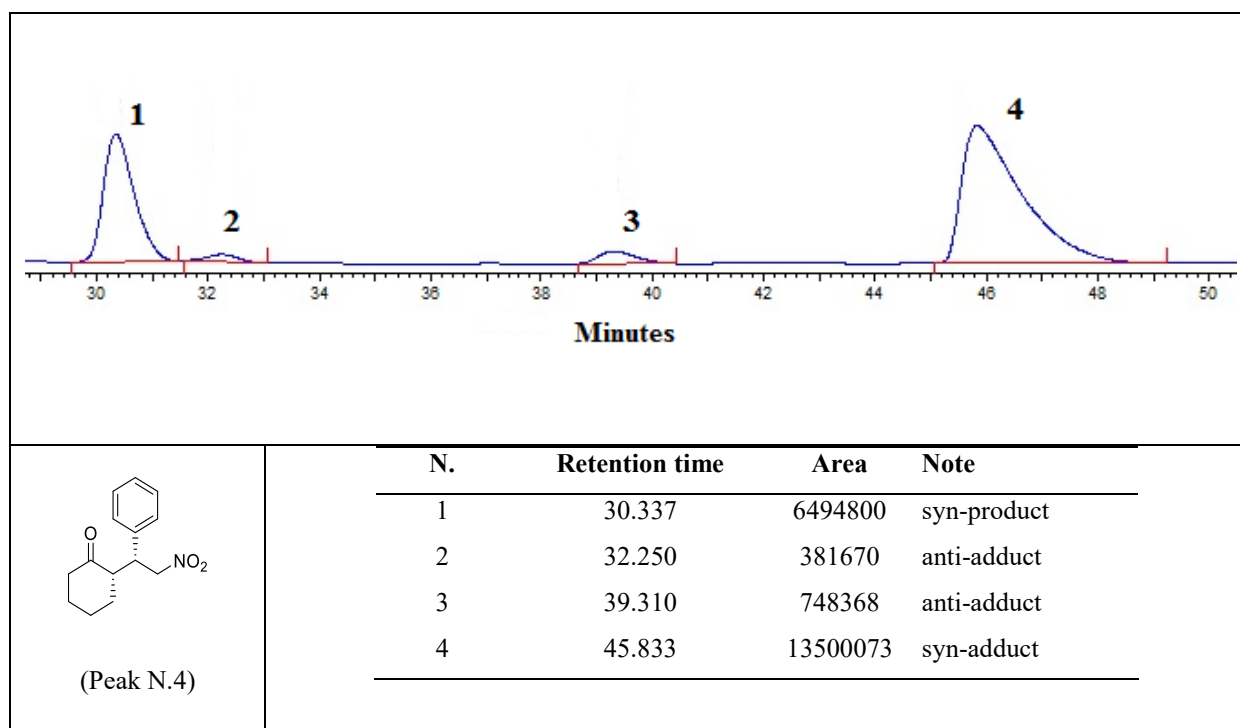


Figure 7.5. HPLC spectrum of the 2-(2-nitro-1-phenylethyl)cyclohexan-1-one enantiomers produced in the presence of DUT-67-Pro as catalyst in isopropanol.

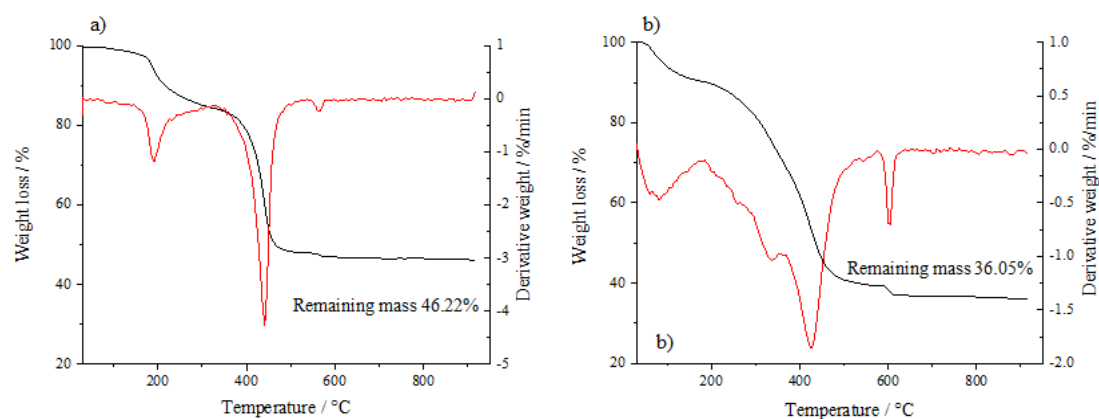


Figure 7.6. (a) TGA curve of DUT-67 obtained from the synthesis in $\text{H}_2\text{O}/\text{CH}_3\text{COOH}/\text{C}_2\text{H}_5\text{OH}$; (b) TGA curve of DUT-67-pro prepared in ethanol.

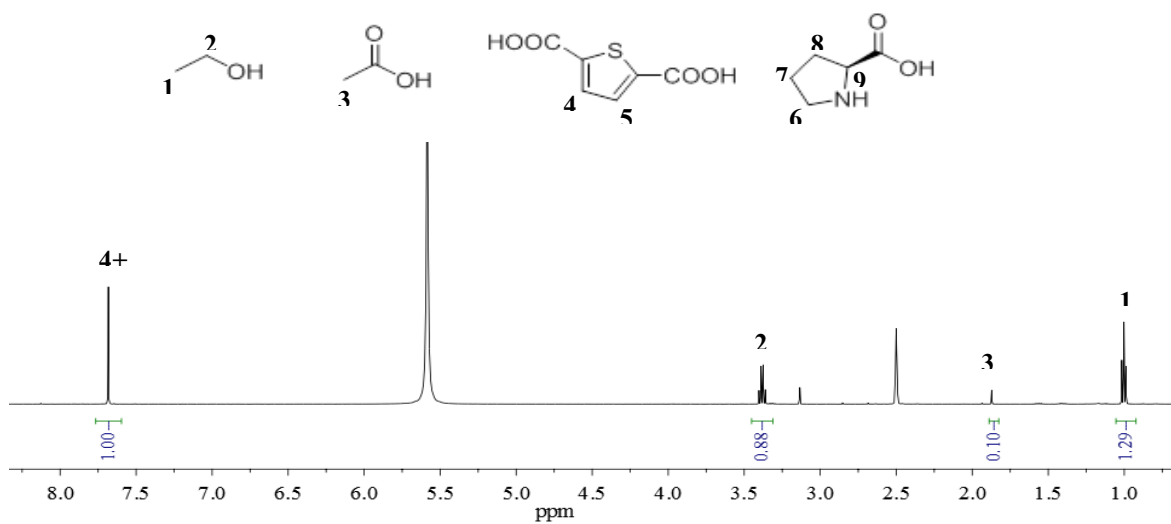


Figure 7.7. $^1\text{H-NMR}$ spectrum of digested activated DUT-67 obtained in the synthesis performed in $\text{EtOH}/\text{H}_2\text{O}/\text{CH}_3\text{COOH}$ as solvent.

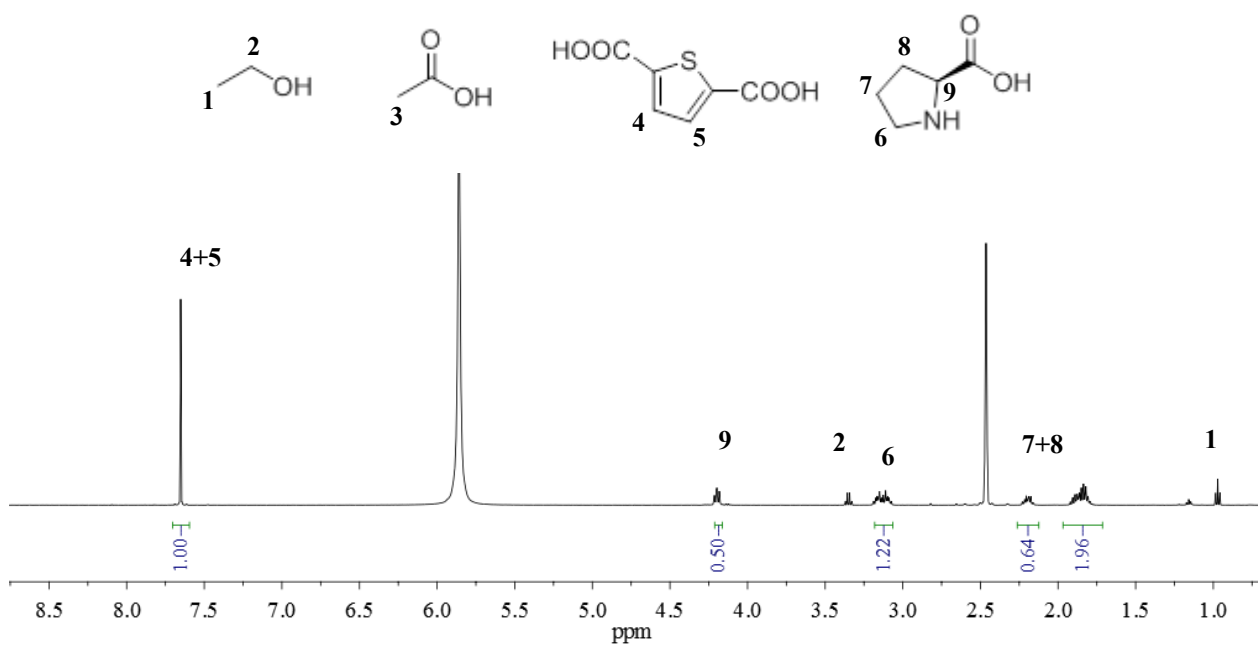


Figure 7.8. $^1\text{H-NMR}$ spectrum of digested activated DUT-67-Pro.

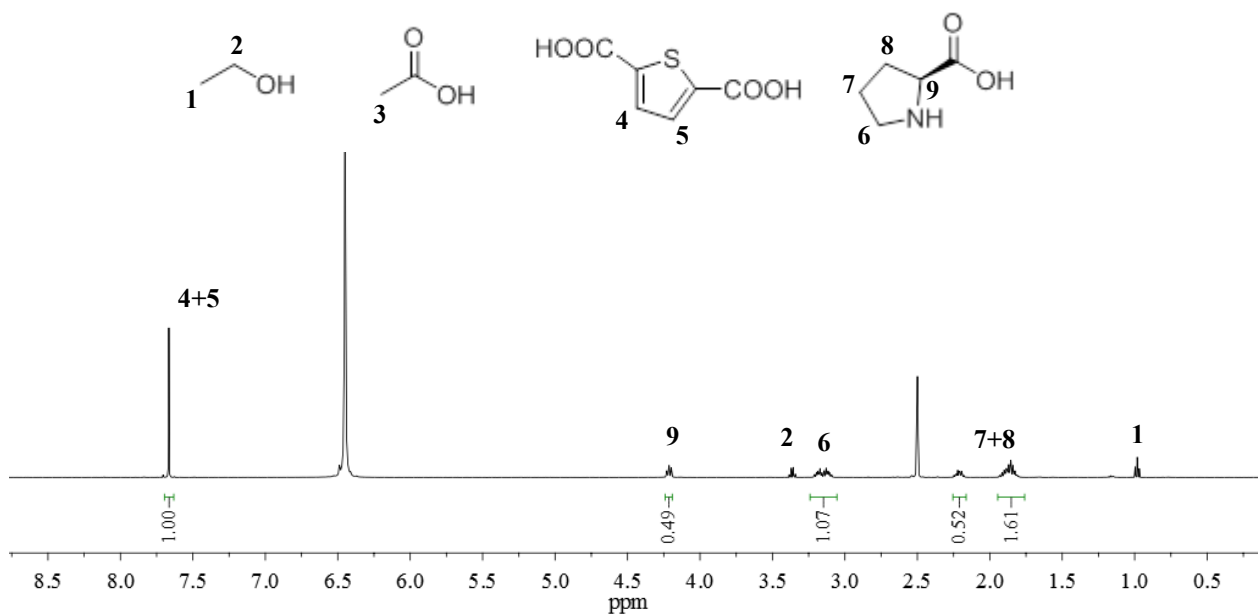


Figure 7.9. $^1\text{H-NMR}$ spectrum of digested activated DUT-67-Pro catalyst applied in the asymmetric Aldol reaction with the presence of benzoic acid as additive.

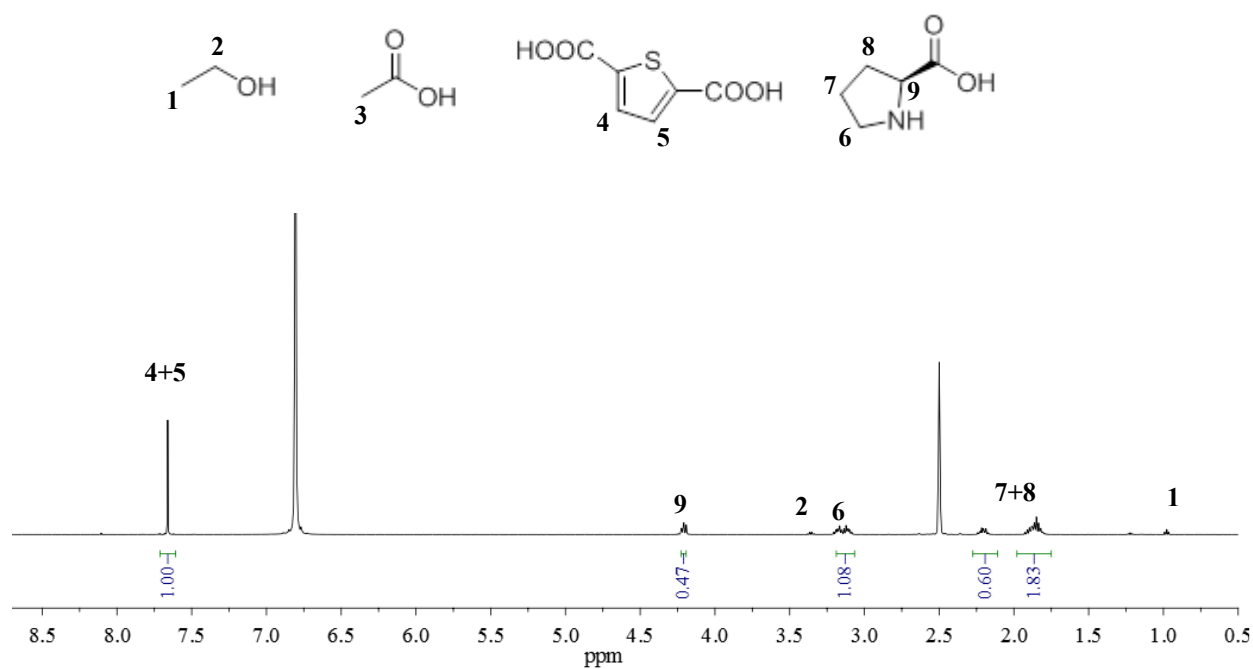


Figure 7.10. $^1\text{H-NMR}$ spectrum of digested activated DUT-67-Pro used in two catalytic cycles.

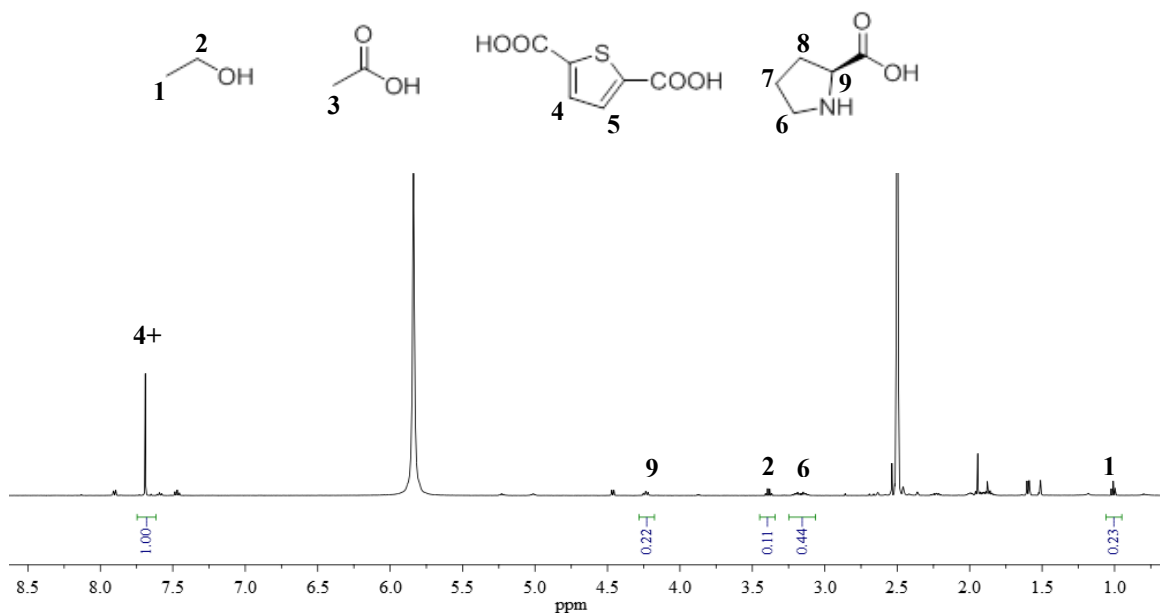


Figure 7.11. $^1\text{H-NMR}$ spectrum of digested DUT-67-Pro catalyst applied in the asymmetric aldol reaction with the presence of CH_3COOH as additive.

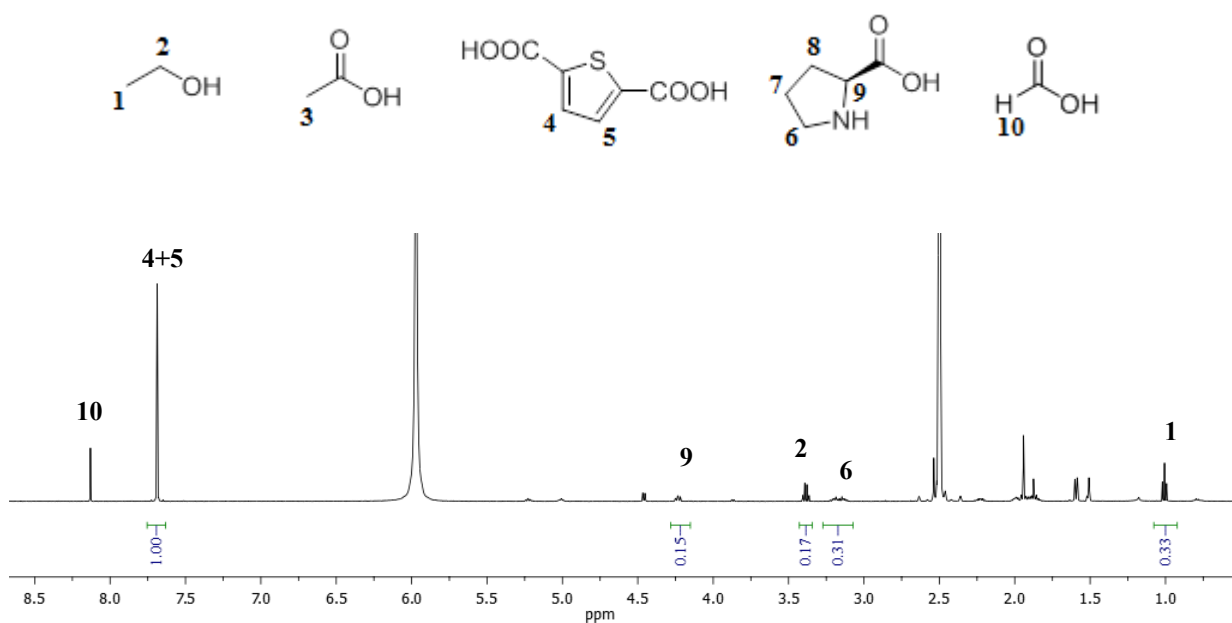


Figure 7.12. $^1\text{H-NMR}$ spectrum of digested DUT-67-Pro catalyst applied in the asymmetric aldol reaction with the presence of HCOOH as additive.

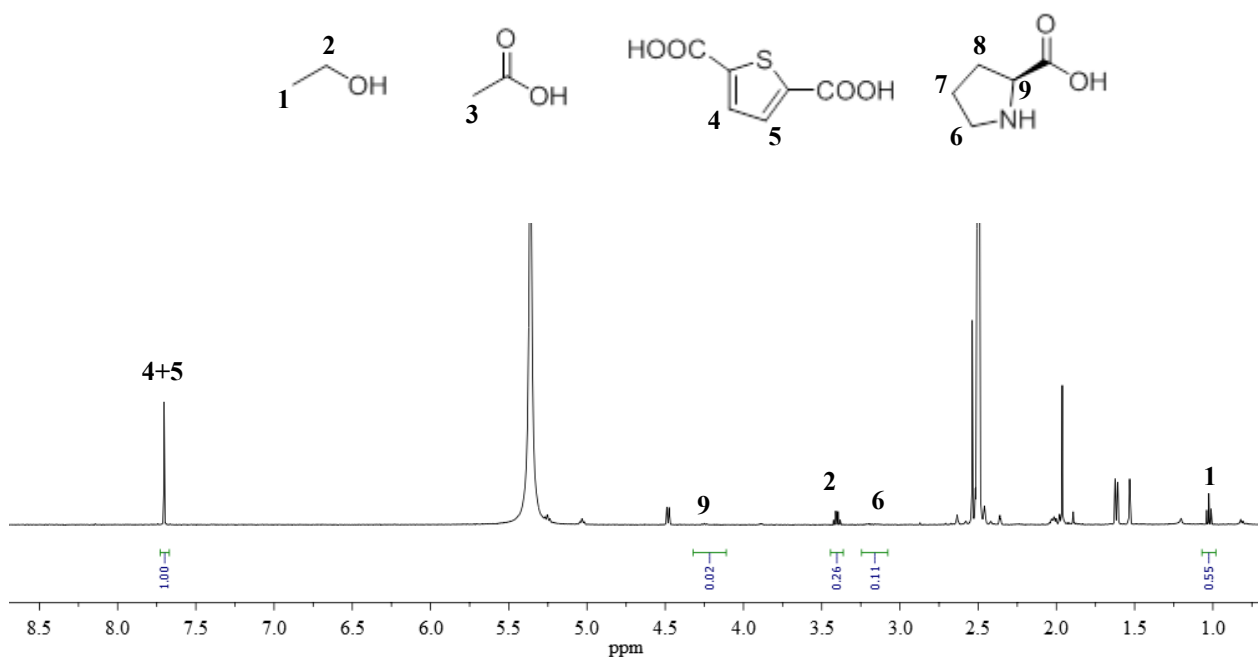


Figure 7.13. $^1\text{H-NMR}$ spectrum of digested DUT-67-Pro catalyst applied in the asymmetric aldol reaction with the presence of CF_3COOH as additive.

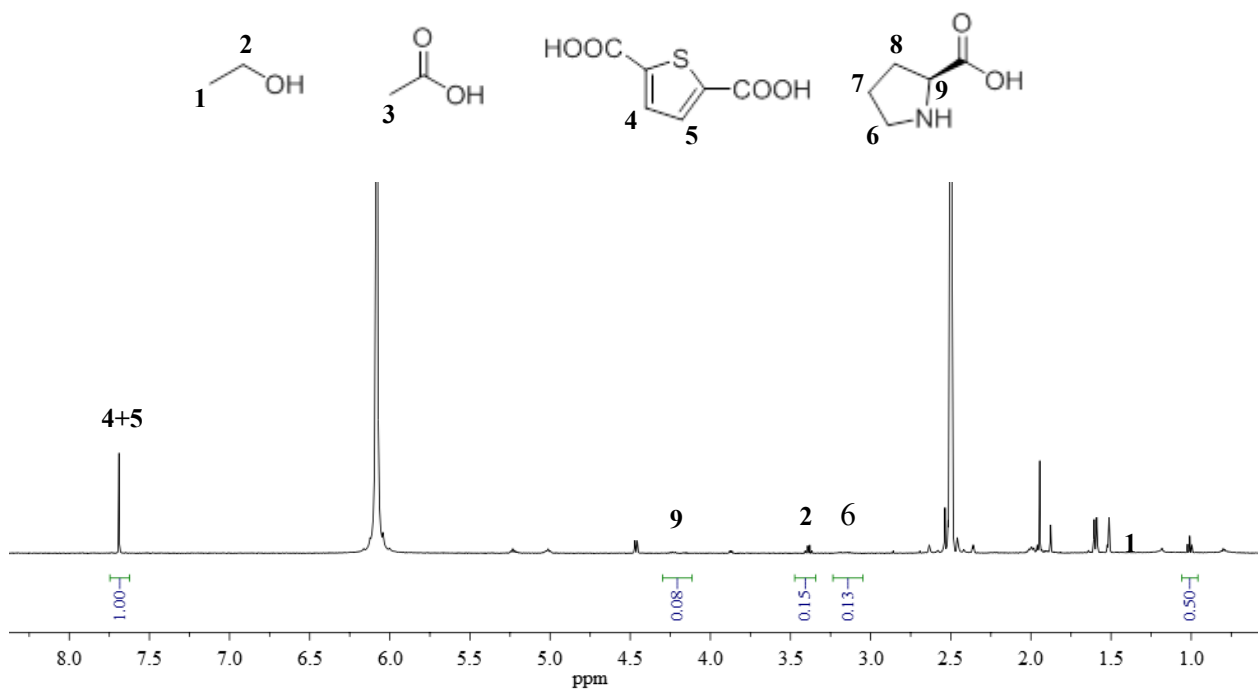


Figure 7.14. $^1\text{H-NMR}$ spectrum of digested DUT-67-Pro catalyst applied in the asymmetric aldol reaction with the presence of HCl as additive.

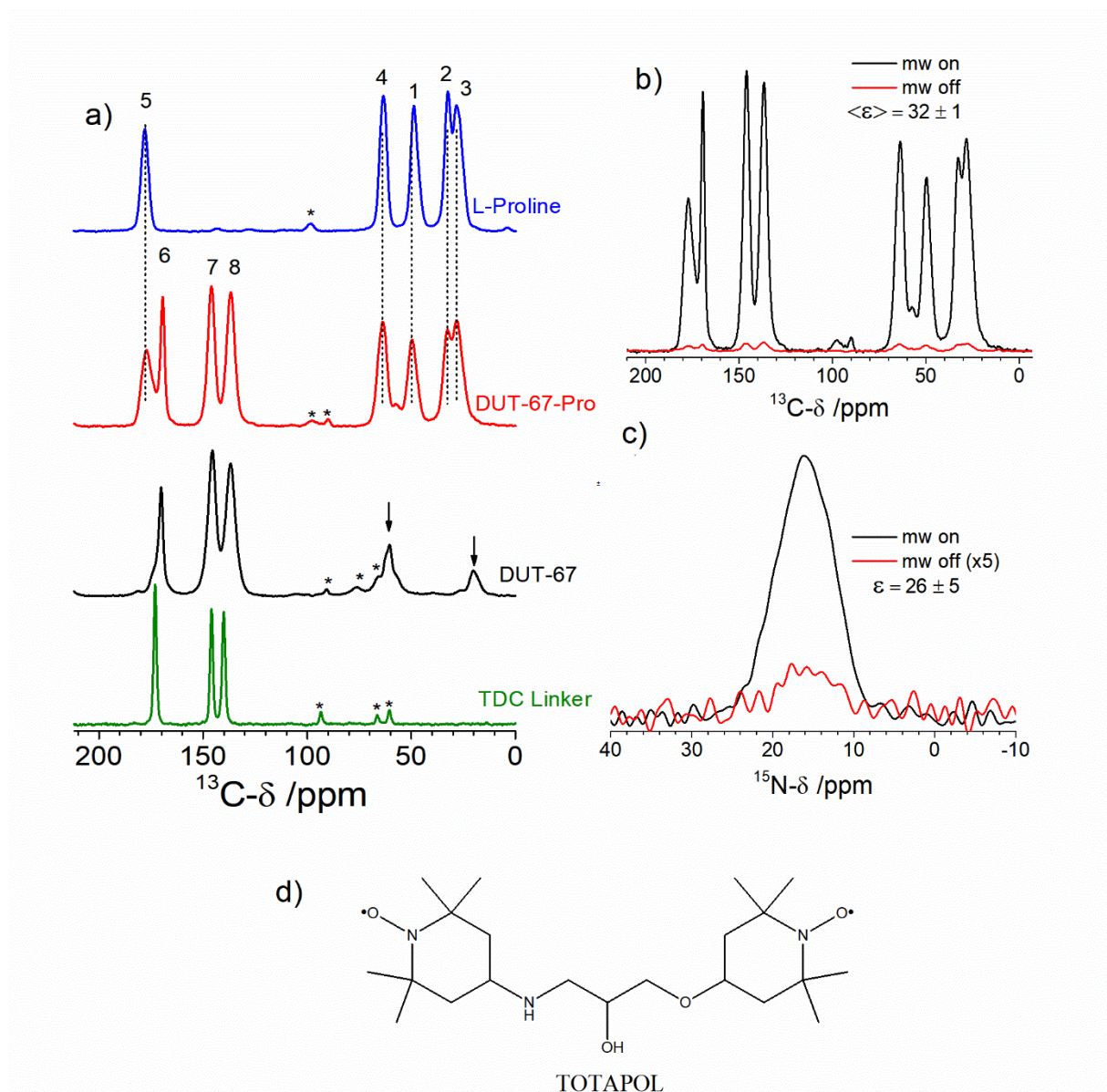


Figure 7.15. a) DNP enhanced $^{13}\text{C}\{^1\text{H}\}$ CP MAS spectra of the compounds studied in this work. b) $^{13}\text{C}\{^1\text{H}\}$ CP MAS and c) $^{15}\text{N}\{^1\text{H}\}$ CP MAS spectra of DUT-67-Pro measured with microwave off (mw off, red line) and microwave on (mw on, black line) to analyze the signal enhancement. Enhancements indicated in the figure were obtained by comparison of the spectral areas. d) Structure of the TOTAPOL radical. Note: The total measurement times were 5 min for the $^{13}\text{C}\{^1\text{H}\}$ CP MAS spectra (mw on and off). For the $^{15}\text{N}\{^1\text{H}\}$ CP MAS spectra the total measurement times were 2 h with mw irradiation (mw on) and 14 h without mw irradiation (mw off), respectively.

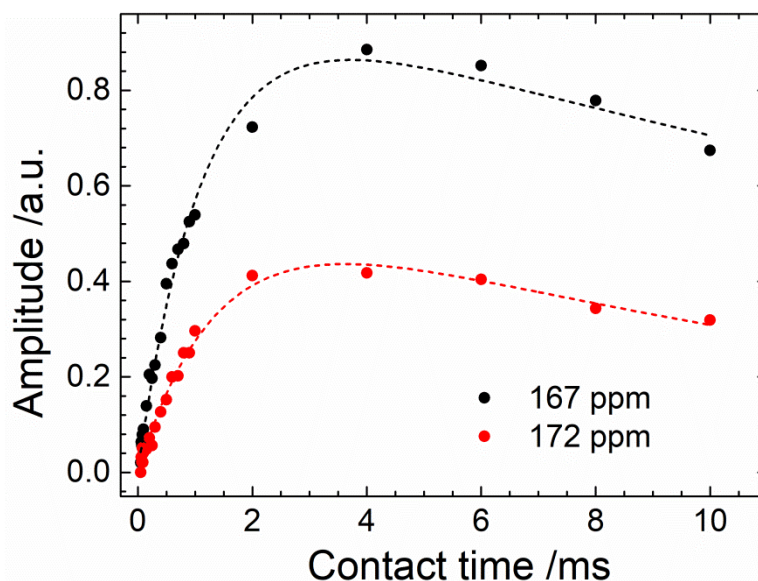


Figure 7.16. Amplitudes of the DNP enhanced ^{13}C CP MAS signals at 167 and 172 ppm in DUT-67 as a function of the contact time. Amplitudes were obtained by Gaussian deconvolutions of the ^{13}C CP MAS spectra for each contact time. Dashed curves represent least-square fittings to Equation 1. The experiment was performed at low temperature (~ 120 K) using DNP enhancement to obtain satisfactory signal-to-noise ratio, in order to clearly resolve the intensity evolution of the signals at 172 ppm and 167 ppm. Characteristic times T_C (the cross-relaxation time between ^1H and ^{13}C , which is the characteristic time for polarization transfer) and T_1^ρ (^1H spin-lattice relaxation time in the rotating frame) can be determined by fitting the curve to the following expression¹⁷²: $I(t) = \frac{I_0}{1-T_C/T_1^\rho} \left(1 - e^{-\frac{1-T_C/T_1^\rho}{T_C}t} \right) e^{-\frac{t}{T_1^\rho}}$, where I_0 is the equilibrium ^{13}C magnetization intensity. The fitting results in T_C values of 1.4 ± 0.1 ms and 1.1 ± 0.1 ms and T_1^ρ of 14 ± 2 ms and 25 ± 1 ms for the lines at 172 ppm and 167 ppm respectively.

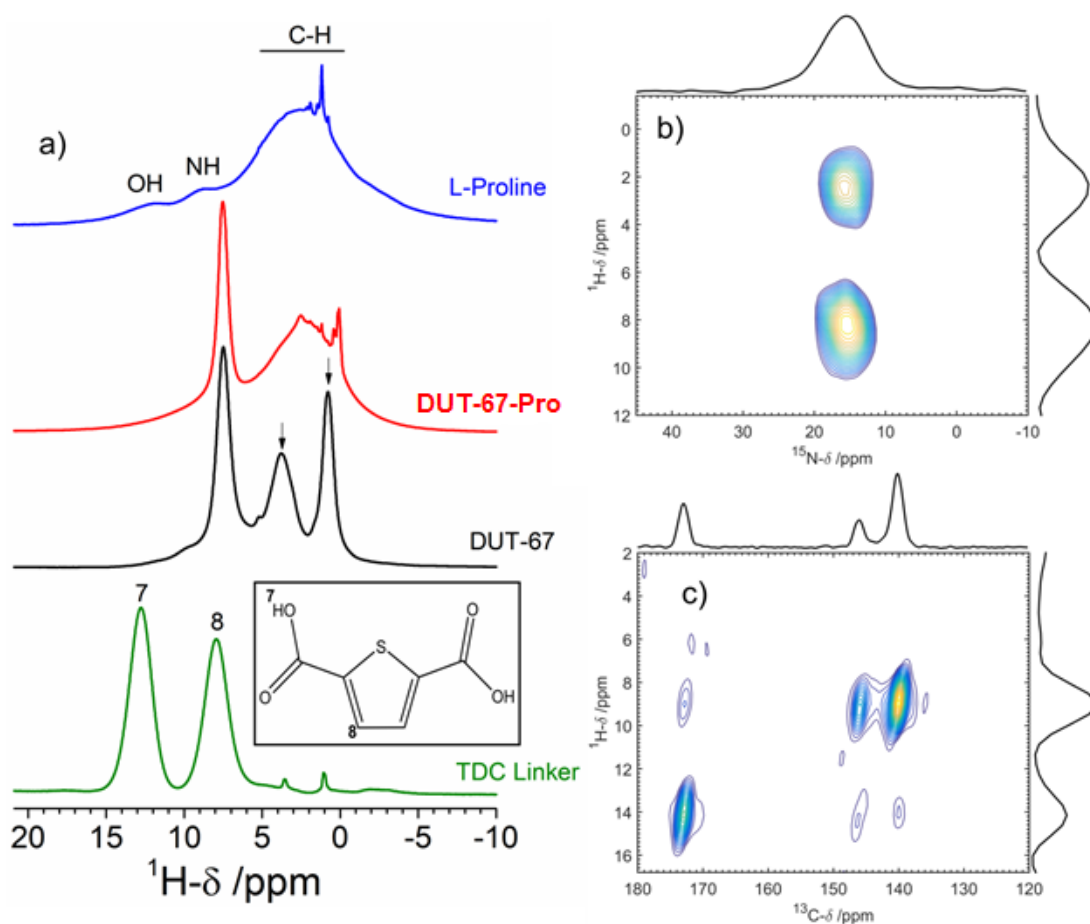
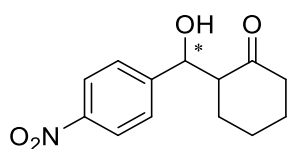


Figure 7.17. a) ^1H MAS NMR spectra of the compounds studied in this work measured at 14.1 T with a spinning frequency of 22 kHz. Peaks marked with arrows probably correspond to adsorbed water and/or ethanol in the MOF structure. b) DNP enhanced $^{15}\text{N}\{^1\text{H}\}$ CP MAS FSLG HETCOR spectra of pure *L*-proline. c) DNP enhanced $^{13}\text{C}\{^1\text{H}\}$ CP MAS FSLG HETCOR spectra of the pure TDC linker. Note: The total measurement times for the DNP enhanced HETCOR spectra were 20 h (b) and 4 h (c), respectively.



2-(hydroxyl(4-nitrophenyl)methyl)cyclohexan-1-one:

$^1\text{H-NMR}$ (500 MHz, CDCl_3): δ (ppm) 1.36-1.84 (m, 6H, 3CH₂), 2.01-2.18 (m, 1H, OH), 2.29 -2.65 (m, 3H, CH, CH₂), 4.88 (d, 1H, anti-CH*), 5.47 (d, 1H, syn-CH*), 7.47 (d, 2H, ArH), 8.19 (d, 2H, ArH);

$^{13}\text{C-NMR}$ (100 MHz, CDCl_3): δ (ppm) 24.67, 27.62, 29.68, 30.74, 42.67, 57.17, 74.02, 123.51, 126.58, 1287.85 147, 148, 215.

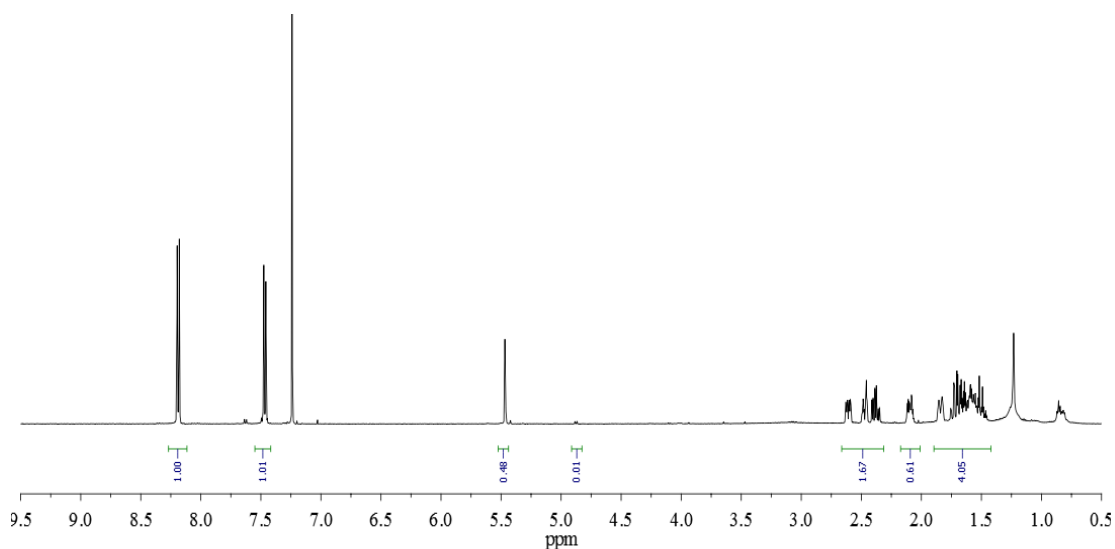


Figure 7.18. $^1\text{H-NMR}$ spectrum of 2-(2-nitro-1-phenylethyl) cyclohexan-1-one (purified orange solid obtained from the of DUT-67-pro catalyzed reaction).

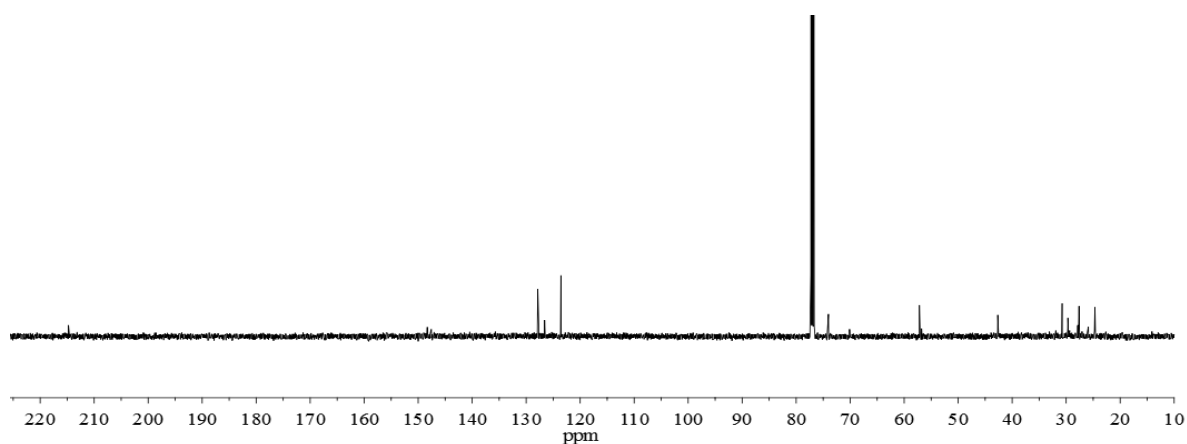


Figure 7.19. $^{13}\text{C-NMR}$ spectrum of 2-(2-nitro-1-phenylethyl) cyclohexan-1-one (purified orange solid obtained from the of DUT-67-pro catalyzed reaction).

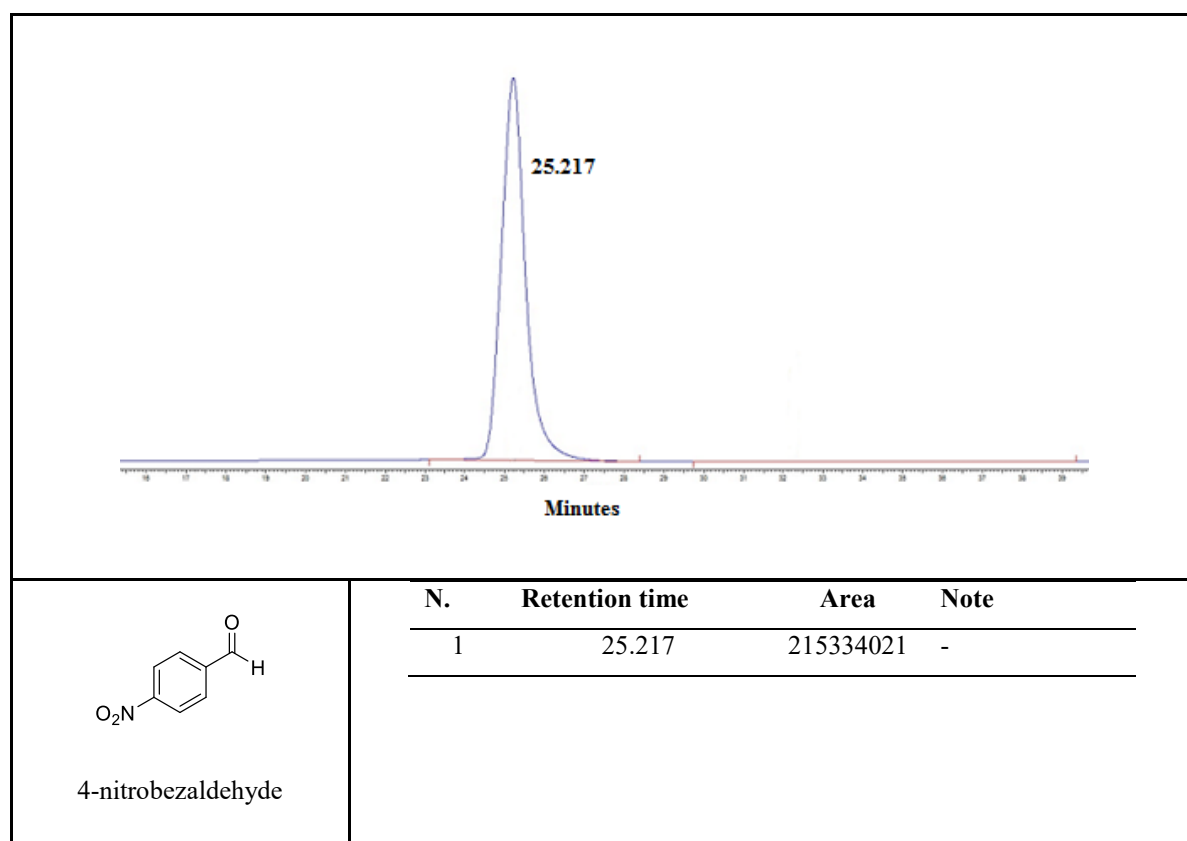


Figure 7.20. HPLC chromatogram of the 4-nitrobenzaldehyde.

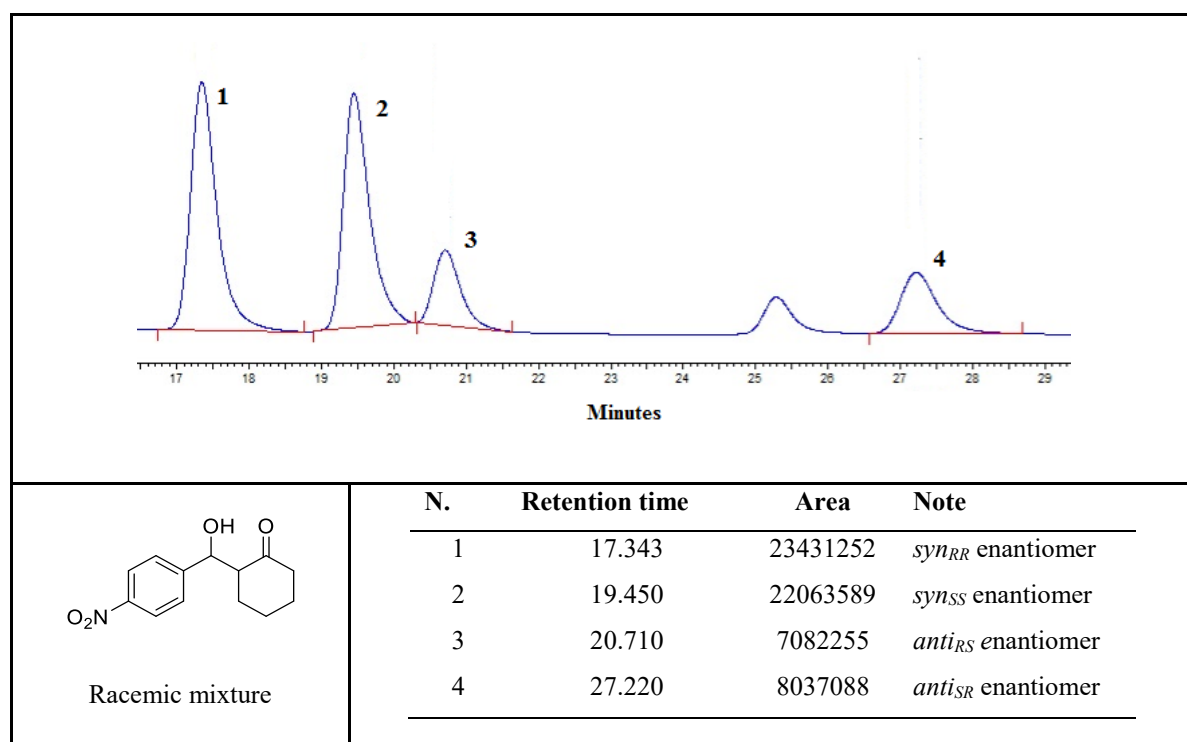


Figure 7.21. HPLC chromatogram of the 2-(hydroxy(4-nitrophenyl)methyl)cyclohexan-1-one enantiomers produced in the presence of DUT-67 as catalyst in DMSO.

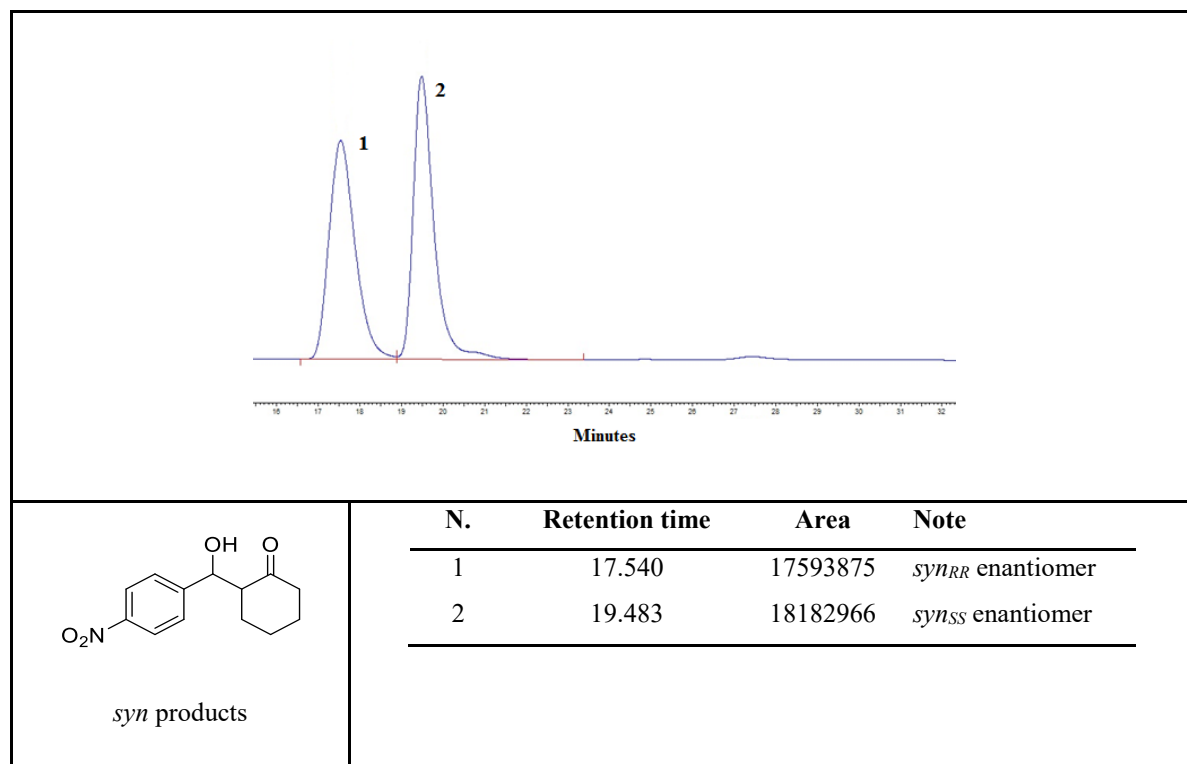


Figure 7.22. HPLC chromatogram of the *syn*-products of 2-(hydroxy(4-nitrophenyl)methyl)cyclohexan-1-one enantiomers.

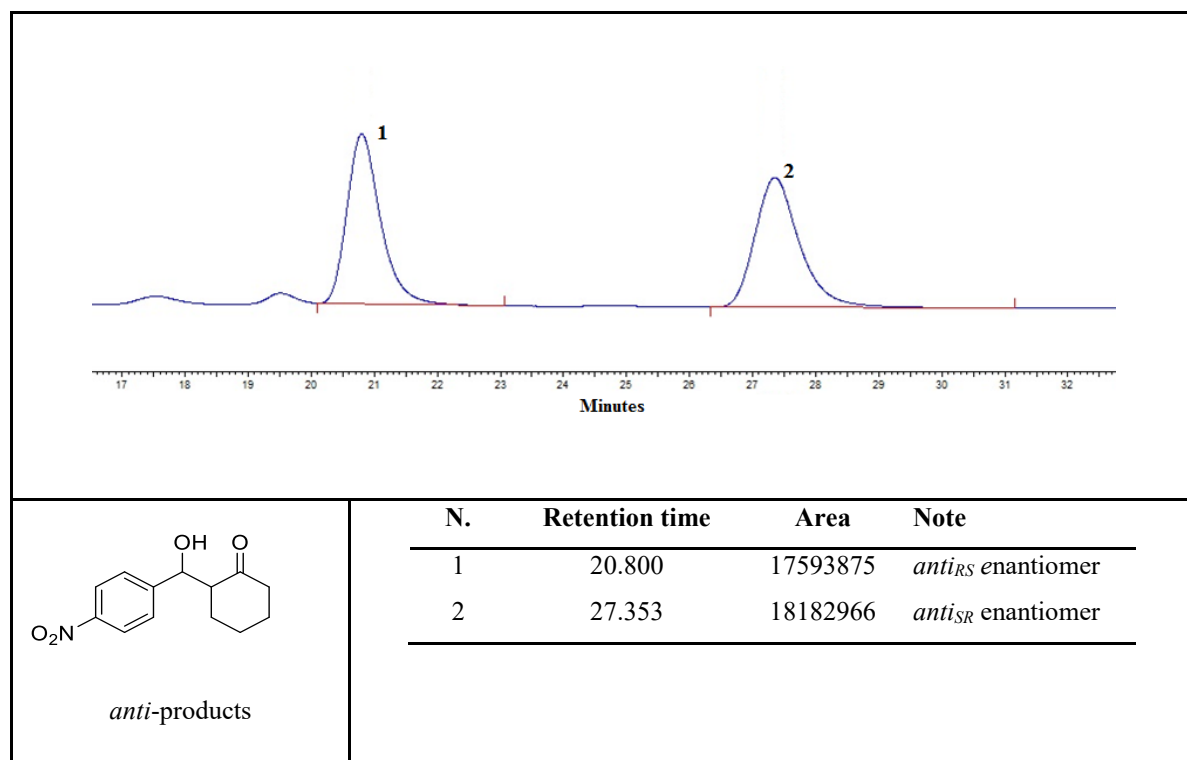


Figure 7.23. HPLC chromatogram of the *anti*-products of 2-(hydroxy(4-nitrophenyl)methyl)cyclohexan-1-one enantiomers.

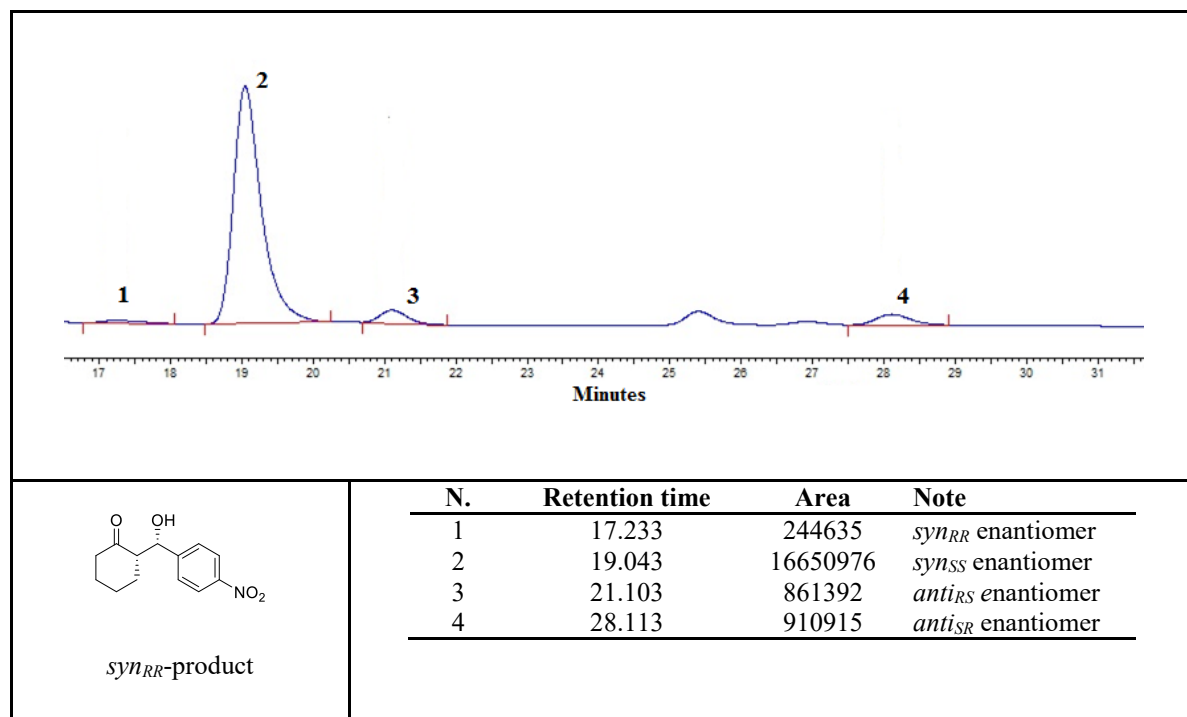


Figure 7.24. HPLC chromatogram of the 2-(hydroxy(4-nitrophenyl)methyl)cyclohexan-1-one enantiomers produced in the presence of DUT-67-pro catalyst in the presence of benzoic acid as additive in DMSO.

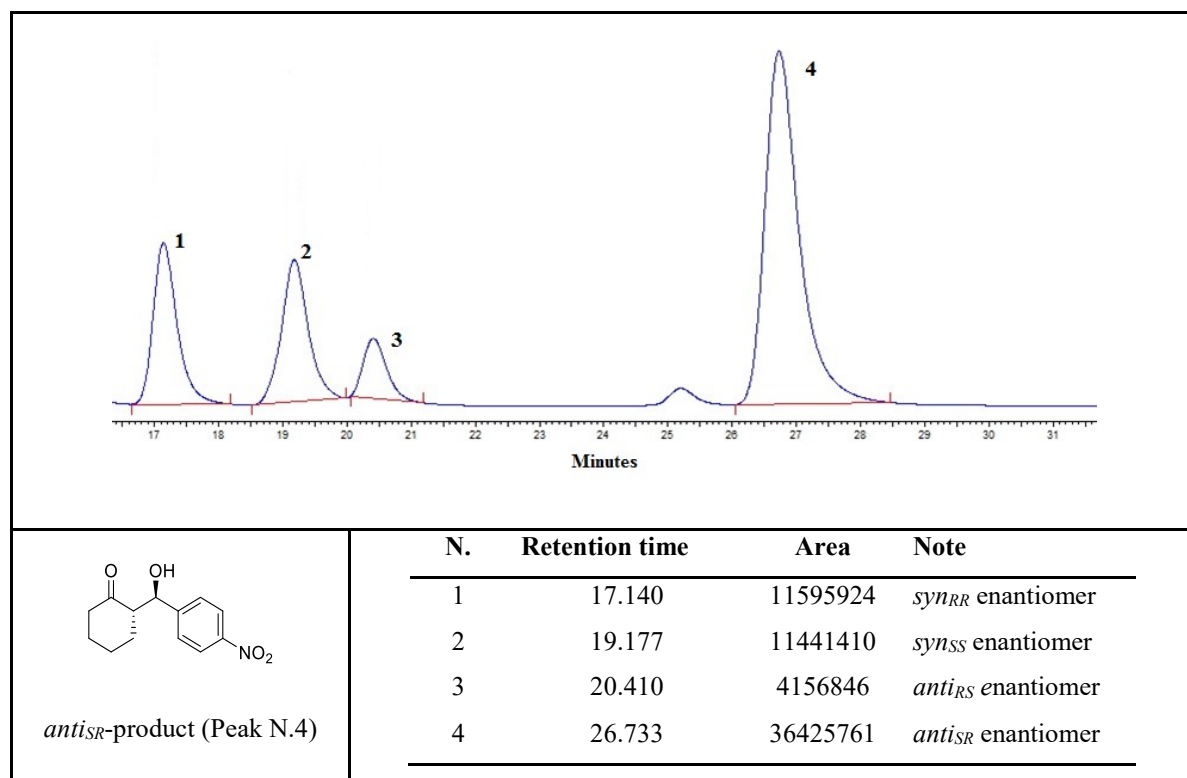


Figure 7.25. HPLC chromatogram of the 2-(hydroxy(4-nitrophenyl)methyl)cyclohexan-1-one enantiomers.

Table 7.1. Crystallographic data of modeled DUT-136.

Phase data				
Chemical formula:	Zr ₆ O ₃₂ N ₆ C ₁₀₂ H ₈₄			
Crystal system:	Trigonal			
Space group:	P3			
Cell parameters:	a=19.7780 Å c=12.5744 Å			
Cell volume:	4259.74 Å ³			
Atomic parameters				
Atom	x	y	z	U, Å ²
Zr1	0.30879	0.56339	0.92051	0.05
Zr2	0.41382	0.64089	1.12784	0.05
O3	0.38301	0.5736	0.79449	0.05
O4	0.21831	0.45272	0.92428	0.05
O5	0.14826	0.46852	1.05762	0.05
O6	0.41315	0.53488	1.125	0.05
O7	0.33596	0.47895	0.97918	0.05
O8	0.41872	0.63834	0.96623	0.05
O9	0.30568	0.55693	1.08112	0.05
O10	0.46328	0.70723	0.78075	0.05
O11	0.47684	0.7154	1.25395	0.05
O12	0.37245	0.57687	1.26879	0.05
O77	1/3	2/3	1.19016	0.05
O78	1/3	2/3	0.86086	0.05
N13	0.24334	0.22497	0.42575	0.05
N14	0.11072	0.20673	0.60722	0.05
C15	0.51212	0.80177	1.40125	0.05
C19	0.46921	0.62569	0.64624	0.05
C23	0.15624	0.42943	0.98009	0.05
C24	0.37107	0.47579	1.0646	0.05
C25	0.43634	0.63612	0.74795	0.05
C26	0.46757	0.76865	1.30072	0.05
C27	0.20047	0.16392	0.50739	0.05
C29	0.25183	0.16623	0.60178	0.06
C30	0.11474	0.15219	0.52584	0.05
C32	0.07704	0.15223	0.41461	0.06
C33	0.26745	0.21193	0.33561	0.05
C35	0.07053	0.18484	0.69436	0.05
C37	0.06974	0.2403	0.77857	0.05
C38	0.29124	0.26836	0.2471	0.05
C39	0.06279	0.30543	0.7513	0.05
C41	0.07212	0.36038	0.828	0.05
C43	0.09308	0.35374	0.93201	0.05
C44	0.08775	0.28276	0.96215	0.05

C46	0.07619	0.22632	0.88582	0.05
C48	0.36847	0.30626	0.20894	0.05
C50	0.39544	0.37094	0.14196	0.05
C52	0.34505	0.39771	1.10946	0.05
C53	0.26537	0.35277	1.13609	0.05
C55	0.23831	0.28883	0.20407	0.05
C57	0.32828	0.18225	0.57952	0.05
C58	0.37182	0.17058	0.65656	0.05
C59	0.33955	0.14264	0.75642	0.05
C60	0.26371	0.12665	0.77949	0.05
C61	0.21986	0.13824	0.7026	0.05
C62	0.03608	0.19288	0.40034	0.05
C63	0.00474	0.19346	0.3017	0.05
C64	0.01357	0.15328	0.2166	0.05
C65	0.05395	0.11263	0.2299	0.05
C66	0.08577	0.11227	0.3282	0.05
H16	0.57578	0.82995	1.38476	0.075
H17	0.49568	0.75433	1.4596	0.075
H18	0.49947	0.84612	1.43526	0.075
H20	0.5169	0.68281	0.6168	0.075
H21	0.42246	0.59971	0.58582	0.075
H22	0.49314	0.58609	0.65937	0.075
H28	0.18852	0.10722	0.47231	0.06
H31	0.0786	0.09129	0.55631	0.06
H34	0.26359	0.15613	0.32131	0.06
H36	0.03867	0.12343	0.71556	0.06
H40	0.05588	0.31688	0.66968	0.06
H42	0.07576	0.41445	0.8023	0.06
H45	0.10155	0.27487	1.04209	0.06
H47	0.0798	0.17547	0.90937	0.06
H49	0.4098	0.29019	0.23822	0.06
H51	0.45732	0.40449	0.12387	0.06
H54	0.22553	0.37207	1.11245	0.06
H56	0.17857	0.2606	0.23271	0.06
H67	0.35423	0.20436	0.5028	0.06
H68	0.43054	0.18328	0.63853	0.06
H69	0.37312	0.13316	0.81588	0.06
H70	0.23888	0.10525	0.857	0.06
H71	0.16131	0.12591	0.722	0.06
H72	0.02921	0.22479	0.46524	0.06
H73	-0.02616	0.22533	0.29116	0.06
H74	-0.01066	0.15385	0.14028	0.06
H75	0.06093	0.08163	0.16388	0.06
H76	0.11777	0.08138	0.33649	0.06

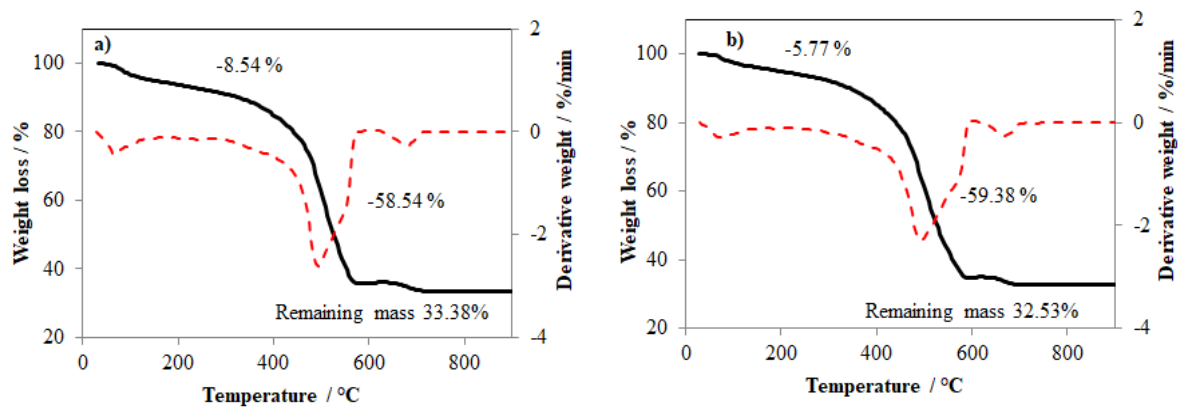


Figure 7.26. TGA curve of fresh amine-DUT-136 (a) and reused amine-DUT-136.

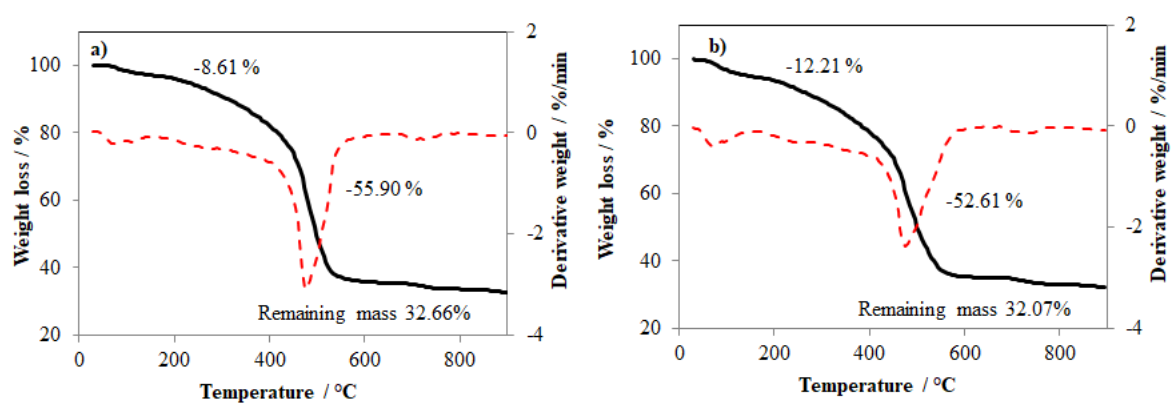


Figure 7.27. TGA curve of fresh amide-DUT-136 (a) and reused amide-DUT-136.

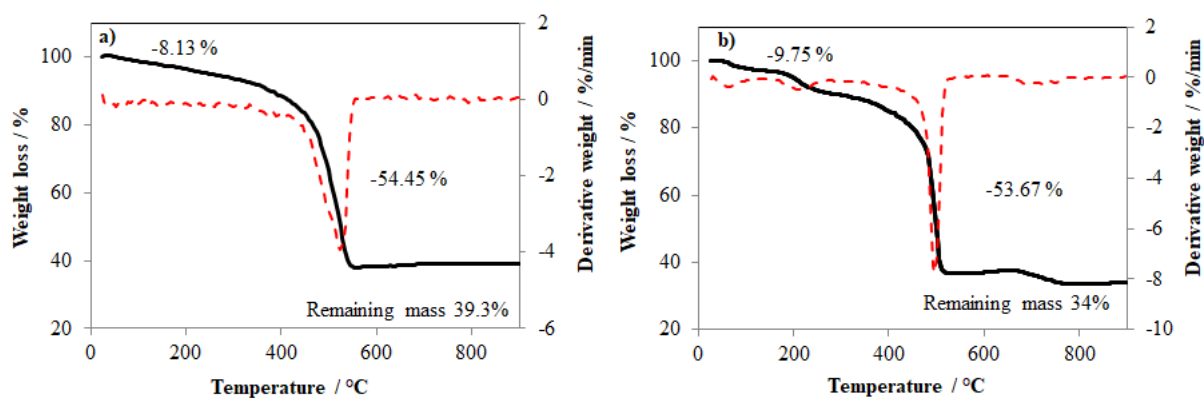


Figure 7.28. TGA curve of fresh Ni-amide-DUT-136 (a) and reused Ni-amide-DUT-136.

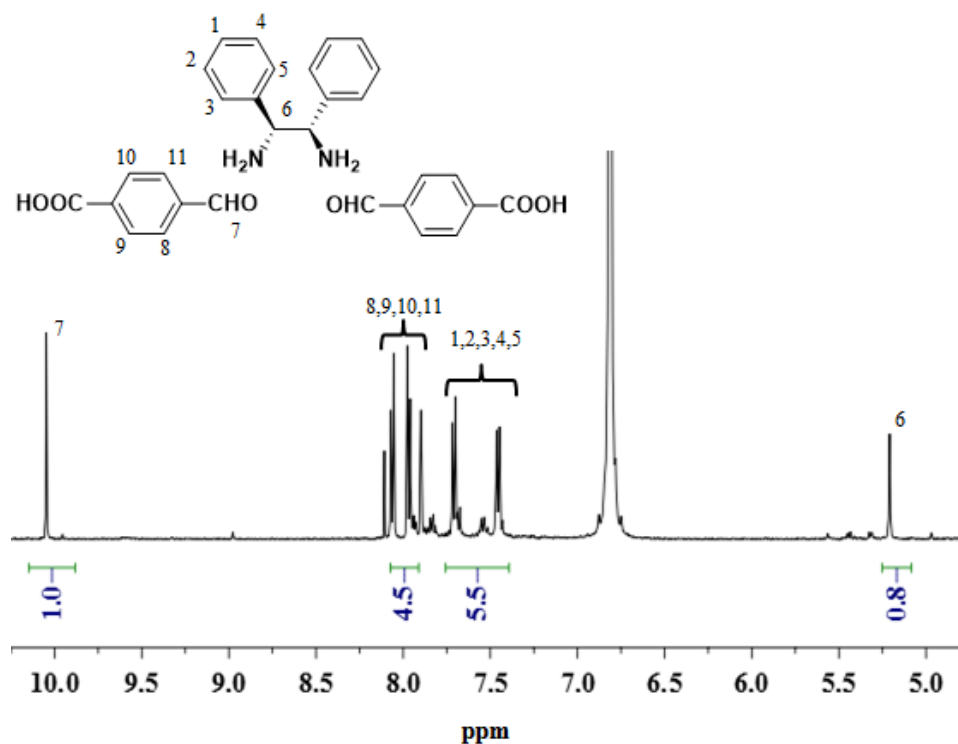


Figure 7.29. ¹H-NMR spectrum of digested imine-DUT-136.

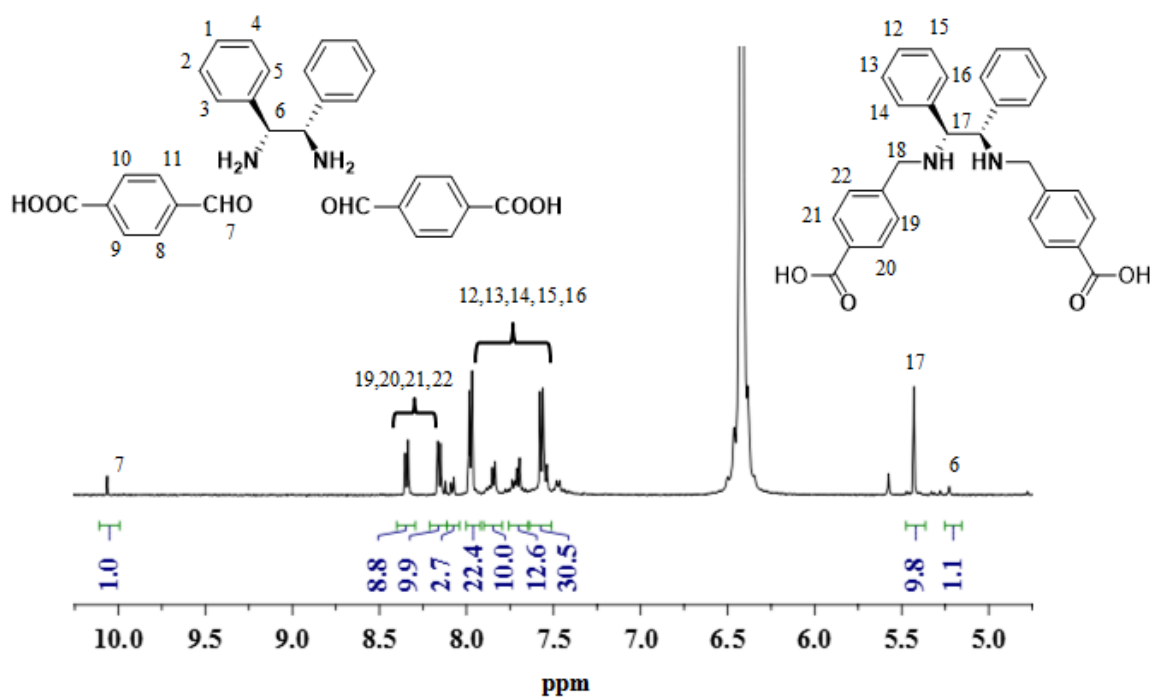


Figure 7.30. ¹H-NMR spectrum of digested amine-DUT-136.

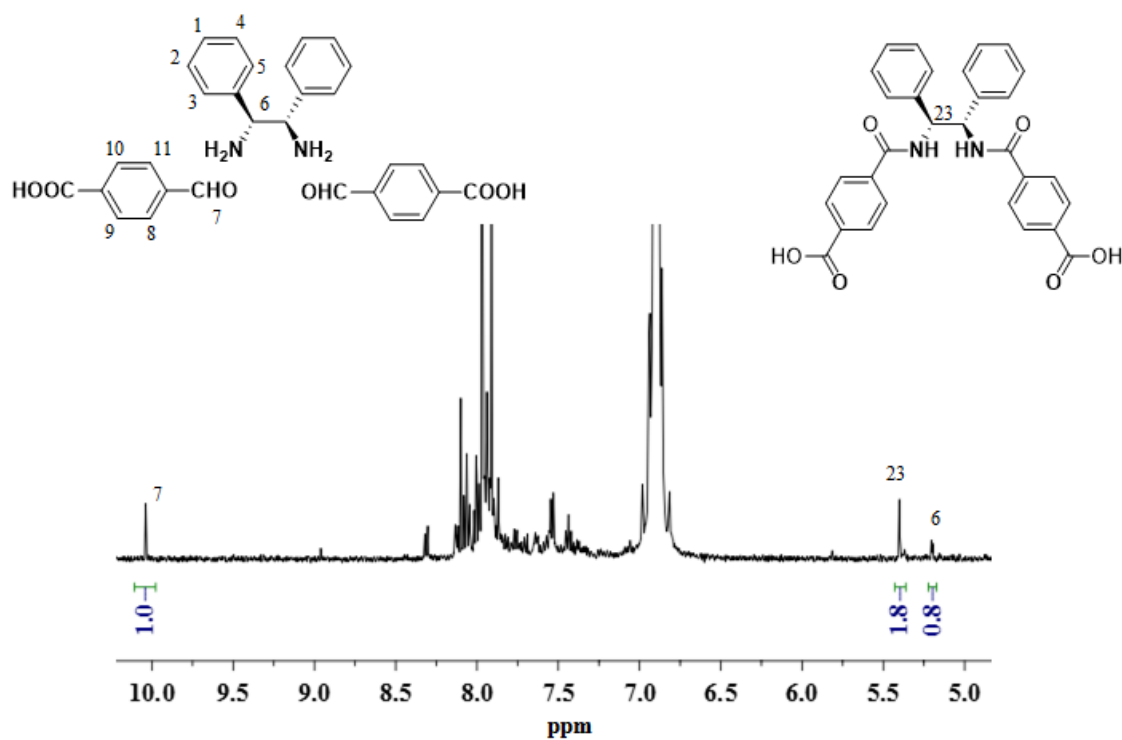
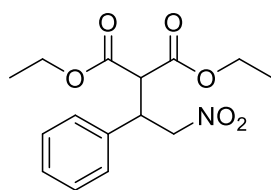


Figure 7.31. ^1H -NMR spectrum of digested amide-DUT-136.



diethyl 2-(2-nitro-1-phenylethyl) malonate:

^1H -NMR (500 MHz, CDCl_3): δ (ppm) 1.01 (t, 3H, CH_3), 1.21 (t, 3H, CH_3), 3.75 (d, 1H, CH), 4.06 (m, 2H, CH_2), 4.17 (m, 3H, CH_2 and CH^*), 4.82 (m, 2H, CH_2), 7.23 (m, 5H, ArH)

^{13}C -NMR (100 MHz, CDCl_3): δ (ppm) 13.83, 42.94, 54.95, 62.01, 77.15, 128.42, 136.19, 167.13.

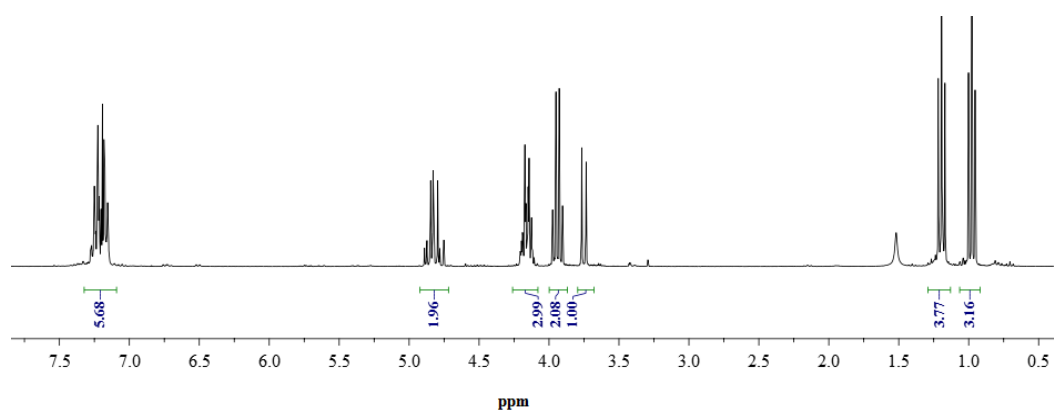


Figure 7.32. ^1H -NMR spectrum of diethyl 2-(2-nitro-1-phenylethyl) malonate.

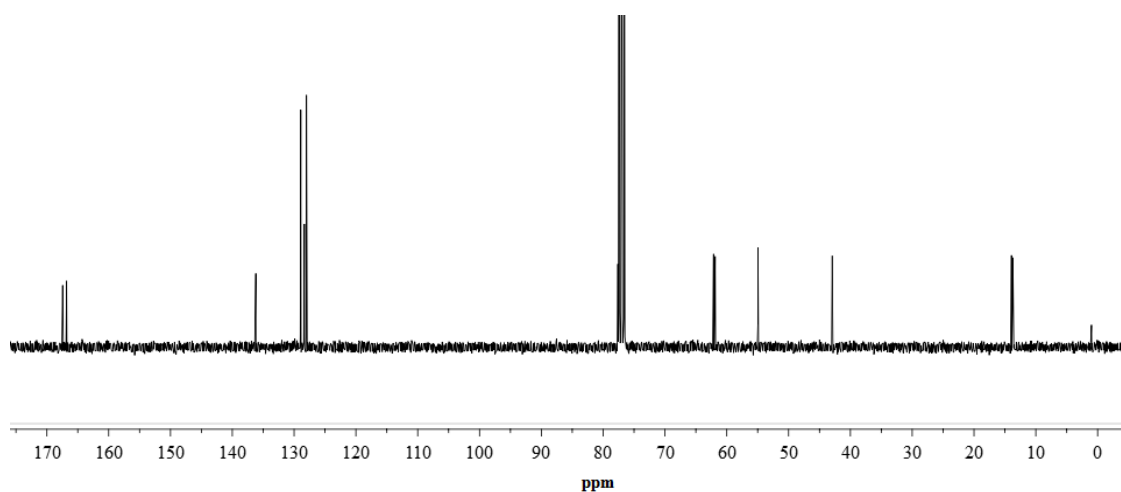


Figure 7.33. ^{13}C -NMR spectrum of diethyl 2-(2-nitro-1-phenylethyl) malonate.

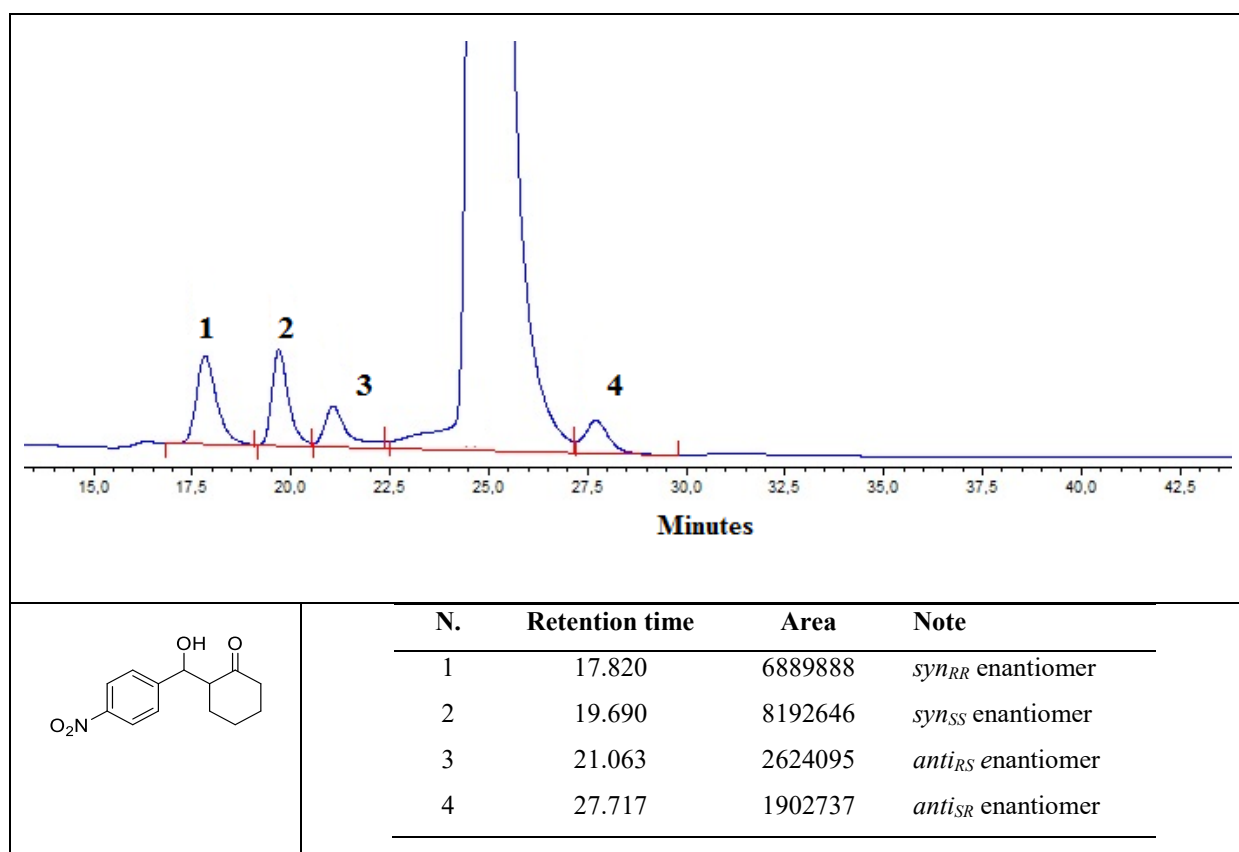


Figure 7.34. HPLC chromatogram of the 2-(hydroxy(4-nitrophenyl)methyl)cyclohexan-1-one enantiomers produced in the presence of amine-DUT-136.

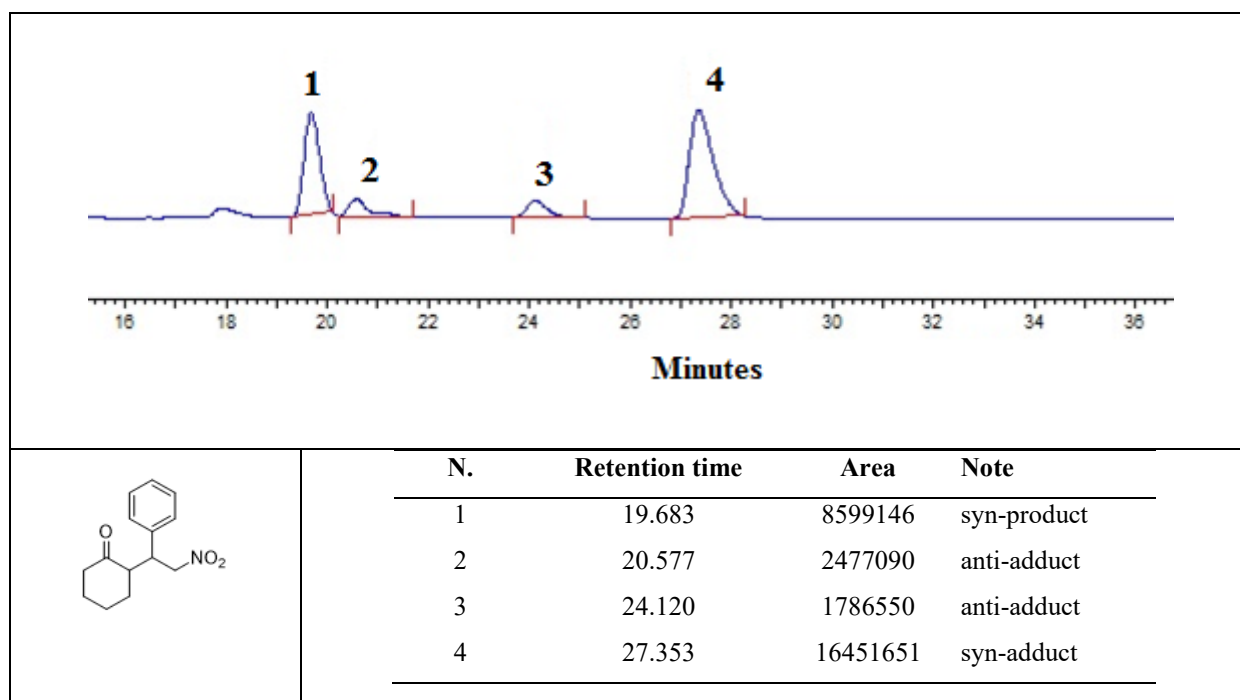


Figure 7.35. HPLC spectrum of the 2-(2-nitro-1-phenylethyl)cyclohexan-1-one enantiomers produced in the presence of amine-DUT-136 catalyst.

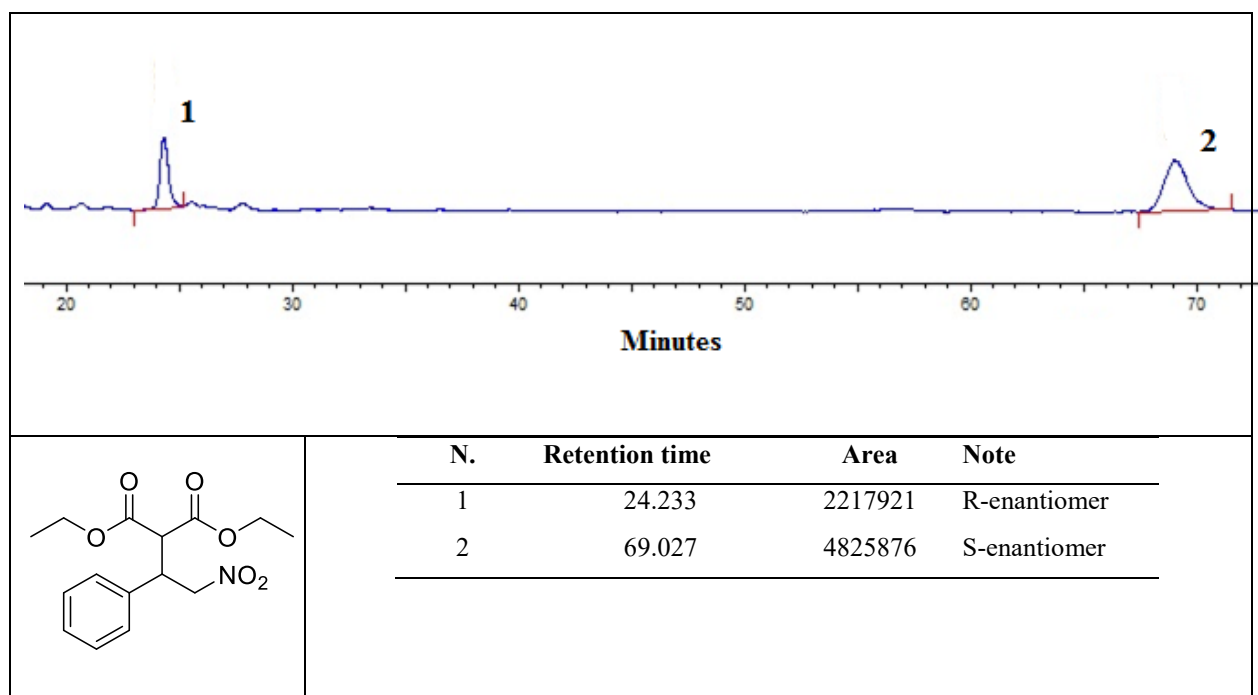


Figure 7.36. HPLC spectrum of diethyl 2-(2-nitro-1-phenylethyl) malonate, produced in the presence of $\text{Ni}(\text{OAc})_2$ and (R,R)-1,2-diphenylenediamine.

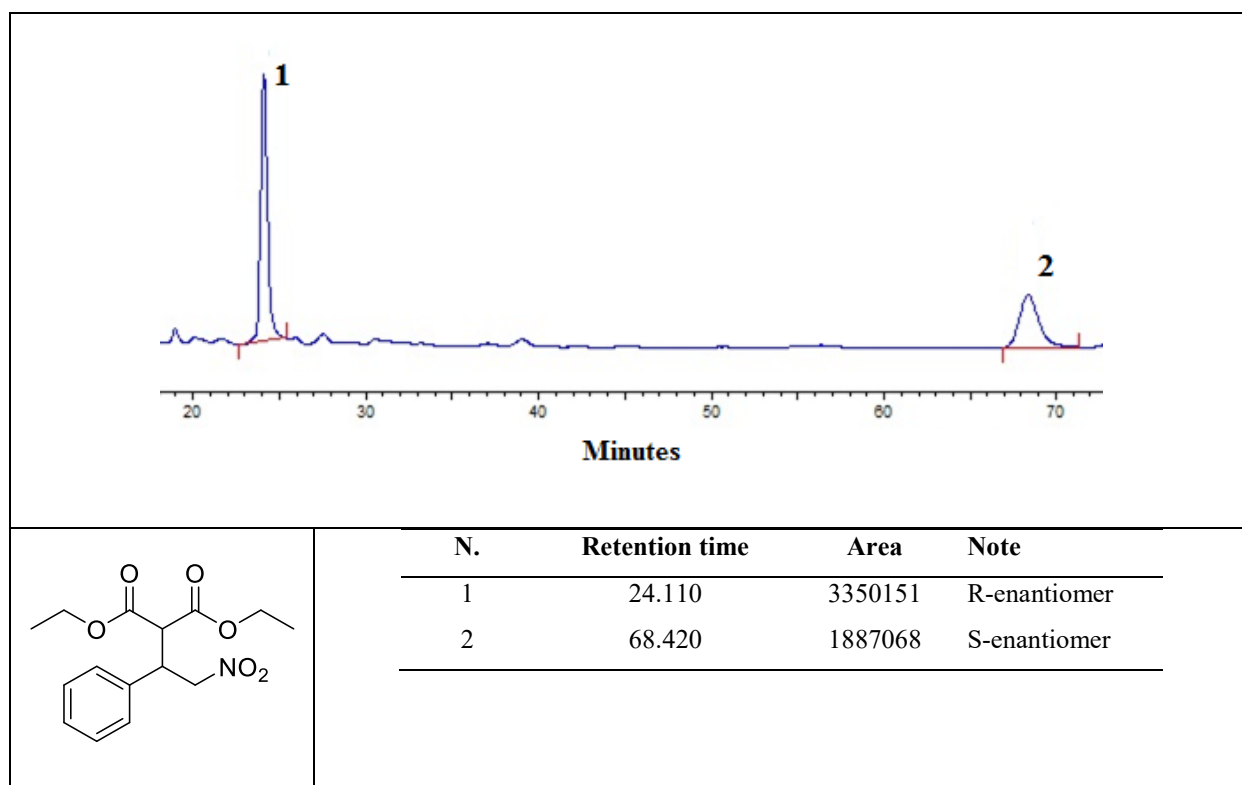


Figure 7.37. HPLC spectrum of diethyl 2-(2-nitro-1-phenylethyl) malonate, produced in the presence of $\text{Ni}(\text{OAc})_2$ and (S,S)-1,2-diphenylenediamine.

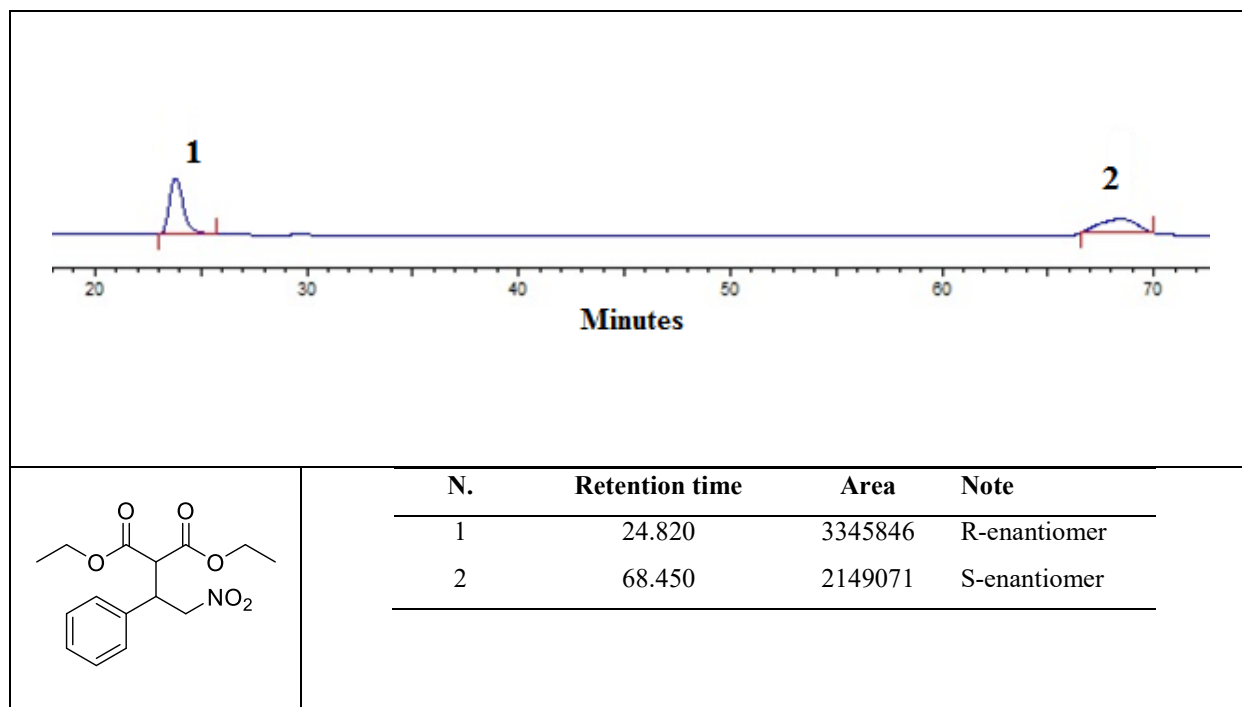


Figure 7.38. HPLC spectrum of the spectrum of diethyl 2-(2-nitro-1-phenylethyl) malonate. enantiomers produced in the presence of Ni-(R,R)-amide-DUT-136 as catalyst.

References

1. J. D. Evans, B. Garai, H. Reinsch, W. Li, S. Dissegna, V. Bon, I. Senkowska, R. A. Fischer, S. Kaskel, C. Janiak, N. Stock and D. Volkmer, *Metal–organic frameworks in Germany: From synthesis to function*, *Coordination Chemistry Reviews*, 2019, **380**, 378.
2. S. Horike, S. Shimomura and S. Kitagawa, *Soft porous crystals*, *Nature Chemistry*, 2009, **1**, 695.
3. H. Furukawa, K. E. Cordova, M. O’Keeffe and O. M. Yaghi, *The chemistry and applications of metal-organic frameworks*, *Science*, 2013, **341**, 1230444.
4. G. Ferey, *Hybrid porous solids: past, present, future*, *Coordination Chemistry Reviews*, 2008, **37**, 191.
5. E. A. Tomic, *Thermal stability of coordination polymers*, *Journal of Applied Polymer Science*, 1965, **9**, 3745.
6. T. D. Bennett, J. M. Tuffnell, C. W. Ashling, J. Hou, S. Li, L. Longley and M. L. R. Gómez, *Novel Metal–Organic Framework Materials: Blends, Liquids, Glasses and Crystal-Glass Composites*, *Chemical Communications*, 2019, **55**, 8705..
7. P. Z. Moghadam, A. Li, S. B. Wiggin, A. Tao, A. G. P. Maloney, P. A. Wood, S. C. Ward and D. Fairen-Jimenez, *Development of a Cambridge Structural Database Subset: A Collection of Metal–Organic Frameworks for Past, Present, and Future*, *Chemistry of Materials*, 2017, **29**, 2618.
8. S. S.-Y. Chui, S. M.-F. Lo, J. P. H. Charmant, A. G. Orpen and I. D. Williams, *A chemically functionalizable nanoporous material*[$\text{Cu}_3(\text{TMA})_2(\text{H}_2\text{O})_3$], *Science*, 1999, **283**, 1148.
9. A. Kirchon, L. Feng, H. F. Drake, E. A. Joseph and H. C. Zhou, *From fundamentals to applications: a toolbox for robust and multifunctional MOF materials*, *Chemical Society Reviews*, 2018, **47**, 8611.
10. Weigang Lu, Zhangwen Wei, Zhi-Yuan Gu, Tian-Fu Liu, Jinhee Park, Jihye Park, Jian Tian, Muwei Zhang, Qiang Zhang, Thomas Gentle, Mathieu Boscha and H.-C. Zhou, *Tuning the structure and function of metal–organic frameworks via linker design*, *Chemical Society Reviews*, 2014, **43**, 5561.
11. O. M. Yaghi, M. O’Keeffe, N. W. Ockwig, H. K. Chae, M. Eddaoudi and J. Kim, *Reticular synthesis and the design of new materials*, *Nature*, 2003, **423**, 705.
12. Mohamed Eddaoudi, Jaheon Kim, Nathaniel Rosi, David Vodak, Joseph Wachter, Michael O’Keeffe and O. M. Yaghi, *Systematic Design of Pore Size and Functionality in Isorecticular MOFs and Their Application in Methane Storage*, *Science*, 2002, **295**, 469.
13. H. Li, M. Eddaoudi, M. O’Keeffe and O. M. Yaghi, *Design and synthesis of an exceptionally stable and highly porous metal-organic framework*, *Nature*, 1999, **402**, 276.
14. D. J. Tranchemontagne, J. L. Mendoza-Cortes, M. O’Keeffe and O. M. Yaghi, *Secondary building units, nets and bonding in the chemistry of metal-organic frameworks*, *Chemical Society Reviews*, 2009, **38**, 1257.

15. O. M. Yaghi, G. Li and T. L. Groy, *Conversion of hydrogen-bonded manganese(II) and zinc(II) squarate ($C_4O_4^{2-}$) molecules, chains and sheets to three-dimensional cage networks*, *Journal of the Chemical Society, Dalton Transactions*, 1995, **0**, 727.
16. Robert W. Gable, Bernard F. Hoskins and R. Robson, *Synthesis and structure of $[NMe_4][CuPt(CN)_4]$: an infinite three-dimensional framework related to PtS which generates intersecting hexagonal channels of large cross section*, *Journal of the Chemical Society, Chemical Communications*, 1990, **0**, 762.
17. H. Furukawa and O. M. Yaghi, *Storage of Hydrogen, Methane, and Carbon Dioxide in Highly Porous Covalent Organic Frameworks for Clean Energy Applications*, *Journal of the American Chemical Society*, 2009, **131**, 8875.
18. J. G. Nguyen and S. M. Cohen, *Moisture-Resistant and Superhydrophobic Metal–Organic Frameworks Obtained via Postsynthetic Modification*, *Journal of the American Chemical Society*, 2010, **132**, 4560.
19. S. Yuan, L. Feng, K. Wang, J. Pang, M. Bosch, C. Lollar, Y. Sun, J. Qin, X. Yang, P. Zhang, Q. Wang, L. Zou, Y. Zhang, L. Zhang, Y. Fang, J. Li and H. C. Zhou, *Stable Metal–Organic Frameworks: Design, Synthesis, and Applications*, *Advanced Material*, 2018, **30**, 1704303.
20. R. Banerjee, A. Phan, B. Wang, C. Knobler, H. Furukawa, M. O’Keeffe and O. M. Yaghi, *High-Throughput Synthesis of Zeolitic Imidazolate Frameworks and Application to CO_2 Capture*, *Science*, 2008, **319**, 939.
21. D. J. Tranchemontagne, J. R. Hunt and O. M. Yaghi, *Room temperature synthesis of metal–organic frameworks: MOF-5, MOF-74, MOF-177, MOF-199, and IRMOF-0*, *Tetrahedron*, 2008, **64**, 8553.
22. Y.-K. Seo, G. Hundal, I. T. Jang, Y. K. Hwang, C.-H. Jun and J.-S. Chang, *Microwave synthesis of hybrid inorganic–organic materials including porous $Cu_3(BTC)_2$ from Cu(II)-trimesate mixture*, *Microporous and Mesoporous Materials*, 2009, **119**, 331.
23. K. Schlichte, T. Kratzke and S. Kaskel, *Improved synthesis, thermal stability and catalytic properties of the metal–organic framework compound $Cu_3(BTC)_2$* , *Microporous and Mesoporous Materials*, 2004, **73**, 81.
24. J. Lee, O. K. Farha, J. Roberts, K. A. Scheidt, S. T. Nguyen and J. T. Hupp, *Metal–organic framework materials as catalysts*, *Chemical Society Reviews*, 2009, **38**, 1450.
25. S. Ma, D. Sun, M. Ambrogio, J. A. Fillinger, S. Parkin and H.-C. Zhou, *Framework-Catenation Isomerism in Metal–Organic Frameworks and Its Impact on Hydrogen Uptake*, *Journal of the American Chemical Society*, 2007, **129**, 1858.
26. H. Furukawa, Y. B. Go, N. Ko, Y. K. Park, F. J. Uribe-Romo, J. Kim, M. O’Keeffe and O. M. Yaghi, *Isorecticular Expansion of Metal–Organic Frameworks with Triangular and Square Building Units and the Lowest Calculated Density for Porous Crystals*, *Inorganic Chemistry*, 2011, **50**, 9147.
27. W. Zhang, O. Kozachuk, R. Medishetty, A. Schneemann, R. Wagner, K. Khaletskaya, K. Epp and R. A. Fischer, *Controlled SBU Approaches to Isorecticular Metal–Organic Framework Ruthenium-Analogues of HKUST-1*, *European Journal of Inorganic Chemistry*, 2015, **2015**, 3913.

28. H. Furukawa and X. Sun, in *The Chemistry of Metal–Organic Frameworks*, ed. S. Kaskel, John Wiley & Sons, Germany, 2016, **chapter 10**, 271.
29. O. K. Farha, I. Eryazici, N. C. Jeong, B. G. Hauser, C. E. Wilmer, A. A. Sarjeant, R. Q. Snurr, S. T. Nguyen, A. Ö. Yazaydin and J. T. Hupp, *Metal–Organic Framework Materials with Ultrahigh Surface Areas: Is the Sky the Limit?*, *Journal of the American Chemical Society*, 2012, **134**, 15016.
30. G. Férey, C. Mellot-Draznieks, C. Serre, F. Millange, J. Dutour, S. Surblé and I. Margiolaki, *A Chromium Terephthalate-Based Solid with Unusually Large Pore Volumes and Surface Area*, *Science*, 2005, **309**, 2040.
31. U. Stoeck, S. Krause, V. Bon, I. Senkovska and S. Kaskel, *A highly porous metal–organic framework, constructed from a cuboctahedral super-molecular building block, with exceptionally high methane uptake*, *Chemical Communications*, 2012, **48**, 10841.
32. I. M. Hönicke, I. Senkovska, V. Bon, I. A. Baburin, N. Bönisch, S. Raschke, J. D. Evans and S. Kaskel, *Balancing Mechanical Stability and Ultrahigh Porosity in Crystalline Framework Materials*, *Angewandte Chemie International Edition*, 2018, **57**, 13780.
33. S. Kaskel, in *The Chemistry of Metal–Organic Frameworks*, ed. S. Kaskel, John Wiley & Sons, Germany, **chapter 1**, 1.
34. S. Yang, L. Peng, S. Bulut and W. L. Queen, *Recent Advances of MOFs and MOF-Derived Materials in Thermally Driven Organic Transformations*, *Chemistry – A European Journal*, 2019, **25**, 2161.
35. Y. Bai, Y. Dou, L.-H. Xie, W. Rutledge, J.-R. Li and H.-C. Zhou, *Zr-based metal–organic frameworks: design, synthesis, structure, and applications*, *Chemical Society Reviews*, 2016, **45**, 2327.
36. K. K. Tanabe and S. M. Cohen, *Postsynthetic modification of metal–organic frameworks—a progress report*, *Chemical Society Reviews*, 2011, **40**, 498.
37. S. M. Cohen, *Postsynthetic Methods for the Functionalization of Metal–Organic Frameworks*, *Chemical Reviews*, 2012, **112**, 970.
38. J. H. Cavka, S. Jakobsen, U. Olsbye, N. Guillou, C. Lamberti, S. Bordiga and K. P. Lillerud, *A New Zirconium Inorganic Building Brick Forming Metal Organic Frameworks with Exceptional Stability*, *Journal of the American Chemical Society*, 2008, **130**, 13850.
39. Z. Chen, S. L. Hanna, L. R. Redfern, D. Alezi, T. Islamoglu and O. K. Farha, *Reticular chemistry in the rational synthesis of functional zirconium cluster-based MOFs*, *Coordination Chemistry Reviews*, 2019, **386**, 32.
40. A. Schaate, P. Roy, A. Godt, J. Lippke, F. Waltz, M. Wiebcke and P. Behrens, *Modulated Synthesis of Zr-Based Metal–Organic Frameworks: From Nano to Single Crystals*, *Chemistry – A European Journal*, 2011, **17**, 6643.
41. V. Bon, V. Senkovskyy, I. Senkovska and S. Kaskel, *Zr(IV) and Hf(IV) based metal–organic frameworks with reo-topology*, *Chemical Communications*, 2012, **48**, 8407.
42. V. Bon, I. Senkovska, M. S. Weiss and S. Kaskel, *Tailoring of network dimensionality and porosity adjustment in Zr- and Hf-based MOFs*, *CrystEngComm*, 2013, **15**, 9572.

43. H. Furukawa, F. Gándara, Y.-B. Zhang, J. Jiang, W. L. Queen, M. R. Hudson and O. M. Yaghi, *Water Adsorption in Porous Metal–Organic Frameworks and Related Materials*, *Journal of the American Chemical Society*, 2014, **136**, 4369.
44. V. Bon, I. Senkovska, I. A. Baburin and S. Kaskel, *Zr- and Hf-Based Metal–Organic Frameworks: Tracking Down the Polymorphism*, *Crystal Growth & Design*, 2013, **13**, 1231.
45. Y. Zhang, X. Zhang, J. Lyu, K.-i. Otake, X. Wang, L. R. Redfern, C. D. Malliakas, Z. Li, T. Islamoglu, B. Wang and O. K. Farha, *A Flexible Metal–Organic Framework with 4-Connected Zr₆ Nodes*, *Journal of the American Chemical Society*, 2018, **140**, 11179.
46. H. Wang, X. Dong, J. Lin, S. J. Teat, S. Jensen, J. Cure, E. V. Alexandrov, Q. Xia, K. Tan, Q. Wang, D. H. Olson, D. M. Proserpio, Y. J. Chabal, T. Thonhauser, J. Sun, Y. Han and J. Li, *Topologically guided tuning of Zr-MOF pore structures for highly selective separation of C₆ alkane isomers*, *Nature Communications*, 2018, **9**, 1745.
47. A. J. Howarth, A. W. Peters, N. A. Vermeulen, T. C. Wang, J. T. Hupp and O. K. Farha, *Best Practices for the Synthesis, Activation, and Characterization of Metal–Organic Frameworks*, *Chemistry of Materials*, 2017, **29**, 26.
48. F. Drache, V. Bon, I. Senkovska, J. Getzschmann and S. Kaskel, *The modulator driven polymorphism of Zr(IV) based metal–organic frameworks*, *Philosophical Transactions of the Royal Society A: Mathematical, Physical and Engineering Sciences*, 2017, **375**, 20160027.
49. G. C. Shearer, S. Chavan, S. Bordiga, S. Svelle, U. Olsbye and K. P. Lillerud, *Defect Engineering: Tuning the Porosity and Composition of the Metal–Organic Framework UiO-66 via Modulated Synthesis*, *Chemistry of Materials*, 2016, **28**, 3749.
50. F. Drache, F. G. Cirujano, K. D. Nguyen, V. Bon, I. Senkovska, F. X. Llabrés i Xamena and S. Kaskel, *Anion Exchange and Catalytic Functionalization of the Zirconium-Based Metal–Organic Framework DUT-67*, *Crystal Growth & Design*, 2018, **18**, 5492.
51. M. Yoon, R. Srirambalaji and K. Kim, *Homochiral Metal–Organic Frameworks for Asymmetric Heterogeneous Catalysis*, *Chemical Reviews*, 2012, **112**, 1196.
52. L. Ma, C. Abney and W. Lin, *Enantioselective catalysis with homochiral metal–organic frameworks*, *Chemical Society Reviews*, 2009, **38**, 1248.
53. K. K. Bisht, B. Parmar, Y. Rachuri, A. C. Kathalikattil and E. Suresh, *Progress in the synthetic and functional aspects of chiral metal–organic frameworks*, *CrystEngComm*, 2015, **17**, 5341.
54. T. Sawano, P. Ji, A. R. McIsaac, Z. Lin, C. W. Abney and W. Lin, *The first chiral diene-based metal–organic frameworks for highly enantioselective carbon–carbon bond formation reactions*, *Chemical Science*, 2015, **6**, 7163.
55. T. Sawano, N. C. Thacker, Z. Lin, A. R. McIsaac and W. Lin, *Robust, Chiral, and Porous BINAP-Based Metal–Organic Frameworks for Highly Enantioselective Cyclization Reactions*, *Journal of the American Chemical Society*, 2015, **137**, 12241.
56. C. Wang, M. Zheng and W. Lin, *Asymmetric Catalysis with Chiral Porous Metal–Organic Frameworks: Critical Issues*, *The Journal of Physical Chemistry Letters*, 2011, **2**, 1701.

57. A. Hu, H. L. Ngo and W. Lin, *Chiral Porous Hybrid Solids for Practical Heterogeneous Asymmetric Hydrogenation of Aromatic Ketones*, *Journal of the American Chemical Society*, 2003, **125**, 11490.
58. H. L. Ngo, A. Hu and W. Lin, *Molecular building block approaches to chiral porous zirconium phosphonates for asymmetric catalysis*, *Journal of Molecular Catalysis A: Chemical*, 2004, **215**, 177.
59. C. Kutzscher, H. C. Hoffmann, S. Krause, U. Stoeck, I. Senkovska, E. Brunner and S. Kaskel, *Proline Functionalization of the Mesoporous Metal–Organic Framework DUT-32*, *Inorganic Chemistry*, 2015, **54**, 1003.
60. C. Kutzscher, G. Nickerl, I. Senkovska, V. Bon and S. Kaskel, *Proline Functionalized UiO-67 and UiO-68 Type Metal–Organic Frameworks Showing Reversed Diastereoselectivity in Aldol Addition Reactions*, *Chemistry of Materials*, 2016, **28**, 2573.
61. J. Jiao, C. Tan, Z. Li, Y. Liu, X. Han and Y. Cui, *Design and Assembly of Chiral Coordination Cages for Asymmetric Sequential Reactions*, *J Am Chem Soc*, 2018, **140**, 2251.
62. S.-H. Cho, B. Ma, S. T. Nguyen, J. T. Hupp and T. E. Albrecht-Schmitt, *A metal–organic framework material that functions as an enantioselective catalyst for olefin epoxidation*, *Chemical Communications*, 2006, **0**, 2563.
63. Z. Li, Y. Liu, Q. Xia and Y. Cui, *Chiral binary metal–organic frameworks for asymmetric sequential reactions*, *Chemical Communications*, 2017, **53**, 12313.
64. C. Zhu, Q. Xia, X. Chen, Y. Liu, X. Du and Y. Cui, *Chiral Metal–Organic Framework as a Platform for Cooperative Catalysis in Asymmetric Cyanosilylation of Aldehydes*, *ACS Catalysis*, 2016, **6**, 7590.
65. J. Li, Y. Ren, C. Qi and H. Jiang, *The first porphyrin–salen based chiral metal–organic framework for asymmetric cyanosilylation of aldehydes*, *Chemical Communications*, 2017, **53**, 8223.
66. J. Li, Y. Ren, C. Yue, Y. Fan, C. Qi and H. Jiang, *Highly Stable Chiral Zirconium–Metallosalen Frameworks for CO₂ Conversion and Asymmetric C–H Azidation*, *Acs Applied Materials & Interfaces*, 2018, **10**, 36047.
67. M. Banerjee, S. Das, M. Yoon, H. J. Choi, M. H. Hyun, S. M. Park, G. Seo and K. Kim, *Postsynthetic Modification Switches an Achiral Framework to Catalytically Active Homochiral Metal–Organic Porous Materials*, *Journal of the American Chemical Society*, 2009, **131**, 7524.
68. O. R. Evans, H. L. Ngo and W. Lin, *Chiral Porous Solids Based on Lamellar Lanthanide Phosphonates*, *Journal of the American Chemical Society*, 2001, **123**, 10395.
69. K. Gedrich, M. Heitbaum, A. Notzon, I. Senkovska, R. Fröhlich, J. Getzschmann, U. Mueller, F. Glorius and S. Kaskel, *A Family of Chiral Metal–Organic Frameworks*, *Chemistry – A European Journal*, 2011, **17**, 2099.
70. A. Dhakshinamoorthy, A. M. Asiri and H. Garcia, *Formation of C–C and C–Heteroatom Bonds by C–H Activation by Metal Organic Frameworks as Catalysts or Supports*, *ACS Catalysis*, 2019, **9**, 1081.

71. D. Yang and B. C. Gates, *Catalysis by Metal Organic Frameworks: Perspective and Suggestions for Future Research*, *ACS Catalysis*, 2019, **9**, 1779.
72. E. R. Andrew and E. Szczesniak, *A historical account of NMR in the solid state*, *Progress in Nuclear Magnetic Resonance Spectroscopy*, 1995, **28**, 11.
73. T. L. James, in *Nuclear Magnetic Resonance*, ed. T. L. James, Bethesda: Biophysical Society, 1998, **chapter 1**, 1.
74. T. Kobayashi, F. A. Perras, I. I. Slowing, A. D. Sadow and M. Pruski, *Dynamic Nuclear Polarization Solid-State NMR in Heterogeneous Catalysis Research*, *ACS Catalysis*, 2015, **5**, 7055.
75. A. Sutrisno and Y. Huang, *Solid-state NMR: a powerful tool for characterization of metal-organic frameworks*, *Solid State Nucl Magn Reson*, 2013, **49-50**, 1.
76. S. I. Brückner, J. Pallmann and E. Brunner, in *The Chemistry of Metal–Organic Frameworks*, ed. S. Kaskel, John Wiley & Sons, Germany, 2016, **chapter 20**, 607.
77. E. R. Andrew, A. Bradbury and R. G. Eades, *Nuclear Magnetic Resonance Spectra from a Crystal rotated at High Speed*, *Nature*, 1958, **182**, 1659.
78. E. R. Andrew, A. Bradbury and R. G. Eades, *Removal of Dipolar Broadening of Nuclear Magnetic Resonance Spectra of Solids by Specimen Rotation*, *Nature*, 1959, **183**, 1802.
79. A. Samoson, E. Lippmaa and A. Pines, *High resolution solid-state N.M.R.*, *Molecular Physics*, 1988, **65**, 1013.
80. A. R. Mouat, C. George, T. Kobayashi, M. Pruski, R. P. van Duyne, T. J. Marks and P. C. Stair, *Highly Dispersed SiO_x/Al₂O₃ Catalysts Illuminate the Reactivity of Isolated Silanol Sites*, *Angewandte Chemie International Edition*, 2015, **54**, 13346.
81. R. P. Sangodkar, B. J. Smith, D. Gajan, A. J. Rossini, L. R. Roberts, G. P. Funkhouser, A. Lesage, L. Emsley and B. F. Chmelka, *Influences of Dilute Organic Adsorbates on the Hydration of Low-Surface-Area Silicates*, *Journal of the American Chemical Society*, 2015, **137**, 8096.
82. T. K. Todorova, X. Rozanska, C. Gervais, A. Legrand, L. N. Ho, P. Berruyer, A. Lesage, L. Emsley, D. Farrusseng, J. Canivet and C. Mellot-Draznieks, *Molecular Level Characterization of the Structure and Interactions in Peptide-Functionalized Metal–Organic Frameworks*, *Chemistry – A European Journal*, 2016, **22**, 16531.
83. T. Kobayashi, F. A. Perras, T. W. Goh, T. L. Metz, W. Huang and M. Pruski, *DNP-Enhanced Ultrawideline Solid-State NMR Spectroscopy: Studies of Platinum in Metal–Organic Frameworks*, *The Journal of Physical Chemistry Letters*, 2016, **7**, 2322.
84. Y. Okamoto and T. Ikai, *Chiral HPLC for efficient resolution of enantiomers*, *Chemical Society Reviews*, 2008, **37**, 2593.
85. C. Yamamoto and Y. Okamoto, in *Chiral Analysis*, ed. K. W. Busch and M. A. Busch, Elsevier, Amsterdam, 2006, **chapter 7**, 215.
86. K. B. Lipkowitz, in *Chiral Analysis*, ed. K. W. Busch and M. A. Busch, Elsevier, Amsterdam, 2006, **chapter 5**, 97.
87. J. Teixeira, M. E. Tiritan, M. M. M. Pinto and C. Fernandes, *Chiral Stationary Phases for Liquid Chromatography: Recent Developments*, *Molecules*, 2019, **24**, 865.

References

88. G. Metz, X. L. Wu and S. O. Smith, *Ramped-Amplitude Cross Polarization in Magic-Angle-Spinning NMR*, *Journal of Magnetic Resonance*, 1994, **110**, 219.
89. B. M. Fung, A. K. Khitrin and K. Ermolaev, *An Improved Broadband Decoupling Sequence for Liquid Crystals and Solids*, *Journal of Magnetic Resonance*, 2000, **142**, 97.
90. B. J. van Rossum, H. Förster and H. J. M. de Groot, *High-Field and High-Speed CP-MAS ¹³C NMR Heteronuclear Dipolar-Correlation Spectroscopy of Solids with Frequency-Switched Lee–Goldburg Homonuclear Decoupling*, *Journal of Magnetic Resonance*, 1997, **124**, 516.
91. K. D. Nguyen, C. Kutzscher, F. Drache, I. Senkovska and S. Kaskel, *Chiral Functionalization of a Zirconium Metal–Organic Framework (DUT-67) as a Heterogeneous Catalyst in Asymmetric Michael Addition Reaction*, *Inorg Chem*, 2018, **57**, 1483.
92. S. Mukherjee, J. W. Yang, S. Hoffmann and B. List, *Asymmetric Enamine Catalysis*, *Chemical Reviews*, 2007, **107**, 5471.
93. D. Enders, C. Wang and J. X. Liebich, *Organocatalytic Asymmetric Aza-Michael Additions*, *Chemistry – A European Journal*, 2009, **15**, 11058.
94. W. Notz, F. Tanaka and C. F. Barbas, *Enamine-Based Organocatalysis with Proline and Diamines: The Development of Direct Catalytic Asymmetric Aldol, Mannich, Michael, and Diels–Alder Reactions*, *Accounts of Chemical Research*, 2004, **37**, 580.
95. T. Ishii, S. Fujioka, Y. Sekiguchi and H. Kotsuki, *A New Class of Chiral Pyrrolidine–Pyridine Conjugate Base Catalysts for Use in Asymmetric Michael Addition Reactions*, *Journal of the American Chemical Society*, 2004, **126**, 9558.
96. A. B. Northrup and D. W. C. MacMillan, *The First Direct and Enantioselective Cross-Aldol Reaction of Aldehydes*, *Journal of the American Chemical Society*, 2002, **124**, 6798.
97. P. I. Dalko and L. Moisan, *In the Golden Age of Organocatalysis*, *Angewandte Chemie International Edition*, 2004, **43**, 5138.
98. N. T. S. Phan, M. Van Der Sluys and C. W. Jones, *On the Nature of the Active Species in Palladium Catalyzed Mizoroki–Heck and Suzuki–Miyaura Couplings – Homogeneous or Heterogeneous Catalysis, A Critical Review*, *Advanced Synthesis & Catalysis*, 2006, **348**, 609.
99. K. D. Nguyen, S. H. Doan, A. N. V. Ngo, T. T. Nguyen and N. T. S. Phan, *Direct C–N coupling of azoles with ethers via oxidative C–H activation under metal–organic framework catalysis*, *Journal of Industrial and Engineering Chemistry*, 2016, **44**, 136.
100. F. Cozzi, *Immobilization of Organic Catalysts: When, Why, and How*, *Advanced Synthesis & Catalysis*, 2006, **348**, 1367.
101. M. Benaglia, A. Puglisi and F. Cozzi, *Polymer-Supported Organic Catalysts*, *Chemical Reviews*, 2003, **103**, 3401.
102. S. Luo, J. Li, L. Zhang, H. Xu and J.-P. Cheng, *Noncovalently Supported Heterogeneous Chiral Amine Catalysts for Asymmetric Direct Aldol and Michael Addition Reactions*, *Chemistry – A European Journal*, 2008, **14**, 1273.
103. S. A. Selkälä, J. Tois, P. M. Pihko and A. M. P. Koskinen, *Asymmetric Organocatalytic Diels–Alder Reactions on Solid Support*, *Advanced Synthesis & Catalysis*, 2002, **344**, 941.

104. E. Gross, J. H. Liu, S. Alayoglu, M. A. Marcus, S. C. Fakra, F. D. Toste and G. A. Somorjai, *Asymmetric Catalysis at the Mesoscale: Gold Nanoclusters Embedded in Chiral Self-Assembled Monolayer as Heterogeneous Catalyst for Asymmetric Reactions*, *Journal of the American Chemical Society*, 2013, **135**, 3881.
105. I. Schrader, S. Neumann, A. Šulce, F. Schmidt, V. Azov and S. Kunz, *Asymmetric Heterogeneous Catalysis: Transfer of Molecular Principles to Nanoparticles by Ligand Functionalization*, *ACS Catalysis*, 2017, **7**, 3979.
106. T. Yasukawa, H. Miyamura and S. Kobayashi, *Chiral Ligand-Modified Metal Nanoparticles as Unique Catalysts for Asymmetric C–C Bond-Forming Reactions: How Are Active Species Generated?*, *ACS Catalysis*, 2016, **6**, 7979.
107. P. Deria, J. E. Mondloch, E. Tylianakis, P. Ghosh, W. Bury, R. Q. Snurr, J. T. Hupp and O. K. Farha, *Perfluoroalkane Functionalization of NU-1000 via Solvent-Assisted Ligand Incorporation: Synthesis and CO₂ Adsorption Studies*, *Journal of the American Chemical Society*, 2013, **135**, 16801.
108. J. E. Mondloch, W. Bury, D. Fairen-Jimenez, S. Kwon, E. J. DeMarco, M. H. Weston, A. A. Sarjeant, S. T. Nguyen, P. C. Stair, R. Q. Snurr, O. K. Farha and J. T. Hupp, *Vapor-Phase Metalation by Atomic Layer Deposition in a Metal–Organic Framework*, *Journal of the American Chemical Society*, 2013, **135**, 10294.
109. P. Deria, W. Bury, I. Hod, C.-W. Kung, O. Karagiari, J. T. Hupp and O. K. Farha, *MOF Functionalization via Solvent-Assisted Ligand Incorporation: Phosphonates vs Carboxylates*, *Inorganic Chemistry*, 2015, **54**, 2185.
110. R. J. Marshall and R. S. Forgan, *Postsynthetic Modification of Zirconium Metal–Organic Frameworks*, *European Journal of Inorganic Chemistry*, 2016, **2016**, 4310.
111. S. M. Cohen, *The Postsynthetic Renaissance in Porous Solids*, *Journal of the American Chemical Society*, 2017, **139**, 2855.
112. F. Drache, V. Bon, I. Senkowska, C. Marschelke, A. Synytska and S. Kaskel, *Postsynthetic Inner-Surface Functionalization of the Highly Stable Zirconium-Based Metal–Organic Framework DUT-67*, *Inorganic Chemistry*, 2016, **55**, 7206.
113. B. List, *Proline-catalyzed asymmetric reactions*, *Tetrahedron*, 2002, **58**, 5573.
114. A. J. A. Cobb, D. A. Longbottom, D. M. Shaw and S. V. Ley, *5-Pyrrolidin-2-yltetrazole as an asymmetric organocatalyst for the addition of ketones to nitro-olefins*, *Chemical Communications*, 2004, **0**, 1808.
115. J. M. Betancort, K. Sakthivel, R. Thayumanavan, F. Tanaka and C. F. Barbas Iii, *Catalytic Direct Asymmetric Michael Reactions: Addition of Unmodified Ketone and Aldehyde Donors to Alkylidene Malonates and Nitro Olefins*, *Synthesis*, 2004, **2004**, 1509.
116. B. List, P. Pojarliev and H. J. Martin, *Efficient Proline-Catalyzed Michael Additions of Unmodified Ketones to Nitro Olefins*, *Organic Letters*, 2001, **3**, 2423.
117. K. D. Nguyen, C. Kutzscher, S. Ehrling, I. Senkowska, V. Bon, M. de Oliveira, T. Gutmann, G. Buntkowsky and S. Kaskel, *Insights into the role of zirconium in proline functionalized metal-organic frameworks attaining high enantio- and diastereoselectivity*, *Journal of Catalysis*, 2019, **377**, 41.

References

118. J. Mlynarski and S. Bas, *Catalytic asymmetric aldol reactions in aqueous media - a 5 year update*, *Chemical Society Reviews*, 2014, **43**, 577.
119. B. Schetter and R. Mahrwald, *Modern aldol methods for the total synthesis of polyketides*, *Angewandte Chemie International Edition*, 2006, **45**, 7506.
120. T. D. Machajewski and C.-H. Wong, *The Catalytic Asymmetric Aldol Reaction*, *Angewandte Chemie International Edition*, 2000, **39**, 1352.
121. U. Eder, G. Sauer and R. Wiechert, *New Type of Asymmetric Cyclization to Optically Active Steroid CD Partial Structures*, *Angewandte Chemie International Edition*, 1971, **10**, 496.
122. Z. G. Hajos and D. R. Parrish, *Asymmetric synthesis of bicyclic intermediates of natural product chemistry*, *The Journal of Organic Chemistry*, 1974, **39**, 1615.
123. B. List, R. A. Lerner and C. F. Barbas, *Proline-Catalyzed Direct Asymmetric Aldol Reactions*, *Journal of the American Chemical Society*, 2000, **122**, 2395.
124. J. Huang, X. Zhang and W. Armstrong Daniel *Highly Efficient Asymmetric Direct Stoichiometric Aldol Reactions on/in Water*, *Angewandte Chemie International Edition*, 2007, **46**, 9073.
125. K. Sakthivel, W. Notz, T. Bui and C. F. Barbas, *Amino Acid Catalyzed Direct Asymmetric Aldol Reactions: A Bioorganic Approach to Catalytic Asymmetric Carbon–Carbon Bond-Forming Reactions*, *Journal of the American Chemical Society*, 2001, **123**, 5260.
126. B. M. Trost and C. S. Brindle, *The direct catalytic asymmetric aldol reaction*, *Chemical Society Reviews*, 2010, **39**, 1600.
127. A. Armstrong, R. A. Boto, P. Dingwall, J. Contreras-Garcia, M. J. Harvey, N. J. Mason and H. S. Rzepa, *The Houk-List transition states for organocatalytic mechanisms revisited*, *Chemical Science*, 2014, **5**, 2057.
128. L. Hoang, S. Bahmanyar, K. N. Houk and B. List, *Kinetic and Stereochemical Evidence for the Involvement of Only One Proline Molecule in the Transition States of Proline-Catalyzed Intra- and Intermolecular Aldol Reactions*, *Journal of the American Chemical Society*, 2003, **125**, 16.
129. P. Zhou, S. Luo and J.-P. Cheng, *Highly enantioselective synthesis of syn-aldols of cyclohexanones via chiral primary amine catalyzed asymmetric transfer aldol reactions in ionic liquid*, *Organic and Biomolecular Chemistry*, 2011, **9**, 1784.
130. J. Gao, S. Bai, Q. Gao, Y. Liu and Q. Yang, *Acid controlled diastereoselectivity in asymmetric aldol reaction of cycloketones with aldehydes using enamine-based organocatalysts*, *Chemical Communications*, 2011, **47**, 6716.
131. M. M. Heravi, V. Zadsirjan, M. Dehghani and N. Hosseintash, *Current applications of organocatalysts in asymmetric aldol reactions: An update*, *Tetrahedron: Asymmetry*, 2017, **28**, 587.
132. R. J. Marshall, C. L. Hobday, C. F. Murphie, S. L. Griffin, C. A. Morrison, S. A. Moggach and R. S. Forgan, *Amino acids as highly efficient modulators for single crystals of zirconium and hafnium metal–organic frameworks*, *Journal of Materials Chemistry A*, 2016, **4**, 6955.

133. J. Bonnefoy, A. Legrand, E. A. Quadrelli, J. Canivet and D. Farrusseng, *Enantiopure Peptide-Functionalized Metal–Organic Frameworks*, *Journal of the American Chemical Society*, 2015, **137**, 9409.
134. M. Rimoldi, A. J. Howarth, M. R. DeStefano, L. Lin, S. Goswami, P. Li, J. T. Hupp and O. K. Farha, *Catalytic Zirconium/Hafnium-Based Metal–Organic Frameworks*, *ACS Catalysis*, 2017, **7**, 997.
135. C. Kutzscher, *Introducing Chirality to the 2nd and 3rd Generation of Metal–Organic Frameworks with L-Proline-Functionalized Linkers*, PhD, Technische Universität Dresden, 2018.
136. G. Kickelbick and U. Schubert, *Oxozirconium Methacrylate Clusters: $Zr_6(OH)_4O_4(OMc)_{12}$ and $Zr_4O_2(OMc)_{12}$ (OMc = Methacrylate)*, *Chemische Berichte*, 2006, **130**, 473.
137. V. L. Rechac, F. G. Cirujano, A. Corma and F. X. Llabrés i Xamena, *Diastereoselective Synthesis of Pyranoquinolines on Zirconium-Containing UiO-66 Metal–Organic Frameworks*, *European Journal of Inorganic Chemistry*, 2016, **2016**, 4512.
138. H. Reinsch, S. Waitschat, S. M. Chavan, K. P. Lillerud and N. Stock, *A Facile “Green” Route for Scalable Batch Production and Continuous Synthesis of Zirconium MOFs*, *European Journal of Inorganic Chemistry*, 2016, **2016**, 4490.
139. A. J. Rossini, C. M. Widdifield, A. Zagdoun, M. Lelli, M. Schwarzwälder, C. Copéret, A. Lesage and L. Emsley, *Dynamic Nuclear Polarization Enhanced NMR Spectroscopy for Pharmaceutical Formulations*, *Journal of the American Chemical Society*, 2014, **136**, 2324.
140. C. Copéret, W.-C. Liao, C. P. Gordon and T.-C. Ong, *Active Sites in Supported Single-Site Catalysts: An NMR Perspective*, *Journal of the American Chemical Society*, 2017, **139**, 10588.
141. K. Märker, M. Pingret, J.-M. Mouesca, D. Gasparutto, S. Hediger and G. De Paëpe, *A New Tool for NMR Crystallography: Complete $^{13}C/^{15}N$ Assignment of Organic Molecules at Natural Isotopic Abundance Using DNP-Enhanced Solid-State NMR*, *Journal of the American Chemical Society*, 2015, **137**, 13796.
142. T. Kobayashi, F. A. Perras, T. W. Goh, T. L. Metz, W. Huang and M. Pruski, *DNP-Enhanced Ultrawideline Solid-State NMR Spectroscopy: Studies of Platinum in Metal–Organic Frameworks*, *The Journal of Physical Chemistry Letters*, 2016, **7**, 2322.
143. M. Werner, A. Heil, N. Rothermel, H. Breitzke, Pedro B. Groszewicz, Aany S. Thankamony, T. Gutmann and G. Buntkowsky, *Synthesis and solid state NMR characterization of novel peptide/silica hybrid materials*, *Solid State Nuclear Magnetic Resonance*, 2015, **72**, 73.
144. A. J. Rossini, A. Zagdoun, M. Lelli, J. Canivet, S. Aguado, O. Ouari, P. Tordo, M. Rosay, W. E. Maas, C. Copéret, D. Farrusseng, L. Emsley and A. Lesage, *Dynamic Nuclear Polarization Enhanced Solid-State NMR Spectroscopy of Functionalized Metal–Organic Frameworks*, *Angewandte Chemie International Edition*, 2012, **51**, 123.
145. J. Duschmalé, S. Kohrt and H. Wennemers, *Peptide catalysis in aqueous emulsions*, *Chemical Communications*, 2014, **50**, 8109.

146. C. Song, K.-N. Hu, C.-G. Joo, T. M. Swager and R. G. Griffin, *TOTAPOL: A Biradical Polarizing Agent for Dynamic Nuclear Polarization Experiments in Aqueous Media*, *Journal of the American Chemical Society*, 2006, **128**, 11385.
147. W. R. Gunther, V. K. Michaelis, M. A. Caporini, R. G. Griffin and Y. Román-Leshkov, *Dynamic Nuclear Polarization NMR Enables the Analysis of Sn-Beta Zeolite Prepared with Natural Abundance ^{119}Sn Precursors*, *Journal of the American Chemical Society*, 2014, **136**, 6219.
148. V. Bon, I. Senkovska, J. D. Evans, M. Wöllner, M. Hölzel and S. Kaskel, *Insights into the water adsorption mechanism in the chemically stable zirconium-based MOF DUT-67 – a prospective material for adsorption-driven heat transformations*, *Journal of Materials Chemistry A*, 2019, **7**, 12681.
149. Y. Nishiyama, *Fast magic-angle sample spinning solid-state NMR at 60–100kHz for natural abundance samples*, *Solid State Nuclear Magnetic Resonance*, 2016, **78**, 24.
150. M. Penhoat, D. Barbry and C. Rolando, *Direct asymmetric aldol reaction co-catalyzed by l-proline and group 12 elements Lewis acids in the presence of water*, *Tetrahedron Letters*, 2011, **52**, 159.
151. Y. Hayashi, S. Aratake, T. Itoh, T. Okano, T. Sumiya and M. Shoji, *Dry and wet prolines for asymmetric organic solvent-free aldehyde-aldehyde and aldehyde-ketone aldol reactions*, *Chemical Communications*, 2007, **0**, 957.
152. T. S. Phan Nam, M. Van Der Sluys and W. Jones Christopher *On the Nature of the Active Species in Palladium Catalyzed Mizoroki–Heck and Suzuki–Miyaura Couplings – Homogeneous or Heterogeneous Catalysis*, *A Critical Review*, *Advanced Synthesis & Catalysis*, 2006, **348**, 609.
153. H. J. Reich, Bordwell pKa Table, <https://www.chem.wisc.edu/areas/reich/pkatable/>.
154. H. Hiramatsu and F. E. Osterloh, *pH-Controlled Assembly and Disassembly of Electrostatically Linked CdSe–SiO₂ and Au–SiO₂ Nanoparticle Clusters*, *Langmuir*, 2003, **19**, 7003.
155. A. Habibi Yangjeh, M. Danandeh Jenagharad and M. Nooshyar, *Prediction Acidity Constant of Various Benzoic Acids and Phenols in Water Using Linear and Nonlinear QSPR Models*, *Bulletin of the Korean Chemical Society*, 2005, **26**.
156. H. L. Nguyen, T. T. Vu, D. Le, T. L. H. Doan, V. Q. Nguyen and N. T. S. Phan, *A Titanium–Organic Framework: Engineering of the Band-Gap Energy for Photocatalytic Property Enhancement*, *ACS Catalysis*, 2017, **7**, 338.
157. S. Yuan, L. Zou, J.-S. Qin, J. Li, L. Huang, L. Feng, X. Wang, M. Bosch, A. Alsalmeh, T. Cagin and H.-C. Zhou, *Construction of hierarchically porous metal–organic frameworks through linker labilization*, *Nature Communications*, 2017, **8**, 15356.
158. H. L. Nguyen, F. Gándara, H. Furukawa, T. L. H. Doan, K. E. Cordova and O. M. Yaghi, *A Titanium–Organic Framework as an Exemplar of Combining the Chemistry of Metal– and Covalent–Organic Frameworks*, *Journal of the American Chemical Society*, 2016, **138**, 4330.
159. S. Yuan, P. Zhang, L. Zhang, A. T. Garcia-Esparza, D. Sokaras, J.-S. Qin, L. Feng, G. S. Day, W. Chen, H. F. Drake, P. Elumalai, S. T. Madrahimov, D. Sun and H.-C. Zhou,

- Exposed Equatorial Positions of Metal Centers via Sequential Ligand Elimination and Installation in MOFs*, *Journal of the American Chemical Society*, 2018, **140**, 10814.
160. M. S. Lohse and T. Bein, *Covalent Organic Frameworks: Structures, Synthesis, and Applications*, *Advanced Functional Materials*, 2018, **28**, 1705553.
161. J. L. Segura, M. J. Mancheño and F. Zamora, *Covalent organic frameworks based on Schiff-base chemistry: synthesis, properties and potential applications*, *Chemical Society Reviews*, 2016, **45**, 5635.
162. X. Feng, X. Ding and D. Jiang, *Covalent organic frameworks*, *Chemical Society Reviews*, 2012, **41**, 6010.
163. T. Hasell and A. I. Cooper, *Porous organic cages: soluble, modular and molecular pores*, *Nature Reviews Materials*, 2016, **1**, 16053.
164. A. G. Slater and A. I. Cooper, *Function-led design of new porous materials*, *Science*, 2015, **348**, aaa8075.
165. Y. Jin, Y. Zhu and W. Zhang, *Development of organic porous materials through Schiff-base chemistry*, *CrystEngComm*, 2013, **15**, 1484.
166. X. Han, Q. Xia, J. Huang, Y. Liu, C. Tan and Y. Cui, *Chiral Covalent Organic Frameworks with High Chemical Stability for Heterogeneous Asymmetric Catalysis*, *Journal of the American Chemical Society*, 2017, **139**, 8693.
167. H.-S. Xu, S.-Y. Ding, W.-K. An, H. Wu and W. Wang, *Constructing Crystalline Covalent Organic Frameworks from Chiral Building Blocks*, *Journal of the American Chemical Society*, 2016, **138**, 11489.
168. J. Zhang, X. Han, X. Wu, Y. Liu and Y. Cui, *Multivariate Chiral Covalent Organic Frameworks with Controlled Crystallinity and Stability for Asymmetric Catalysis*, *Journal of the American Chemical Society*, 2017, **139**, 8277.
169. F. Song, C. Wang, J. M. Falkowski, L. Ma and W. Lin, *Isorecticular Chiral Metal–Organic Frameworks for Asymmetric Alkene Epoxidation: Tuning Catalytic Activity by Controlling Framework Catenation and Varying Open Channel Sizes*, *Journal of the American Chemical Society*, 2010, **132**, 15390.
170. Q. Xia, Z. Li, C. Tan, Y. Liu, W. Gong and Y. Cui, *Multivariate Metal–Organic Frameworks as Multifunctional Heterogeneous Asymmetric Catalysts for Sequential Reactions*, *Journal of the American Chemical Society*, 2017, **139**, 8259.
171. P. Deria, J. E. Mondloch, O. Karagiari, W. Bury, J. T. Hupp and O. K. Farha, *Beyond post-synthesis modification: evolution of metal–organic frameworks via building block replacement*, *Chemical Society Reviews*, 2014, **43**, 5896.
172. M. Mehring, *Principles of High Resolution NMR in Solids*, ed. M. Mehring, Springer Verlag, Berlin, Heidelberg, New York, 1983, **chapter 8**, 260.

Publications and Presentations

Publications

1/ **Khoa D. Nguyen**, Christel Kutzscher, Franziska Drache, Irena Senkovska, and Stefan Kaskel, *Chiral Functionalization of a Zirconium Metal–Organic Framework (DUT-67) as a Heterogeneous Catalyst in Asymmetric Michael Addition Reaction*, *Inorganic Chemistry*, **2018**, 57, 1483–1489.

2/ **Khoa D. Nguyen**, Christel Kutzscher, Sebastian Ehrling, Irena Senkovska, Volodymyr Bon, Marcos de Oliveira Jr., Torsten Gutmann, Gerd Buntkowsky, and Stefan Kaskel, *Insights into the Role of Zirconium in Proline Functionalized Metal–Organic Frameworks attaining high Enantio- and Diastereoselectivity*, *Journal of Catalysis*, **2019**, 377, 41-50.

3/ Erik Troschke, **Khoa D. Nguyen**, Silvia Paasch, Johannes Schmidt, Georg Nickerl, Irena Senkovska, Eike Brunner, and Stefan Kaskel, *Integration of an N-heterocyclic carbene precursor into a covalent triazine framework for organocatalysis*, *Chemistry – A European Journal*, **2018**, 24, 18629-18633.

4/ Franziska Drache, Francisco G Cirujano, **Khoa D. Nguyen**, Volodymyr Bon, Irena Senkovska, Francesc X Llabrés i Xamena, and Stefan Kaskel, *Anion exchange and catalytic functionalization of the zirconium-based metal-organic framework DUT-67*, *Crystal Growth & Design*, **2018**, 18 (9), 5492–5500.

5/ Philipp Müller, Volodymyr Bon, Irena Senkovska, **Khoa D. Nguyen**, and Stefan Kaskel, *A bifunctional metal–organic framework platform for catalytic applications*, *Polyhedron*, **2018**, 1, 382-286.

Oral presentation

1/ **Khoa D. Nguyen**, Christel Kutzscher, Sebastian Ehrling, Irena Senkowska, Volodymyr Bon, Marcos de Oliveira Jr., Torsten Gutmann, Gerd Buntkowsky, and Stefan Kaskel, *Proline Functionalization of a Zr-based MOF(DUT-67): A highly enantioselective catalyst for the syn-Aldol addition*, The 6th International Conference on Metal-Organic Framework (MOF 2018), 12/2018, Auckland, New Zealand.

2/ **Khoa D. Nguyen**, Sebastian Ehrling, Irena Senkowska, Volodymyr Bon, and Stefan Kaskel, *Diastereo- and enantioselectivity control in asymmetric Aldol condensation reaction through an efficient chiral heterogeneous Zr-MOF catalyst*, The 10th International Symposium on Nano & Supramolecular Chemistry (ISNSC 10), 07/2018, Dresden, Germany.

Poster presentations

1/ **Khoa D. Nguyen**, Christel Kutzscher, Franziska Drache, Claudia Eßbach, Irena Senkowska, and Stefan Kaskel, *Chiral DUT-67 synthesized via solvent-assisted linker incorporation as a heterogeneous catalyst for the asymmetric Michael addition reaction*, The 2nd European Conference on Metal-Organic Frameworks and Porous Polymers (EuroMOF 2017), 10/2017, Delft, Netherlands.

Curriculum Vitae

Full name: Khoa Dang Nguyen

Date of birth: 19/01/1989

Place of birth: Ho Chi Minh city, Vietnam

Education

01/2016 – present: Ph.D. in chemistry, Technische Universität Dresden, Germany

Supervisors: Prof. Dr. Stefan Kaskel

Thesis: Synthesis of chiral zirconium-based metal-organic frameworks using as solid catalysts in asymmetric Carbon-Carbon coupling reactions

09/2012 – 04/2014: M.Eng. in chemical engineering, Ho Chi Minh City University of Technology, Vietnam.

Supervisors: Prof. Dr. Nam Phan

Thesis: Cu-MOFs as the heterogeneous catalyst for organic reactions

09/2007 – 04/2012: B.Eng. in chemical engineering, Ho Chi Minh City University of Technology, Vietnam.

Supervisors: Prof. Dr. Nam Phan

Thesis: Metal-organic framework MOF-199 as an efficient heterogeneous catalyst for the aza-Michael reaction

Erklärung

Hiermit versichere ich, dass ich die vorliegende Arbeit ohne unzulässige Hilfe Dritter und ohne Benutzung anderer als der angegebenen Hilfsmittel angefertigt habe; die aus fremden Quellen direkt oder indirekt übernommenen Gedanken sind als solche kenntlich gemacht. Die Arbeit wurde bisher weder im Inland noch im Ausland in gleicher oder ähnlicher Form einer anderen Prüfungsbehörde vorgelegt.

Die vorliegende Arbeit wurde am Institut für Anorganische Chemie der Technischen Universität Dresden in dem Zeitraum vom Januar 2016 bis Dezember 2019 unter wissenschaftlicher Betreuung von Herrn Prof. Dr. Stefan Kaskel angefertigt.

Dresden, 25.11.2019

Nguyen Dang Khoa